

STUDIES OF GEOMAGNETISM AND
IONOSPHERE AT LOW LATITUDES

043
IYE
7526

BY
K. NARAYANA IYER

A THESIS
SUBMITTED FOR THE DEGREE OF
DOCTOR OF PHILOSOPHY
OF THE

GUJARAT UNIVERSITY

JUNE 1976

043



B7526

PHYSICAL RESEARCH LABORATORY
AHMEDABAD
INDIA

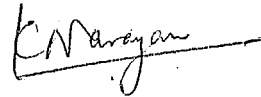
7526

DEDICATED TO

MY PARENTS

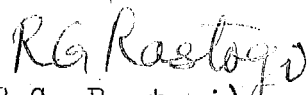
C E R T I F I C A T E

I hereby declare that the work presented in this thesis is original and has not been formed the basis for award of any degree by any University or Institution.



(K. Narayana Iyer)
Author

Certified



(R.G. Rastogi)
Professor-in-Charge

P R E F A C E

When a plane polarized radio wave from a satellite traverses through the ionosphere, its plane of polarization is rotated through an angle which depends on the distribution of ionization and the geomagnetic field along the ray path. This phenomenon known as Faraday Rotation provides a method of calculating the total number of electrons in a column of unit area of cross section extending from the ground to the top of the ionosphere or upto the satellite altitude. This quantity is generally denoted as the Total Electron Content (TEC) of the ionosphere. Although an integrated parameter of the ionosphere it gives useful insight into the behaviour of F-region and gives information about the large scale processes at work in the ionosphere. The elegance lies in the fact that with relatively simple equipments Faraday rotation can be measured by a large number of observatories.

For the measurement of TEC one can use either a low orbiting satellite at an altitude of about 1000 km. or a geostationary satellite at an altitude of 36,000 km. With geostationary satellites one gets continuous information over a particular location with high time resolution. With a low orbiting satellite one gets for a particular instant (in about 15 minutes) information over a large section of the ionosphere from a single observing station. Thus for temporal structure geostationary

satellites are most suited while for studies of spatial variation low orbiting satellites are ideal. However, because of the precession of the satellite orbit observations with a low orbiting satellite spanning over a few months will be distributed into the different hours of the day so that a few months observations will give one diurnal curve.

In November 1964 a receiving system to record the Faraday Rotation of VHF signals transmitted from satellites was set up at Physical Research Laboratory, Ahmedabad. The initial work was carried out by Dr.S.Ramakrishnan and later by Dr.R.P.Sharma and afterwards by the present author. The present author was closely associated with all aspects of tracking the satellite signals, their recording, data reduction and analysis and day to day maintenance. Similar receiving stations were in operation at Thumba and Kodaikanal also for short duration from 1964 to 1969.

The present thesis deals with the study of TEC of the equatorial and low latitude ionosphere in Indian zone using Faraday Rotation of 40 and 41 MHz signals from the satellites Explorer 22 (BE-B) and Explorer 27 (BE-C) recorded at Ahmedabad, Kodaikanal and Thumba during the years 1964 - 1969. Some preliminary results of the geostationary satellite ATS-6 data are also discussed.

At times irregular fluctuations, known as scintillations, are superposed on the regular Faraday fading which could be even so severe as to mask the Faraday fades. These amplitude scintillations are due to the plasma irregularities imbedded in the ionosphere along the path of the radio wave. A study of this feature is also included in this thesis which gives information about the nature and extent of the equatorial ionospheric irregularity belt.

The unique feature of the present study is that the beacon satellite data at Ahmedabad, Kodaikanal and Thumba are compared with the bottomside ionograms taken at the same place.

The lay-out of the thesis is as follows:

Chapters I, II and III

Starting with an introduction to Ionosphere and Geomagnetism at low latitudes in Chapter I, the detailed theory and methods of measuring TEC are given in Chapter II. A description of the experimental set up used and the method used for obtaining TEC from the Faraday rotation records are given in Chapter III. Preliminary results from the Faraday rotation of 140 MHz signals from the geostationary satellite ATS-6 are also given in this Chapter.

Chapter IV

In this Chapter the diurnal seasonal and solar cycle

variations of TEC at Ahmedabad, Kodaikanal and Thumba are described. The bottomside ionograms recorded at Ahmedabad and Kodaikanal at the nearest times of the satellite pass within $\pm \frac{1}{2}$ hr are used to derive the parameter equivalent slab-thickness $\tau = \frac{N_T}{N_m}$ where N_T is the TEC and N_m the maximum electron density in the F-region. This parameter gives the thickness the ionosphere would occupy had it been distributed with a uniform electron density equal to that at the peak of the F-layer. This parameter is also called the layer shape factor as it sensitively depends on the neutral temperature which determines the scale height and hence the layer shape. The diurnal seasonal and solar cycle variations of τ and $\frac{N_a}{N_b}$ where N_a is the total content above the peak and N_b that below the peak of the layer are described. The ratio N_a/N_b gives information about the topside ionosphere which could not be studied using conventional ionospheric sounding techniques. This ratio is indicative of the departures from thermal equilibrium i.e. $T_e \neq T_i \neq T_n$, the temperature gradients in the topside and composition changes in the topside. Results of the study of these parameters are presented in Chapter IV.

Chapter V

The best advantage of the low orbiting satellite is then taken in the present investigation by studying the latitudinal variation of TEC in the Indian equatorial anomaly region, by combining the observations from Kodaikanal, Thumba and Ahmedabad.

The satellite BE-B with an orbital inclination of 79° is most ideal for such studies to obtain the largest geographical coverage with little local time differences. Therefore only data from BE-B satellite have been used for this part of the study. These results are presented as contours of TEC over a grid of latitude (-5° to 25° N dip latitude) vs. local time in Chapter V. These studies bring out the details of the equatorial anomaly in TEC, its diurnal developments, its seasonal variation, its association with equatorial electrojet strength and the effects of solar and magnetic activity on it.

Chapter VI

Other ionospheric parameters derived from TEC measurements are the integrated production rate (Q_o) for an overhead sun and the effective loss rate (β') of the ionosphere. These parameters are computed and their dependence on solar XUV flux and season are investigated. These are presented in Chapter VI.

Chapter VII

In Chapter VII, the results of the studies about the occurrence of satellite signal scintillations, the width of the equatorial high scintillation belt, the characteristics of scintillations imposed by sporadic E patches and spread F irregularities and the most probable time of occurrence of scintillations are investigated.

Chapter VIII

In Chapter VIII some of the input parameters required for the communication systems engineers to plan out the communication links such as group delay, range error, polarization rotation etc are computed and presented using the observed TEC as the basic input to show the utility of the results.

Chapter IX

Another field of investigations carried out in this thesis is the study of a special type of ionospheric irregularities first discovered by Rastogi (1970) called kinks, observed as sharp discontinuities in the ionograms. Results of their occurrence, properties and the calculation of vertical $E \times B$ drift velocities from the temporal variation of the position of these kinks are presented in this Chapter.

Chapter X

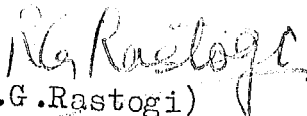
To understand a clearer relation between the ionosphere and equatorial electrojet the author has studied in detail, the diurnal, seasonal and solar cycle variations of the geomagnetic H field at Indian stations. The relative merits of the different definitions of the daily range of the geomagnetic H field, how they are affected by the magnetic disturbances, the amplitude and phase of the diurnal and semidiurnal components of the H field, the dependence of these amplitudes

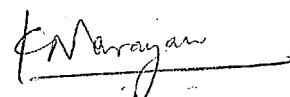
and phases on solar activity, the annual and semiannual variations of the diurnal range of H field ($rS_q H$) and the reasons for the time delay of diurnal maximum by about $\frac{1}{2}$ hr in high sunspot years are also the subject of the present investigations. These are presented in this Chapter.

Chapter XI

The conclusions of the studies are summarised in this Chapter.

It is hoped that these new results will enable to understand better, the complex ionospheric processes and the intricate control of the equatorial ionosphere by the equatorial electrojet. The measurement of TEC will be of immense practical value for the design of communication links via satellites and knowledge about the scintillations will be essential for satellite communication and TV links.


(R.G. Rastogi)
Professor-in-Charge


(K. Narayana Iyer)
Author

A C K N O W L E D G E M E N T S

The author expresses his deep gratitude and indebtedness to Professor R.G. Rastogi for introducing the author to the subject of Aeronomy, his invaluable guidance, advice and encouragement throughout the study and in the preparation of this thesis.

The author expresses his gratitude and respectful regards to Professor K.R.Ramanathan for his keen interest and encouragement in this work.

The author is extremely grateful to Dr.M.R. Deshpande for various stimulating and fruitful discussions at different stages of the work and leaving at the author's disposal the invaluable data of Faraday Rotation and Scintillations of the ATS-6 transmissions recorded by his set up at different stations in India.

The recording of Faraday Rotation at Ahmedabad and Thumba was first started by Dr.S. Ramakrishnan and later continued by Dr.R.P.Sharma. The initial infra-structure laid by them has eased the author's work greatly for which the author expresses his sincere thanks to them.

The author is indebted to Drs.M.K.V.Bappu and J.C.Bhattacharyya of the Indian Institute of Astrophysics, Kodaikanal for supplying their original Faraday Rotation records and ionograms used in this study and the hospitality provided, during the author's stay at Kodaikanal.

Various discussions with **Drs.**(Mrs.) Girija Rajaram and H. Chandra are thankfully acknowledged.

The computational assistance liberally provided by Mr.S.S.Deshikachar, Mr.K.C.Patel, Mr.I.P.Sutaria, Mrs.B.K.Bhatt and Mrs.S.D.Desai are also thankfully acknowledged.

The painstaking job of elegantly typing the thesis was most efficiently done by Mr.P.Raghavan in the shortest possible time. The author records his sincere thanks and appreciation to Mr.P.Raghavan.

The efficient service and facilities of the Telemetry Section, the Computer Centre and Photography and Documentation Section, deserve gratitude to the staff of these sections.

To avoid the long list of names, the author expresses his thanks to all his colleagues with whom he has had fruitful discussions.

Financial support from the Ministry of Education and Department of Space, Government of India is acknowledged.

The author is thankful to the Government of Kerala for sanctioning him long study leave to facilitate this work.

Finally a warm hug goes to the author's wife Mani and sweet kisses to our little daughter Anju for their patience and moral support.

LIST OF PUBLICATIONS

1. K.Narayana Iyer,
Geomagnetic disturbance effect on the solar daily range
of H field,
Curr. Sci., 42, 450-452 (1973).
2. K.Narayana Iyer and R.G. Rastogi,
On the occurrence and vertical movement of kink at
Kodaikanal,
J. Geophys. Res., 79, 209-214 (1974).
3. K.N. Iyer and R.G. Rastogi,
Vertical drift calculations from upward moving
ionospheric irregularities (kinks) over the magnetic
equator,
Ind. J. Radio. Space Phys., 4, 6-9 (1975).
4. R.G. Rastogi, J.C. Bhattacharyya and K.Narayana Iyer,
Ionospheric total electron content over the magnetic
equator,
Proc. Beacon Satellite Investigations of Ionosphere
Structure and ATS-6 Data, Nov. 1974, I, 129-132 (1975).
5. R.G. Rastogi, R.P. Sharma, K.N. Iyer and V. Shodhan,
Contours of total electron content derived from
Faraday rotation of beacon satellite signals at
Ahmedabad,
Proc. Beacon Satellite Investigations of Ionosphere
Structure and ATS-6 data, Nov. 1974, I, 133-136 (1975).
6. R.G. Rastogi, K.N. Iyer and J.C. Bhattacharyya,
Total electron content of the ionosphere over the
magnetic equator,
Curr. Sci., 44, 531-533 (1975).
7. R.G. Rastogi and K.N. Iyer,
Quiet day variation of geomagnetic H field at low
latitudes,
J. Geomag. Geoelect. (accepted for publication) 1976.
8. K.N. Iyer, M.R. Deshpande and R.G. Rastogi,
Equatorial anomaly in total electron content and the
equatorial electrojet strength,
Proc. Ind. Acad. Sci. (communicated) 1976.
9. R.G. Rastogi and K.N. Iyer
Ionospheric scintillations induced by cloud of intense
sporadic E-layer,
Curr. Sci. (communicated) 1976.

10. M.R.Deshpande, R.G. Rastogi, R.V.Bhonsle, H.S.Sawant,
K.N.Iyer, Banshi Dhar, A.V.Jarve, R.K.Rai, Malkiat Singh,
H.S.Gurm, A.R.Jain, B.N. Bhargava, V.M.Patwari and B.S.
Subbarao,
Multistation investigations of low latitude ionosphere
using low orbiting and geostationary satellites,
Presented in the COSPAR Satellite Beacon Symposium,
Boston University, June 1976.

C O N T E N T S

	<u>Page</u>
Dedications	
Certificate	
Preface	i
Acknowledgements	viii
List of publications	x
Contents	xii
CHAPTER-I : INTRODUCTION TO IONOSPHERE AND GEOMAGNETISM AT LOW LATITUDES	
1.1 Introduction	1
1.2 Equatorial electrojet	3
1.3 Conductivity of the ionosphere	6
1.3.1 General theory	6
1.3.2 Special geometry at the dip equator	9
1.3.3 Longitudinal differences	9
1.4 Anomalies in the equatorial F ₂ region	10
1.4.1 Equatorial anomaly in the latitudinal variation of foF ₂	10
1.4.2 Diurnal development of the equatorial anomaly	11
1.4.3 Equatorial anomaly in the diurnal variation of foF ₂	13
1.4.4 Daily variation of h _{max} F ₂	17
1.4.5 Equatorial anomaly in topside ionosphere	18

	<u>Page</u>
1.5 Explanation of the equatorial anomaly	19
1.5.1 Early explanations of the anomaly	19
1.5.2 Theoretical investigations of the equatorial anomaly	20
1.6 Scope of the thesis - Study of the ionosphere using artificial satellites	22
1.7 Satellites and satellite orbits	23
1.8 Characteristic requirements of beacon satellite and transmissions	25
1.9 Details of the two beacon satellites used in this study.	26
 CHAPTER-II : METHODS OF MEASURING TEC USING BEACON SATELLITES AND THEORY OF FARADAY ROTATION	
2.1 Introduction	30
2.2 Different methods of measurement of TEC	30
2.2.1 Angle of arrival measurement	30
2.2.2 Measurement of optical path difference - differential doppler method	32
2.2.3 Faraday rotation	35
2.2.4 Group delay method	35
2.2.5 Combined use of differential doppler and faraday data	36
2.3 Theory of faraday rotation, approximations, assumptions and second order corrections	37
2.3.1 First order theory of faraday rotation	37
2.3.2 Errors involved in first order theory	41
2.4 Approximations and higher order corrections	45
2.4.1 QL approximation	45
2.4.2 High frequency approximations	46

2.4.3 Refraction	46
2.4.4 Departure from the geomagnetic field or ionosphere model	47
2.4.5 Extrapolated field	47
2.4.6 Experimental accuracy	47

CHAPTER-III : EXPERIMENTAL SET UP OF MEASURING TEC USED IN THIS STUDY

3.1 Receiving set up at Ahmedabad	49
3.2 Formalism of satellite predictions	53
3.3 Description of the method of calculation of TEC	54
3.3.1 Geometrical aspects of the ray path calculations	54
3.3.2 Spherical harmonic expansion for the magnetic field	59
3.4 Methods of analysing faraday rotation records	64
3.4.1 Total rotation method	64
3.4.2 Differential faraday rotation (rotation rate or faraday frequency method)	66
3.4.3 Double frequency method	66
3.4.4 Second order methods of Ross (1965), Hudson (1969) and Nancy Uss Crooker (1970)	67
3.4.5 Intercomparison of TEC obtained by the different methods	70
3.4.6 Method used in the present study	71
3.5 Preliminary results of TEC and scintillations using ATS-6 satellite	72

CHAPTER-IV : RESULTS OF TOTAL ELECTRON CONTENT STUDIES AT AHMEDABAD, THUMBA AND KODAIKANAL

4.1 Introduction	78
------------------	----

	<u>Page</u>
4.2 Total electron content at Ahmedabad	81
4.2.1 Diurnal variation of TEC	81
4.2.2 Comparison of diurnal variation of TEC and Nm	83
4.2.3 Comparison of diurnal variation of TEC and Nm for different seasons	83
4.3 Total electron content at Thumba	85
4.3.1 Diurnal variation of TEC at Thumba	85
4.3.2 Comparison of daily variation of TEC and Nm	88
4.4 Total electron content at Kodaikanal	90
4.4.1 Diurnal variation of TEC at Kodaikanal in relation to related ionospheric parameters	90
4.4.2 Comparison of mean diurnal variation of TEC at Kodaikanal and Ahmedabad	93
4.4.3 Comparison of diurnal variation of TEC and Nm for different seasons and solar activity epochs	94
4.5 Seasonal variation of TEC	96
4.5.1 Seasonal variation of daytime and nighttime TEC at Ahmedabad	96
4.5.2 Seasonal variation of daytime and nighttime TEC at Thumba/Kodaikanal	97
4.6 Solar cycle variation of TEC	99
4.6.1 Variation of daily maximum and minimum TEC at Ahmedabad with solar activity	99
4.6.2 Variation of TEC at Kodaikanal/Thumba with solar activity	101
4.7 Equivalent slab-thickness of the ionosphere	102
4.7.1 Diurnal variation of slab-thickness at Ahmedabad	102

	<u>Page</u>
4.7.2 Diurnal variation of slab-thickness at Thumba	104
4.7.3 Diurnal variation of slab-thickness at Kodaikanal	104
4.7.4 Comparison of daily variation of slab-thickness and $h_p F_2$	106
4.7.5 Seasonal variation of daytime and nighttime τ at Ahmedabad	108
4.7.6 Seasonal variation of daytime and nighttime τ at Kodaikanal/Thumba	108
4.7.7 Solar cycle variation of slab-thickness at Ahmedabad	108
4.7.8 Dependence of equivalent slab-thickness on solar activity	111
4.7.9 Distribution of $\tau / 2Y_m$	111
4.8 Distribution of electrons above and below the peak of the ionosphere	112
4.8.1 Diurnal variation of N_a/N_b at Ahmedabad	112
4.8.2 Diurnal variation of N_a/N_b at Thumba	114
4.8.3 Diurnal - seasonal variation of N_a/N_b at Kodaikanal	114
4.8.4 Dependence of N_a/N_b on N_m .	116
4.8.5 Distribution of N_a/N_b	119
4.9 Discussion of the results	119
4.9.1 Diurnal variation of TEC	119
4.9.2 Seasonal variation of TEC	122
4.9.3 Slab-thickness and its implications	124

CHAPTER-V : LATITUDINAL VARIATION OF TOTAL
ELECTRON CONTENT AND SLAB-THICKNESS
IN INDIAN ZONE

5.1 Introduction	127
5.2 Latitudinal variation of TEC	129
5.2.1 Combined observation of TEC from two stations	129
5.2.2 Absence of equatorial anomaly in the diurnal variation of TEC	131
5.2.3 Contours of total electron content in equinoxes	133
5.2.4 Contours of TEC in winter	138
5.2.5 Contours of TEC in summer	138
5.3 Comparison of latitudinal variation of TEC and foF2	138
5.3.1 Contours of foF2 in equinoxes	138
5.3.2 Contours of foF2 in winter	142
5.3.3 Contours of foF2 in summer	142
5.4 Latitudinal/diurnal variation of peak TEC	142
5.5 Latitudinal variation of equivalent slab- thickness	144
5.6 Association of the equatorial anomaly in TEC with the equatorial electrojet strength	147
5.6.1 Comparison of latitudinal variation of TEC on pairs of strong and weak electrojet days	148
5.6.2 Diurnal development of equatorial anomaly in TEC	150
5.6.3 Time lag between anomaly and electrojet	151
5.6.4 Correlation between anomaly parameters and electrojet parameters	151

	<u>Page</u>
5.7 Discussion of the results	151
5.7.1 Latitudinal variation of TEC	154
5.7.2 Latitudinal variation of slab- thickness	157
5.7.3 Dependence of equatorial anomaly on electrojet strength	158
 CHAPTER-VI : INTEGRATED PRODUCTION AND EFFECTIVE LOSS RATES IN THE IONOSPHERE	
6.1 Introduction	161
6.2 Integrated production rate	164
6.2.1 Method of calculation of integrated production rate	164
6.2.2 Variation of production rate with season	166
6.2.3 Solar cycle variation of production rate	168
6.3 Effective loss rate (β')	170
6.3.1 Method of calculation of β'	170
6.3.2 Variation of effective loss rate with season	171
6.4 Discussion of the results	173
6.4.1 Production rate	173
6.4.2 Effective loss rate	176
 CHAPTER-VII : IONOSPHERIC SCINTILLATIONS OF RADIO SIGNALS	
7.1 Introduction	178
7.2 Seasonal variation of scintillation occurrence	181
7.3 Nocturnal variation of scintillation	183

	<u>Page</u>
7.4 Latitudinal variation of scintillation	185
7.5 Dependence of scintillation on sporadic E	189
7.6 Discussion of the results	191
CHAPTER-VIII: APPLICATIONS OF BEACON SATELLITE MEASUREMENTS	
8.1 Introduction	198
8.2 Direct application of beacon measurements	200
8.3 Application of beacon methods in space research	201
8.4 Application of satellite beacon data in the construction of engineering parameters	201
8.5 Application of scintillation data	202
8.6 Computation of engineering parameters from the results of present studies	204
8.6.1 Method of computation	204
8.6.2 Theory of computation of engineering parameters	204
8.6.3 Results of computation of engineering parameters	209
CHAPTER-IX : UPWARD MOVING IONOSPHERIC IRREGULARITIES	
9.1 Introduction	216
9.2 Analysis and results	223
CHAPTER-X : GEOMAGNETIC H FIELD AT LOW LATITUDES	
10.1 Introduction	224
10.2 Solar daily variation of H near the equator in different longitudes	226

	<u>Page</u>
10.3 Diurnal variation of H field at low latitudes	229
10.4 Seasonal variation of $S_q(H)$ field	235
10.5 Interrelationship between the annual and daily variation of electrojet current	240
10.6 Effect of geomagnetic disturbance on the solar daily range of H	243
10.7 Daily range of H on quiet and disturbed days	246
10.8 Discussion of the results and conclusions	251
CHAPTER-XI : SUMMARY AND CONCLUSIONS	260
REFERENCES	263
Appendix I	AI-1
Appendix II	AII-2

CHAPTER - I

INTRODUCTION TO IONOSPHERE AND GEOMAGNETISM AT LOW LATITUDES

1.1 Introduction

The ionosphere is a region of the upper atmosphere which contains free electrons and ions. It begins at a height of about 50 kms with no well defined upper limits. The ions and electrons are most abundant at heights of around 300 km but they represent only one thousandth of the air density even at that level; so the ionosphere can be regarded as a weakly ionized plasma embedded in earth's magnetic field. But as regards its practical utility and scientific interest, the ionization has attracted as much attention as the neutral air from which it is produced by the action of solar radiation. The most important property of the ionosphere is to reflect - under suitable conditions - long, medium and short waves used for broadcasting and radio communication.

The early investigations mainly by sounding the ionosphere using radio waves (Breit and Tuve, 1925; Appleton and Barnett, 1925) have revealed the existence of distinct layers conventionally designated as D(70 to 90 km), E(90 to 150 km) and F(150 to 500 km) regions whose reflecting properties and physical characteristics are distinct and show marked variations, partly systematic and partly irregular. A detailed description of various techniques of probing the ionosphere is given in the April issue of J. Atmos. Terr. Phys., 1970.

Once such routine monitoring of the ionosphere had become widespread soon it became apparent that certain aspects of the behaviour of the equatorial ionosphere differed greatly from the behaviour of the ionosphere elsewhere. It was also found that these differences were not determined by the geographic equator but by the dip equator.

The major influence of the geomagnetic field on the equatorial ionosphere arises because charged particles move more freely along the magnetic lines of force than across them. This means that in order to move the ionization vertically or in an east-west direction electric fields will have to be set up in the horizontal or vertical directions. It is known that electric fields are produced by the neutral wind attempting to blow the ionization across the magnetic field lines in the 100 - 130 km height range (dynamo region); this electric field drives the Sq current system (Matsushita and Campbell, 1967). In practice it appears that the large scale electric fields set up in the dynamo region at 10° - 15° latitude travel up the highly conducting magnetic field lines and appear virtually undiminished over the equatorial F-region (above 150 km) (Rishbeth, 1974).

The above mentioned Sq current system causes a diurnal variation of the geomagnetic field with a range of $\sim 100 \gamma$ (at the magnetic equator) which again depends on the latitude of the observation point relative to the Sq current focus. Ground based magnetometers when placed near the magnetic equator show an

abnormally large amplitude for the daily variation of the horizontal component (H) of the earth's magnetic field (Chapman and Bartels, 1940). The enhancement is known to be caused by an electric current flowing eastward in the dynamo region above the dip equator which has a width of about 500 km. The source of this current is the special geometry of the field at the dip equator which causes a vertical Hall polarization field resulting in enhanced conductivity in the eastward direction. This extra current known as the equatorial electrojet (Chapman, 1951) causes several interesting phenomena in the equatorial ionosphere.

1.2 Equatorial Electrojet

One of the most spectacular variation exhibited by all geomagnetic elements is daily variation (24 hourly) with fairly constant values at night, the field increasing shortly after sunset, reaching a maximum value around noon and falling thereafter to attain the night time level after sunset. Such a smooth pattern is known as Sq (S - solar, q - quiet) variation. However this quiet day pattern varies largely from day to day and season to season. The pattern of daily maximum reverses at a latitude of 30-40° and this latitude is called the Sq focus latitude. The range of variation in the course of a day, day time maximum value - night time minimum, is known as the daily range in the concerned element. This daily range is season and solar activity dependent and exhibits day to day variability also depending on the position of the focus. The daily range is normally expected to fall of from

a broad maximum value around the equator to zero value at the focus latitudes.

As early as 1922, when a geomagnetic observatory at Huancayo near the dip equator was established a few new features of the daily variation of earth's magnetic field came into light. Whereas the daily range in the declination, D and vertical intensity Z at Huancayo are comparable to those at station in similar geographical latitudes, the diurnal range in the horizontal component of H is abnormally large being often more than double the expected value. This abnormal range in H was interpreted by McNish (1937) as being due to locally concentrated eastward electric currents. Egedal (1947, 1948) reported that the diurnal range of H at six stations near the equator showed a sharply peaked curve symmetrical about the dip equator and smoother than a plot against dipole latitude. Subsequent measurements at other places viz. in Uganda (Chapman, 1948), Nigeria (Onwumechilli and Alexander, 1959), Peru (Forbush and Casaverde, 1961) and in India (Pramanik and Yegnanarayanan, 1952; Pramanik and Hariharan 1953; Thiruvengadhan, 1954), showed that this abnormal increase in the diurnal range of H happens at all places near the dip equator. It now became clear that the enhancement was due to overhead current. This enhancement of electric current flowing in a narrow zone of $\pm 3^\circ$ over the magnetic equator on the sunlit hemisphere was named 'Equatorial electrojet' by Chapman (1951). Figure 1.1 illustrates the abnormally large diurnal range in the electrojet region.

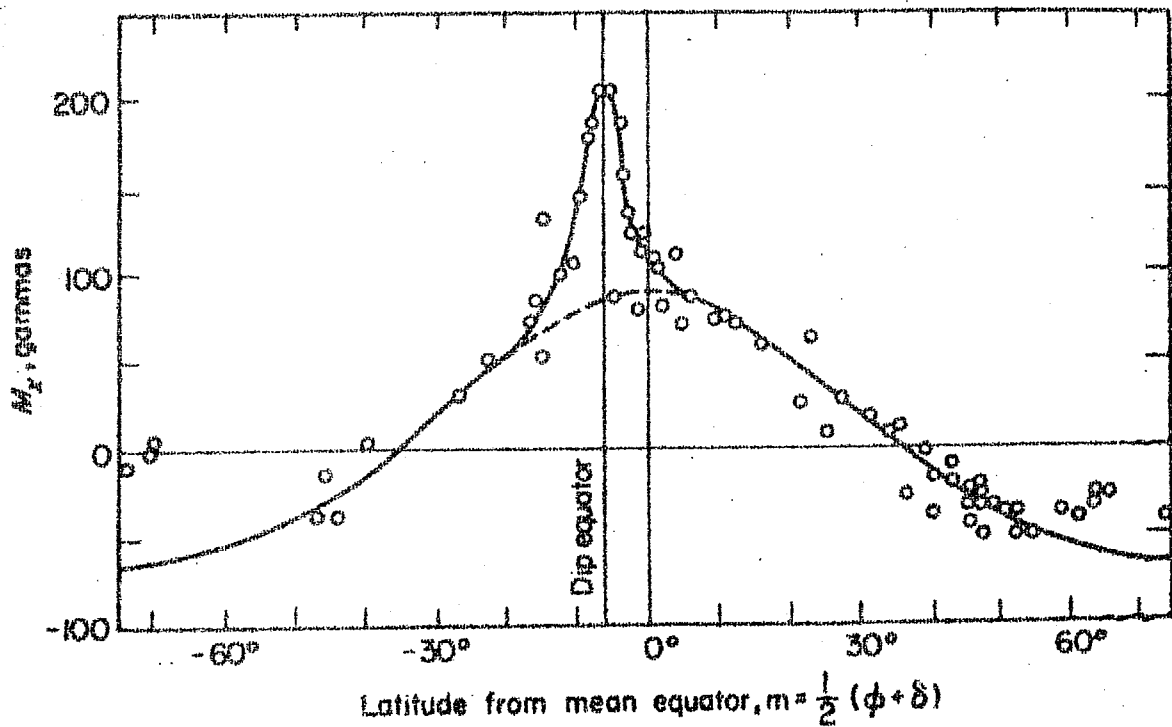


Figure 1.1 : Variation of the Daily range in H field with magnetic dip indicating the abnormally large range in the equatorial electrojet region (after Matsushita and Campbell, 1967).

1.3 Conductivity of the ionosphere

1.3.1 General theory

The cause of the equatorial electrojet lies in a special feature of the electrical conductivity and hence a brief description about conductivity is presented below.

Based on simple gas kinetic theory conductivity of an ionized gas, which is anisotropic in presence of a magnetic field, is represented by a tensor. Taking a cartesian coordinate system with its Z axis along the magnetic field direction \vec{B} , the conductivity tensor σ is given by

$$[\sigma] = \begin{bmatrix} \sigma_0 & -\sigma_2 & 0 \\ \sigma_2 & \sigma_1 & 0 \\ 0 & 0 & \sigma_3 \end{bmatrix} \quad (1.1)$$

where σ_0 , σ_1 and σ_2 are respectively the longitudinal, Pederson and Hall conductivities and are given by

$$\begin{aligned} \sigma_0 &= \frac{1}{B} \sum_i \frac{n_i \Omega_i}{\nu_i} e_i \\ \sigma_2 &= \frac{1}{B} \sum_i \frac{n_i \nu_i \Omega_i}{\nu_i^2 + \Omega_i^2} e_i \\ \sigma_1 &= -\frac{1}{B} \sum_i \frac{n_i \Omega_i^2}{\nu_i^2 + \Omega_i^2} e_i \end{aligned} \quad (1.2)$$

where subscript i denotes the i^{th} species of charged particles, e is the charge of the particle (-e for electrons), $\Omega_i = \frac{e_i B}{m_i c}$ is the gyrofrequency, ν_i is the collision frequency of the i^{th}

ion species with neutrals, n_i is the number density of charged particles and m_i mass of the charged particle. The collisions between charged particles is excluded in equation (1.2). In a weakly ionized plasma like the lower ionosphere, this is reasonably true, but becomes serious with increasing altitude and must be taken into account.

From equation (1.2) it is found that σ_0 , σ_1 and σ_2 are function of n_i , m_i and ν_i which depend on neutral number density. These parameters vary with time and space. The height distribution of σ_0 , σ_1 and σ_2 show that σ_1 and σ_2 are smaller than σ_0 and reach maximum at 110 to 140 km (E region); this result is independent of the model used for n_i and ν_i . The ratio $\frac{\sigma_2}{\sigma_1}$ is about 10 around 100 km during day time.

When the magnetic and electric fields are orthogonal and in the horizontal plane, which is true near the magnetic equator, a vertical Hall current flows. But since the medium is bound in the vertical direction, the flow of this current is inhibited resulting in the setting up of polarization fields. If this Hall polarization field inhibits further the Hall current, the effective conductivity of the medium (parallel to the electric field) is greater than σ_1 . In the ionosphere, Hall current leads to polarization fields which leaks away easily along the conducting geomagnetic field lines except at the dip equator where the field lines are horizontal and the Hall current is completely inhibited. The resulting conductivity is sufficient to explain the observed Sq field.

To derive the effective conductivity the coordinates are changed with X, Y and Z representing the magnetic south, east and vertically upward directions respectively. The conductivity tensor (1.1) then takes the general form

$$[\sigma] = \begin{bmatrix} \sigma_{xx} & \sigma_{xy} & \sigma_{xz} \\ \sigma_{yx} & \sigma_{yy} & \sigma_{yz} \\ \sigma_{zx} & \sigma_{zy} & \sigma_{zz} \end{bmatrix} \quad (1.3)$$

If we consider ionosphere as a conducting thin spherical shell, then currents cannot flow vertically and hence $J_z = 0$. The current density

$$\vec{J} = [\sigma] \vec{E} \quad (1.4)$$

then becomes

$$\begin{aligned} J_x &= \sigma_{xx} E_x + \sigma_{xy} E_y \\ J_y &= \sigma_{yx} E_x + \sigma_{yy} E_y \end{aligned} \quad (1.5)$$

with $J_z = 0$

where

$$\begin{aligned} \sigma_{xx} &= \sigma_0 \sigma_1 / (\sigma_0 \sin^2 \phi + \sigma_1 \cos^2 \phi) \\ \sigma_{xy} &= -\sigma_{yx} = \sigma_0 \sigma_2 \sin \phi / (\sigma_0 \sin^2 \phi + \sigma_1 \cos^2 \phi) \\ \sigma_{yy} &= (\sigma_0 \sigma_1 \sin^2 \phi + \sigma_1 \sigma_3 \cos^2 \phi) / (\sigma_0 \sin^2 \phi + \sigma_1 \cos^2 \phi) \end{aligned} \quad (1.6)$$

where ϕ is the dip angle and $\sigma_3 = \sigma_1 + \sigma_2^2 / \sigma_1$ is the

effective or cowling conductivity to be used in the dynamo theory. Since $\sigma_2 \gg \sigma_1$ in the 100 km region σ_3 is very much enhanced or σ_{xx} , σ_{yy} and σ_{xy} being function of ϕ , vary with latitude. Estimations show that height integrated effective conductivity over most part of earth is 5 to 10 times greater than the Pederson conductivity, even though the inhibition of Hall current is not complete at most places (Hirono 1950a,b, 1952; Martyn 1948a; Maeda 1952; Baker and Martyn 1953; Chapman 1956; and Maeda and Matsumoto, 1962).

1.3.2 Special geometry at the dip equator

At the dip equator $\phi = 0$ and $\sigma_{xx} = \sigma_0$, $\sigma_{xy} = 0$ and $\sigma_{yy} = \sigma_3$. Thus the cowling conductivity is enhanced by a further factor of 2 to 5 because of the total inhibition of Hall current. The enhancement of σ_{yy} occurs in a narrow zone of half width 3° latitude (Baker and Martyn 1953) flanking the dip equator and this is the cause of the equatorial electrojet.

1.3.3 Longitudinal differences

Subsequent studies (Rastogi, 1962) of the electrojet in different longitudes have shown significant longitudinal differences with strongest electrojet in the American zone and weakest in Indian zone. This is confirmed in recent rocket measurements of electrojet currents intensity in Peru (Maynard, 1967; Davies et al., 1967) and in India (Sastry, 1968). This longitudinal inequality may be due to longitudinal differences in the geomagnetic field \vec{B} ,

which gives rise to inequalities in the conductivity σ_{yy} (Suguiira and Cain, 1966). Untied (1967) has modified σ_{yy} model of Suguiira and Cain (1966) to take into account meridional currents also. This model yields a stronger current and a substantially large ($\sim 7^\circ$) width of the electrojet. Untied (1967) assumed a dipole field. Suguiira and Poros (1969) have improved upon this model by using a spherical harmonic expansion for the magnetic field.

1.4 Anomalies in the equatorial F2 region

1.4.1 Equatorial anomaly in the latitudinal variation of foF2

Even the earliest observations had demonstrated that the F₂ layer behaves anomalously in various ways. The first example of such unexpected behaviour was shown by Appleton and Naismith (1935) that the f_oF₂ at Slough was less at summer noon than winter noon, whereas the E and F₁ regions ionization increased with decrease of solar zenith angle as expected from Chapman's (1931) simple theory of production of ionization in planetary atmospheres. Another abnormal behaviour of the F₂ region of the ionosphere was noted by Berkner and Wells (1934) with the establishment of an equatorial observatory at Huancayo where he found the magnitude of f_oF₂ had two peaks during the day around 0800 and 1600 hr with a bite-out around noon. Maeda et al. (1942) showed that f_oF₂ data of American and Asian stations fitted well with each other when the geomagnetic latitude was considered rather than geographic latitude thus detecting geomagnetic control in the F₂ region. However, Appleton (1946) was first to show that when equinox noon values

of f_oF_2 were plotted against magnetic dip a curve is resulted which had two peaks at $\pm 28^\circ$ dip with a trough around dip equator. The existence of these two peaks north and south of the dip equator has come to be known as Equatorial anomaly, geomagnetic anomaly or Appleton anomaly. Figure 1.2 illustrates the equatorial anomaly in the latitudinal variation of f_oF_2 (after Rastogi 1966).

Burkard (1954) and Maeda (1955) tried to examine the relative importance of the geomagnetic (dipole) and magnetic (dip) latitude in the distribution of noon f_oF_2 but no significant difference could be found. Rastogi (1959a,b) using an extended set of data showed that when noon f_oF_2 is plotted against the magnetic dip the scatter of points is much less than if it is plotted against dipole or geographic latitude indicating that the anomaly is controlled by the magnetic dip.

1.4.2 Diurnal development of the equatorial anomaly

By examining the relation between N_m and geomagnetic latitude for hours of the equinox day other than noon, Appleton (1954) found that the latitudinal anomaly persists throughout the day and is absent at night hours. A detailed investigation of the equatorial anomaly's daily variation during equinoxial months of 1953-54 - a period of extremely low solar activity was carried out by Rastogi (1959c). He found that two peaks begin forming close to the dip equator around 0900 LT, move poleward until they reach 16° dip latitude by 1600 LT and then move back towards the equator finally disappearing by 2100 LT. It is observed in all

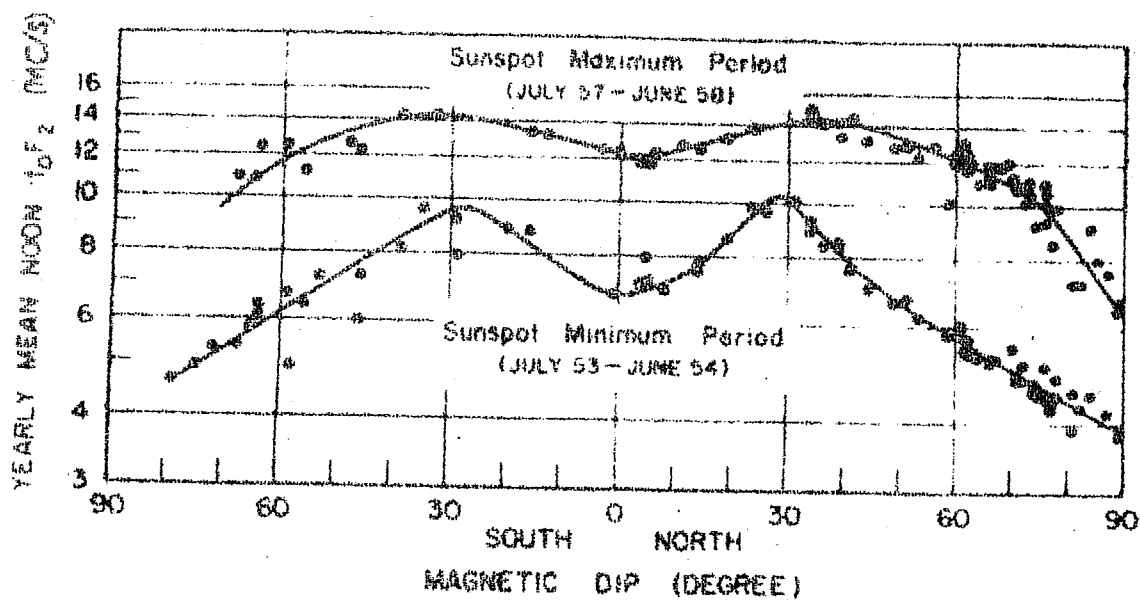


Figure 1.2 : Equatorial anomaly in noon foF2 for sunspot maximum and sunspot minimum period (after Rastogi 1966).

cases that while the peaks move poleward their amplitude increases and while they move equatorward their amplitude decreases.

The situation during solar maximum is quite different. Although the development of the anomaly begins at the same time the peaks maintain their poleward motion upto 2000 LT where maximum development occurs before moving back to the equator. Lyon and Thomas (1963) found that the anomaly persists at least till 0200 LT during equinox of 1958. The same observations were confirmed by Rao and Malhotra (1964) also. Rastogi (1966) compared the daily development of the anomaly for each hour of March for low sunspot year (1964) and high sunspot year (1959). The anomaly is most pronounced at 1400 LT during 1964 and 2000 LT during 1959. His findings are reproduced in Figure 1.3.

Longitudinal differences in the equatorial anomaly were first pointed out by Eyfrig (1962). He found that the numerical values of the peaks and troughs are different in the eastern and western hemispheres, lower values being found at 90°W than 60°E. The difference is also found to be larger in the southern than in the northern hemisphere.

1.4.3 Equatorial anomaly in the diurnal variation of f_oF_2

Berkner and Wells (1934) were the first to note a noon bite-out in the daily variation of f_oF_2 at Huancayo, i.e. a peak of f_oF_2 is reached in morning and again in the late afternoon with a valley around noon. Rastogi (1959b) found that the

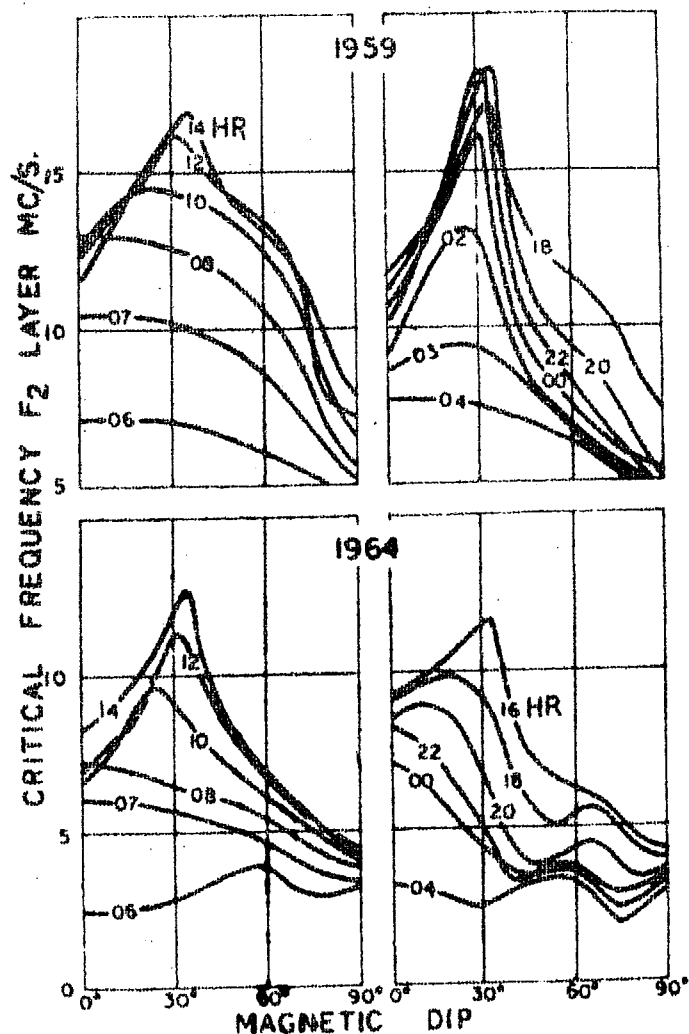


Figure 1.3 : Diurnal development of equatorial anomaly during low (1964) and high (1959) sunspot years (after Rastogi 1966)

diurnal variation of f_oF_2 is considerably different at stations having the same geomagnetic latitude, but when the true magnetic dip of the station is considered these discrepancies disappear. Rastogi (1959c) found that the double maximum in the diurnal variation of f_oF_2 are less separated with increasing latitude and finally converge to a single maximum at a dip of 25° . Studies of the daily variation of f_oF_2 have also been carried out by Rao (1963). Rastogi and Sanatani (1963) have described the longitudinal effect in the daily variation of f_oF_2 at the equatorial stations. At Huancayo (dip $2^\circ N$) the noon bite-out and the evening peak become less important with increasing solar activity so much so that in 1958 the daily variation has only a single prominent peak in the forenoon. At Kodaikanal (dip $3.5^\circ N$) one finds a very distinct noon bite-out in any of the years 1954-62. The daily variation of f_oF_2 at Natal (dip $2^\circ S$) is quite different. These results are reproduced in Figure 1.4. The equatorial stations Huancayo, Ibadan and Kodaikanal represent the American, African and Asian sectors respectively.

In the American sector, during solar minimum year (1954), two peaks are observed, a morning and an afternoon peak separated by a trough around noon known as the noon bite-out. As sunspot number increases, the morning peak gains importance while the afternoon peak and the noon bite-out becomes less significant. At 1800 hr LT during solar maximum (1958) f_oF_2 as a function of local time begins decreasing rapidly whereas its behaviour during solar minimum is much less precipitous.

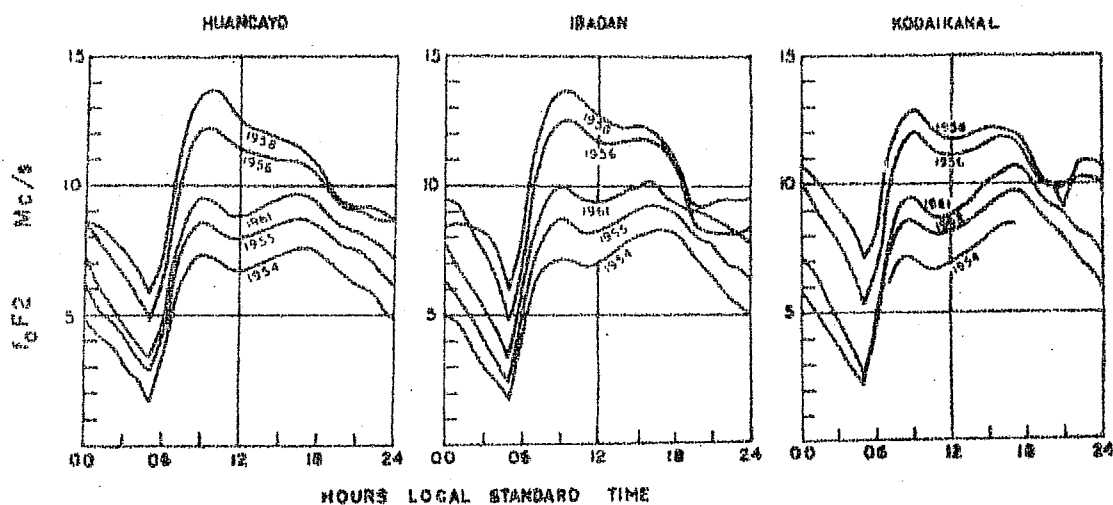


Figure 1.4 : Daily variation of f_oF_2 at equatorial stations Huancayo, Ibadan and Kodaikanal representing American, African and Indian zones for years of varying solar activity.

Overall, the solar cycle change in the daily variation of f_oF_2 in the African and American sector is similar with two exceptions: during solar minimum the afternoon peak is greater than the morning peak, and during solar maximum the noon bite-out is more evident. In the Asian sector, Rastogi (1970) found that at Kodaikanal, close to the dip equator, the morning maximum in f_oF_2 is weaker than the afternoon one during solar minimum while as solar activity increases, f_oF_2 increases more rapidly in the morning than in the afternoon so that during solar maximum the morning maximum gains importance.

When the equatorial anomaly is studied in the American, African and Asian sectors characteristic differences are observed which depend on solar cycle.

1.4.4 Daily variation of $h_{max} F_2$

Observations of $h_{max} F_2$, the height, of peak F_2 ionization density, are much fewer than those of $N_{max} F_2$ primarily because of the greater difficulty in obtaining the measurements from ionosonde data. Incoherent scatter radar yields the height directly but there are very few stations employing this technique.

During solar minimum years on quiet equinoctial days near the dip equator (African sector), Olatunji (1965) and Lyon (1965) find that $h_{max} F_2$ lies between 300 km and 350 km from 1200 LT to 1800 LT. Farley (1966) using incoherent scatter radar find the same values of $h_{max} F_2$ in the American sector. During the night

all these investigators find that $h_{\max} F_2$ slowly decreases to around 275 km by 0500 LT.

A different daily variation of $h_{\max} F_2$ is found during solar maximum years. In the African sector Olatunji (1965) finds that the F_2 peak increases from 300 km at 0700 LT to 500 km by 1400 LT maintaining this altitude till 1800 LT. Soon after 1800 LT $h_{\max} F_2$ rises rapidly attaining 600 km by 2100 LT. This same post sunset behaviour is also seen in the American zone (Lyon and Thomas, 1963). $h_{\max} F_2$ then decreases throughout the night so that by 0400 LT it has reached its minimum value of 300 km. Rastogi (1971) has shown that the effects of solar activity on $f_o F_2$ and $h_p F_2$ are diametrically opposed; $f_o F_2$ increases at its maximum rate when the corresponding change in $h_p F_2$ is least.

Chandra et al. (1973) have done true height analysis of $N(h)$ distribution at an equatorial station Thumba. They found that $h_{\max} F_2$ and $h_p F_2$ tally each other for night time records only. $h_{\max} F_2$ was found to show midday maximum in the low sunspot year, 1965; but as solar activity increased, largest values of $h_{\max} F_2$ were seen in post sunset period.

1.4.5 Equatorial anomaly in topside ionosphere

The equatorial anomaly is also seen from topside sounding satellite (Lockwood and Nelms, 1964). It is evident that the ionosphere above the F_2 peak is also controlled by the geomagnetic field. If electron density is plotted as a function of altitude,

a ledge is observed (between 1600 and 2400 LT) whose height variation depends on magnetic latitude. In fact this ledge occurs on the magnetic field line which passes through the crests of the anomaly called the anomaly field line (Lockwood and Nelms, 1964; Raghava Rao and Sivaraman, 1974).

1.5 Explanation of the equatorial anomaly

1.5.1 Early explanation of the anomaly

Soon after Appleton's observations concerning the equatorial anomaly was published, Mitra (1946) suggested that the formation of the anomaly was due to production of ionization by solar ultra-violet radiation high in the atmosphere from 600 to 1100 km and subsequent downward diffusion along magnetic field lines to F_2 altitudes causing an increase in ionization at magnetic latitudes of $\pm 15^\circ$.

Martyn (1947, 1953) on the other hand proposed that most of the ionization was produced in the lower atmosphere, near 200 km and lifted vertically with a velocity $\frac{\vec{E} \times \vec{B}}{B^2}$ where \vec{E} represents an eastward electrostatic field and \vec{B} the earth's magnetic field. The combined effect of this $E \times B$ drift and diffusion along the magnetic field lines by gravitational and pressure gradients forces effectively transports the ionization from the magnetic equator towards higher latitudes. However as latitude increases the downward diffusion velocity also increases so that beyond a certain latitude, the plasma's horizontal velocity component starts

to decrease with increasing latitude. In this way crests in ionization are produced north and south of the magnetic equator.

The electrostatic field E required in Martyn's theory is produced in the E-region as a consequence of neutral winds moving ionization across magnetic field lines thereby generating currents and electric fields. This so called 'dynamo' theory first proposed by Stewart (1882) (see Matsushita 1967 and Tarpley 1970).

Investigations by Duncan (1960), Baxter (1964) and others seem to indicate that Martyn's theory is better able to account for the observations than Mitra's. The investigations by Duncan (1960) and Matsushita (1968) suggested that ionization is being transported to one latitude region at the expense of the other. Mitra's theory cannot explain transport of ionization toward equator.

1.5.2 Theoretical investigations of equatorial anomaly

Solving the steady state continuity equation which included the effects of production, loss, diffusion, $\vec{E} \times \vec{B}$ drift and neutral wind, Hanson and Moffett (1966) found that the crests in ionization reached 20° latitude for a drift of 15 m/sec and only 8° when drift was neglected. Bramley and Peart (1964) solving the continuity equation assuming similar conditions produced the same results. They also found that a drift speed of 10 m/sec would produce crest at 17° geomagnetic latitude with a peak to trough ratio of 1.55; an upward velocity of 5 m/sec would produce crest at 12.5° latitude with peak to trough ratio of 1.22.

Investigating the vertical drift effects in more detail, Bramley and Young (1968) found that the peak to trough ratio increased linearly with drift speed from a ratio 1 at zero drift to 5 at 33 m/sec. The latter drift speed produces crest at 25° latitude.

Baxter and Kendall (1968) have solved the complete time dependent continuity equation, to take into account corotation of the ionization with the earth.

Abur-Robb and Windle (1969) solving the time dependent continuity equation investigated the effect of neutral wind on producing the north-south asymmetry. They found that a wind speed of 40 m/sec blowing from north to south across the dipole equator transported ionization from northern to southern hemisphere causing the southern crest to be larger than the northern one.

Further studies by Abur-Robb (1969) and Sterling et al. (1969) not only confirmed that drift is a necessary ingredient for producing the equatorial anomaly but showed that the position of the crests depend only on $\vec{E} \times \vec{B}$ drift and not on neutral wind velocity.

Anderson (1971) using a more realistic geomagnetic field model has theoretically reproduced the diurnal development of the equatorial anomaly in the American and Asian sectors using different electrostatic field models.

The anomalous diurnal variation of $f_o F_2$ at an equatorial station showing a depletion around noon is a direct consequence of

the above discussed processes in the equatorial F_2 region.

1.6 Scope of the thesis - Study of the ionosphere using artificial satellites

Till the advent of the satellites orbiting round the earth it was impossible to study the major portion of the ionosphere above the F-region peak (topside) because of the inherent difficulty that radio waves with frequency $f > f_c$ become transparent to the ionosphere and hence the conventional radio sounding techniques from ground fail to probe beyond the F-region peak. However satellites equipped with stable coherent radio beacon transmitters of several suitable frequencies have been used in the past two decades for studying the topside ionosphere. By measuring on the ground one or more of the characteristics such as polarization, amplitude, phase, frequency etc of the coherent transmissions from satellites it is possible to study the gross properties of the ionosphere on short and long time scales. The most usually and easily measured parameter for such studies is the total electron content (TEC) of the ionosphere which is defined as the total number of electrons in a vertical column of unit area of cross section extending from satellite to the ground (Browne et al., 1956). The study of the behaviour of the parameter is of great practical utility for the communication engineer and throws light into the physical processes at work in the ionosphere. A phenomenon which can be studied with no extra equipment than that required for measuring TEC is the scintillation of HF and VHF signals imposed by the electron density irregularities in the ionospheric plasma,

as these waves traverse through the ionosphere. Information on the morphology of scintillation is of great practical value for communication engineers to correct for the phase distortions of trans-ionospheric signals caused by the scintillations. Characteristic features of scintillation also carry information about the nature of these irregularities, their scale sizes and distribution and the physical mechanisms responsible for the production of these (Swenson, 1963). In the present work a study of the equatorial and low latitude ionosphere by measuring the TEC using low orbiting satellites over a period covering half a solar cycle is presented. Part of the thesis is devoted for the study of scintillations in the ionosphere. A chapter is also added on the study of geomagnetic field and its variations at low latitudes in the Indian zone.

1.7 Satellites and satellite orbits

The advantage with satellite studies is that once a satellite is placed in orbit it continues to be in operation for a large number of years. Most of the satellites used for such studies are at or above about 1000 km altitude, where the air density is so small that the drag effects on the satellite orbit are almost negligible. The motion of a satellite around the earth is guided by the well known gravitational force balance equation

$$\frac{m_s v_s^2}{r} = \frac{G M_E m_s}{r^2} \quad (1-7)$$

where m_s is the satellite mass, M_E the mass of the earth, v_s the orbital velocity of the satellite, G the gravitational constant

and r the distance of the satellite from the centre of the earth. Satellite orbit could be chosen to be circular or to have any desired eccentricity. It follows from the equation (1.7) that the period of revolution of the satellite when it is at any given altitude is given by

$$T = 2\pi \sqrt{\frac{r^3}{GM_E}} \quad (1.8)$$

and varies as $r^{3/2}$. Satellites at around 1000 km altitude will thus have a period of roughly 105 minutes. Of course small nonuniformities in the gravitational field give rise to slight perturbations in the orbit. So such satellites can be used to scan a few hundred kms of the ionosphere in about a few minutes' time (King Hele, 1964). The orbits could be chosen to have any inclination with the equatorial plane. Polar circularly orbiting satellites with almost a N-S transit are preferred in the study of TEC in order to avoid local time changes. Such low orbiting satellites have the advantage that from a single observing station we can cover about $\pm 10^\circ$ latitudinal extent in about a few minutes' time. However there is the limitation that we do not get continuous data over any location.

This could be overcome by employing geostationary satellites which have their period of revolution same as that of the spinning period of the earth (viz 24 hours) so that with respect to any observer the satellite appears to be always at a fixed location.

For this the satellite should be placed over the equator at the geostationary altitude of $6.6 R_E$ (earth radii). Such a satellite will give continuous information over a given place but at the same time spatial coverage has to be forgone. However data from the geostationary satellite ATS-6 have just started to emerge from Indian observations.

1.8 Characteristic requirement of beacon satellite and transmissions

To give the widest geographical coverage and to permit the study of polar ionosphere the satellite orbit should be inclined approximately 90° from the earth's equatorial plane. In order to keep the source well above most of the electrons in the ionosphere and above the scintillation producing irregularities the satellite altitude should be at least 1000 kms. Circular orbit can simplify the analysis. Polar orbiting satellites can avoid the local time dependence in latitudinal variation studies. It is desirable that the satellite has electromagnetic symmetry about the spin axis or the satellite be spin stabilized in such a way that the antenna aspect presented to the ground observer changes only very little. It is very useful to have several frequencies and that they be locked together in phase. Sufficient power must be transmitted to facilitate reception with good signal to noise ratio even by simple equipments on ground (Ref. Swenson 1963, COSPAR information bulletin No. 15, 20).

1.9 Details of the two beacon satellites used in this study

The explorer 22 research satellite known as Beacon Explorer-B (BE-B) or S₆₆ was launched by means of a Scout rocket on October 9, 1964 from Vandenberg Air Force Base, USA. The satellite went into an orbit with an inclination of 79°, apogee of 674 miles (1084.4 kms) and perigee 878.5 km. The anomalistic period is 104.7 minutes.

Explorer 27 satellite known as BE-C was also launched from the same launching site by a similar rocket on 29 April 1965. This satellite went into an orbit with an inclination of 41°, an apogee of 1321 km and perigee of 933.2 km and an initial period of 108 minutes.

Both the satellites are identical in construction

Weight = 116 lbs

Shape = octogonal cylindrical shell from the sides of which
four solar panels extend like wind mill blades

Material = Made of honey comb nylon and fibre glass

Height = 12"

Diameter = 18"

The cut away view of the satellite Explorer 22 is shown in Figure 1.5.

Solar panels are 10° wide and 5.5' long and contain twice as many solar cells as needed for initial power. As the solar cells deteriorate due to radiation effects a reserve bank of solar

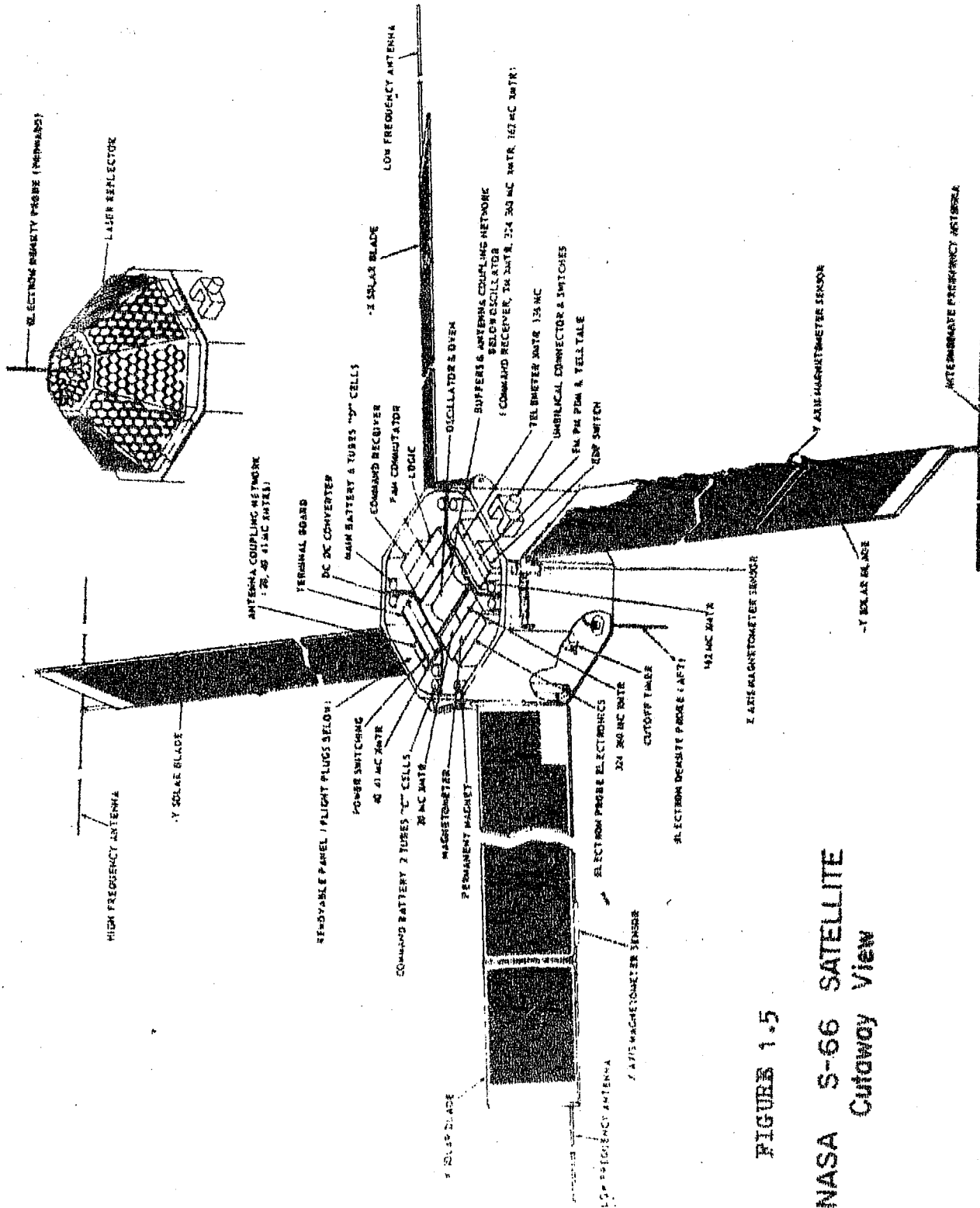


FIGURE 1-5

NASA S-66 SATELLITE
 Cutaway View

cells would be brought into operation.

Antennas: Extending from the ends of opposite solar panels are two 5' long whip antennas which radiate 20.005, 40.010 and 41.010 MHz. Two bar magnets 5.75" long are used for passive orientation of the satellite. They align it along the magnetic field.

To protect the instrument from large temperature variations vacuum insulation is provided between the instrument and the satellite shell. When the internal temperature of the shell drops below the desired 21°C any one of the eight thermostats located throughout the satellite, triggers an adjacent heater.

Centrifugal forces cause the weighted antispin cables to deploy and allow the four solar panels to erect themselves. The first of these two actions bring down the spin rate to 40 rpm from 160 rpm. The solar panel deployment causes a further decrease of spin rate to 3 rpm. The rate is then gradually reduced to zero by magnetic antispin rods.

S₆₆ satellites have 3 basic transmitting systems:

- (1) NASA Ionospheric beacons at 20, 40, 41 and 360 MHz
- (2) APL doppler system at 162 and 324 MHz
- (3) Telemetry channel at 136 MHz.

The ionospheric beacon frequencies are derived from 5 MHz crystal oscillator which is enclosed in a package containing a dual oven with high thermal stability. The transmissions are

coherent and linearly polarized. All the low frequency transmitters radiate at approximately 250 mW.

A clock marker or timing pulse appears on the 20 MHz signal. This modulation is a rectangular pulse which occurs every 22.018 sec. BE-B provides one pulse and BE-C provides two pulses. These timing pulses can be used as identification marks for the two satellites. Signals for the time markers are derived from a tuning fork oscillator with a stability of 1 part in 10^9 .

C H A P T E R - I I

METHODS OF MEASURING TEC USING BEACON SATELLITES AND THEORY OF FARADAY ROTATION

2.1 Introduction

We divide the various methods of measuring TEC according to the measured parameter of the wave as follows:

- (a) Method based on measurement of angle of arrival of the wave
- (b) Method based on measurements of the polarization angle of wave (Faraday Rotation)
- (c) Method based on the measurement of the shift of the frequency of the receiving wave (Doppler technique)
- (d) Method based on the measurement of group delay of two different frequencies.

The above methods will be briefly explained in this chapter and a detailed account of the theory of Faraday Rotation which has been used in the present study will be postponed to section 2.3.

2.2 Different methods of measurement of TEC

2.2.1 Angle of arrival measurement

One of the effects of the ionospheric medium is the refraction of the incoming wave thus causing a change in its propagation direction. For a frequency $\omega > \omega_p$ the ray path is bent while crossing the ionosphere but it is almost straight in the

lower atmosphere where the refractive index $\mu \approx 1$. Denoting by ϵ and ϵ' the refraction angle errors as seen by the observer and transmitter respectively, the angle $i = \epsilon + \epsilon'$ is called the ray bending. Under simplified conditions it has been shown that it is a function of the zenith angle χ at the observing point and the quantity $\int_T^R N ds$ where ds is an element of path along the ray direction. If $\omega \gg \omega_p$ and χ is small, the path \overline{RS} is $\approx R$, the range of the satellite and hence one can write

$$i = \int_R^T N ds = \sec \chi \int_0^{R_s} N dh = N_t \sec \chi \quad (2.1)$$

where N_t is the vertical columnar electron content (TEC).

The early measurements of this kind made use of the rise and set of signals. χ can be calculated from the orbital ephemeris of the satellite and measured using directional antennas. Thus TEC can be evaluated. More accurate and spatially continuous measurement can be obtained using interferometers (Titheridge, 1966). In this the dispersive property of the ionosphere is made use of. The difference in the angle of arrival of two widely spaced frequencies is measured using which TEC can be derived. This is very useful in detecting slight horizontal gradients in TEC.

The disadvantage with this method is that the orbital ephemeris would not be accurate enough for rigorous measurements and otherwise sophisticated ray tracing techniques will have to be employed.

2.2.2 Measurement of the optical path difference

At a single receiving station, the difference of phase path followed by different signals emitted by the satellite can be used for TEC measurements. The two waves being measured can be either waves of two different frequencies or two magnetoionic components of the same frequency giving rise to the two corresponding widely used methods - the differential doppler and faraday rotation.

Differential doppler method - In spite of the name, in practice the time behaviour of two received frequencies is measured. This is actually a phase difference method. The optical phase path of a wave transmitted from a satellite S and received on ground at R is $P = \int_Y \mu ds$ where Y is the phase path of the wave. Let P' denote the geometrical path of the wave. Then $P' = \int ds$. This path Y is not in general coincident with the straight line joining R and S. If the operating frequency $\omega \gg \omega_p, \omega_H$ and ν , we can use the no collision no magnetic field Appleton-Hartree formula

$$\mu^2 = 1 - \frac{\omega_p^2}{\omega^2} \quad (2.2)$$

which reduces to
$$\mu = 1 - \frac{Ne^2}{2\epsilon_0 m \omega^2} = 1 - a \frac{N}{\omega^2} \quad (2.3)$$

where $a = \frac{e^2}{2\epsilon_0 m} = 510 \text{ mks units.}$

Denoting by ΔP the difference between the optical path

and geometric path we write,

$$\Delta P = P' - P = \int (1 - \mu) ds = \frac{a}{\omega^2} \int N ds \quad (2.4)$$

where $\int N ds$ represents the total electron content (TEC) along the line of sight. Now due to higher frequency used and small zenith angle χ , the refraction effect can be neglected by putting

$SR = R = \int ds$. In this case we can write

$$P = \frac{a}{\omega^2} \int_0^{h_s} N \sec \chi dh = \frac{a}{\omega^2} \overline{\sec \chi} \int_0^{h_s} N dh \quad (2.5)$$

h_s being the satellite height and $\overline{\sec \chi}$, a weighted mean of $\sec \chi$ such that

$$\overline{\sec \chi} = \frac{\int_0^{h_s} \sec \chi N dh}{\int_0^{h_s} N dh} \quad (2.6)$$

By choosing a suitable value χ' of χ along the geometrical path, we have

$$R = h_s \sec \chi'.$$

Therefore
$$N_t = \frac{\omega^2}{a} \frac{\Delta P}{\overline{\sec \chi}} = \frac{\omega^2}{a} \frac{h_s \sec \chi'}{\sec \chi} \frac{\Delta P}{R} \quad (2.7)$$

at $\sec \chi' = \overline{\sec \chi}$. Therefore
$$N_t = \frac{\omega^2}{a} h_s \frac{\Delta P}{R} \quad (2.8)$$

We can now make use of the dispersive property of the ionosphere. If the satellite emits two coherent frequencies then the difference between ΔP_1 and ΔP_2 of the frequencies ω_1 and ω_2 can be written

as

$$\Delta P_1 = P'_1 - P_1 = \int_R^S (1 - \mu_1) ds = \frac{a}{\omega_1^2} \int_R^S N ds$$

$$\text{and } \Delta P_2 = P'_2 - P_2 = \int_R^S (1 - \mu_2) ds = \frac{a}{\omega_2^2} \int_R^S N ds$$

The difference

$$\delta = \Delta P_1 - \Delta P_2 = \frac{m^2 - 1}{m^2} \frac{a}{\omega_1^2} \int_R^S N ds \quad (2.9)$$

or $\delta = \frac{m^2 - 1}{m^2} \Delta P_1$, assuming same geometrical path for ω_1 and ω_2 where $m = \frac{\omega_2}{\omega_1}$.

Thus the total electron content

$$N_t = \frac{\omega_1^2}{a} h_s \frac{m^2}{m^2 - 1} \frac{\delta}{R} \quad (2.10)$$

In practice one measures the relative phase rather than the phase path.

$$\text{Therefore } \Delta \phi = \Delta \phi_1 - \frac{1}{m} \Delta \phi_2 = \frac{P_1 \omega_1}{c} - \frac{1}{m} \frac{P_2 \omega_2}{c} \quad (2.11)$$

so that an ambiguity of 2π will exist. This can be solved as follows. If there are no horizontal gradients,

$$\frac{\Delta P}{R} = \frac{\Delta \dot{P}}{R} = \frac{\Delta \ddot{P}}{\ddot{R}} \quad (2.12)$$

$$N_t = \frac{\omega^2}{a} h_s \frac{m^2}{m^2 - 1} \frac{\delta}{R} \quad (2.13)$$

Since $\dot{R} = \dot{P}_1 = \dot{P}_2$ and recalling that $\Delta \omega_1 = \frac{\omega_1 \dot{P}_1}{c}$

and $\Delta \omega_2 = \frac{\omega_2 \dot{P}_2}{c}$ and $\omega_{DD} = \Delta \omega_1 - \frac{\Delta \omega_2}{m}$ we get

$$N_t = \frac{\omega_1^2}{a} h_s \frac{m^2}{m^2 - 1} \frac{\omega_{DD}}{\Delta \omega_1} \quad (2.14)$$

hence the name differential doppler to the method. What is actually measured is the phase difference between the two waves as a function of time using a polarimeter and a phase comparator or phase sensitive detector.

2.2.3 Faraday rotation

In traversing a magnetoionic medium (such as the ionosphere) a plane wave undergoes a rotation of its plane of polarization the total angle of rotation depending approximately on the average magnetic field component in the direction of propagation and on the total number of electrons in a column of unit cross-section along the ray path. The earth's magnetic field is known to the desired accuracy. Therefore if the angle of rotation of the plane of polarization of a wave of known frequency can be measured on the ground the total number of electrons in a unit column along the ray path and therefrom the vertical columnar electron content can be derived. The principal advantage of this method is its simplicity both in data collection and analysis. Ever since this effect was first suggested by Murray and Hargreaves (1954) this is widely used for measuring TEC. Early such measurements of TEC were done using Lunar echoes (Browne et al., 1956, Evans and Taylor, 1961) and later using artificial satellites (Little and Lawrance, 1960).

2.2.4 Group delay method

Measurement can be made of the time of flight of a signal from satellite to ground using the relation

$$P_r = \left(\frac{1}{u} \right) ds \quad (2.15)$$

where P_g is the group path and $\frac{1}{\mu} = \mu'$, the group refractive index. As is done in the phase path method, assuming $P_g = \int \mu' ds$ and $P_g' = \int ds$ and with the same approximation used in differential doppler method, we can write

$$\Delta P_g = P_g' - P_g = \int_{\gamma} (\mu' - 1) ds = \frac{a}{\omega^2} \int N ds \quad (2.16)$$

and

$$\Delta T_g = \frac{\Delta P_g}{c} = \frac{a}{c \omega^2} \int_{\gamma} N ds \quad (2.17)$$

If, as usual, we have two frequencies ω_1 and ω_2

$$\Delta T_{g12} = \frac{a}{c} \left(\frac{1}{\omega_1^2} - \frac{1}{\omega_2^2} \right) \int N ds \quad (2.18)$$

This gives the value of $\int N ds$ which can be reduced to the vertical content $N_t = \int N dh$ using a suitable value of $\overline{\sec \chi}$.

It must be mentioned that unlike the Faraday method, differential Doppler and Group delay methods give N_t upto the satellite height. Attempts have therefore been made to measure TEC above 2000 km by subtracting the results of Faraday method from those of group delay technique. The results will be contaminated by the errors involved in both the methods. However, using a geostationary satellite variations in protonospheric TEC can be monitored using the principles.

2.2.5 Combined use of differential doppler and faraday data

Recalling that

$$\Omega(t) = \frac{b}{\omega^2} B \overline{\cos \theta} \int_R^S N ds \quad (2.19)$$

and
$$\Delta P(t) = \frac{a}{\omega_1^2} \int_R^S N ds = \Delta P_0 + \Delta P_c(t) \quad (2.20)$$

We can write
$$\Omega(t) = \frac{b}{a} \overline{B \cos \theta} \Delta P(t)$$

The differential rotation
$$\Delta \phi = \frac{\omega_1}{c} \frac{m^2 - 1}{m^2} \frac{1}{\omega_1^2} \int N ds$$

where $m = \frac{\omega_2}{\omega_1}$

If $m = 1 + \xi$ and $\xi \ll 1$, $\frac{m^2 - 1}{m^2} = 2\xi$

Therefore
$$\Delta \phi = \frac{a}{c} \frac{2\xi}{\omega} N_t$$

$$\frac{\Delta \phi}{\Delta \omega} = - \frac{2a\xi}{c\omega^2} N_t \quad (2.21)$$

$$\lim_{\xi \rightarrow 0} \frac{\Delta \phi}{\Delta \omega} = T_g \text{ the group delay}$$

Consequently if there is a satellite emitting three frequencies ω_1 , ω_2 and ω_3 , the first two closely spaced and ω_3 much higher, one can measure the differential phase without ambiguity and with great accuracy.

2.3 Theory of faraday rotation approximations, assumptions and second order corrections

2.3.1 First order theory of faraday rotation

The basic theory was developed by Browne, Evans, Hargreaves and Murray (1956). Due to the free electrons present and the imposed earth's magnetic field the ionosphere behaves like a birefringent medium. Consequently if a wave of given linear of

elliptic polarization is emitted by a satellite, when traversing through the ionosphere, such a wave splits into two characteristic modes i.e. the ordinary and the extra-ordinary. They propagate with different phase velocity due to their different index of refraction. If a particular experimental condition is fulfilled (i.e. the zenith angle χ is not too large and $\omega \gg \omega_p, \omega_H$) the two waves proceed, to a first degree of approximation along nearly coincident paths. Emerging from the bottom of the ionosphere the two waves recombine again giving rise to a new wave polarization which is modified with respect to the original.

If in particular the emitted wave is linearly polarized and the QL condition satisfies (i.e. $Y_1^4 / 4(1-X)^2 \ll Y_L^2$) the emerging wave is again linearly polarized but with an angle different from the original one. From this effect, which is known as the Faraday effect, if the geomagnetic field is known, the total electron content can be derived (Murray and Hargreaves, 1957).

Under QL and high frequency approximations the collisionless Appleton-Hartree refractive index formula becomes, (Garriott, 1960)

$$\mu_o^2 = 1 - \frac{X}{1 + Y_L} \quad (2.22)$$

and $\mu_e^2 = 1 - \frac{X}{1 - Y_L}$

o and e signifying the ordinary and extra-ordinary modes

where $X = \frac{\omega_p^2}{\omega^2}$ and $Y_L = \frac{\omega_H}{\omega} \cos \theta$

An incoming linearly polarized wave can be decomposed into two circular counter rotating ones. In crossing the ionosphere the

two components are shifted in phase relative to one another by an angle β . It is easy to show that while recombining they give rise again to a linearly polarized wave whose direction is rotated by an angle $\Omega = \frac{\beta}{2}$ with reference to the incoming wave, towards the lagging component. The phase for each wave is written as

$$\Phi = \frac{\omega}{c} \int_Y \mu ds \quad (2.23)$$

where Y is the signal phase path. The phase difference is given by

$$\beta = \Phi_o - \Phi_e = \frac{\omega}{c} \int (\mu_o - \mu_e) ds = 2\Omega \quad (2.24)$$

Therefore

$$\Omega = \frac{\omega}{2e} \int \frac{(\mu_o - \mu_e)}{2} ds = \frac{\omega}{2c} \int \chi \chi_L ds \quad (2.25)$$

assuming $\omega \gg \omega_p, \omega_H$

$$\begin{aligned} \Omega &= \frac{\omega}{2e} \int \frac{eB \cos \theta}{\omega^3} \frac{Ne^2}{\epsilon_o m^2} ds \\ &= \frac{e^3}{2\epsilon_o m^2 c \omega^2} \int_0^{h_s} N B \cos \theta \sec \chi dh \end{aligned} \quad (2.26)$$

All the quantities within the integrals are functions of height, h .

While $B \cos \theta$ is known N is not known. The problem can be solved with some degree of approximation by writing

$$\Omega = \frac{K}{f^2} \bar{M} \int_0^{h_s} N dh \quad (2.27)$$

where

$$\bar{M} = \frac{\int_0^{h_s} B \cos \theta \sec \chi f(h) dh}{\int_0^{h_s} f(h) dh}$$

and $f(h) = \frac{N(h)}{N_{yn}}$

Figure 2.1 illustrates how faraday rotation takes place.

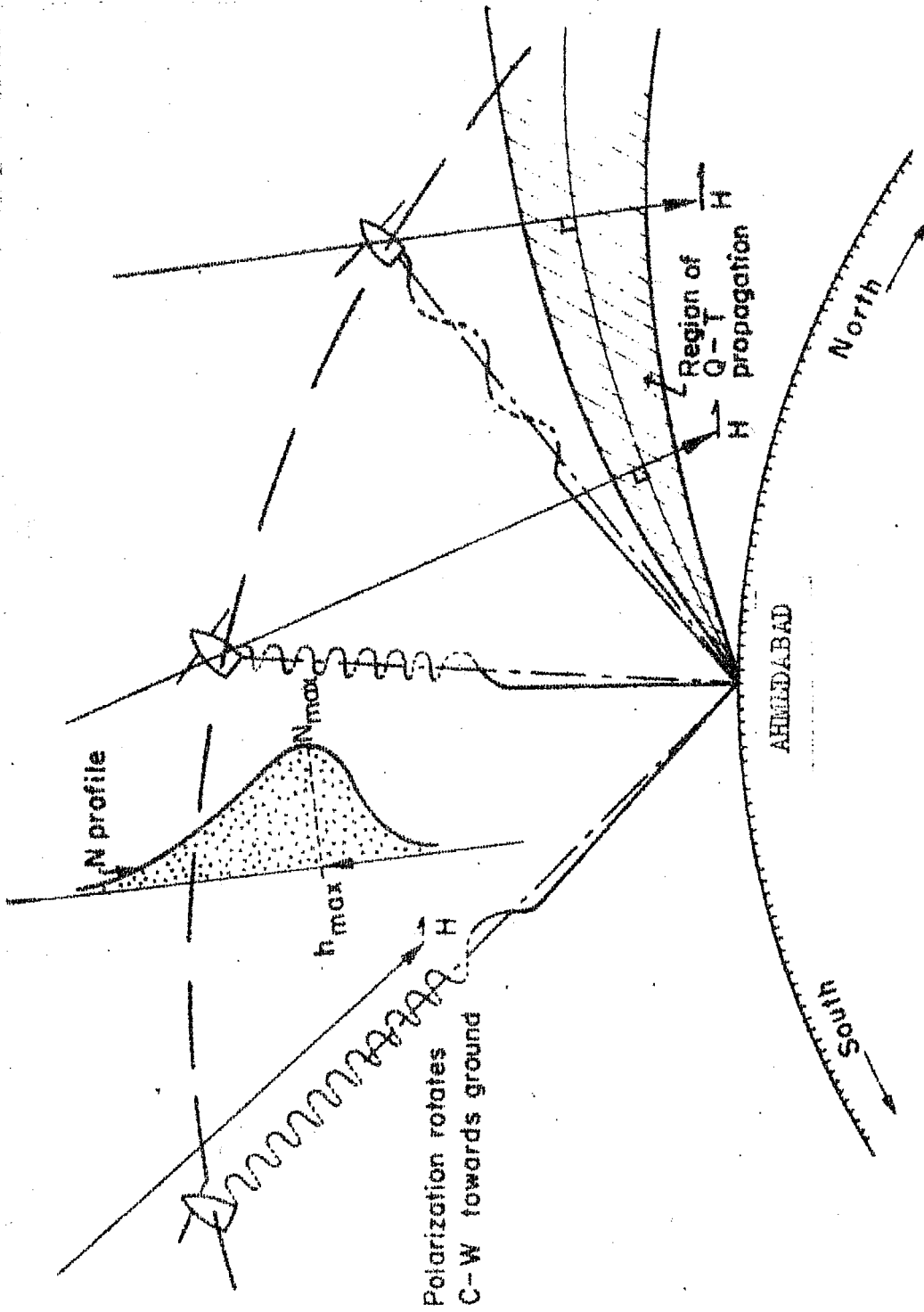


Figure 2.1 : Pictorial sketch of the way in which the Faraday Rotation Angle varies during a satellite passage.

This \bar{M} will correspond to a particular value of $M (= B \cos \theta \sec \lambda)$ along the path at a height called the mean ionospheric height (Yeh and Swenson 1961). This position, although exact for a particular case, is no longer true if the $N(h)$ profile and the direction are changed maintaining the ionospheric height as is generally done. This height strongly depends on the distribution of ionization and magnetic field along the ray path. In order to ascertain the error introduced by this approximation, it is a good rule to theoretically analyse the behaviour of M over the station sky. This has been done by various authors (e.g. Yeh and Gonzales 1960) and the errors are estimated to be less than 5%.

2.3.2 Errors involved in the first order theory

The main sources of error in the Faraday rotation method are those due to vertical motions of the source and horizontal gradients in TEC. Other errors are due to taking fixed height for M , that too same for day and night, high frequency approximations, QL approximations, neglect of collisions in the Appleton-Hartree formula, low zenith angle approximation, geometry of the magnetic field used in M calculations, neglect of wave normal splitting and magnetoionic mode coupling which are discussed one by one in what follows.

Browne et al. (1956) have shown that most of the rotations $\int \Omega$ occur within the first 1000 kms above the earth. Titheridge (1968) has shown that 92% of the total electron content and 95% of the Faraday rotation occurs below 1000 kms. Figure 2.2 shows the dependence of $\int \Omega$ on the satellite height, i.e., the upper

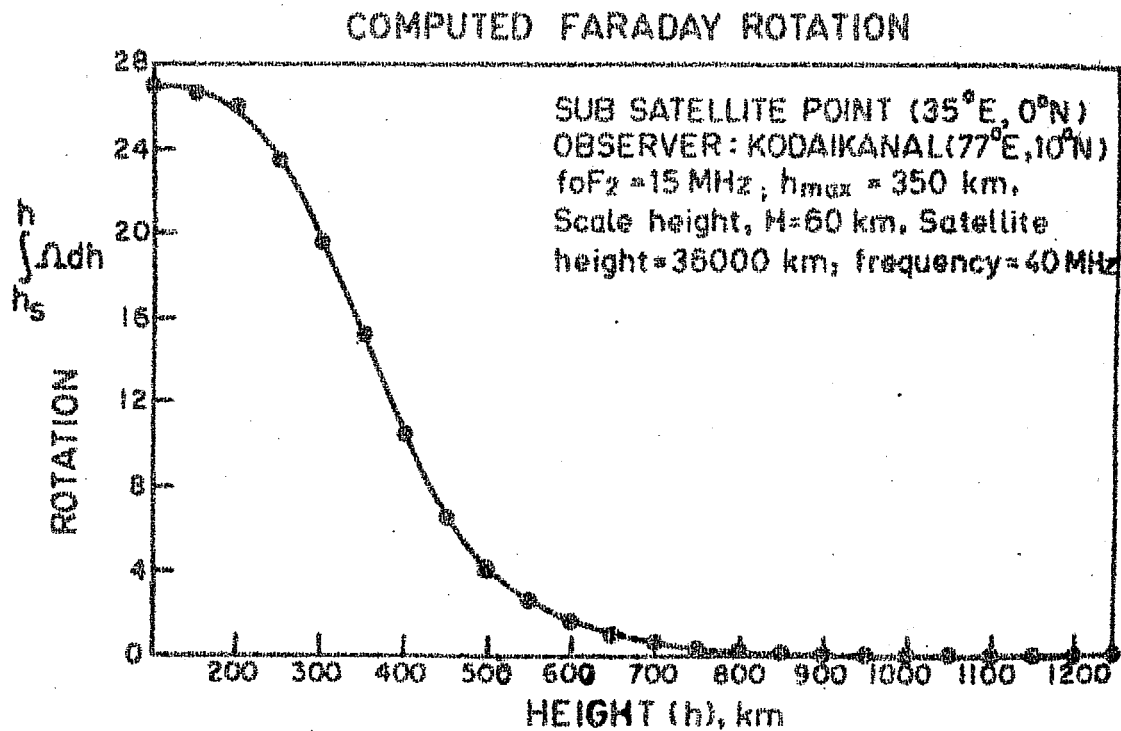


Figure 2.2 : Dependence of Faraday Rotation suffered by a wave on height computed using model ionosphere and model magnetic field.

limit of the integral. As B decreases as $\frac{1}{r^3}$ above a certain limit (~ 1400 km) the increase of this upper limit does not affect h . This means that the faraday rotation measured is due to the ionization upto a height where B has a value independent from the satellite height. Thus vertical motion of the satellite of a perturbation nature do not affect the Faraday rotation measured on ground. It is thus concluded that Faraday rotation methods gives the TEC only upto a maximum height of 2000 kms. This virtual drawback has been made use of to derive the protonospheric electron content by subtracting faraday content from differential doppler content, which is sensitive upto the satellite height (36000 kms). The errors involved in assuming a mean field height for \bar{M} ($B \cos \theta \sec \chi$) have been discussed by Yeh and Gonzales (1960). Figure 2.3, computations of $M(h)$ for different satellite elevations and azimuths are shown. It is shown that for high elevation passes the variation of M with height is very small and hence will not cause serious errors. The appropriate value taken for M depends on the geometry of the magnetic field. M can be computed for a selected path of propagation over the observing point. By using the model profiles \bar{M} and the mean \bar{h} have been computed for various paths by Chiccacci (1972). He finds that h ranges from 315 to 347 km during the day and 405 - 415 km for night. In Figure 2.4 the value of $M/\bar{M}(\bar{h})$ is plotted vs h for the worst condition of a large zenith angle χ , in order to show the errors involved by choosing a fixed height for M . We can observe that for night, $\bar{h} = 400$ km, no appreciable errors are present while during the day the error is below 10% only for about a 120° azimuth centred around the south of

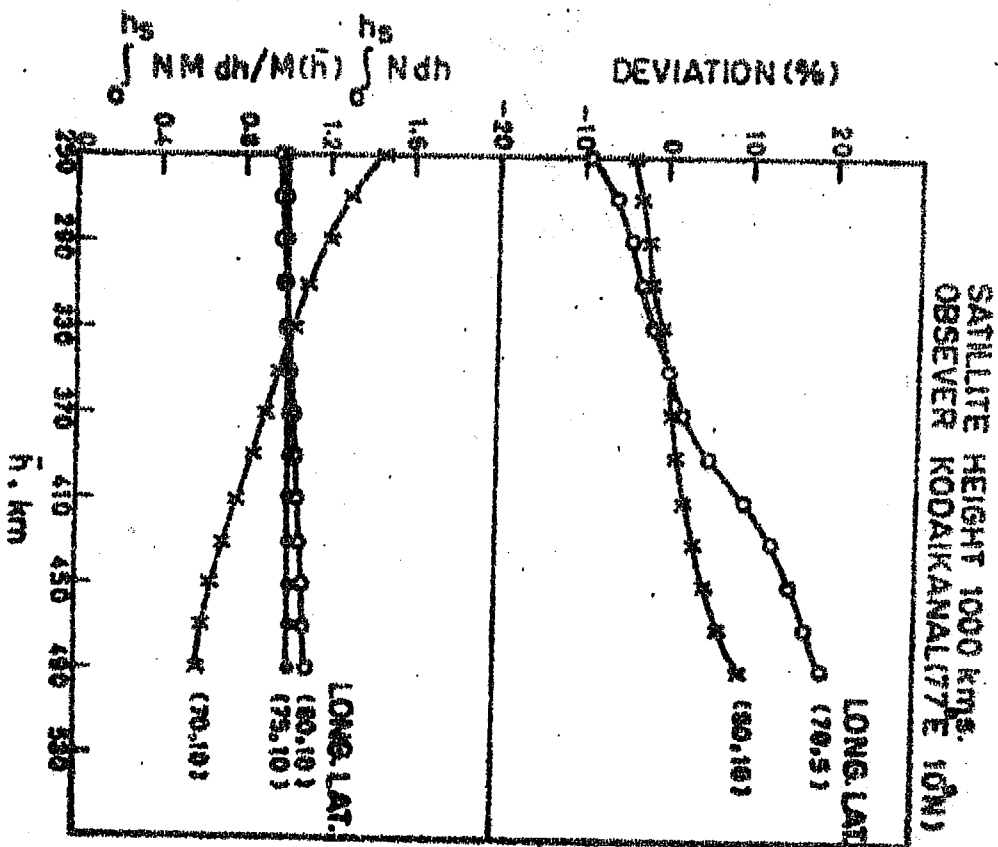


Figure 2.4 : Figure indicates the error involved in assuming a fixed mean height (h) for M computation at different sub-satellite points.

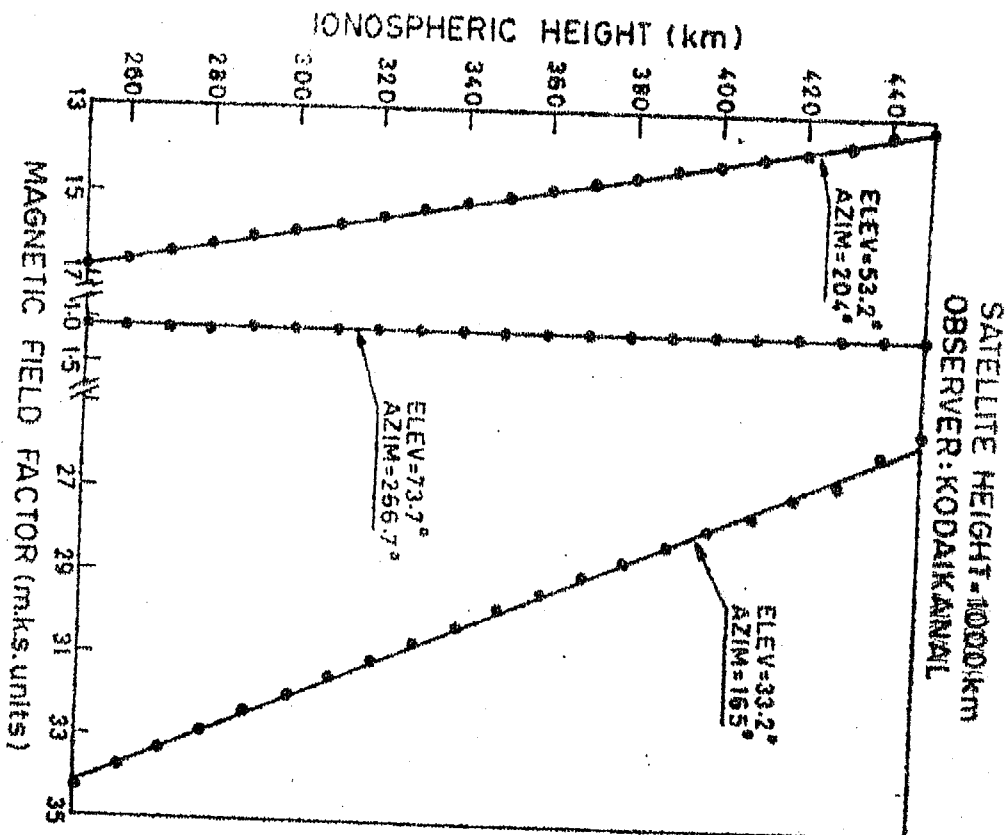


Figure 2.3 : Variation of magnetic field factor with height for satellite look angles.

the station. On the other hand this ratio for $\bar{h} = 400$ km at the zenith of the station ranges from 1.015 and 0.989 for day and night respectively. It has been generally accepted that the centroid of the $N(h)$ distribution which is one scale height above h_{\max} is reasonably correct for the mean field height. Therefore \bar{M} is taken at a height $h = h_{\max} + 50$ kms (Yeh and Gonzales, 1960; Basu and Basu, 1971). Consequently by using $\bar{h} = 400$ km and restricting to $\chi < 450$ the data can be ascertained to have an error $< 10 - 15\%$, which for studying the variation of TEC is quite accurate considering the very simple technique used. Basu and Basu (1971) have estimated the error due to assuming fixed mean field height. A change of height by 10 km introduces 3% error in TEC. The measured value of TEC is taken to be corresponding to the sub-ionospheric point which is the point on the surface of the earth lying below the crossing of the ray path with a thin shell placed at h .

2.4 Approximations and higher order corrections

2.4.1 QL approximation

In deriving the basic Faraday rotation formula it has been assumed that the waves are propagating in the quasi-longitudinal mode. Ratcliffe (1959) has shown that this approximation is valid provided that

$$\frac{Y_4^2}{4Y_2^2} < |1 - X - rZ|^2 \quad (2.28)$$

At frequencies $(\omega > \omega_p, \omega_H \text{ and } \omega_c)$ Z is negligible and X does

not exceed 0.01 anywhere along a ray path under these conditions

it can be shown that QL approximation holds unless for $89^\circ < \theta < 91^\circ$.

However, in the QT region the assumption fails. Jonathan Mass (1966) has calculated the effect of QT propagation on the above approximation. He finds that the width of the rate anomaly where QL propagation does not hold is $\sim 2^\circ$ for 20 MHz and 1° for 40 MHz. Thus the error introduced is 2% for 20 MHz and 1% for 40 MHz. Thus for all practical purposes QL propagation is a reasonable approximation.

2.4.2 High frequency approximation

When Browne et al. (1956) derived the equation, they expanded the difference between μ_o and μ_e in powers of X. Subsequently they neglected all terms in X except of order 1. This is justified if $\omega_p^2/\omega^2 \ll 0.01$ (Titheridge, 1971). Basu and Basu (1969) have studied the effect of magnetoionic mode coupling and wave normal splitting. They found that the effect is strong at low geomagnetic latitudes at 40 MHz and the coupling region is large at night than in day. Elsewhere the errors involved are not very serious at 40 MHz and above where $\frac{\omega_p^2}{\omega^2} \ll 0.01$. Errors are 5% by day and 15% at night. Hudson (1969) has further found that second order effect is of order $\frac{1}{f^4}$ and is serious at QT. This can be eliminated by $\frac{d\Omega}{dM}$ method.

2.4.3 Refraction

At small elevation angles ionospheric refraction will cause deviations from the straight line path. Thus the O and E modes will not travel through the same path. However, at low elevation angles $< 30^\circ$ refraction will produce a path splitting as great as 1° . This will not introduce an error of more than 3% in TEC at high

frequencies. Tyagi and Bhatnagar (1969) have found that the effect of refraction will introduce a time lag between the occurrence of QT on two widely spaced frequencies.

2.4.4 Departures from the geomagnetic field or ionosphere model

The work of Bramley and Ross (1951) and Bramley (1953) has shown that at least in the lower ionosphere departures from spherical stratification are small and of short duration. Systematic tilts are found to occur only near dawn when the isoionic surfaces in the lower ionosphere are tilted from west to east. Tilts from east to west may be expected to occur in the upper ionosphere at the same time such that these two tilts may cancel each other to some extent in their effect on Faraday rotation. It may be noted that the results will be most sensitive to tilts when $\sec \chi_{400}$ is large, in other words at low elevation transits. The effect of horizontal gradients and TID's will also lead to erroneous results.

2.4.5 The extrapolated field

To find \vec{B} at the mean field height the earth's magnetic field is generally extrapolated outwards using dipole model and inverse cube law which will introduce errors. But we have used spherical harmonic expansion of the magnetic field using 48 Gaussian coefficients and \vec{M} is separately computed for each sub-ionospheric position using IBM 360 computer. This should enhance the accuracy.

2.4.6 Experimental accuracy

Counting the number of Faraday fades from the chart records

can introduce errors as large as $\frac{1}{2}$ rotation. The largest uncertainties are in the post midnight period when TEC is so low that during a whole transit there may be only 1 or 2 fades at 40 MHz. This will introduce an error of $\pm 3\%$ by day and as large as 50% in the predawn period. By far this is the most severe error out of all.

Kersley and Taylor(1974) have compared TEC obtained from 26 overhead passes of BE-B with that obtained by integrating the incoherent scatter profiles at Malvern. In 19 cases agreement was obtained with a fixed value of M. In few cases when F_2 layer was unusually high, an adjustment in mean field height (h_F) was necessary. h_F is proportional to h_{max} and a mean field height of 375 km is recommended for general use.

C H A P T E R - III

EXPERIMENTAL SET UP AND METHOD OF MEASURING TEC USED IN THIS STUDY

The details of the characteristics of the beacon satellites used in this study and their transmissions were given in Chapter I. In the present chapter, the experimental set up used at Ahmedabad, Kodaikanal and Thumba for recording Faraday rotation will be described.

3.1 Receiving set up at Ahmedabad

Block diagram of the receiving system is shown in Figure 3.1. The dipole antennas are erected in the E-W direction at a height of $\frac{\lambda}{4}$ from the ground. E-W direction is chosen to have the antenna reception pattern symmetrical in the N-S direction (as most of the passes are in the N-S direction).

The receiver has unbalanced inputs with an impedance of 50 ohms. The dipole antenna gives an impedance of 72 ohms (balanced). Impedance matching is achieved by using a wide-band balun matching transformer. This impedance matching transformer is mounted near the antenna itself. Amphenol RG - 8/U coaxial transmission line is used to connect the antenna outputs to the receiver inputs.

Figure 3.2 gives the block diagram of the transistorized Magnavox receiver used for receiving the satellite signals. It is a double superheterodyne receiver using crystal controlled local oscillators. The preamplifier section is a fully shielded

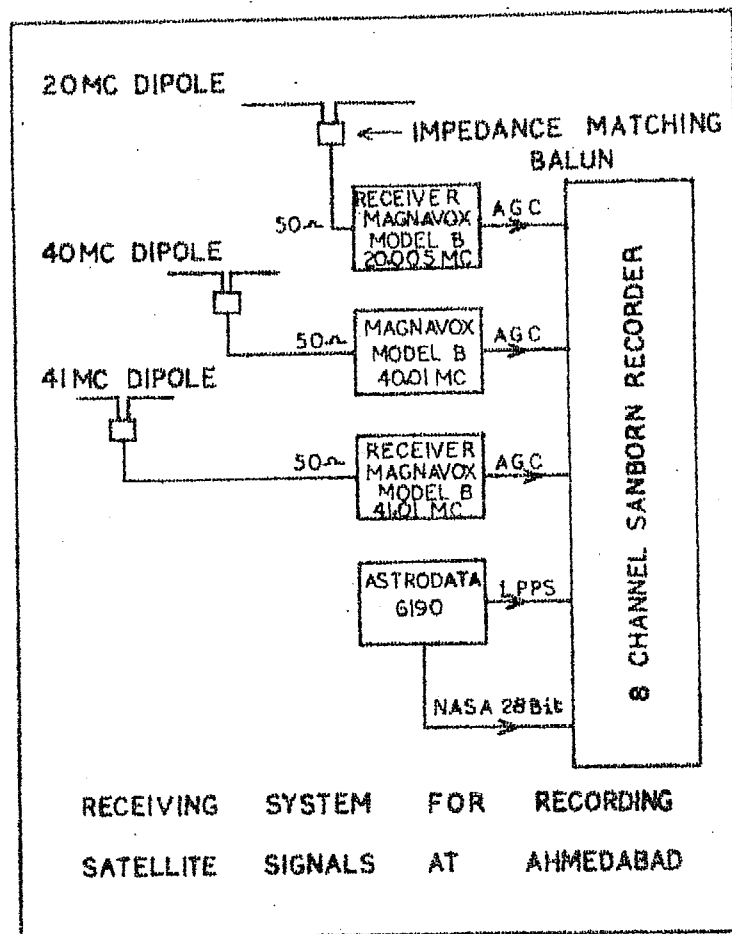


Figure 3.1 : Schematic diagram of the satellite signal receiving system at Ahmedabad.

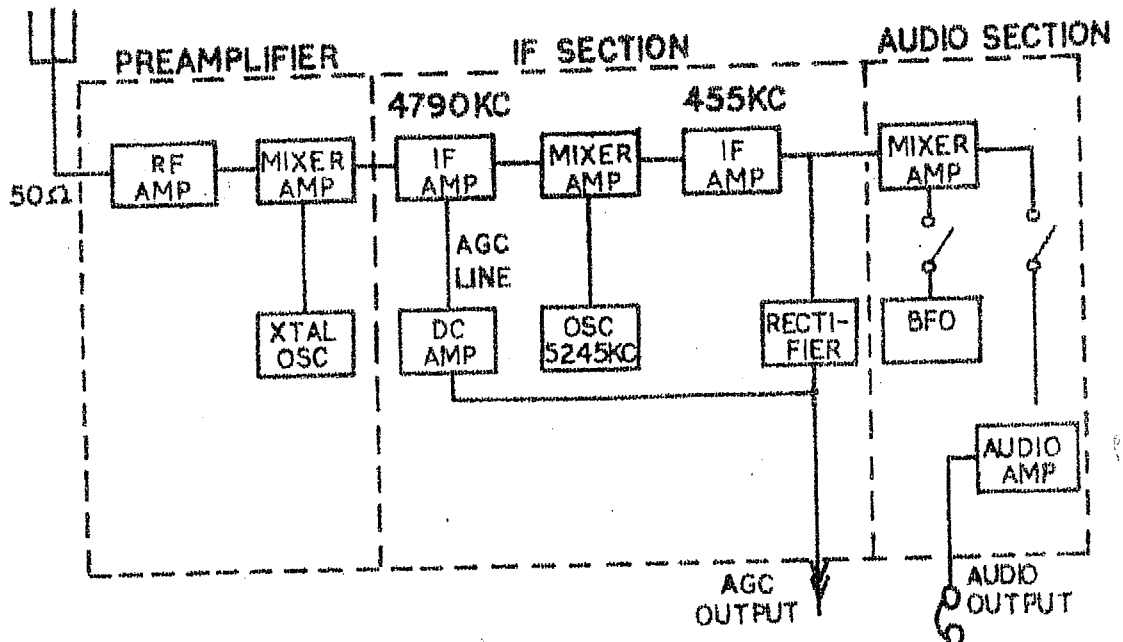


Figure 3.2 : Block diagram of the receiver.

plug in unit. By plugging in the appropriate P/A into the front end of the main receiver the receiver frequency can be altered.

The preamplifier plug in unit consists of an RF stage, a mixer stage and an oscillator stage. This gives an output of 4790 kHz. The RF amplifier has approximately a gain of 35 db. The mixer stage has a conversion gain of 5 db. The front end unit contains the first IF stage, the second local oscillator, second IF amplifier, second detector and audio stage. Second local oscillator is crystal controlled at 5245 kHz. This stage mixes with the 4790 kHz and gives an output of 455 kHz. The AGC incorporated in the circuitry is such that it is logarithmically related to the amplitude of the incoming signal. This is to make the nulls sharp and to have broad maxima from an otherwise sinusoidal wave. The second IF stage has a gain of 90 db.

Complete electrical specification of the R_x is as under:

- (1) Voltage requirements +8.4V and -12.4V DC. The total current drain of each receiver is nominally 15 milliamps.
- (2) The sensitivity of the R_x is 135 dbm.
- (3) The bandwidth of R_x at 3 db point is 2500 Hz.
- (4) The AGC output impedance is 15 k ohms and the AGC time constant is 8 milliseconds.

Due to the velocity of the satellite the signals suffer doppler shift. But the 2.5 kHz bandwidth is sufficient to accommodate this frequency change.

The AGC output is fed to the DC amplifier manufactured by Sanborn company. DC amplifier drives the galvanometer of Sanborn strip chart recorder. The frequency response of the recording system is 0 - 50 Hz. Strip chart recorder has 8 channels. Two channels are used twice by shifting the position of stylus. These channels are reversed for the time marker pulses. Chart speed can be varied from 0.25 mm/sec to 100 mm/sec. The overall gain of the whole system is 145 db roughly.

Amplitude calibration is not necessary for faraday rotation records. Since the AGC has logarithmic response, amplitude calibration is essential for scintillation studies. A standard signal generator was used for calibrating the whole system.

Since the satellites move with very high velocity a time standard correct to a fraction of a second is essential. At Ahmedabad a time standard manufactured by 'Astrodata' company which gives 1 pulse output/sec which is derived from a crystal controlled 1 MHz oscillator of high stability is used.

Many countries broadcast standard time signals in the HF band. The frequencies allotted for these signals are 2.5 MHz, 5 MHz, 10 MHz, 15 MHz, 20 MHz and 25 MHz. At Ahmedabad 10 MHz and 15 MHz transmissions from Japan or Hawaii (JWWH) are used for synchronizing the local time standard. The time standard is never allowed to have an error more than 100 milli.sec. Exactly identical receiving systems were used at Thumba and Kodaikanal.

3.2 Formalism of satellite predictions

Before planning any observation schedule with satellites it is necessary to have fairly accurate predictions about the expected satellite transits across the station sky. A computer programme has been developed to be used in IBM 360 for this purpose. The basic input to this is the information from the NASA prediction bulletins periodically received for each satellite. For a selected orbit at every 5 or 10° of latitude the incremental longitude and incremental time and height of the satellite are given in this bulletin. Knowing the coordinates of the observing site, the period of the satellite, change in longitude between successive equatorial crossings the predictions can be generated for any desired period.

From the known parameters, the rate of change of latitude, longitude and height of the satellite with respect to time are computed and stored as coefficients. From the desired starting time and date, for each minute the satellite position can be extrapolated with the help of these coefficients. Knowing the satellite position and observer position, the azimuth, elevation and slant range of the line of sight can be computed. These information are printed out for transits having maximum elevation greater than a pre-desired value ($\sim 10^\circ$). The Fortran IV programme used has been appended as Appendix I.

3.3 Description of the method of calculation of TEC

3.3.1 Geometrical aspects of the ray path calculations

Once such predictions are available, recording schedule is made. From the records the Faraday rotation angle for every minute from the QT point is scaled off. Using the Faraday rotation angle and the sub-satellite coordinates (obtained from NASA refined world maps films) at every minute during the transit as input parameters TEC is calculated according to the method described below with the help of another computer programme acceptable to IBM 360 which is also appended in Appendix II.

Having calculated the above parameters the sub-ionospheric points of the satellite at every minute during a transit are derived using a fixed height (350 km for Ahmedabad and 400 km for Kodaikanal) for the mean field factor. Now, the zenith angle χ_c of the ray path at the ionospheric point is calculated.

The next step is to compute the magnetic field vector at the point where the ray path crosses the ionosphere and hence to calculate the angle θ between the ray path and the field. From this the magnetic field factor $\bar{M} = B \cos \theta \sec \chi_c$ is calculated. From the inputs of time, subsatellite points and number of Faraday fades Ω , the total electron content TEC is calculated using the formula $\Omega = \frac{k}{f^2} \bar{M} N_T$, where $k = 2.97 \times 10^{-2}$ mks units f is the frequency of the wave in Hz \bar{M} in Gauss and N_T in el. m⁻². Ω is in radians. For 40 MHz, this reduces to

$$N_T = 1.69 \frac{\Omega}{\text{m}} \underline{\underline{=}}$$

N_T being expressed in units of 10^{17} el. m^{-2} and Ω the number of fades.

From this skeleton sketch each part may be elaborated as follows:

(a) Calculation of elevation, azimuth, range and sub-ionospheric points (Spherical Astronomy, Smart)

In Figure 3.3(a), let C denote the centre of the earth, O observer, λ_o longitude of observer ϕ_o latitude of observer, S subsatellite point λ_s sub-satellite longitude ϕ_s subsatellite latitude. $CS = CI = CO = \text{Earth's radius, } R$, $SS_o = \text{height of satellite} = h_s$ $II_o = \text{height of ionosphere } h_i$. The above quantities are known.

Let λ_i and ϕ_i be the sub-ionospheric longitude and latitude respectively which is also to be computed. In Figure 3.3(c)

$$PO = \text{observer's colatitude} = (90 - \phi_o) = b,$$

$$PS = \text{subsatellite co-latitude} = (90 - \phi_s) = c. \text{ Let } OS = a$$

In the spherical triangle POS

$$\cos a = \cos b \cos c + \sin b \sin c \cos A$$

$$\text{But } A = \lambda_o - \lambda_s$$

$$\text{Therefore } \cos a = \cos b \cos c + \sin b \sin c \cos(\lambda_o - \lambda_s) \quad (3.1)$$

$$\text{and } \sin a = \sqrt{1 - \cos^2 a} \quad \text{and } a = \tan^{-1} \left(\frac{\sin a}{\cos a} \right)$$

To find the range OSo

In OCSO of Figure 3.3(a)

$$OS_o^2 = CO^2 + CS_o^2 - 2CO \cdot CS_o \cdot \cos OCS_o$$

$$= R^2 + (R + h_s)^2 - 2R(R + h_s) \cdot \cos a$$

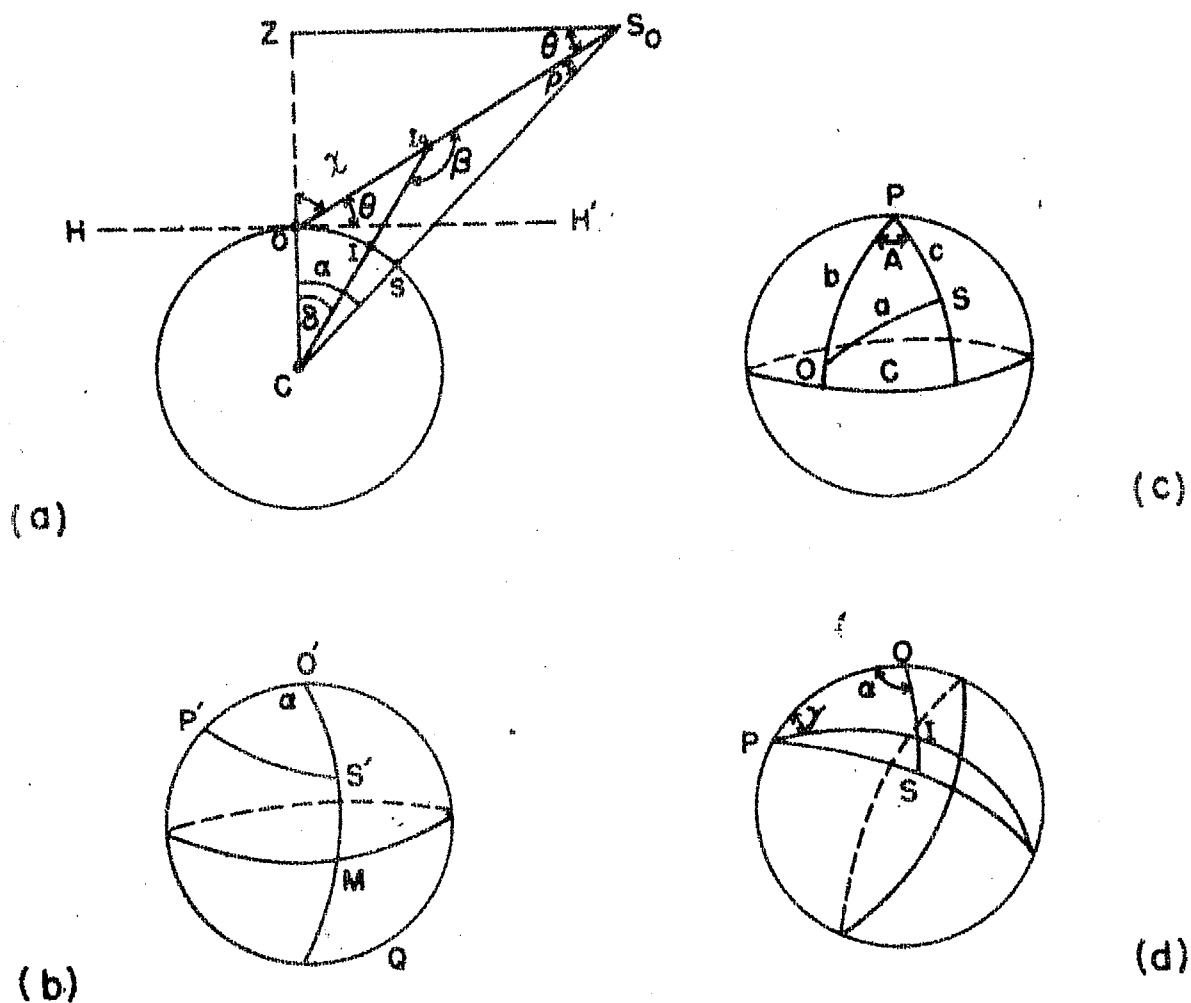


Figure 3.3 : Geometry for the calculation of elevation, azimuth and sub-ionospheric point.

$$OS_0 = \left[R^2 + (R+h_s)^2 - 2 \cdot R \cdot (R+h_s) \cos a \right]^{\frac{1}{2}} \quad (3.2)$$

To find the elevation $\hat{S_0 O H'} = \theta$

$$\text{In } \triangle^{le} OZS_0, \cos \theta = \frac{ZS_0}{OS_0} = \frac{CS_0 \sin a}{OS_0}$$

$$\text{Therefore } \cos \theta = (R+h_s) \frac{\sin a}{OS_0}$$

$$\text{Hence } \theta = \cos^{-1} \left[(R+h_s) \frac{\sin a}{OS_0} \right] \quad (3.3)$$

To find the zenith angle $ZOS_0 = \chi_0$

From Figure 3.3(a), $\chi_0 = 90 - \theta$, and the zenith angle χ_0 at the ionospheric point is simply related to χ_0 by

$$\sin \chi_i = \frac{R+h_s}{R+h_s+h_i} \sin \chi_0 \quad (3.4)$$

In Figure 3.3(b) O' and S' correspond to the observer and the satellite on the celestial sphere. $PO' = b$, $PS' = c$ and $O'S' = a$.

Now azimuth is the angle between PO' and $O'S' M = \alpha$

$$\text{Let } s = \frac{a+b+c}{2}$$

From spherical trigonometry,

$$\sin \frac{\alpha}{2} = \left[\sin(s-b) \sin(s-a) / (\sin b \sin a) \right]^{\frac{1}{2}}$$

$$\text{Therefore } \alpha = 2 \sin^{-1} \left[\sin(s-b) \sin(s-a) / (\sin b \sin a) \right]^{\frac{1}{2}} \quad (3.5)$$

To find sub-ionospheric points

In Figure 3.3(a) let $CI_0S_0 = \beta$ and $O CI_0 = \delta$

Therefore $\beta = COI_0 + OCI_0 = (90 + \theta + \delta)$

Now
$$\frac{CS_0}{\sin \beta} = \frac{CI_0}{\sin \beta}$$

But
$$\frac{CO}{\sin \beta} = \frac{OS_0}{\sin a}$$

i.e.
$$\sin \beta = \frac{CO \sin a}{OS_0} = \frac{R \sin a}{OS_0}$$

$$\sin \beta = \frac{CS_0 \sin \beta}{CI_0} = \frac{(R+h_s) \sin \beta}{R+h_i}$$

Therefore
$$\beta = \sin^{-1} \left[\frac{(R+h_s) \sin \beta}{R+h_i} \right]$$

and
$$\delta = \beta - (90 + \theta) \quad (3.6)$$

In Figure 3.3(c), $PO = b$, $PS = c$. Let $IPO = \gamma$

In spherical $\Delta^{le} IPO$ of Figure 3.3(d)

$$\tan \gamma = \sin \delta \sin \alpha / (\cos \delta \sin \beta - \sin \delta \cos b \cos \alpha)$$

Therefore
$$\gamma = \tan^{-1} \left[\frac{\sin \delta \sin a}{\cos \delta \sin \beta - \sin \delta \cos b \cos \alpha} \right]$$

$$\lambda_i = \lambda_0 - \gamma = \text{sub-ionospheric longitude} \quad (3.7)$$

In Figure 3.3(d), $PI = \text{sub-ionospheric colatitude} = d$ (say)

In spherical $\Delta^{le} POI$,

$$\frac{\sin d}{\sin d} = \frac{\sin \delta}{\sin \gamma}$$

Therefore
$$\sin d = \frac{\sin \delta \sin \alpha}{\sin \gamma}$$

or
$$d = \sin^{-1} \left[\frac{\sin \delta \sin \alpha}{\sin \gamma} \right]$$

Sub-ionospheric latitude $= 90 - d = \phi_i$

3.3.2 Spherical harmonic expansion for the magnetic field

The upto date computer programme given by R.H.Eckhouse Jr. which again is a modification of the programme of Jones and Melotte (1953) and Yeh and Gonzales (1960) is used in the present study. The mathematical expressions are those given by Jones and Melotte (1953). The spherical harmonic expansion uses 48 coefficients of Jensen and Cain (1962) which expands the magnetic potential upto terms of 6th order and 6th degree. These equations require only very little computer time.

The magnetic vector potential in spherical harmonic coordinate system is given by

$$V = a \sum_{n=1}^{\infty} \sum_{m=0}^n \left(\frac{a}{r}\right)^{n+1} H_n^m(\mu) (g_n^m \cos m\phi + h_n^m \sin m\phi) \quad (3.9)$$

where a is the radius of the earth, r is the distance of the point at which field is required, from the centre of earth. θ is the geographic colatitude of this point. ϕ geographic longitude g_n^m, h_n^m are Gaussian coefficients, $\mu = \cos \theta$

$$H_n^m = \frac{2^n n! (n-m)!}{2n!} P_n^m(\mu) \quad (3.10)$$

and
$$P_n^m(\mu) = (1-\mu^2)^{m/2} \frac{d^m}{d\mu^m} P_n(\mu) \quad (3.11)$$

$P_n^m(\mu)$ is the associated Legendre polynomial. The Legendre and associated Legendre polynomials are taken from Morse and Feshbach (1953). The X, Y and Z components representing the south,

east and vertically upward components of the field are

$$X = \frac{1}{\sin \theta} \sum_{n=0}^6 \left(\frac{a}{r}\right)^{n+2} C_{\theta, n} = H_{\theta} \quad (3.12)$$

$$Y = \frac{1}{\sin \theta} \sum_{n=0}^6 \left(\frac{a}{r}\right)^{n+2} C_{\phi, n} = H_{\phi} \quad (3.13)$$

$$Z = - \sum_{n=0}^6 (n+1) \left(\frac{a}{r}\right)^{n+2} C_{rn} = H_r \quad (3.14)$$

where

$$C_{\theta n} = \sum_{m=0}^n K_n^m (g_n^m \cos m\phi + h_n^m \sin m\phi) \quad (3.15)$$

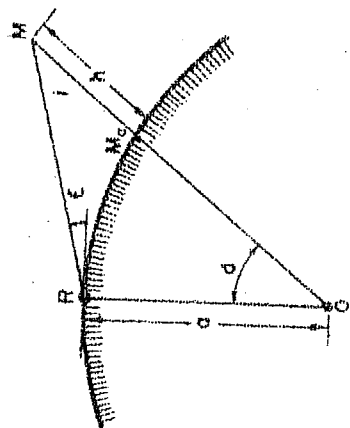
$$C_{\phi n} = \sum_{m=0}^n m H_n^m (-g_n^m \sin m\phi + k_n^m \cos m\phi) \quad (3.16)$$

$$C_{rn} = \sum_{m=0}^n H_n^m (g_n^m \cos m\phi + h_n^m \sin m\phi) \quad (3.17)$$

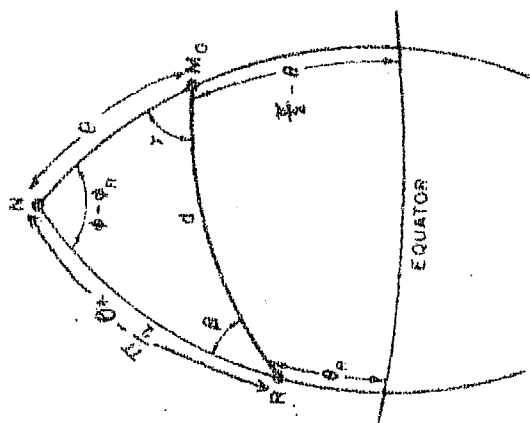
$$K_n^m = - \sin \theta \frac{d H_n^m}{d \theta} \quad (3.18)$$

It should be noted that although the summation indices begin with zero, the Gaussian coefficients do not exist for $n = m = 0$, since free magnetic charges do not exist as compared to free electric charges. Thus the monopole term cannot exist in practice, and the expansion begins with dipole term only. One further obvious point is that the expansion is written for a spherical earth.

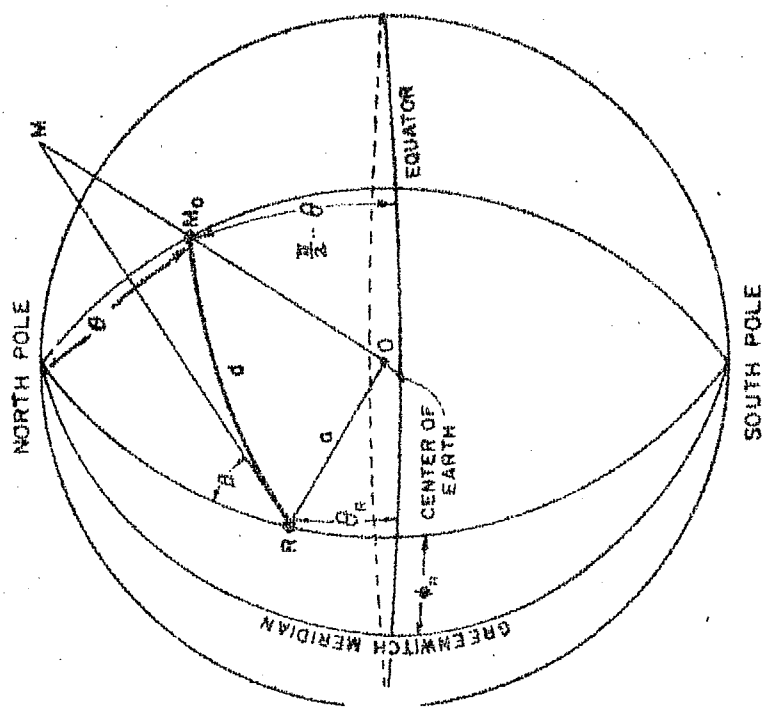
In Figure 3.4(a), let the receiving station be represented by (a, θ_R, ϕ_R) in the spherical polar coordinate system, where a = earth radius, 6371.2 kms. M is the point of magnetic field computation given by (ϵ, β, h)



b



c



R: RECEIVING STATION GIVEN BY ϕ_R, θ_R

C: EARTH RADIUS (6371.2 km)

M: POINT OF MAGNETIC FIELD COMPUTATION GIVEN

BY ϕ, β, θ (SEE FIGURES 5 & 6)

M': SUBFIELD POINT GIVEN BY β, δ

Figure 3.4(b) and (c): Satellite receiver geometry; plane view and spherical triangle respectively.

Figure 3.4(a): Satellite receiver geometry for magnetic field computation.

M_0 is the subfield point given by β and δ .

$$\text{Then } \sin i = \frac{a}{a+h} \cos \epsilon \quad (3.19)$$

$$\cos i = \sqrt{1 - \sin^2 i} \quad (3.20)$$

$$\delta = \frac{\pi}{2} - \epsilon - i \quad (3.21)$$

$$\cos \theta = \sin \theta_R \cos \delta + \cos \theta_R \cos \beta \quad (3.22)$$

$$\text{and } \sin \theta = \sqrt{1 - \cos^2 \theta} \quad (3.23)$$

$$\sin \gamma = \frac{\sin \beta}{\sin \theta} \cos \theta_R \quad (3.24)$$

$$\cos \gamma = \frac{\sin \theta_R - \cos \delta \cos \theta}{\sin \delta \sin \theta} \quad (3.25)$$

$$\sin(\phi - \phi_R) = \frac{\sin \beta}{\sin \theta} \sin \delta \quad (3.26)$$

$$H_0^0 = 1 \quad (3.27)$$

The recursion relation for H_n^m is

$$H_{n+1}^m = \mu H_n^m - \frac{n^2 - m^2}{4n^2 - 1} H_{n-1}^m \quad (3.28)$$

$$\text{and } H_{n+1}^{m+1} = \sqrt{1 - \mu^2} H_n^m \quad (\text{for } n=m) \quad (3.29)$$

$$K_n^m = -n \mu H_n^m + \frac{n^2 - m^2}{2n - 1} H_{n-1}^m \quad (3.30)$$

$$\bar{M} = -H_r - H_\theta \cos \gamma \tan i - H_\phi \sin \gamma \tan i \quad \rightarrow (3.31)$$

The full computer flow chart, Gaussian coefficients and final Fortran IV computer programme listing acceptable to IBM 360 are appended in Appendix II.

3.4 Methods of analyzing faraday rotation records

3.4.1 Total rotation method

Whenever the incoming polarization is orthogonal to the dipole antenna a null is present in the records. Assuming QI propagation and no horizontal gradients, the rate of Faraday rotation will be almost constant except near the QT region. At this point the rate of rotation undergoes a drastic change and this can be identified in clear records in the absence of scintillation and other disturbances. At the QT point since the electric vector of the incoming signal is parallel to the magnetic field the plane of polarization remains unchanged. Thus this portion of the record when the trace remains almost flat is the QT point. Here the rotation of the plane of polarization can be taken as zero or it represents the initial polarization at the satellite. A typical record taken on 2-4-65 for BE-B is shown in Figure 3.5. Jonathan Mass (1966) has discussed the errors in this assumption. He concludes that the errors are not more than 2 - 5% in the worst case. From the QT point the number of fades Ω at every full minute can be scaled and the TEC corresponding to the sub-ionospheric latitude at each minute computed knowing the sub-satellite position at each minute supplied by NASA refined world

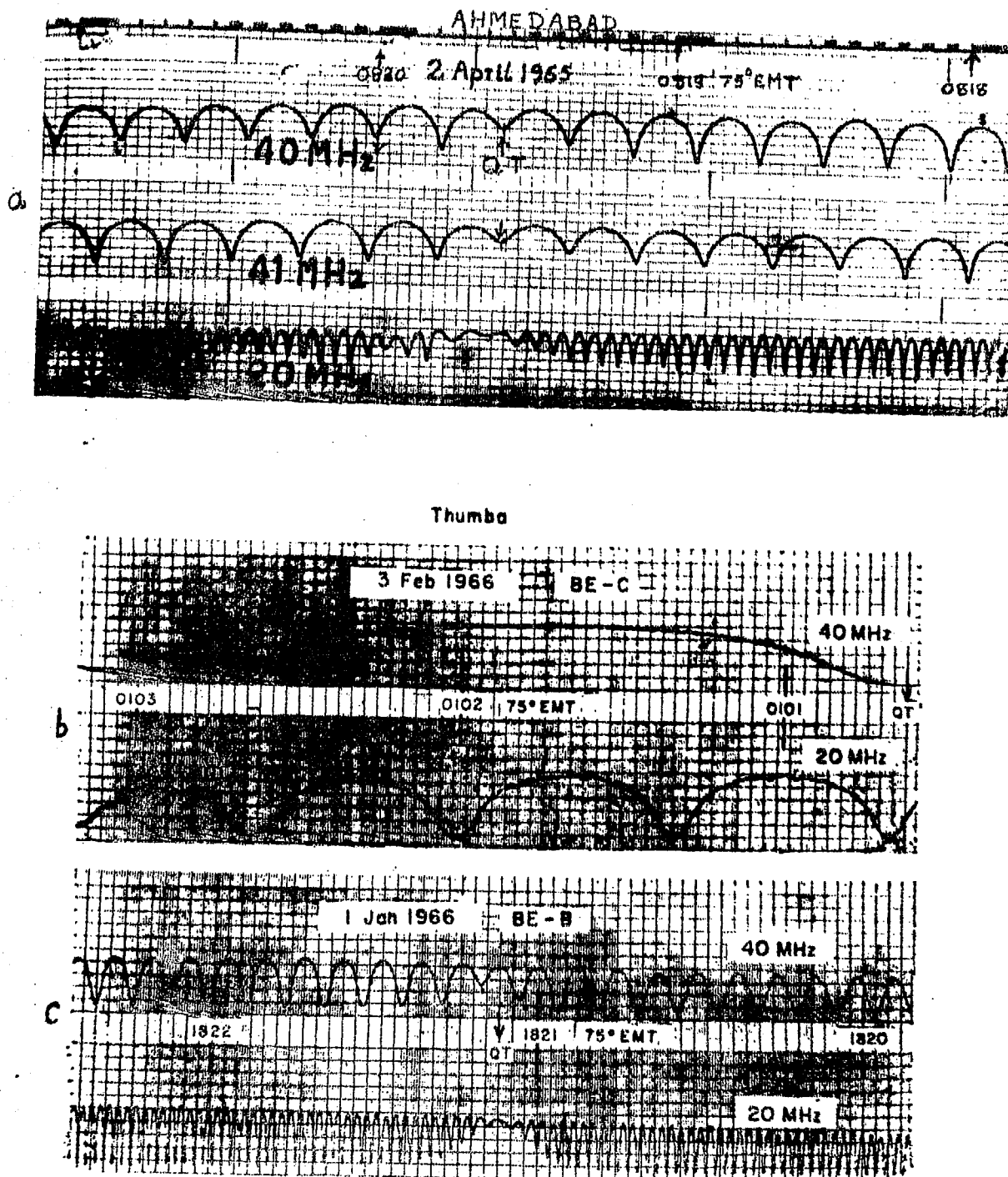


Figure 3.5 : Typical Faraday rotation records-

- (a) at Ahmedabad on 2 April 1966 around 0820 75° EMT
- (b) at Thumba on 3 February 1966 around 0102 75° EMT and
- (c) at Thumba on 1 January 1966 around 1821 75° EMT

The clear QT points and the frequencies are also marked in the figure.

maps. Then we can use the formula

$$N_t = \frac{\Omega f^2}{k \bar{M}}$$

3.4.2 Differential faraday rotation (Rotation rate or Faraday frequency method)

We know that $\Omega = \frac{k}{f^2} \bar{M} N_t$ (3.32)

In case the QT point is not clear or to correct for the errors occurring near the QT point, we can use this method to find out the absolute value of TEC. When no horizontal gradient is present,

$$\Delta \Omega = \frac{k}{f^2} (\Delta \bar{M} \cdot N_t + \bar{M} \cdot \Delta N_t)$$

or $N_t = \frac{\Delta \Omega}{\Delta \bar{M}} \frac{f^2}{k}$ (3.33)
assuming no horizontal gradients
(i.e. $\Delta N_t = 0$)

3.4.3 Double frequency method

The most accurate way to solve the ambiguity of the factor $n\hat{n}$ is to use two closely spaced frequencies ω_1 and ω_2 so that

$$\Omega_1 = \frac{b}{\omega_1^2} \bar{M} N_t$$

$$\text{and } \Omega_2 = \frac{b}{\omega_2^2} \bar{M} N_t$$

$$\text{Therefore } \delta \Omega = \Omega_1 - \Omega_2 = b \bar{M} N_t \cdot \frac{\omega_2^2 - \omega_1^2}{\omega_1^2 \omega_2^2}$$

$$\text{i.e., } \delta \Omega = \Omega_1 \frac{\omega_2^2 - \omega_1^2}{\omega_2^2}$$

$$\text{or, } \Omega_1 = A \delta \Omega \quad \text{where } A = \frac{\omega_2^2}{\omega_2^2 - \omega_1^2} \quad (3.34)$$

The polarization of the two received signals will coincide if $\delta\Omega = n\pi$ using this method, the coincidence will resolve the ambiguity if ω_1 and ω_2 are suitably chosen. Using $\omega_1 = 40$ and $\omega_2 = 41$ MHz, $A = 20.75$ i.e. there will be coincidence every 20.75 rotations of the 40 MHz signal. Since Ω is a function of time during a pass and due to variations in TEC and \bar{M} it is generally easy to see more than one coincidence. It is obvious that when $\Omega_1 = \Omega_2 - m\pi$ the polarization is not orthogonal to the antenna and an error of $<\pi$ is possible. In such case it is advisable to plot $\delta\Omega$ vs Ω and to find the exact value of $\delta\Omega$ from the extrapolated best fitted straight line curve.

3.4.4 Second order methods of Ross (1965), Hudson (1969) and Nancy Uss Crooker (1970)

The original first order formula of Browne et al. (1956) for Faraday rotation does not account the higher order terms in the Appleton-Hartree refractive index formula for a magnetoionic medium. This will lead to erroneous results of TEC especially when magnetoionic mode coupling between the ordinary and extra-ordinary rays takes place. This happens generally near the QT region. Therefore Ross (1965) has derived a second order Faraday rotation formula

$$\Omega = \Omega_0 \left[1 + \frac{1}{2} \beta \bar{X} + \frac{1}{2} (\beta - 1) G_1 \bar{X} \right] \quad (3.35)$$

where Ω_0 is the first order Faraday rotation angle, β is a factor proportional to $\frac{\bar{X}^2}{\bar{X}^2}$ which in turn is proportional to $\frac{\int N^2 dh}{\int N dh}$.

G is a geometrical factor and

$$G = \tan \chi \left[\tan \chi - \frac{Y_1}{Y_2} \right]$$

$\beta = 1$ for a completely uniform distribution of $N(h)$. For a Chapman distribution of the form,

$$N = N_m \exp \left[1 - z - e^{-z} \sec \chi \right] \quad (3.36)$$

We can take $\beta = 0.159 h$, h being in units of scale height.

For $h = 1000$ km, $H = 67$ km we can write $\beta = 2.5$. This formula can be used only with a proper knowledge of the factors β and G which require information about the electron density distribution with height.

Therefore Hudson (1969) had made a simple extension to the first order formula by expanding the refractive index formula in a series expansion as

$$n = 1 - \frac{x}{2} + \frac{xy \cos \theta}{2} - \frac{xy^2 \sin^2 \theta}{4(1-x)} + \frac{xy^3 \sin^3 \theta \tan \theta}{16(1-x)^2} \quad \rightarrow (3.37)$$

Now the angular rotation $d\Omega$ as the wave of frequency ω passes through a distance ds is

$$d\Omega = \frac{\omega}{2c} (n_1 - n_2) ds \quad (3.38)$$

where n_1 and n_2 are the two characteristic refractive indices.

Thus

$$\Omega = \frac{\omega}{2c} \left[xy \cos \theta + \frac{xy^3 \sin^3 \theta \tan \theta}{4} + \frac{x^2 y^3 \sin^3 \theta \tan \theta}{16} \right] ds$$

Neglecting the third term in the bracket,

$$\Omega = \frac{\omega}{2e} \int XY \cos \theta ds + \frac{\omega}{16e} \int XY^3 \sin^3 \theta \tan \theta ds \quad (3.40)$$

i.e. $\Omega = \Omega_0 + \Delta\Omega \quad (3.41)$

where $\Delta\Omega$ now becomes the second order correction.

Now
$$\Delta\Omega = \frac{K_2 \bar{M}_2}{f^4} \int N dh \quad (3.42)$$

where $K_2 = 4.595 \times 10^{-6} \text{ m.k.s. units}$ and

$$\bar{M}_2 = (B \sin \theta)^3 \tan \theta \sec \chi$$

It may be noted that the second order correction is inversely proportional to the 4th power of wave frequency and hence negligible at VHF.

An improvement in the closely spaced first order formula of Blackband (1960) for deducing ionospheric electron content from Faraday rotation measurements was made by Nancy Uss Crooker (1970) as follows:

$$N_t = \left(n \pm \frac{\Delta t}{P_L} \right) \frac{f_L^2}{f_H^2 - f_L^2} \frac{f_H^2}{k M} \quad (3.43)$$

where Δt is the time shift between the nulls of the higher frequency f_H and the lower frequency f_L at any instant of time t under consideration. P_L is the period of fading for the lower frequency and

$$P_L = 1/2 \frac{d\Omega}{dt}$$

Assuming no horizontal gradients,

$$P_c(t) = \frac{f^2}{2k} \frac{1}{N_t \frac{dM}{dt}} \quad (3.44)$$

For different values of n , $P_c(t)$ can be calculated and plotted. The observed $P(t)$ curve coincides best with the $P_c(t)$ curve for a particular value of n . This is selected as the actual value of n . $P(t)$ is read off from the records.

3.4.5 Inter-comparison of TEC obtained by the different methods

In this section, to show the intercompatibility and the relative accuracies of the different methods of analysing Faraday rotation records, we have analysed a typical satellite pass on 17-3-1965 of the satellite BE-B at about 0441 UT. The values of TEC given by the different methods and difference with respect to the first order formula are shown below:

0441 UT of 17-3-65

Author	TEC (el/m ²)	% Difference
Browne et al. (1956) (First order)	3.474 x 10 ¹⁷	Standard
Blackband (1960)	3.351 x 10 ¹⁷	3.5%
Ross (1965)	3.544 x 10 ¹⁷	2.0%
Hudson (1969)	3.684 x 10 ¹⁷	6.0%
Nancy Uss Crooker (1970)	3.143 x 10 ¹⁷	2.8%

The above results indicate that the higher order corrections

are not greater than 5 - 10% and therefore for routine use the simple first order total rotations formula of Browne et al.(1956) is quite reliable.

3.4.6 Method used in the present study

However, second order formulas are not amenable to routine use while handling large amount of data. Therefore in this study the single frequency first order faraday rotation formula is used, and records in which QT is very clear are only used. The closely spaced frequency method $\left(\frac{d\Omega}{df}\right)$ is used for records in which QT point is not clearly identifiable unambiguously. Again, at the QT region where the simple formula fails, the differential faraday fading formula $\frac{d\Omega}{dM}$ method is used. The mean ionospheric height is chosen as 400 km for Thumba, 400 km for Kodaikanal and 350 for Ahmedabad. The magnetic field at this height is computed using the 48 Gaussian coefficients spherical harmonic expansion for each minute's position of the satellite. The elevation, azimuth and range of the satellite for each minute are computed for the known sub-satellite coordinates supplied by NASA refined world maps. A fixed satellite height of 1000 km is chosen throughout the analysis. No variation of \bar{h} with day and night is considered.

Thumba data for 1965-68, Kodaikanal for 1964 Oct - 69 and Ahmedabad 1964 Oct - 1969 have been used to derive the total electron content. Almost simultaneous ionogram information is used to study the parameters of bottomside ionosphere.

3.5 Preliminary results of TEC and scintillations using ATS-6 satellite

With the positioning of the geostationary satellite ATS-6 at 35°E in July 1975 it was possible for experimenters in India to obtain continuous records of total electron content from different stations in the Indian subcontinent. Thus a chain of ATS-6 receiving stations were established with the collaboration of Physical Research Laboratory, Ahmedabad. The details of the stations are given in Table 3.1. All these stations have identical receiving systems and record Faraday rotation at 140 MHz. In addition to this, a major establishment is in operation at Ootacamund (Ooty) to record Faraday rotation at 40, 140 and 360 MHz, Amplitude and phase scintillations at 40, 140 and 360 MHz and Group delay at 40 and 140 MHz with respect to 360 MHz.

Table 3.1

Station	Geographic		Magnetic Dip ° N
	Longitude ° E	Latitude ° N	
Ooty	76.70	11.43	4.00
Bombay	72.91	19.09	24.75
Ahmedabad	72.62	23.03	34.00
Rajkot	70.74	22.31	33.00
Udaipur	73.67	24.58	35.00
Patiala	76.38	30.32	45.00

Some preliminary results of this study are given below. The main advantage of geostationary satellite is to study the diurnal variation of TEC over a particular location with high time resolution. The Faraday rotation data at the above mentioned stations have been analysed to obtain the diurnal variation of TEC at each of these stations. As the ratio of the change in Faraday rotation angle ($\Delta\Omega$) to \bar{M} is directly proportional to the Total Electron content we show here only the ratio $\Delta\Omega/\bar{M}$ typically for 24 October 1975. The results are shown in Figure 3.6 where the diurnal variation of $\Delta\Omega/\bar{M}$ at 140 MHz at Ooty, Bombay, Rajkot, Ahmedabad, Udaipur and Patiala has been compared, thus covering a range of latitudes right from near the magnetic equator to latitudes beyond the equatorial anomaly peak. f_oF_2 at Ahmedabad is also plotted at the top of the diagram for comparison. It is seen from Figure 3.6 that the diurnal curve at Ooty is quite flat and that during the course of the day at Ooty less than one rotation only has taken place at Ooty. As one goes away from the dip equator we see that the diurnal curve becomes more and more sharp and the amount of rotation within the day is more than two at Ahmedabad and Udaipur indicating that the electron content increases with latitude giving a peak near about the latitude of Ahmedabad or Udaipur. With further increase of latitude, at Patiala the Faraday rotation curve again tends to be flat.

From Figure 3.6 thus the diurnal as well as latitudinal variation of TEC is indicated. The latitudinal variation of TEC clearly indicates the Appleton anomaly. These results lend support

ATS-6 140 MHz 24-OCTOBER, 1975

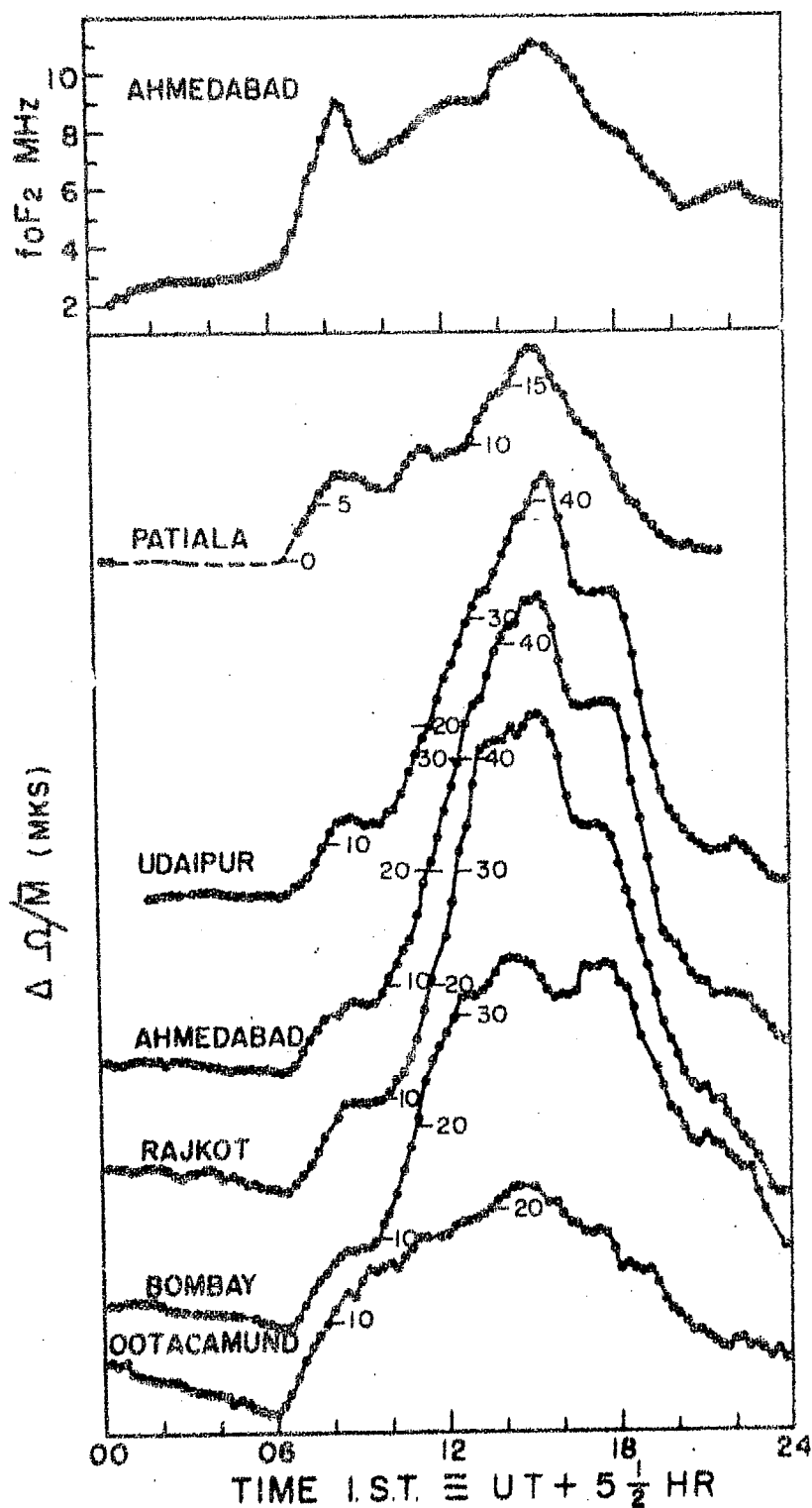


Figure 3.6 : Daily variation of $\Delta \Omega / \bar{M}$ (proportional to TEC) at the chain of Indian stations on 24 October 1975.

to the results in the following chapters derived from low orbiting satellites' data.

To indicate the presence of satellite signal scintillations at frequencies as large as 360 MHz, we have shown in Figure 3.7 typical records of scintillations recorded at Ooty at 40, 140 and 360 MHz. Three typical night time scintillation records for 19 October 1975, 20 October 1975 and 25-26 October 1975 are shown in Figure. Generally one expects the scintillation strength to follow inverse frequency law, i.e. scintillation will be stronger at lower frequency than at higher frequency. But we see, often this law is not obeyed in equatorial scintillation. On 19 October 1975, and on 20 October 1975, the scintillation at 360 MHz is much deeper than at 40 or 140 MHz. But on 25-26 October 1975, scintillation at 40 MHz is stronger than at 140 and 360 MHz. This violation of frequency law is indicative of the different nature of the equatorial scintillating irregularities.

Although scintillation is known to be a night time phenomenon (Koster, 1972), we show here instances when considerable scintillation is seen in day time. Figure 3.8 shows a few records on 7 November 1975, 5 November 1975 and 3 November 1975 when scintillation was seen during day time. However the inverse frequency dependence of scintillation strength seems to be obeyed by these day time scintillating irregularities. This again indicates the different physical nature of day time and night time irregularities. These day time scintillations are seen to be associated with strong blanketing type Es patches.

ATS-6 OOTACAMUND

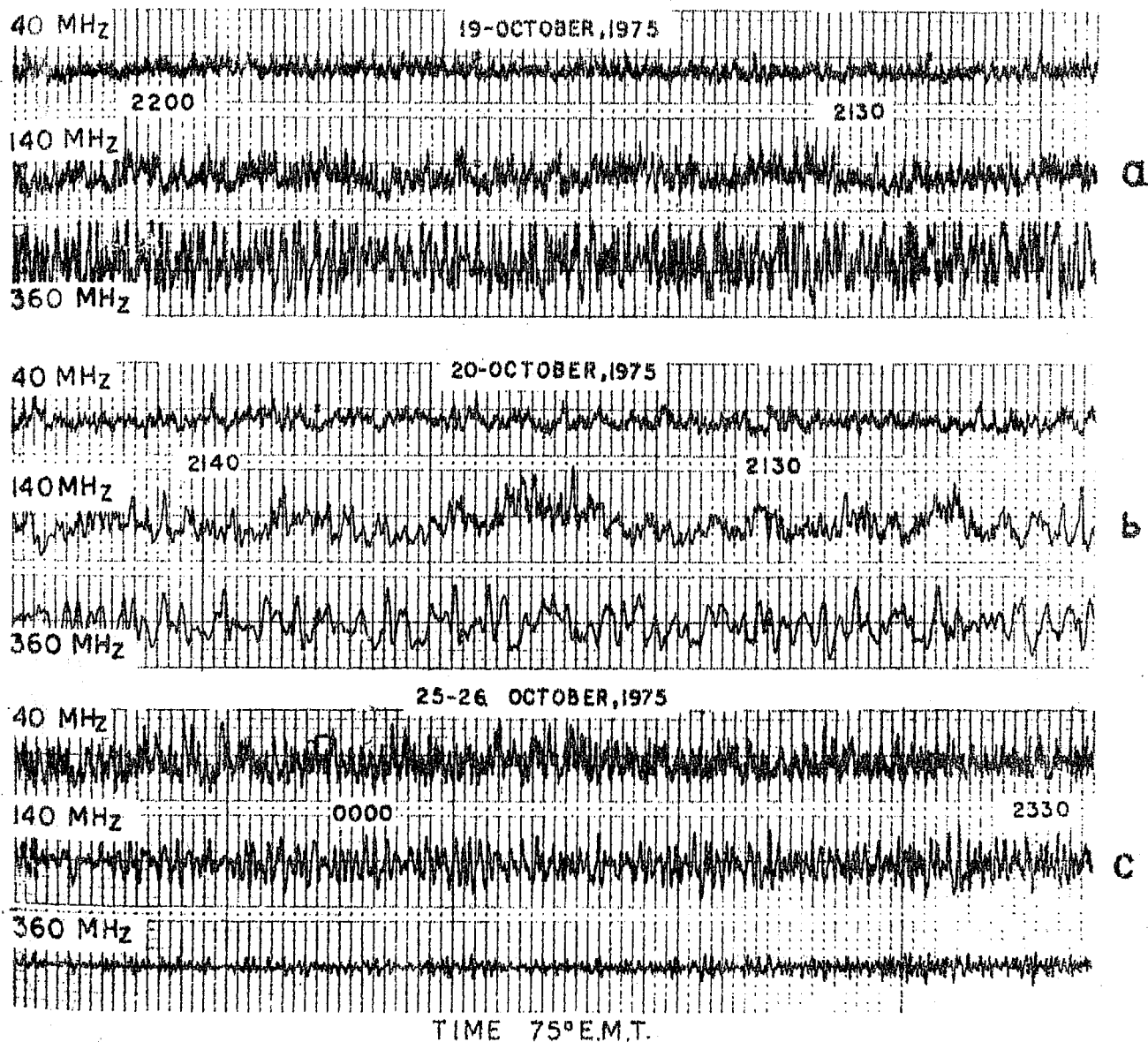


Figure 3.7 : Night time scintillations at Ootacamund showing the frequency law inversion in (a) and (b) and frequency law obeyed in (c).

ATS-6 OOTACAMUND

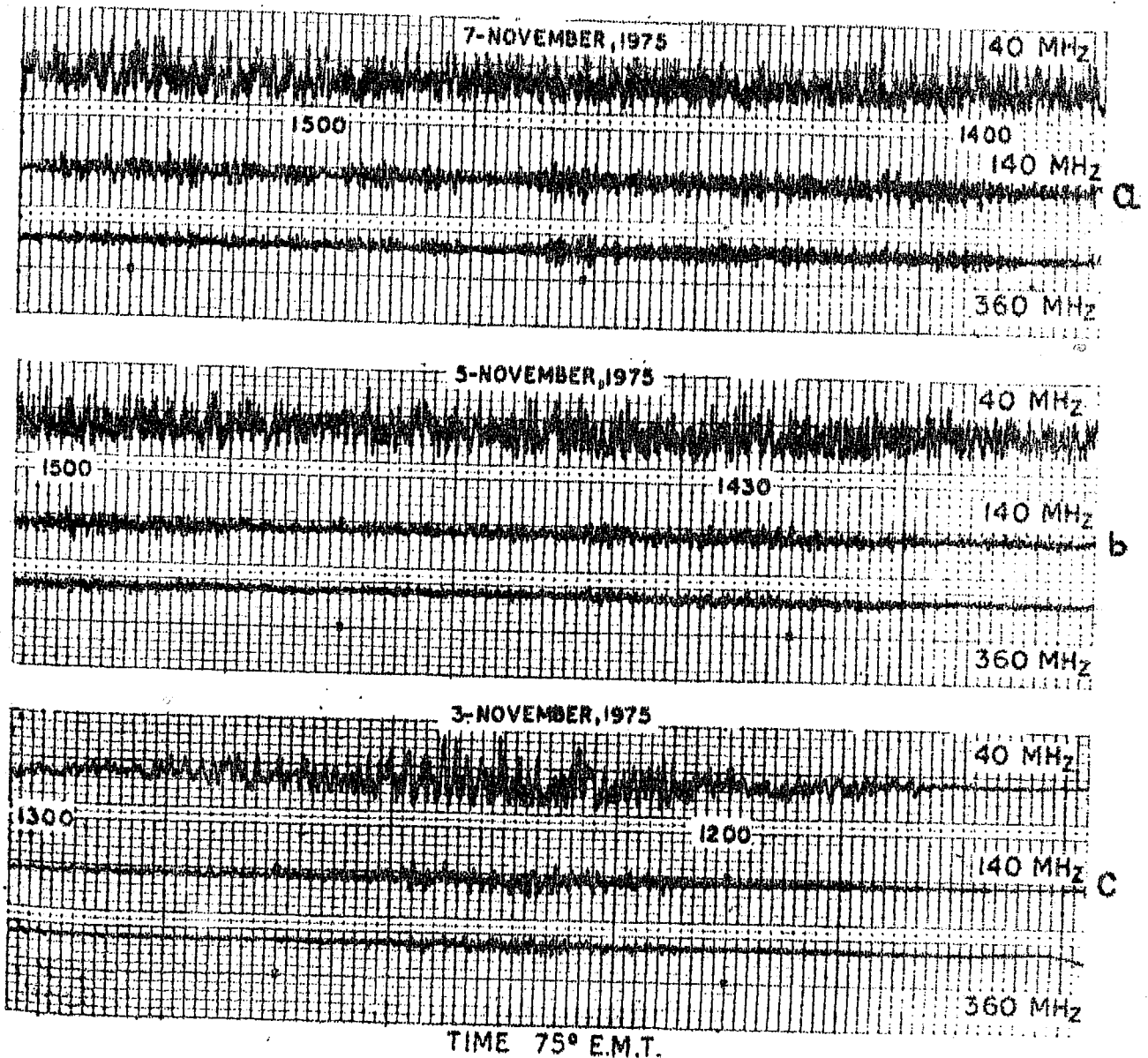


Figure 3.8 : Day time scintillations at Ootacamund showing the frequency law obeyed in (a) and (b) and burst of scintillation in (c).

C H A P T E R - I V

RESULTS OF TOTAL ELECTRON CONTENT STUDIES AT AHMEDABAD, THUMBA AND KODAIKANAL

4.1 Introduction

Until fairly recently most of the data on equatorial and low latitude Total Electron Content has been obtained by low orbiting satellites, in particular from BE-B and BE-C. Over 90 observatories are reported to have been recording the signals from these satellites, out of which 8 are in India (Tyagi and Mitra 1970). However, some measurements also exist using geostationary satellites (Garriott et al. 1965, Koster 1966, Yeboah-Amankwah and Koster 1972 and Deshpande et al. 1976). Measurements using orbiting satellites are most suited to study the spatial variations of Total Electron Content while geostationary satellites are superior in respect of continuous monitoring with high time resolution.

The main features of TEC studied are the diurnal and seasonal changes of TEC (Goodman 1966, Yuen and Roclofs 1966, 1967, Da Rosa and Smith 1967, Titheridge 1968a,b, Taylor and Earnshaw 1970 and Young et al. 1970) integrated production and effective loss rates (Garriott and Smith 1965 and Smith 1968), changes produced by solar flares and magnetic storms (Garriott et al. 1967, Titheridge and Andrews 1967, Goodman 1968, Taylor and Earnshaw 1970, Webb 1969 and Mendillo et al. 1969, 1970) and the occurrence and

characteristics of large scale irregularities and scintillations (Titheridge 1968e,d, Elkins and Slack 1969, Dieminger et al. 1970 and Davies and da Rosa 1969).

Studies also exist on the related parameters such as equivalent slab thickness $(\tau) = \frac{N_T}{N_m}$ which is a parameter dependent on temperature (Yeh and Flaherty 1966, Bandopadhyay 1970, Walker 1971 and Chance and Chin 1972).

In the present chapter, the results of the study of Faraday Rotation at 40 and 41 MHz signals recorded at Ahmedabad, Thumba and Kodaikanal during the period November 1964 through December 1969 from the low orbiting beacon satellites BE-B and BE-C are presented.

Recording of satellite signals, prediction of passes and the analysis of the records were first started at Ahmedabad in November 1964 by Dr.S.Ramakrishnan and continued later by Dr.R.P.Sharma and afterwards by the present author. Only passes having a maximum elevation $> 30^\circ$ were recorded at Ahmedabad. The time of sub-satellite point passing over Ahmedabad on each day has been plotted in Figure 4.1. It is found from this figure that the time of closest approach of northbound or southbound passes of BE-B recedes through 24 hours in a period of 177 days. On any particular day the northbound and southbound passes of BE-B occur at a time interval of $11\frac{1}{2}$ hours in between. Thus combining both northbound and southbound passes together, a minimum of about 3 months are required to obtain one full diurnal curve. In the

SEE FARADAY FADING RECORDINGS AT AHMEDABAD

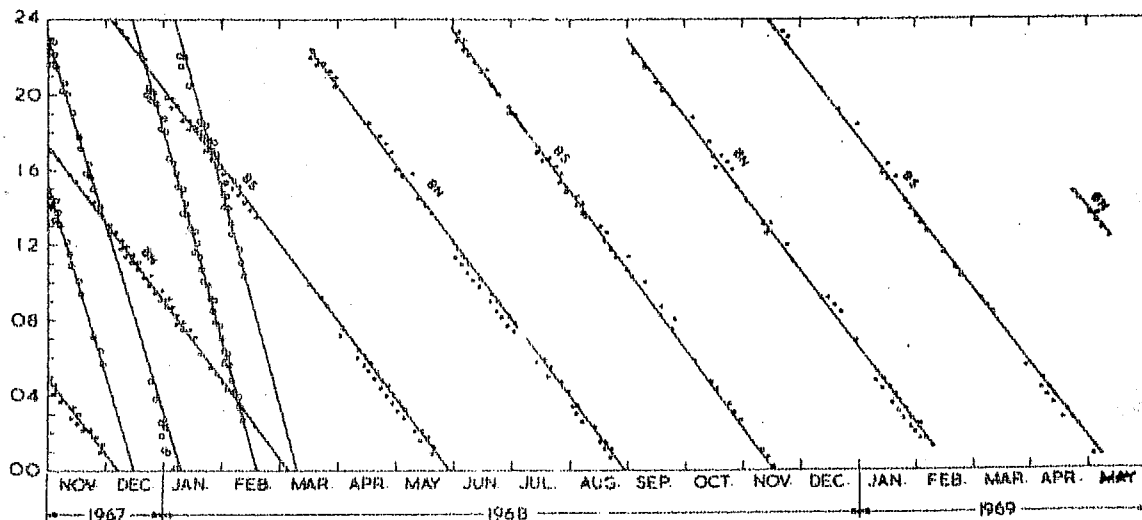
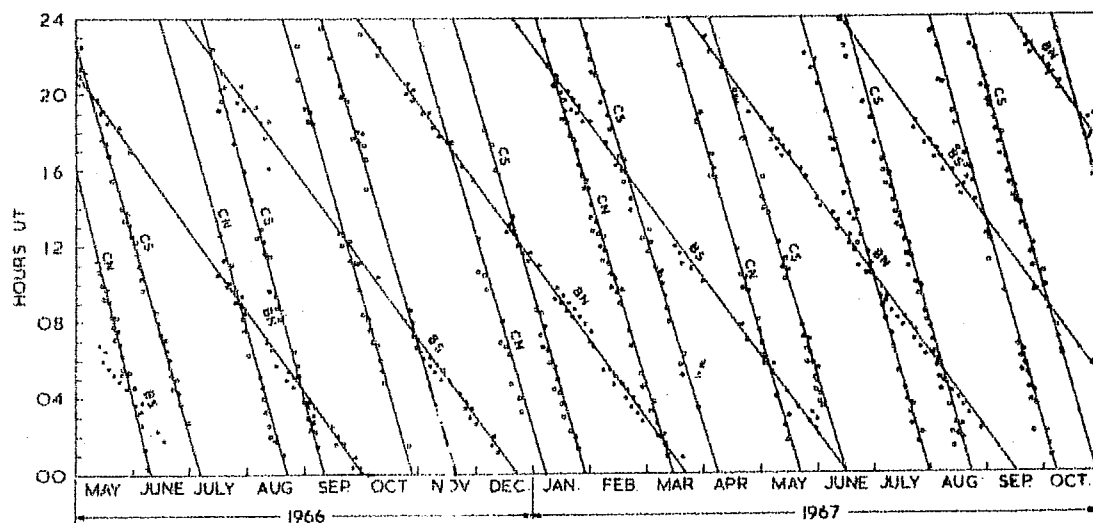
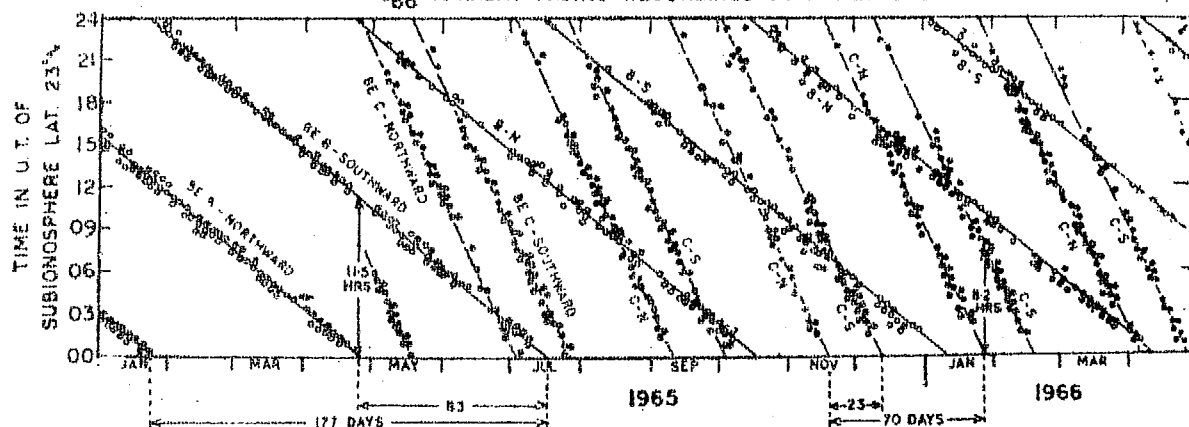


Figure 4.1 : Time of all the passes at sub-ionospheric latitude of 23°N plotted against days for RE-A

case of satellite BE-C the passes recede through 24 hours in about 70 days and the time interval between northbound and the corresponding southbound pass is 8.2 hours. Therefore combining both BE-B and BE-C data at any place a full diurnal curve can be obtained in less than two months' time. Even then it is to be borne in mind that the diurnal variations derived thus will however be contaminated to some extent by day to day and seasonal changes.

It is found that at Ahmedabad QT condition is achieved at a sub-satellite latitude of 29°N geographic. QT point can clearly be identified in almost all records.

4.2 Total electron content at Ahmedabad

4.2.1 Diurnal variation of TEC

For each pass the TEC has been calculated at every minute during the pass and the observed TEC plotted against sub-ionospheric point at every minute. A smooth curve is fitted through the observed points and from the smooth curve the value of TEC corresponding to the latitude of Ahmedabad is read off. All such obtained TEC values are plotted against time for the period December 1964 through May 1969 separately for northbound and southbound passes of BE-B. These are shown in Figure 4.2. It is seen that about 9 daily curves are obtained within a period of 50 months. It is also seen that the daily curves of northbound and southbound passes are shifted from each other by roughly 12 hours.

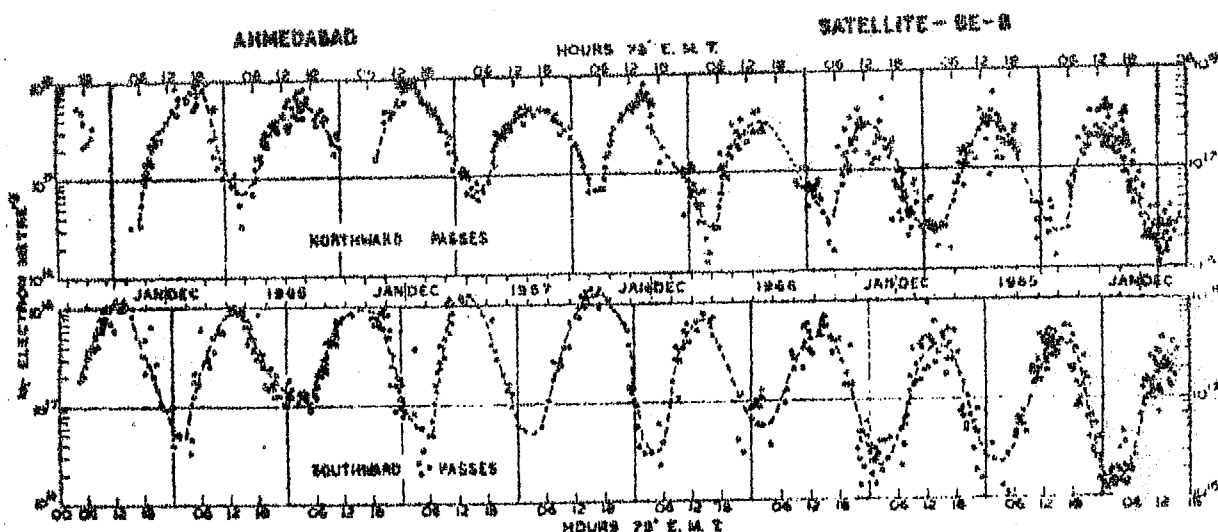


Figure 4.2 : Mass plot of TEC at Ahmedabad separately obtained for Northbound and Southbound passes of the satellite BE-B for the period December 1964 - May 1969.

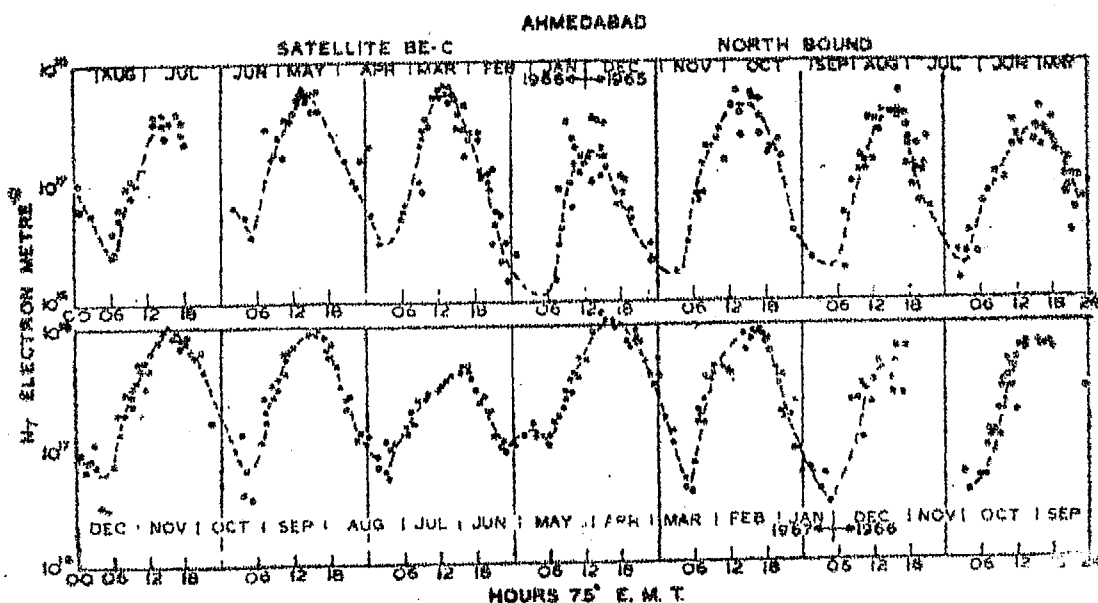


Figure 4.3 : Mass plot of TEC values obtained from Northward passes of satellite BE-C between the period May 1965 - December 1967.

Similar data for the northbound passes of BE-C for a period of 32 months from May 1965 through December 1967 are plotted in Figure 4.3. During this period 14 daily curves have resulted. From both Figures 4.2 and 4.3, the diurnal trend of TEC is quite clear. TEC attains minimum value around 04 hr LT and then increases very rapidly after sunrise. Peak values of TEC are reached around 14-16 hr LT, thereafter TEC decreases. It is seen that there is considerable amount of scatter in these daily plots which are due to genuine day to day changes of TEC.

4.2.2 Comparison of diurnal variation of TEC and N_m

In order to compare the daily variation of TEC and the maximum electron (N_m) of the ionosphere, in Figure 4.4, in the upper portion, TEC derived from northbound passes of BE-B and in the lower portion the N_m values interpolated from the hourly ionograms at Ahmedabad to the time of satellite pass are plotted against 75° EMT. For any particular period the diurnal variations of TEC and N_m are very similar to each other, thus showing that the information of any physical parameter obtained from TEC measurements will be weighted heavily by the ionization around F-region peak.

4.2.3 Comparison of diurnal variation of TEC and N_m for different seasons

Next, we have compared the diurnal variation of TEC and N_m for the different seasons. For this purpose, the data is grouped into four different seasons of 3 months each, viz., Spring (March, April, May), Summer (June, July, August), Autumn (September,

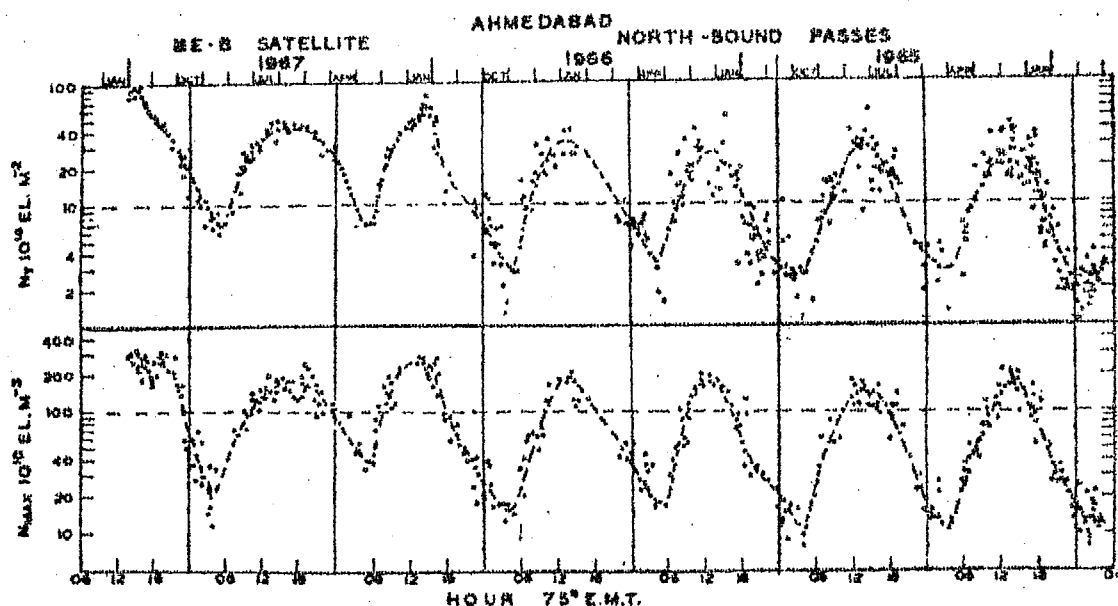


Figure 4.4 : Comparison of TEC and Nm for the northbound passes of satellite SE-B for the period December 1964 through May 1969.

AHMEDABAD SATELLITES SE-B & SE-C
SPRING - (MAR. APR. MAY)

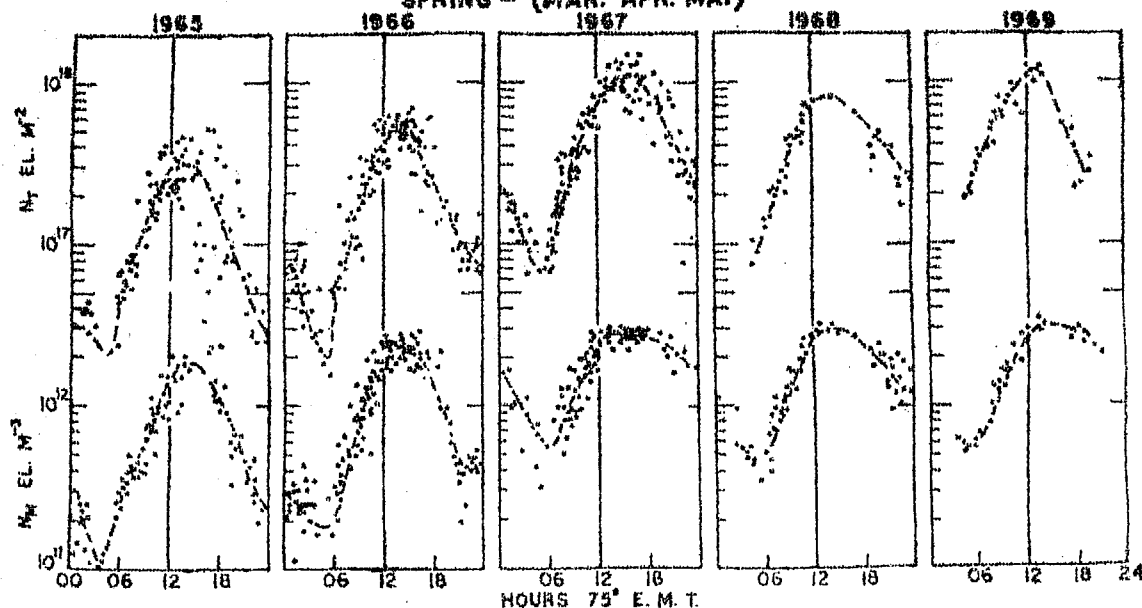


Figure 4.5 : Daily variation of TEC and Nm during Spring season of the years 1965 through 1969.

October, November and Winter (December, January, February). The data from all the passes of BE-B and BE-C are put together to obtain diurnal curves for each season of each year from 1965 through 1968. These results are shown in Figures 4.5 through 4.8. TEC reaches minimum values during pre sunrise hours, around 04-06 hr LT, and attains maximum values in the afternoon (13-16 hr LT). The time of maximum has a tendency to be delayed in any season as the solar activity progresses. TEC and N_{\max} curves are similar in any season. With increasing solar activity TEC progressively increases in any season with the exception of summer season in which the diurnal range becomes smaller with higher solar activity. During any particular year, the diurnal range of TEC is largest in equinoxes. The range of TEC variation during the course of a day is measured by the ratio of daily maximum to minimum TEC. In Figure 4.9 the variation of this ratio with 10.7 cm solar flux is shown. It is seen that in winter months diurnal ratio of TEC remains at a constant value of about 16 for all solar activity levels, while in summer it decreases from a value of 20 at a solar flux value of 80 units to 5 at a flux value of 150 units. Diurnal ratio of N_{\max} plotted in the same figure also shows similar variation with solar activity.

4.3 Total electron content at Thumba

4.3.1 Diurnal variation of TEC at Thumba

With a view to study the behaviour of ionospheric electron content near the magnetic equator two recording stations for

SUMMER - (JUN. JUL. AUG.)

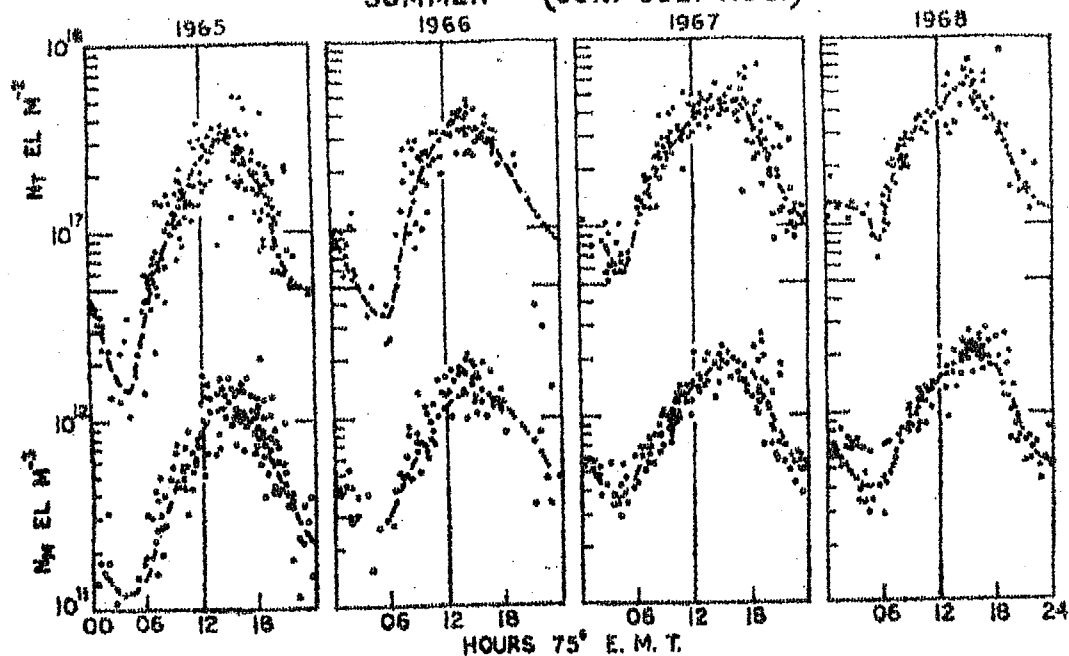


Figure 4.6 : Comparison of daily variation of TEC (marked in the figure as NT) and maximum electron density in the F-region Nm for summer season of the years 1965 through 1968.

AHMEDABAD

SATELLITES BE-B & BE-C

AUTUMN - (SEP. OCT. NOV.)

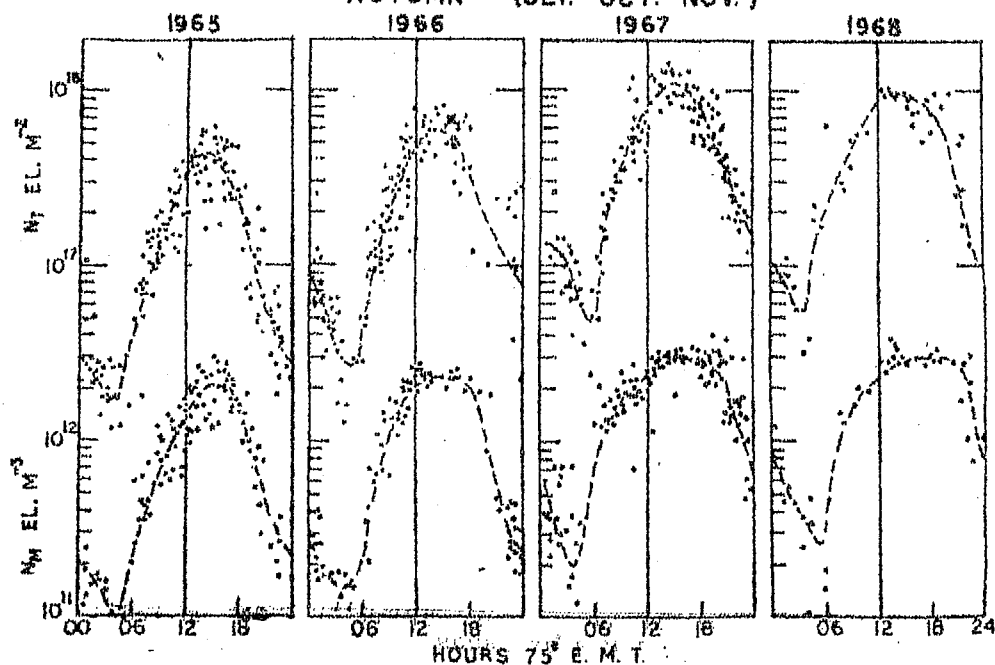


Figure 4.7 : Comparison of daily variation of TEC and Nm

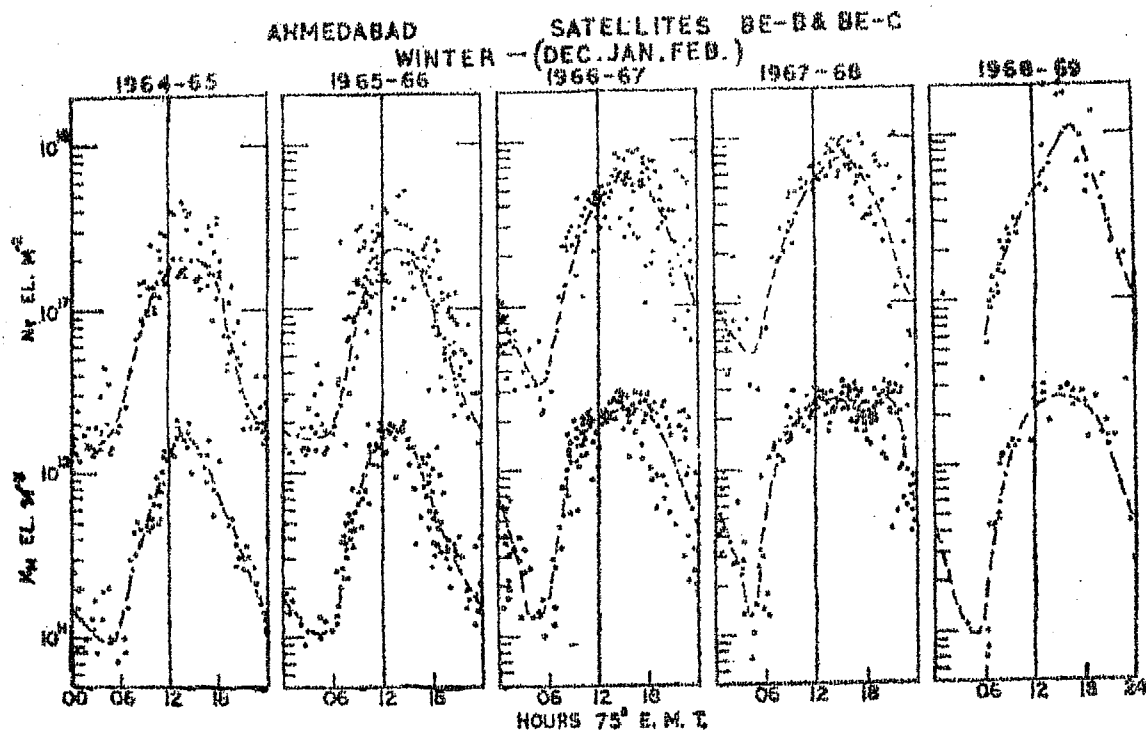


Figure 4.8 : Comparison of daily variation of TEC and Nm for winter season of 1964 - 65 through 1968 - 69.

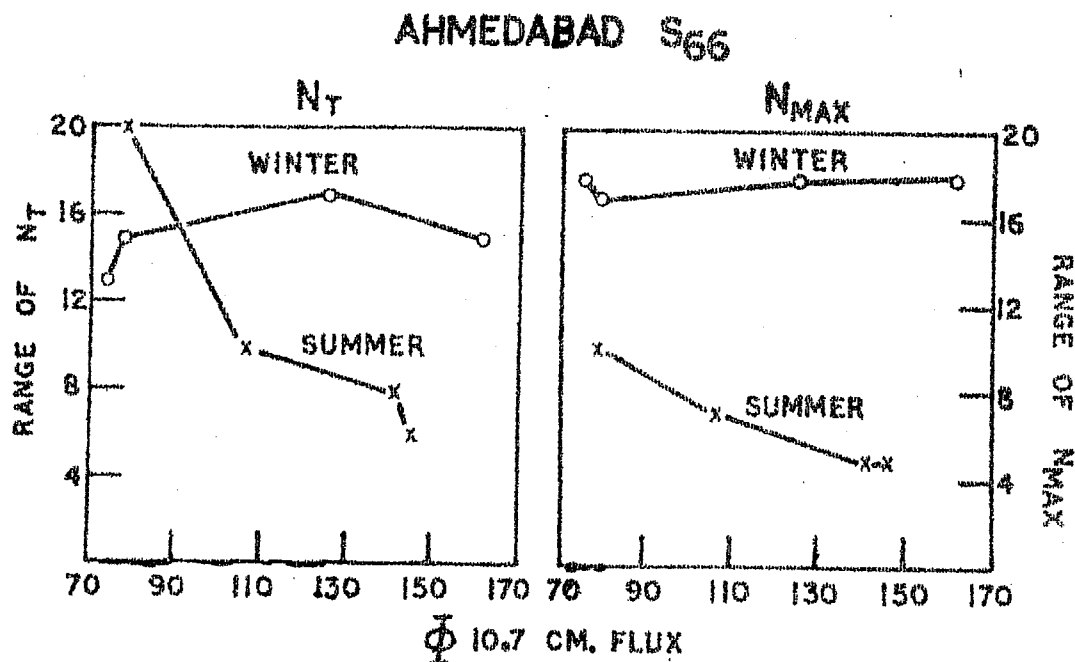


Figure 4.9 : Variation of daily range in TEC (marked as NT in figure) and Nmax with 10.7 cm solar flux

measuring the Faraday rotation of 40 and 41 MHz signals were established at Thumba and Kodaikanal, with receiving systems exactly identical at both places to the one used at Ahmedabad. All the recorded passes at Thumba during the period 1965 to August 1968 were analysed to obtain TEC. To study the diurnal variation of equatorial TEC, in Figure 4.10, TEC is plotted against 75° EMT. TEC is denoted in the figure by N_T . As the total number of passes analysed in any particular season or year were not high enough, we have put together the data of all seasons and all years to obtain the mean daily variation of TEC. Therefore the scatter of points is so large that no mean line has been drawn through the observed points. Yet, the diurnal trend of minimum values of TEC around 04 hr LT and maximum value around 14-18 hr LT which agrees well with the earlier observation of TEC at equatorial stations in African and American longitudes (Blumle 1962, Skinner 1966, Olatunji 1967 and Bandopadhyay 1970). A point of arbitration about equatorial TEC is whether it shows a noon bite-out similar to the one in f_oF_2 . No conclusion about this aspect can be drawn from the above observations. However, this point is further elaborated in the next section and discussed in Section 4.9.

4.3.2 Comparison of daily variation of TEC and N_m

In order to compare the diurnal variation of TEC and N_{\max} we have used the ionograms at Kodaikanal. This is because the ionospheric soundings at Thumba were done at hourly intervals,

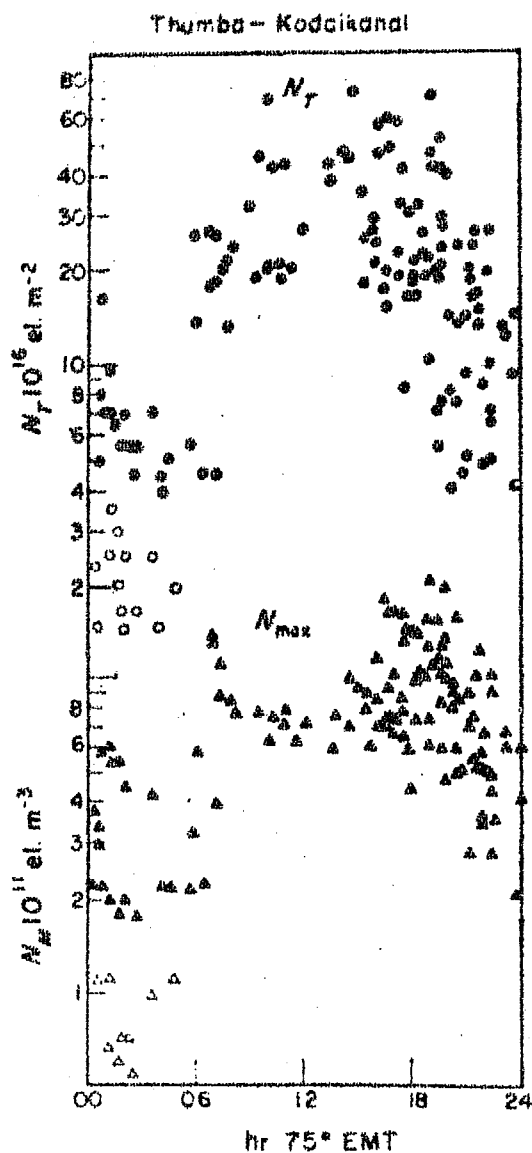


Figure 4.10 : Mass plot of TEC and maximum electron density in the F-region (N_m) against time obtained at Thumba. Note that N_m is obtained from Kodaikanal ionograms and TEC was recorded at Thumba.

while at Kodaikanal, a neighbouring equatorial station, soundings are done at 15 minutes interval; this will give an ionogram as close to the satellite pass as possible. It may be noted that the value of N_{\max} at these two stations are shown to be almost equal (Harish and Rastogi, 1971). As is well known for equatorial stations, N_{\max} indicates a midday minimum with peaks in the forenoon and evening hours.

At Thumba during low sunspot years reflections are not observed from the ionosphere during the early morning hours (Chandra and Rastogi, 1971). These no echo conditions are variedly ascribed to excessive absorption, decrease of ionization or loss of echo due to large gradients in the ionosphere. It is seen from Figure 4.10 that some of the TEC values between 02 and 06 hrs are abnormally low and these are indicated by open circles. These are also found to be associated with extremely low values of N_m (indicated by open triangles). Thus it may be inferred that the no echo condition at equatorial regions correspond to a genuine decrease of N_{\max} with f_oF_2 at these hours falling below the lower limit of the ionosonde.

4.4 Total electron content at Kodaikanal

4.4.1 Diurnal variation of TEC at Kodaikanal in relation to related ionospheric parameters

At Kodaikanal another station near to the magnetic equator (dip $3.4^\circ N$) TEC has been measured using the Faraday rotation of 40 and 41 MHz signals from the satellites BE-B and BE-C for the

period November 1964 through 1969. In this section, the mean daily variation of TEC at Kodaikanal is compared with other ionospheric parameters, viz., the F-region peak electron density (N_m), height of maximum F_2 region ionization ($h_m F_2$), the semithickness parameter of the F_2 region ($Y_m F_2$) and the horizontal drift speeds measured by the spaced receiver technique at Thumba. The parameters N_m , $h_m F_2$ and $Y_m F_2$ are reduced from the true height analysis using Budden's matrix method (Budden, 1954) of the ionograms taken by C_4 ionosonde nearest to the time of satellite transit at Kodaikanal. Horizontal drift velocity (V_h) at F region heights was measured at Thumba using Mitra's spaced receiver technique (Mishra et al. 1971). Figure 4.11 shows the average diurnal variation over the period 1964-66 of the parameters N_T (representing TEC), $N_m F_2$, $h_m F_2$, $Y_m F_2$ and $V_h(F_2)$. The number of observations for N_T for any particular hour are written at the top of the figure. The observations around midnight are very few but for daytime hours there are sufficient observations for any hour. The standard deviation for N_T and N_m are shown by the vertical flags.

The mean N_T curve shows exactly similar behaviour as seen at Thumba, viz., minimum around 04 hr; increases rapidly after sunrise reaching a peak around 15 hr thereafter decreasing steadily till 04 hr. There is no evidence of the midday bite-out in TEC. N_m curve also shows minimum value around 05 hr and two day time maxima around 08 hr and around 16-17 hr separated by a valley around 11 hr. The height of peak ionization is minimum around 06 hr and maximum around 13 hr. The semithickness $Y_m F_2$

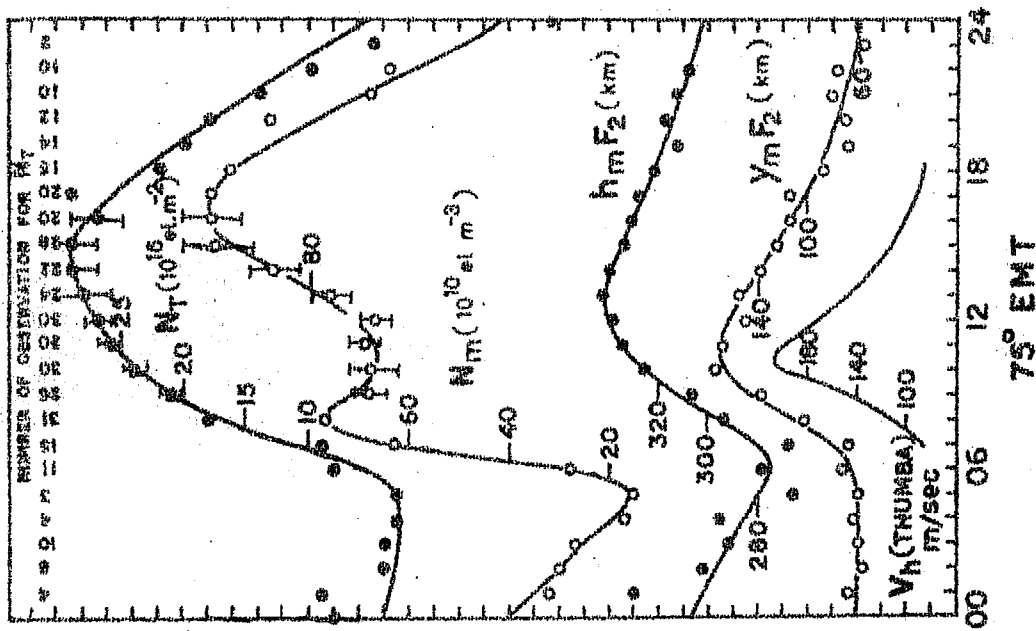


Figure 4.11 : Comparison of daily variation of TEC, N_m , $h_m F_2$, $y_m F_2$ and V_h at Kodaikanal during 1964 - 66.

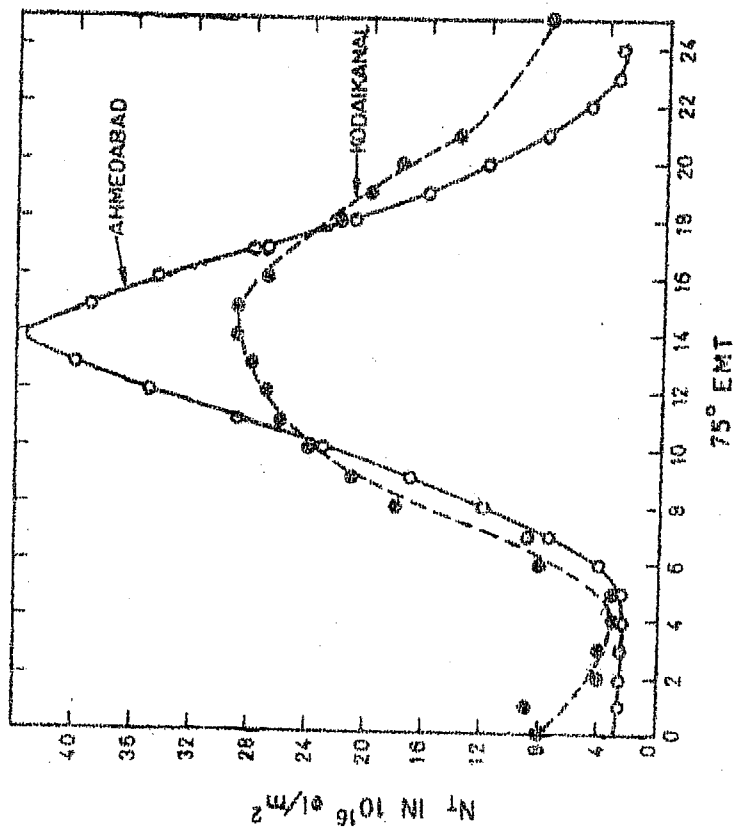


Figure 4.12 : Comparison of diurnal variation of TEC at Kodaikanal and Ahmedabad showing the extra ionization at Ahmedabad between 11 and 16 hrs.

maximises round 11 hr. The F-region ionospheric horizontal drift velocity is also maximum around 11 hr. The coincidence in time of the maxima of $Y_m F_2$ and $V_h(F_2)$ and minimum in $N_m F_2$ shows clearly that the decrease of $N_m F_2$ is due to the electrodynamic uplift of ionization over the magnetic equator during the midday hours which in turn increases the thickness of the layer. Further implications of this feature and the absence of diurnal anomaly in TEC will be discussed in Section 4.9.

4.4.2 Comparison of mean diurnal variation of TEC at Kodaikanal and Ahmedabad

In order to understand better, the absence of noon bite-out in TEC, in contrast to the N_m variation, in this section the mean diurnal variation of TEC at Kodaikanal and Ahmedabad are compared, for the same solar activity conditions. This result is shown in Figure 4.12. It is clearly seen that the diurnal variation of TEC (marked in the figure as N_T) is very similar at both the stations. However, the TEC values between 11 and 16 hrs are reasonably larger at Ahmedabad than at Kodaikanal. This difference cannot be accounted for by the differences in production and loss balance alone even after allowing for the presence of a neutral density latitudinal anomaly (Chandra and Goldberg 1964, Newton and Pelz 1969 and Hedin and Mayr 1973). This hence suggests that transport of ionization from equator to tropical latitudes is definitely present through vertical drift and diffusion but it is not severe enough to create a depression of TEC at noon. The change of slope of TEC curve of Kodaikanal (Figure 4.12) as compared to that

of Ahmedabad itself is suggestive of this effect.

4.4.3 Comparison of diurnal variation of TEC and N_m for different seasons and solar activity epochs

The data of Kodaikanal have been grouped into different seasons namely Equinox (March, April, September, October), Winter (November, December, January, February) and Summer (May, June, July, August) of low solar activity (1964-1966) and high solar activity (1967-69) epochs. Comparatively lesser amount of data for any individual month or year for Kodaikanal does not permit a division into 4 seasons as done for Ahmedabad or separate seasonal studies of each year. Then a scatter plot of the diurnal variation of TEC is made against time putting together all the measurements for northbound as well as southbound passes of BE-B and BE-C. The results are shown in Figure 4.13 for low solar activity period. For comparison with the diurnal variation of corresponding values of maximum electron density of F_2 region N_m is also plotted on the lower part of this diagram. TEC reaches peak values around 14 hr LT in equinox and winter of low solar activity period while the peak is delayed to about 16 hr LT in summer.

Similar results for high solar activity period are shown in Figure 4.14. In high sunspot period TEC is found to reach minimum value around 05 hr LT in all seasons. The maxima occur around 14 hr LT in equinoxes and 15 hr LT in winter and summer. The diurnal ratios are 16.8, 11.8 and 8.0 in equinox, winter and summer of low solar activity and 10.8, 10.8 and 7.6 respectively

KODAIKANAL 1967-69

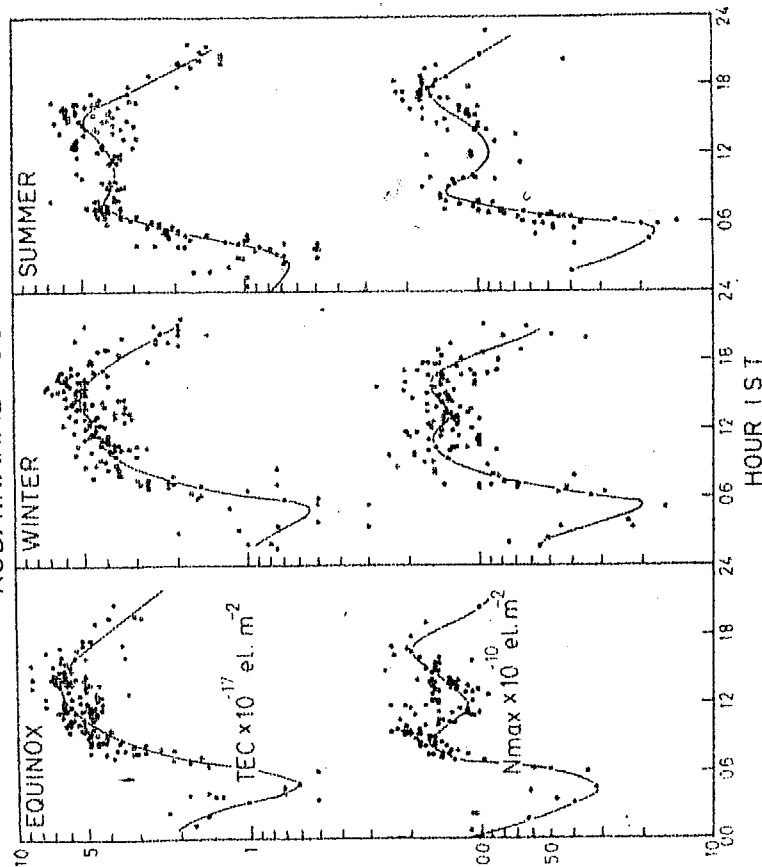


Figure 4.14 : Daily variation of TEC and N_{max} at Kodaikanal for equinox, winter and summer seasons of high solar activity period (1967-69).

KODAIKANAL 1964-66

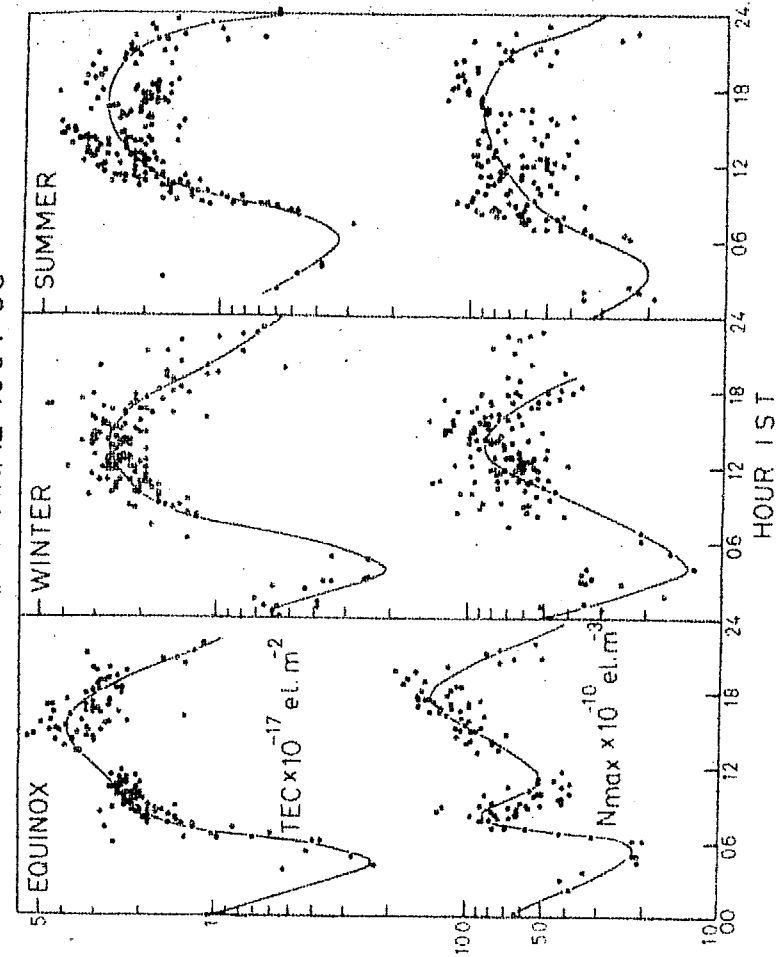


Figure 4.13 : Daily variation of TEC and N_{max} at Kodaikanal for equinox, winter and summer seasons of low solar activity period (1964-66).

in the corresponding seasons of high solar activity. Thus the diurnal ratio is seen to decrease with increasing solar activity.

It has already been seen from the diurnal curves at Thumba and Kodaikanal that TEC does not show a noon bite out on average. This is a basic difference between the daily variation of TEC at equator and at other latitudes where the variations of TEC and N_m are very similar. Here again on a seasonwise study we see that the variations of TEC and N_m are not similar at equator. Referring to Figure 4.13 equinox curves we see that although a clear bite-out is seen in N_{max} no such tendency is shown by TEC. For other seasons also, TEC does not show the noon bite-out while N_m has a tendency to show noon bite-out. It may be mentioned that the N_m points are also at the time of satellite pass and hence around noon time the measurements are relatively few in both. In the high sunspot curves of Figure 4.14 N_{max} curves in all seasons clearly indicate the noon bite-out but TEC curves again do not show except in summer where there is a slight tendency for noon bite-out in TEC. Thus on the whole the conclusion that can be drawn is that noon bite-out is absent in TEC unlike in N_{max} . There is no clear indication of a midday bite-out in TEC.

4.5 Seasonal variation of TEC

4.5.1 Seasonal variation of daytime and nighttime TEC at Ahmedabad

Having studied the diurnal variation of TEC next attempt is to study the seasonal variation of TEC. For this, the daily

maximum value of TEC lying in the time interval of 12-16 hrs LT and the daily minimum value in the interval 23-04 hrs have been separately studied. The mean value of TEC in these time windows for each month from November 1964 through 1967 have been computed. Data of Delhi and Hyderabad available for this period have also been used. In Figure 4.15 these values are plotted against months for each of these years. The daily maximum TEC shows a clear semiannual variation with maxima around April and October (Equinoxes) and minima in solstices. This trend is seen in all the years rather more conspicuously for high sunspot year 1967. The general upward trend of the curve as the solar cycle is on the progressive phase also indicates the long term solar cycle changes.

Looking at the curves of daily minimum TEC plotted in the lower part of Figure 4.15 for the years 1965, 1966 and 1967 more or less an annual trend is observed, with maximum occurring in summer and minimum in winter. It is also seen that in the winter of 1967-68 i.e. during high sunspot winter the daily maximum TEC is larger than in the corresponding summer value, thereby indicating the presence of winter anomaly in high solar activity. The absence of winter anomaly at night is also quite evident.

4.5.2 Seasonal variation of daytime and nighttime TEC at Thumba/Kodaikanal

In this section, the seasonal variation of daytime and nighttime TEC at the equatorial stations is studied. As the

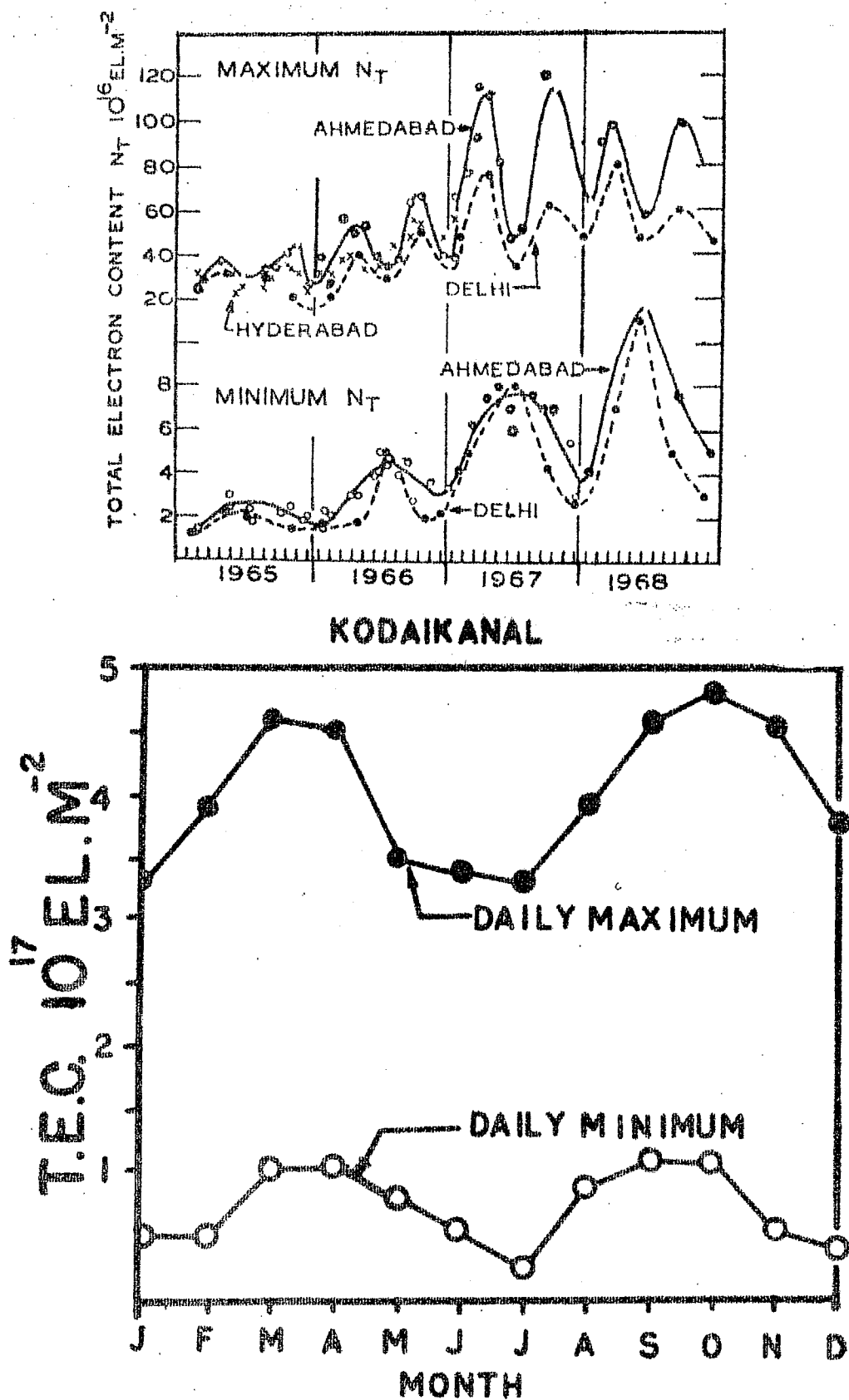


Figure 4.15 : Seasonal variation of daily maximum and daily minimum TEC at low latitudes - Hyderabad, Ahmedabad and Delhi-(top) and at equatorial station Kodaikanal (bottom).

number of observations in the time interval to be considered are not sufficient, we have put together the data from both the stations and the mean seasonal variation averaged over the years 1964 through 1969 is shown. This result is shown in Figure 4.16 where the daily maximum (between 12 and 16 hrs LT) and the daily minimum (between 23 and 05 hrs LT) are plotted separately against months. A clear semiannual wave with peaks in equinoxes and minima in solstices is seen predominantly in daytime TEC and to a lesser extent in nighttime TEC. This observation is in conformity with observations at equatorial stations in other longitudes thus establishing that semiannual variation of TEC is a permanent feature of low latitudes in all longitude sector.

4.6 Solar cycle variation of TEC

4.6.1 Variation of daily maximum and minimum TEC at Ahmedabad with solar activity

The dependence of daily maximum TEC on solar activity is investigated in this section. 10.7 cm solar radio flux has been used for measuring the level of solar activity. The data has been grouped into summer, winter, spring and autumn seasons and the variation of daily maximum and daily minimum TEC with 10.7 cm flux has been plotted separately for each season. These results are shown in Figure 4.17. A linear increase of both maximum as well as minimum TEC is seen for all the seasons with varying slopes and intercepts. Linear equations are fitted for each of these of the form $N_t = a [1 + b(\Phi - 70)]$ and the coefficients

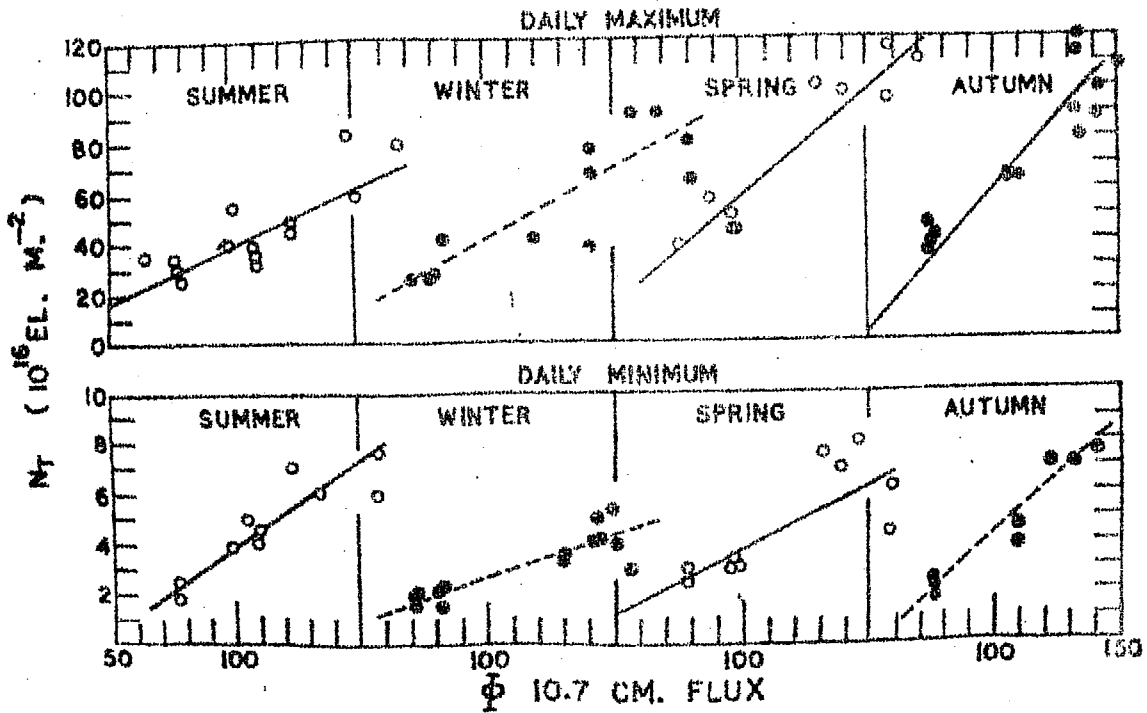


Figure 4.17 : Variation of daily maximum and daily minimum TEC (marked as NT in the figure) with 10.7 cm solar flux for the different seasons.

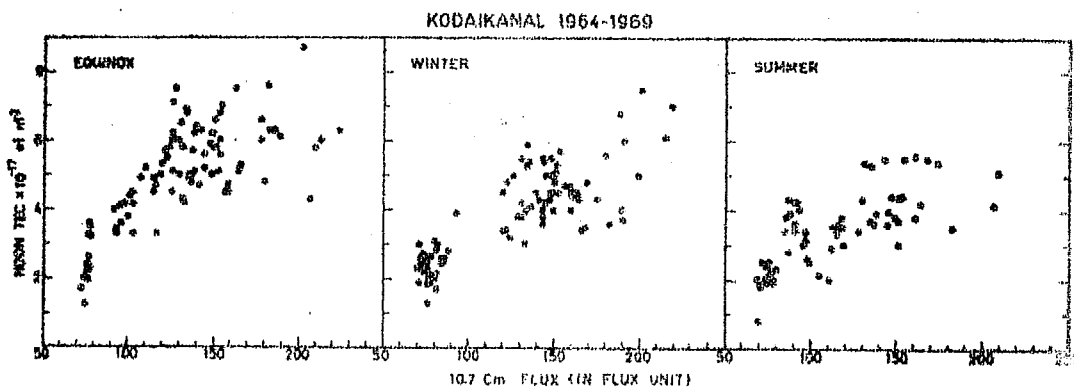


Figure 4.18 : Variation of noon TEC (11-14 hrs) at Kodaikanal with 10.7 cm solar flux.

'a' and 'b' for each season for TEC (Max.) and TEC (Min.) are given in Table 4.1. The threshold value of 70 flux units corresponds to zero sunspot number or no solar activity.

Table 4.1

Coefficients 'a' and 'b' of the variation of total electron content (N_t) with solar flux (ϕ) at Ahmedabad according to the expression:

$$N_t = a [1 + b (\phi - 70)]$$

Maximum TEC	Ahmedabad	
	a	b
Winter	20.34	0.0285
Summer	29.31	0.0175
Spring	24.52	0.0299
Autumn	24.45	0.0453
	$\times 10^{16} \text{ el/m}^2$	
Minimum TEC		
	a	b
Winter	1.68	0.0185
Spring	2.19	0.0228
Summer	1.80	0.0417
Autumn	1.56	0.0436
	$\times 10^{16} \text{ el/m}^2$	

4.6.2 Variation of TEC at Kodaikanal/Thumba with solar activity

As mentioned earlier, the data at Kodaikanal and Thumba have been combined to study the dependence of TEC on solar activity. Variation of noon TEC (averaged over 11-16 hrs LT) with 10.7 cm flux is plotted in Figure 4.18 separately for Equinox, Winter and Summer

seasons using the data over the years 1964 through 1969. A threshold of 70 flux units is again observed, above which TEC increases linearly with progress of solar flux. The slope is seen to be maximum in equinox, less in winter and still less in summer. This feature is common at Ahmedabad as well as the equatorial stations in equinoxes but the rate of increase of TEC with solar flux is least in winter at Ahmedabad. This reversed nature of winter and summer TEC's at Ahmedabad at equator is again the manifestation of winter anomaly. It may be mentioned that $\phi = 90^\circ$ corresponds to zero sunspot or the quietest period.

4.7 Equivalent slab thickness of the ionosphere

4.7.1 Diurnal variation of slab thickness at Ahmedabad

The equivalent slab thickness of the ionosphere has been defined as the ratio of the total electron content to the maximum electron density in F region. This represents the thickness the ionosphere would occupy had it been distributed at a uniform density equal to that at the peak. Physically this parameter is dependent on the neutral, ion and electron temperatures and hence on the scale height of $N(h)$ distribution. From the nearest hourly ionograms at Ahmedabad the N_{\max} value for the time of satellite pass is interpolated and this value is used to derive the slab thickness (τ). In Figure 4.19 a scatter plot of equivalent slab thickness against time for each measurement is shown, separately for the years 1964 through 1967, for different seasons. For comparison, the mean daily variation of $h_p F_2$, the height of peak ionization for a single parabolic distribution of

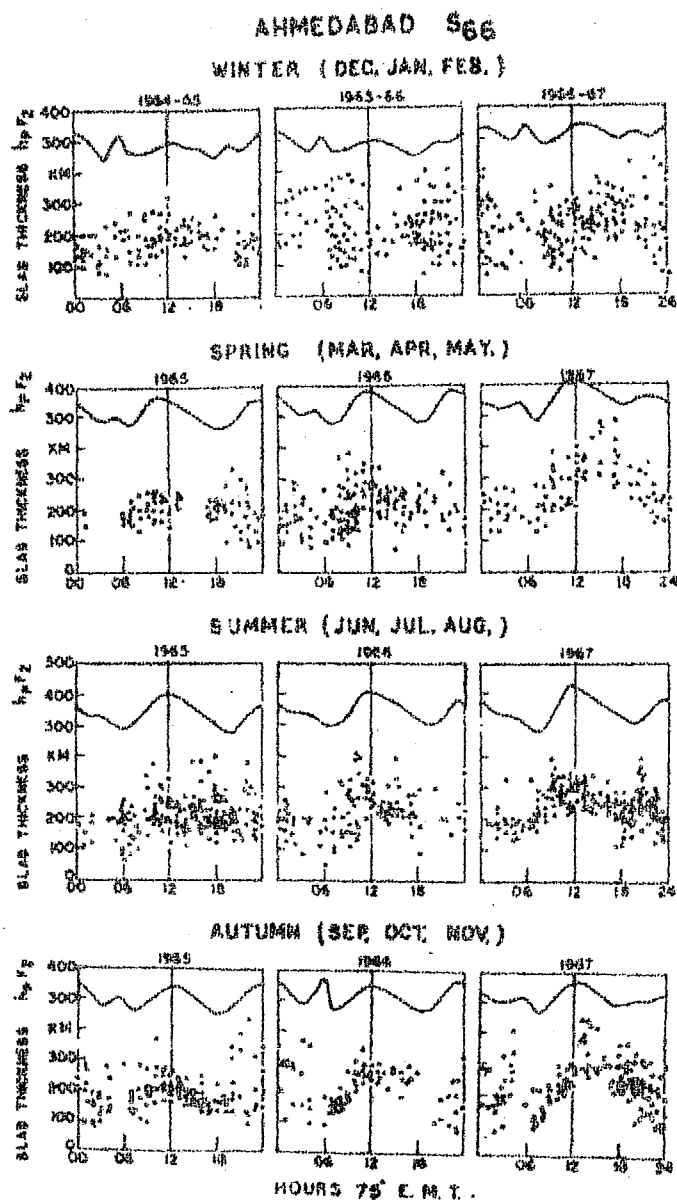


Figure 4.19 : Daily variation of slab thickness at Ahmedabad and hpF2 for different seasons from 1965 to 1967.

electron density with height, scaled from the ionograms is also shown in the upper part of the figure for the concerned season and year. Although there is some indication of a peak in τ around noon, the large scatter of points prevents any firm conclusion to be drawn.

4.7.2 Diurnal variation of slab thickness at Thumba

Slab thickness at Thumba has been calculated using Thumba TEC data and Kodaikanal ionosonde data. The values of from individual measurements are shown in Figure 4.20. The mean diurnal variation is indicated by the dashed line curve. Slab thickness at Thumba thus shows a broad maximum around 14 hr LT reaching a value as high as 500 km. There seems to be a secondary peak in τ around 01 hr LT. The afternoon peak of τ is in good agreement with the results of previous workers at other equatorial stations (Blumle 1962, Skinner 1966 and Bandopadhyay 1970). However predawn peak reported by Skinner (1966) at Zaria, by Yuen and Roelofs (1966) at Hawaii and by Bandopadhyay (1970) at Huancayo is missing at least in the average picture at Thumba.

4.7.3 Diurnal variation of slab thickness at Kodaikanal

The diurnal variation of slab thickness at Kodaikanal for the different seasons of low and high solar activity is shown in Figure 4.21. The missing points at certain early morning and night times are due to lack of data. It is seen that τ has a smooth diurnal variation with low values of about 200 km at night

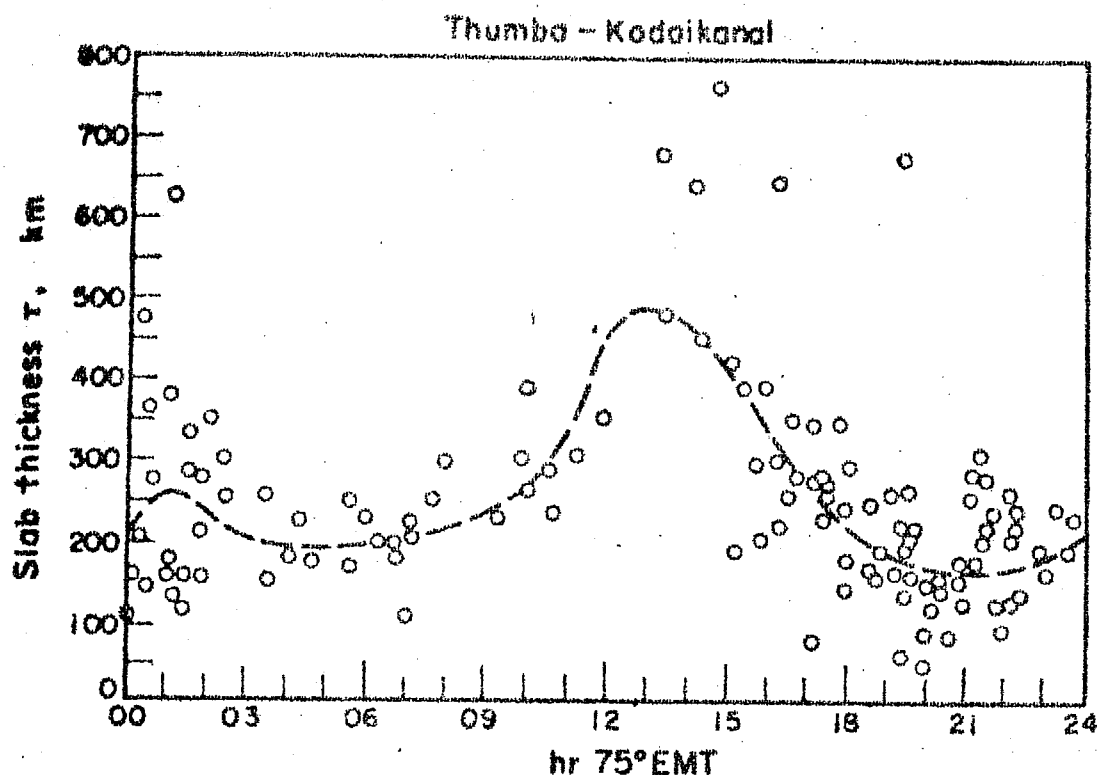


Figure 4.20 : Daily variation of slab thickness at Thumba-Kodaikanal averaged for the period 1965 through 1968.

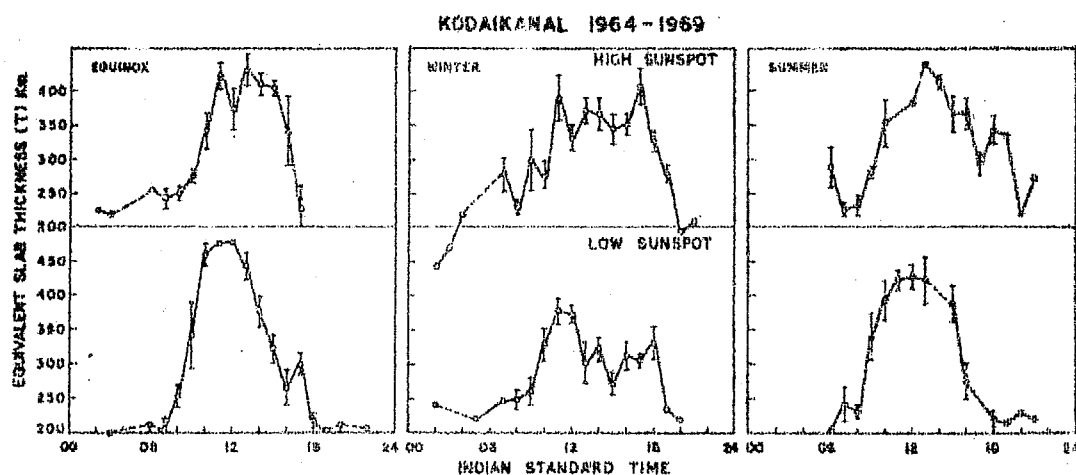


Figure 4.21 : Daily variation of slab thickness at Kodaikanal for the different seasons of low (1964-66) and high (1967-69) solar activity conditions.

and peak values around noon (11-13 hrs LT). In all seasons of both low and high solar activity the minimum τ is constant at about 200 km. The noontime peak values are 480 km, 370 km and 430 km in low sunspots and 430 km, 390 km and 430 km in high sunspots respectively for equinox, winter and summer months. Thus it is seen that there is no significant difference between low sunspot and high sunspot values of τ for equatorial stations. This is a major difference between the equatorial and tropical latitudes in the behaviour of τ . This point will be further elaborated in the study of variation of τ with solar flux.

4.7.4 Comparison of daily variation of slab thickness and $h_p F_2$

In Figure 4.19 because of the large scatter of points in the slab thickness plot it was not possible to draw a direct comparison of τ and $h_p F_2$. Therefore an alternate way of presenting the results is followed. Thus in Figure 4.22, the values of τ obtained from the mean diurnal curves of TEC and N_m are plotted against time for the different seasons. The corresponding $h_p F_2$ variation is shown in the upper part of the diagram. The full lines represent the data for 1965 and dashed line for 1967. Now a midday peak in τ is seen except in the winter of low sunspot year (1965). Further a predawn peak in τ is seen for winter and autumn seasons of the high solar activity year 1967. Similar presunrise peak in bottomside has been noted by Rastogi and Sanatani (1966). Observations at other equatorial and low latitude stations (Ross and Blumle 1963, Garriott et al. 1965, Bandopadhyay 1970 and Klobuchar and Allen 1970) also support the presence of

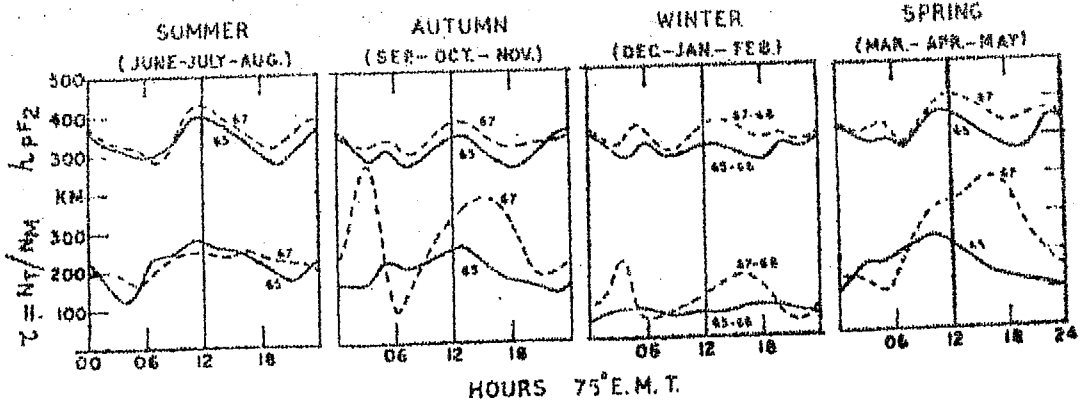


Figure 4.22 : Comparison of daily variation of mean slab thickness at Ahmedabad and hpf2 for the different seasons of low (1965) and high (1967) solar activity years.

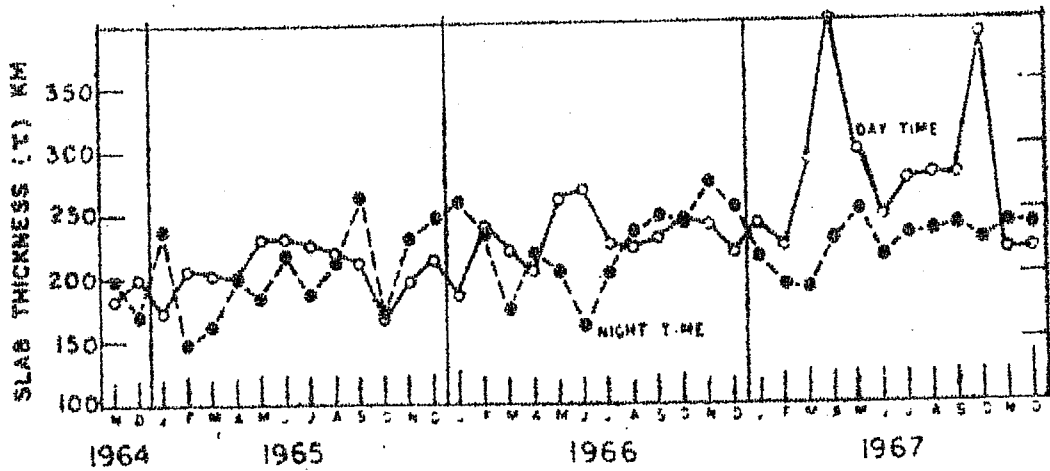


Figure 4.23 : Seasonal variation of daytime and nighttime slab thickness at Ahmedabad for the period November 1964 to December 1967.

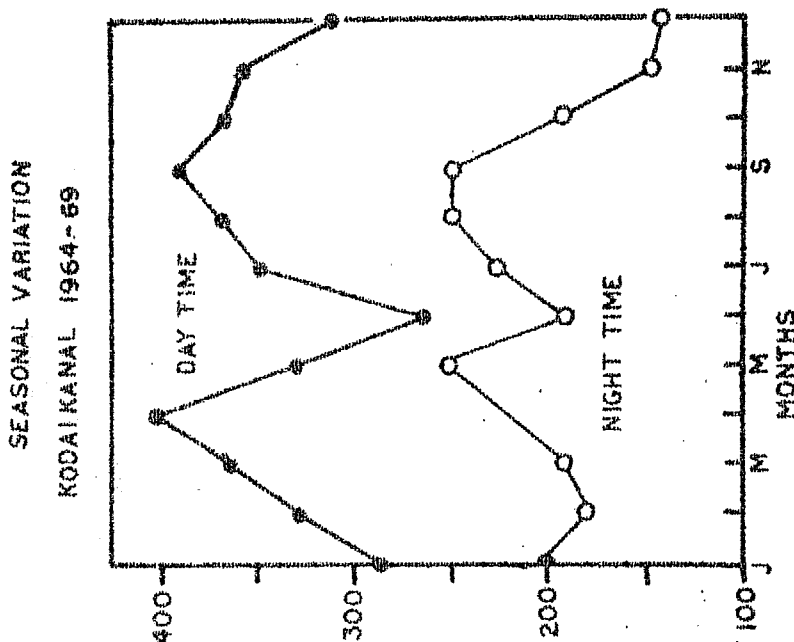


Figure 4.24 : Mean seasonal variation of daytime (filled circles) and nighttime (open circles) slab thickness at Kodaikanal averaged over the period 1964 to 1969.

predawn peak in τ which is further discussed in Section 4.9.

4.7.5 Seasonal variation of daytime and nighttime τ at Ahmedabad

The monthly mean value of τ at Ahmedabad in the time interval 11-16 hrs LT and 23-05 hrs LT have been separately plotted in Figure 4.23 against months to investigate the seasonal variation of daytime and nighttime τ . A significant semiannual component is seen for daytime τ while no such definite trend is exhibited by the nighttime slab thickness. The daytime seasonal peak is seen during equinoxes.

4.7.6 Seasonal variation of daytime and nighttime τ at Kodaikanal/Thumba

Coming to the equatorial latitudes, the seasonal variation of slab thickness is studied by combining the data of Thumba and Kodaikanal and for all the years 1964-69. The mean seasonal curves are shown in Figure 4.24. Daytime slab thickness is shown in the upper portion and nighttime value in the lower part of the diagram. It is seen that both daytime and nighttime slab thickness shows a clear semiannual variation at equatorial stations, even though a clear semiannual trend is not evident in Ahmedabad nighttime slab thickness.

4.7.7 Solar cycle variation of slab thickness at Ahmedabad

Since we have at Ahmedabad data of slab thickness for more than half a solar cycle the solar activity dependence of this parameter could be studied. 10.7 cm solar noise flux has been

chosen as an index of solar activity. The data is separated into the four seasonal groups and the variation with 10.7 cm flux is separately studied for each season for the daytime and nighttime slab thickness. The results are shown in Figure 4.25. For daytime slab thickness a linear regression line could be fitted of the form

$$\tau = a [1 + b (\Phi - 70)]$$

for all the seasons. However, for the nighttime slab thickness the scatter of points is so large as not to permit fitting of such line for Winter and Autumn. For other seasons linear increase of τ with 10.7 cm flux is seen. The coefficients 'a' and 'b' for daytime and nighttime τ are separately given in Table 4.2.

Table 4.2

Coefficients 'a' and 'b' of the variation of the equivalent slab-thickness (τ) with solar flux (Φ) at Ahmedabad according to the equation:

$$\tau = a [1 + b (\Phi - 70)]$$

Daytime		
	a	b
Winter	196	0.0023
Spring	199	0.0060
Summer	209	0.0040
Autumn	169	0.0086
	km	
Nighttime		
Winter	172	0.0065
Spring	161	0.0044
Summer	164	0.0054
Autumn	206	0.0023
	km	

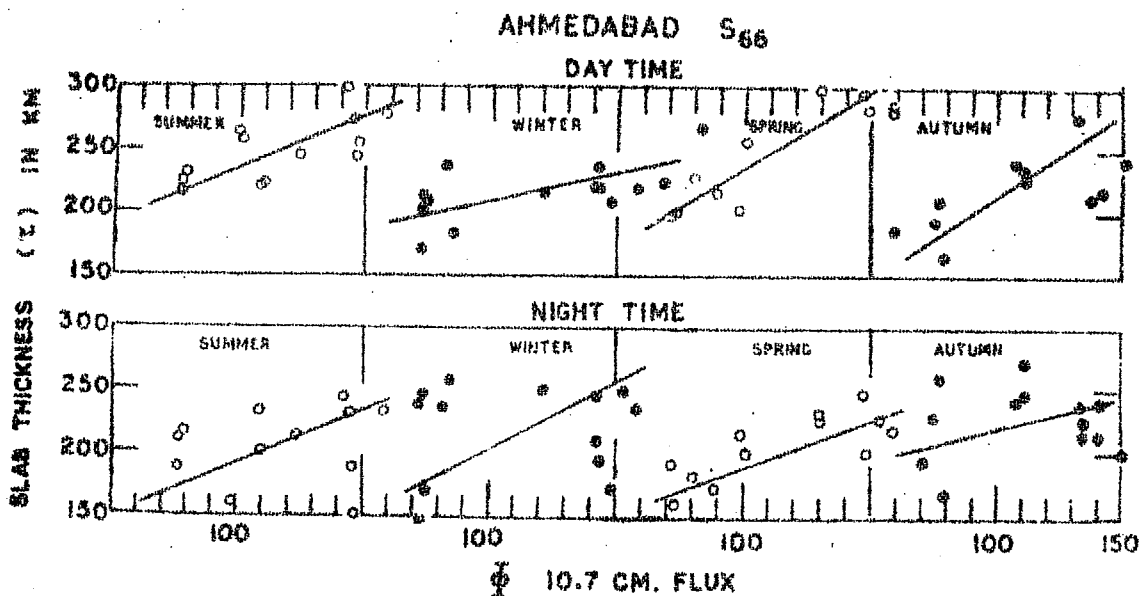


Figure 4.25 : Variation of daytime and nighttime slab thickness at Ahmedabad with 10.7 cm solar flux for different seasons.

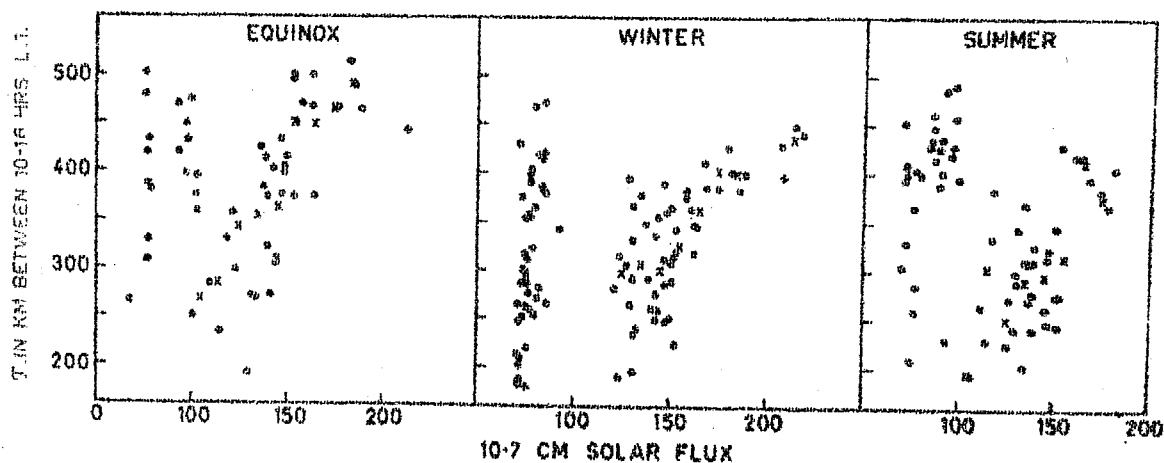


Figure 4.26 : Dependence of slab thickness (marked in figure) at Kodaikanal with 10.7 cm solar flux for different seasons.

It is seen that the daytime winter τ increases very slowly with 10.7 cm flux and the rate of increase is maximum in equinoxes.

4.7.8 Dependence of equatorial slab thickness on solar activity

Daytime values of τ for the three seasons of equinox winter and summer are separately plotted against 10.7 cm solar flux to obtain the dependence of equatorial slab thickness on solar activity. These results are represented in Figure 4.26. The scatter of points is so large that the slab thickness seems to be independent of solar activity. This is contrary to the behaviour at Ahmedabad where slab thickness was found to increase with solar flux. This means that slab thickness has different implications at equatorial latitudes as compared to tropical latitudes.

4.7.9 Distribution of $\tau / 2 Y_m$

Wright (1960) has shown that for an α Chapman layer the slab thickness $\tau = 4.13 H$, where H is the scale height of the ionizable constituent. Another parameter known as semi thickness of the layer, Y_m (used earlier in Section 4.4.1) is half the latus rectum of the parabola which is fitted to the $N(h)$ profile near the level of maximum electron density N_m is equal to $2H$. Therefore, for a Chapman layer

$$\tau / 2 Y_m = \frac{4.13 H}{4 H} = 1.03$$

In order to investigate the actual value of $\tau / 2 Y_m$ in comparison

to the theoretically expected value of 1.03, in Figure 4.27 histograms of occurrence of $\tau/2Y_m$ values are shown. It is seen that the most likely value of $\tau/2Y_m$ is approximately one; the mean value is 1.45. However there are a number of cases when the layer departs from Chapman distribution and $\tau \gg 2Y_m$ giving a large value for $\tau/2Y_m$. This means that at these times, the thickness of the theoretical parabola fitted at the N_{\max} region falls short of the mean thickness. The implications of this are discussed in Section 4.9.

4.8 Distribution of electrons above and below the peak of the ionosphere

4.8.1 Diurnal variation of N_a/N_b at Ahmedabad

The ionograms taken at the nearest time of satellite passes are subjected to true height analysis by Budden's (1954) lamination method. From this the bottomside content (N_b) or the electron content below the peak of F region is computed. Now the content below the peak is subtracted from the total electron content obtained from Faraday rotation measurements to obtain the content above the peak (N_a). Then the ratio N_a/N_b is computed for each pass and its diurnal variation at Ahmedabad is studied. This is shown in Figure 4.28 where a scatter plot of N_a/N_b against 75° EMT is made, separately for each season, for the years 1965 and 1966. No attempt is made to draw a mean line through the points because of the large scatter. However the general trend is that large values of N_a/N_b are seen during nighttime hours and low values around noon hours. This pattern is same for all the seasons.

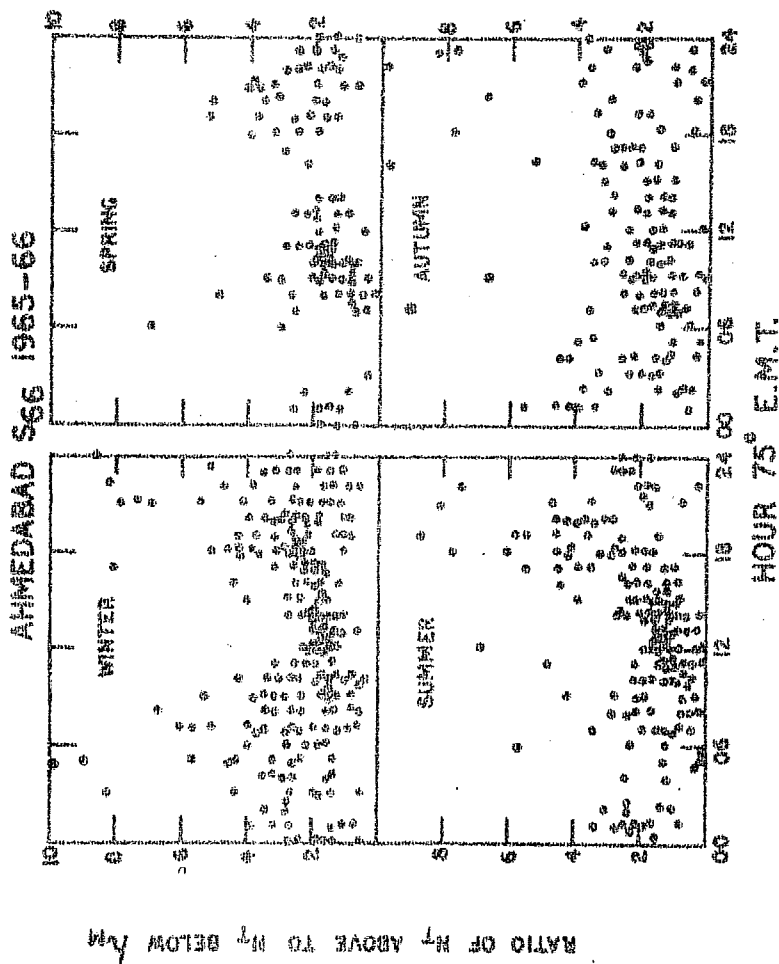


Figure 4.28 : Scatter plot of N_a/N_b ratio (N_T above to N_T below the peak H_M) at Ahmedabad with time.

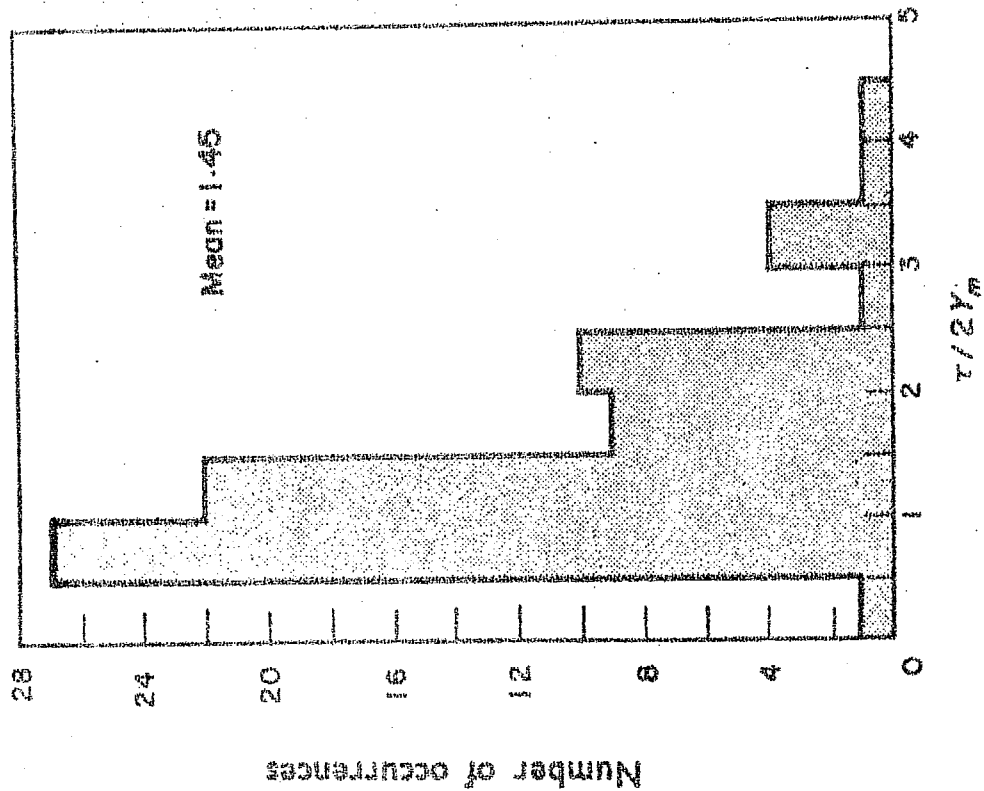


Figure 4.27 : Occurrence histogram of $\tau/2Y_m$

4.8.2 Diurnal variation of N_a/N_b at Thumba

As the available data at Thumba was not sufficient to make any seasonal studies, all the available data were combined to obtain mean diurnal variation of N_a/N_b at Thumba. This result is shown in Figure 4.29. On the top of the diagram it is indicated as Thumba - Kodaikanal to imply that the TEC data is from Thumba while the ionograms are from Kodaikanal. N_a/N_b has a maximum value of about 6 around 03 hr LT. The daytime values are constant around 1. After sunset it again increases, thereby indicating that with the ceasing of production after sunset, the layer moves up and bottom side content is decaying fast which will enhance the N_a/N_b ratio.

4.8.3 Diurnal seasonal variation of N_a/N_b at Kodaikanal

Kodaikanal data has been classified into equinox, winter and summer seasons of low and high solar activity periods as described earlier and for each pass the ionograms at nearest 15 minute interval are subjected to true height analysis to obtain N_b . Hence N_a/N_b ratio is calculated for each pass. From these data the mean N_a/N_b values for each hour are plotted against time, separately for each season. These results are shown in Figure 4.30. For any season N_a/N_b has low values between 1 and 2 in the daytime and values as high as 4 at night. Especially at low sunspot N_a/N_b shows presunrise peaks at about 04-05 hr LT and again a large peak after sunset. These peaks are not very clear at high sunspot.

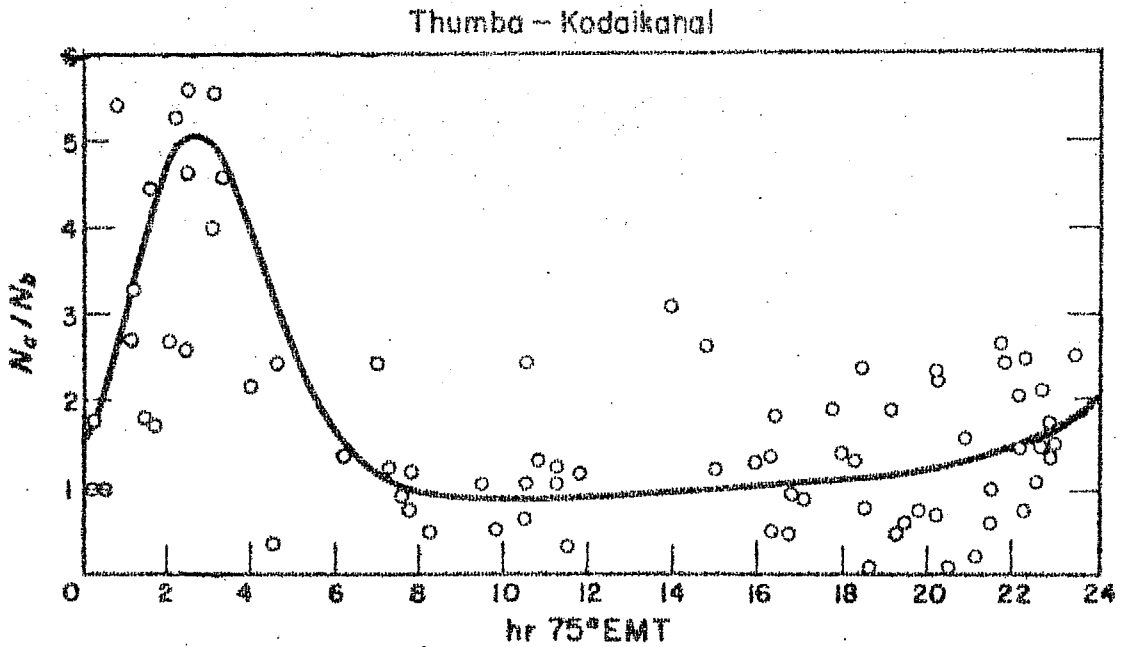


Figure 4.29 : Scatter plot of Na/Nb at Thumba - Kodaikanal with time for the period 1965 - 1968.

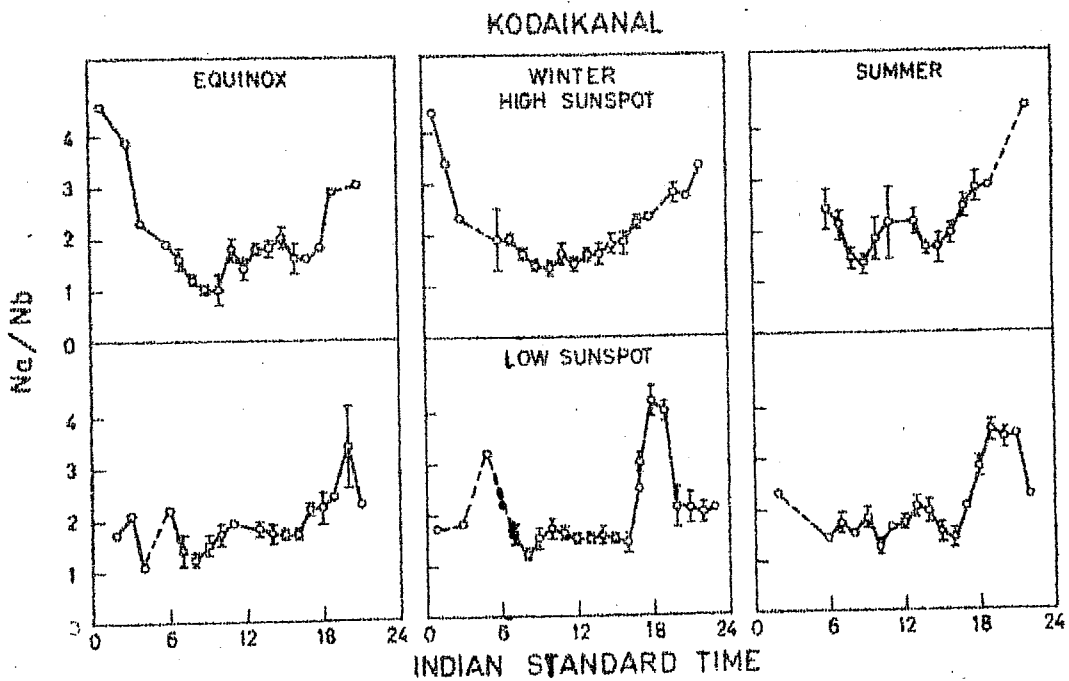


Figure 4.30 : Daily variation of Na/Nb at Kodaikanal for different seasons of low (lower part) and high (upper part) sunspot conditions.

The implications of these presunrise peak in N_a/N_b are discussed in Section 4.9.

4.8.4 Dependence of N_a/N_b on N_m

From the previous results of large values of N_a/N_b at nighttime, a dependence of N_a/N_b on N_m is sought. Also the question arises whether the changes of N_a/N_b are brought about by N_a or N_b . To investigate this point we have compared in Figure 4.31 a few typical nighttime $N(h)$ profiles obtained at Jicamarca, Peru using the incoherent back scatter technique. The different profiles are labelled and their times are indicated in the Figure. It can be seen that the topside of the profiles does not show any diurnal variation while the electron density near the peak changes considerably with time. During the early morning hours the layer moves down (profile, F, 0323 hr) and N_{max} decreases to a very low value. It is evident that the bottomside has decreased much more and hence N_a/N_b ratio increases. For the profile F at 0323 hr this ratio is calculated to be about 9 while for the profiles A at 2248 and B at 2325 it is about 5. Thus the ratio N_a/N_b attains maximum values at predawn hours when N_m and hence N_b is very low.

That N_a/N_b attains peak values at times when N_m is very low is further emphasised by the variation of N_a/N_b with N_m shown in Figure 4.32. This is derived by grouping the observed N_a/N_b into different intervals of N_m and finding the mean N_a/N_b for each group of N_m . Thus each point on the figure is a mean of a number of

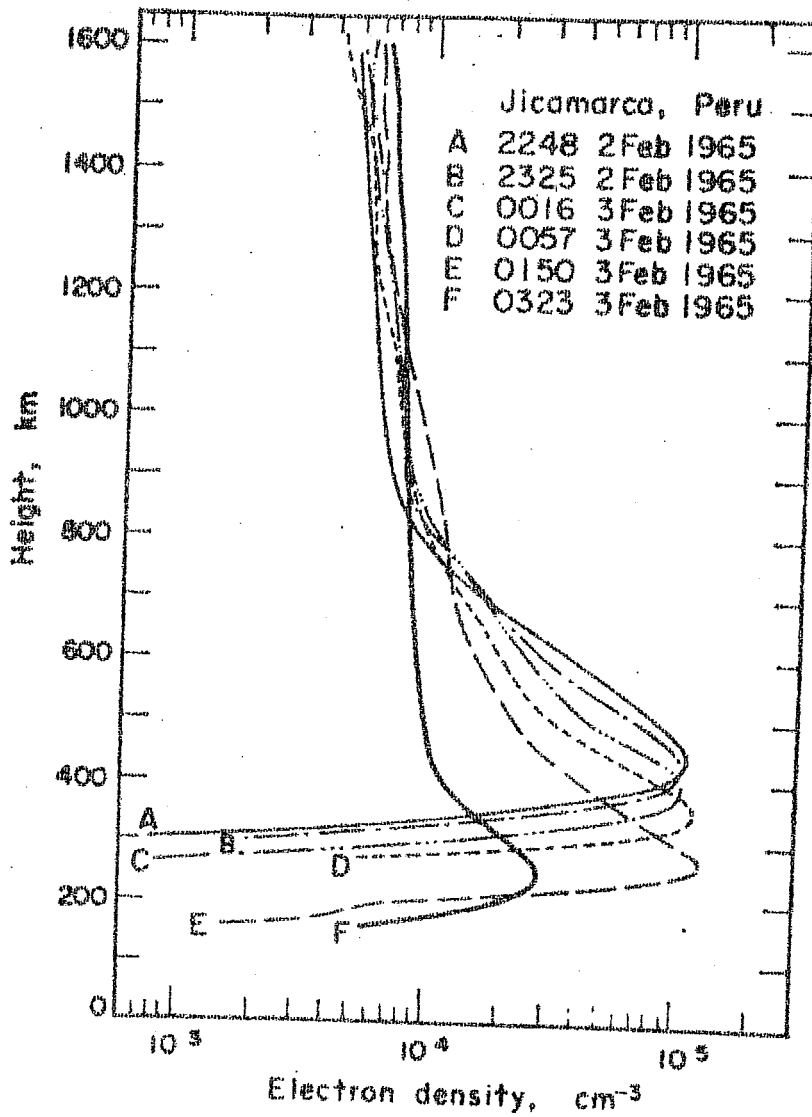


Figure 4.31 : Observed electron density profiles at Jicamarca, Peru by incoherent scatter technique on the night of 2-3 February 1965 for different hours.

KODAIKANAL 1964-66

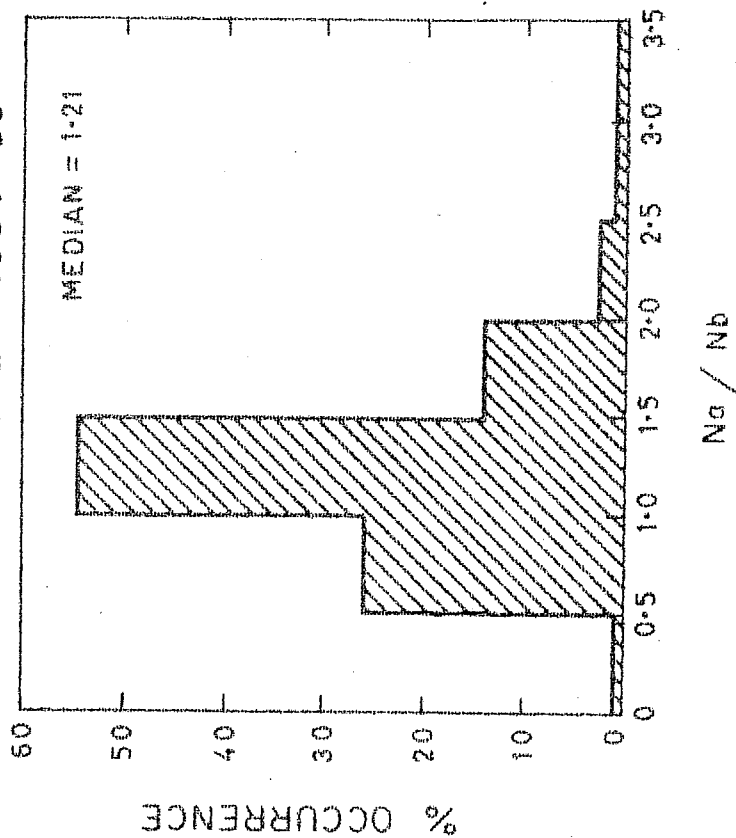


Figure 4.33 : Occurrence histogram of Na/Nb at Kodaikanal during 1964-66.

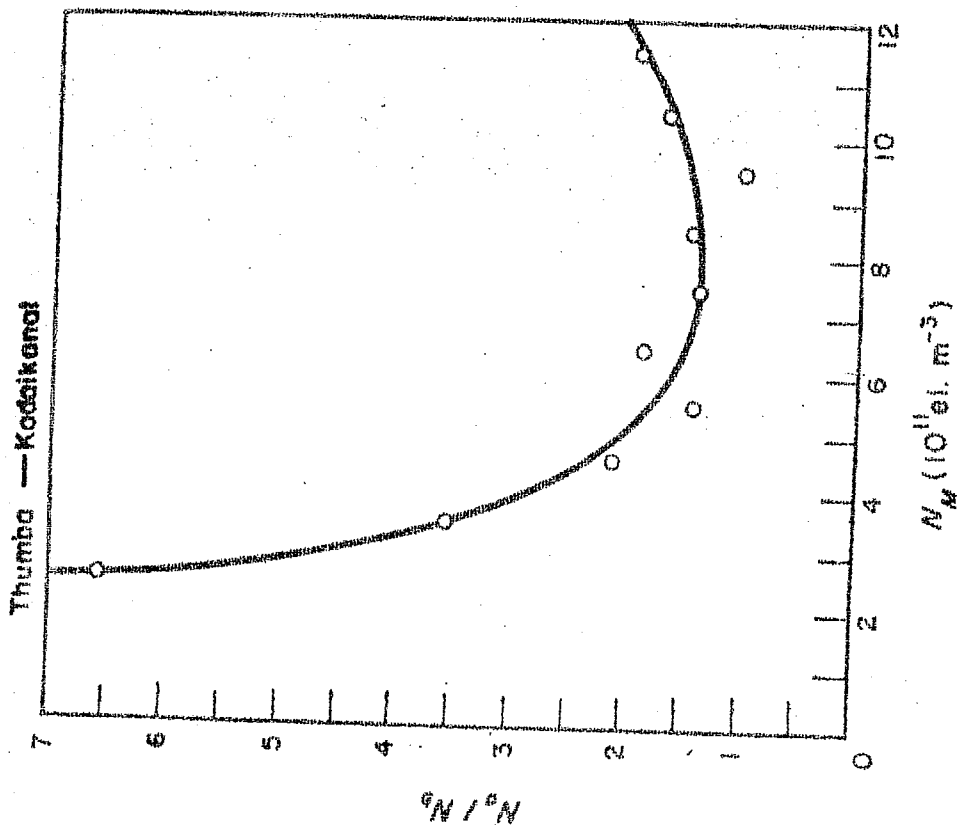


Figure 4.32 : Dependence of Na/Nb on N_w at Thumba-Kodaikanal.

observations. The figure indicates that large values of N_a/N_b are associated with very low values of N_m . However this relationship between N_a/N_b and N_m need not be unique. These low values of N_m occur at predawn hours (03-04 hrs LT). So only for this time interval this may be true.

4.8.5 Distribution of N_a/N_b

The percentage occurrence of the different values of N_a/N_b are plotted in Figure 4.33 in the form of histograms from Kodaikanal data for low sunspot years 1964-66. It is found that about 55% of the cases are in the N_a/N_b ratio range of 1.0 - 1.5 with median value of N_a/N_b as 1.21. The occurrence of large values of N_a/N_b are possible, though infrequent. The median value of 1.21 obtained for N_a/N_b is much smaller than the theoretically expected value of 2.15 (Wright 1960) for an α -Chapman layer. Thus, at most of the time Chapman distribution is not found to be satisfied.

4.9 Discussion of the results

4.9.1 Diurnal variation of TEC

The main results obtained can be summarised as follows.

At a tropical station Ahmedabad, the diurnal variation of TEC and N_m are similar to each other. At the equatorial stations, Thumba and Kodaikanal, the diurnal variation of TEC and N_m are dissimilar; the former does not show the noon bite-out shown by the later.

At this stage it is worthwhile to compare the results reported by other workers for similar latitudes. Tyagi and

Somayajulu (1966) have reported the results of Total Electron Content studies at Delhi. The diurnal variation of TEC observed by them at Delhi is similar to what is observed at Ahmedabad from the present study. They report diurnal ratio of about 7 for October-December 1964, 10 for January-March 1965 and 25 for April-June 1965. As the solar activity is not much progressed during this period these changes of diurnal ratios are attributed to mainly seasonal effects, thus showing large diurnal ratio in low sunspot years, northern summer months. Garriott and Smith (1965) report values of 30:1 for Hawaii (20°N) and 10:1 for Stanford (34°N). Other published results indicate values of 10:1 for Boulder (40°N) and 6:1 for Washington (40°N). But for Auckland (36°S) Titheridge (1973) reported a diurnal ratio of 3:1 only. Thus in southern hemisphere the diurnal ratio seems to be much reduced as compared to northern hemisphere. The very small values of diurnal ratio for northern summer months of high solar activity are corroborated by the observation of low diurnal ratios at southern winter.

Seasonal changes in diurnal ratio are brought about mainly by the changes of night time electron content. Measurement of mean rate of change of TEC after sunset indicates an integrated loss rate of $7 \times 10^{-5} \text{ sec}^{-1}$ (Titheridge, 1966). If this loss rate persisted throughout the night, the electron content would be reduced by a factor of 10 in summer and 40 in winter at mid latitudes. But this factor is very much reduced in practice through different mechanisms that contribute to maintain the night time ionosphere below 2000 kms.

(a) Vertical drifts produced by horizontal neutral winds at mid latitudes raise the ionization into a region of low loss rate.

(b) Cooling and contraction of the exosphere produce a flow of ionization down the tubes of force to enhance the ionization below 1000 km.

(c) The height of O^+ to H^+ transition level decreases at night giving rise to an increase in topside scale height. This appreciably enhances the measured TEC.

The least value of diurnal range in summer during high solar activity indicates that mechanisms (a) and (b) are most predominant at these times. Effect (c) becomes important in winter. Near the equator, the diurnal ratios are found to be larger because the horizontal magnetic field obstructs the vertical movements required in (a), (b) and (c).

As regards the diurnal variation, in particular the noon bite-out in TEC at magnetic equatorial stations there are varied findings by different workers. Measurements of TEC at Huancayo by Blumle (1962) and at Ibadan by Olatunji (1967) showed no noon bite-out. Rufenach et al. (1968) analysing Faraday rotation of 54 MHz signals from transit 4A satellites recorded at Bangkok showed that TEC monotonically increased till noon or even afternoon hours while N_m showed noon bite-out. Observation to the contrary are also available in literature. Noon bite-out in TEC was

observed by Skinner (1966) at Zaria (dip 2°N) and by Yeboah-Amankwah and Koster (1972) at Legon (dip 9.4°N). Bandopadhyay (1970) showed a dip in TEC at about 14 hr LT at Huancayo and Onwukwe (1974) observed a dip in TEC at Ibadan around 15 hr LT. Thus there seems to be evidence equally for the presence as well as absence of noon bite-out in TEC at equatorial station. In the light of these we should examine our results. Neither our mean diurnal curve for low sunspot years at Kodaikanal nor the scatter plots of TEC at Kodaikanal or Thumba show the presence of noon bite-out in TEC. But it must be noted that this cannot be interpreted as the absence of vertical uplift of ionization from the dip equator. This can be better understood from Figure 4.12 where the daily variation of TEC at Kodaikanal and Thumba are compared. The very change of slope of Kodaikanal TEC curve at about 10 hr LT and the relatively flat maximum of TEC at Kodaikanal indicates that definitely ionization is diffusing from dip equator to tropical latitudes.

The presence or absence of clear noon bite-out in TEC seems to be longitude dependent. It can be concluded that at least in Indian zone a clear noon-bite out in TEC is absent.

4.9.2 Seasonal variation of TEC

There are distinct seasonal effects in electron content behaviour. It is known that the diurnal maximum is quite flat during low solar activity winter, while in summer and equinoxes it is relatively sharp. As the solar activity progresses the

winter maximum also becomes sharper, the summer maximum becomes little flat while the equinox maximum remains sharp (Tyagi and Somayajulu 1970 and Tyagi and Mittal 1971). Thus during high sunspot years the winter values of peak electron content is larger than summer values indicating the winter anomaly (Walker 1971). Nighttime TEC remains moderately constant between 00 and 06 hr in all seasons. Daily minimum TEC shows an annual variation at all solar activity levels the maximum being in summer and minimum in winter. This has been confirmed by our observations (Rastogi and Sharma 1971) and by Somayajulu et al. (1972). The variation of daily maximum is a little complicated. For Hawaii it shows a semiannual variation in all years from 1964 through 1968. At Ahmedabad, Delhi and Hong Kong the semiannual variation is quite discernible only in high sunspot years. For the low solar activity period 1964-65 the annual component seems to predominate. It therefore seems that the annual component dominates whenever the seasonal anomaly is absent and semiannual component dominates when seasonal anomaly is present.

As regards the seasonal effects at the equator, our results are in conformity with earlier observations at other equatorial stations, Huancayo and Ibadan, viz., no seasonal anomaly is noticeable. Both daytime and nighttime TEC shows semiannual variation. At low to mid latitudes seasonal anomaly becomes evident as solar activity progresses. In southern hemisphere no seasonal anomaly is seen upto at least 34°S even during moderate to high solar activity (Titheridge and Smith 1959).

Thus it seems there is an asymmetry in regard to the presence of winter anomaly between northern and southern hemisphere. Olatunji (1967) suggested that the latitude at which winter anomaly appears is determined by its proximity to the magnetic equator rather than the geographic equator. Thus, centred on the dip equator there is a belt of latitudes in which winter anomaly is absent. Titheridge (1973a) had suggested that in northern hemisphere the annual and semiannual components may augment each other while in southern hemisphere they may cancel each other so as to have no seasonal anomaly there.

4.9.3 Slab-thickness and its implications

Diurnal, seasonal and solar cycle variations of τ have been studied at low latitudes by several authors (Bhonsle et al. 1965, Skinner 1966, Yuen and Roclofs 1967, Klobuchar and Allen 1970, Bandopadhyay 1970 and Walker and Ting 1972). Generally during daytime τ increases with solar activity and is more in summer than in winter in conformity with the present results. However Klobuchar and Allen (1970) have reported abnormal diurnal variation with nighttime value more than daytime value. Large pre sunrise peaks have also been observed by Skinner (1966) and Bandopadhyay (1970) in winter. Various theories have been advanced to explain this feature. Titheridge has discussed the dependence of τ on different ionospheric parameters and he concluded that is primarily a measure of the neutral temperature and not plasma temperature. Yeh and Flaherty (1966) have studied the dependence

of τ on T_e/T_i ratio. Furnan and Prasad (1973) have shown that τ is neither a measure of neutral temperature nor of T_e/T_i ratio. But the departures of τ from the Chapman value decided by 4.15 H is a measure of the departure from diffusive equilibrium at topside.

Coming to the theories for presunrise peaks, Bandopadhyay (1970) suggested it as due to conjugate photo-electrons from summer pole heating the winter polar ionosphere. Skinner (1966) attributed it to early sunrise above the layer peak. The presence of significant amount of H_e^+ and H^+ above the layer peak was suggested by Garriott et al. (1965). The first two mechanisms are inadequate. Chance (1972) has investigated the third possibility and found that lowering of O^+ to H^+ transition level in winter could cause significant gradients in topside plasma scale heights causing large values of τ before sunrise. Scale height gradients of 0.36 km/km in winter and 0.2 km/km were computed at 04 hr LT. The transition level is lowered to 670 km in winter from 870 km in summer.

The above mechanisms would imply that the topside content is increasing to give large values of τ at presunrise hours. But our studies of τ and N_a/N_b at Thumba indicate that the topside content does not change much with time, and hence most of the changes of τ and N_a/N_b are brought about by changes of bottomside content. Thus we suggest that the very fast decay of bottomside electron density at the predawn hours reduces the

values of N_b and N_m very much at these hours, thus producing the presunrise peaks in τ and N_a/N_b .

Thus, the changes of N_a/N_b are brought about by changes of N_b . Model calculations using different models such as Chapman model and diffusive equilibrium model for topside show that none of the theoretical values coincide with experimental values. The disparity also could be by the contribution of E and F_1 regions into the measured TEC which are not taken care of by Chapman model.

C H A P T E R - V

LATITUDINAL VARIATION OF TOTAL ELECTRON CONTENT AND SLAB THICKNESS IN INDIAN ZONE

5.1 Introduction

Low orbiting satellites at an altitude of about 1000 km offer a powerful tool to study, within a very short duration, the spatial variation of F region ionization. Measurement of Faraday rotation of VHF signals from such satellites enables one to study the spatial distribution of Total Electron Content. From a single observing station about $\pm 10^\circ$ of latitude can be studied about the observing station using this technique with reasonably good accuracy. Latitudinal variation of Total electron content has been studied by Basu and Das Gupta (1968), Titheridge and Smith (1968), de Mendonca et al (1969) Golton and Walker (1971) and Rastogi et al. (1973, 1975) in the equatorial and low latitudes using Faraday Rotation of VHF signals from the satellites BE-B and BE-C. The results of joined observations at Singapore (dip 18°S), Bangkok (dip 13°N) and Hong Kong (dip 30.5°N), all in the same longitude sector have indicated a distinct trough of TEC near the dip equator, and crests at $\pm 30^\circ$ dip (Rufenach et al. 1968). Thus the above referred studies clearly indicate the existence of the equatorial anomaly in TEC similar to the one in f_oF_2 , in its latitudinal variation. de Mendonca et al (1969) have derived contours of TEC in the southern hemisphere low

latitudes which also indicates the equatorial anomaly in TEC.

Dumford (1967) obtained a positive correlation between E region current system near the magnetic equator and equatorial anomaly using topside sounder data. MacDonal (1969) and Rastogi and Rajaram (1971) using f_oF_2 values near the magnetic equator have given evidence that the equatorial anomaly shows high correlation with electrojet strength and poor correlation with S_q current strength. Rush and Richmond (1973) have obtained positive correlation between several parameters characterizing the equatorial anomaly in f_oF_2 and electrojet strength. As for the equatorial anomaly in TEC is concerned geomagnetic control of this anomaly has been studied by Das Gupta and Basu (1971). Influence of solar flux and equatorial electrojet on the diurnal development of equatorial anomaly in TEC was investigated by Walker and Ma (1972). It must be noted that the above two investigations are from a single station near the peak of the equatorial anomaly and hence a complete coverage of the anomaly region from dip equator to and beyond the anomaly crest is not obtained. Studies of TEC in Indian equatorial region by Rastogi et al. (1973,1975) have shown that the latitudinal anomaly in TEC is present while the diurnal anomaly in TEC is absent. This led us to a detailed investigation of latitudinal distribution of TEC and slab thickness in the Indian zone combining the observations taken at Kodaikanal and Ahmedabad during the period 1964-1969.

The latitudinal variation of TEC, f_oF_2 , and slab thickness are presented in this Chapter. Also the equatorial electrojet control of the development of equatorial anomaly is presented in this chapter.

5.2 Latitudinal variation of TEC

5.2.1 Combined observation of TEC from two stations

From a single observing station TEC can be measured over a latitude range of $\pm 10^\circ$ about the station. Thus if we have the data from two stations Ahmedabad (dip 34°N) and Kodaikanal (dip 3.4°N) we can have a large latitudinal coverage. Further more, in the intervening region between the two stations an overlapping zone, where observations can be simultaneously had from both the stations is available. In this overlapping zone, the values of TEC obtained from both the stations can be matched reasonably well. In order to show the range of observations covered, in Figure 5.1 the contours of constant satellite zenith angles as seen from Ahmedabad and Kodaikanal are shown. The full line contours refer to Ahmedabad and dashed line contours to Kodaikanal. For instance, if the satellite is any where on the full line circle labelled $\chi = 60^\circ$ it will be visible from Ahmedabad at a zenith angle of 60° or elevation of 30° . Thus we can see that there is a reasonably large overlapping zone in between. Two typical sub-satellite trajectories of the satellite BE-B are also shown in the figure. The line joining the open circle points is the

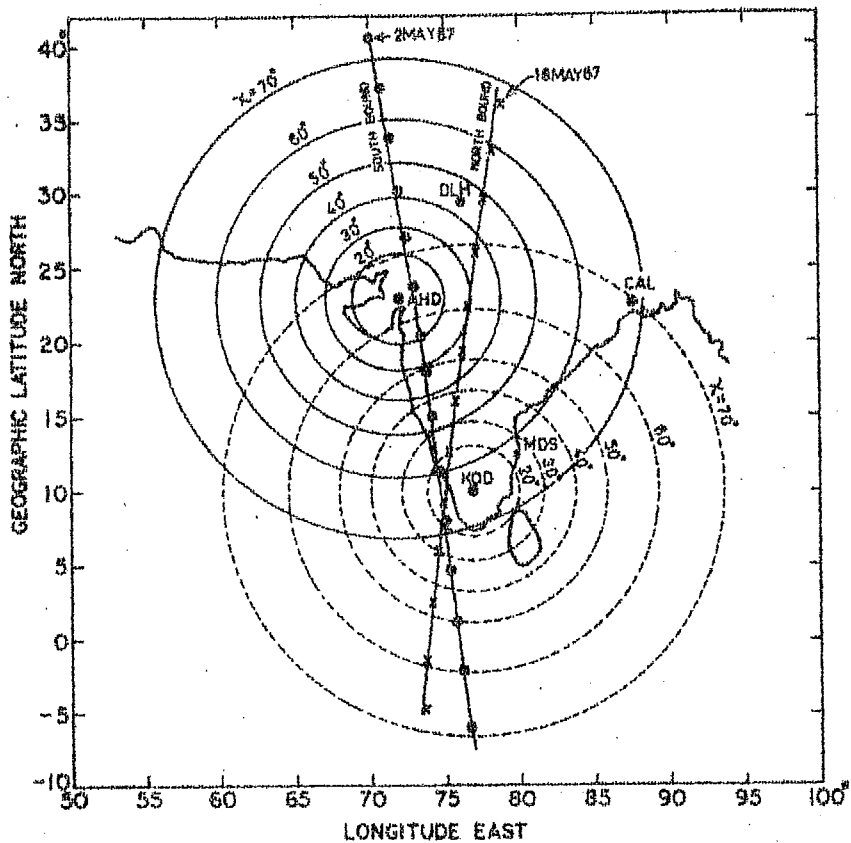


Figure 5.1 : Contours of constant zenith angle for a satellite at 1000 km altitude as observed from Ahmedabad (full lines) and Kodaikanal (dashed lines). Two typical sub-satellite tracks for 18 May 1967 (Northbound) and 2 May 1967 (Southbound) for satellite BH-B are also shown to indicate the region of coverage when observed from both the stations.

sub-satellite track for a southbound pass on 2 May 1967 and the crosses refer to a northbound pass on 18 May 1967. We can see that latitudes right from the geographic equator to 35°N are covered by the southbound pass on 2 May 1967 with zenith angles less than 60° . Thus from the combined observations of Ahmedabad and Kodaikanal the whole equatorial anomaly belt can be investigated.

Some of the typical latitudinal plots of TEC are shown in Figure 5.2. In these plots the filled circles are observations from Kodaikanal and the open circles are observations from Ahmedabad. We can see that there is good agreement between the TEC values obtained in the overlapping zone on the latitudinal plot on 16-11-1965. A clear latitudinal anomaly is seen on these plots taken around noon time. Also we see that from day to day there is variability in the position and strength of the latitudinal peak in TEC.

5.2.2 Absence of equatorial anomaly in the diurnal variation of TEC

In Section 4.4.2 the diurnal variation of TEC was compared at the equatorial station Kodaikanal (dip 3.4°N) and the station near the crest of equatorial anomaly, viz., Ahmedabad (dip 34°N). It was seen that no noon bite-out or diurnal anomaly in TEC was observed in the diurnal plot of TEC at Kodaikanal. For convenience Figure 4.12 is again reproduced in this section as Figure 5.3. Comparing the diurnal curves in Figure 5.3 for Kodaikanal and Ahmedabad we see that there is a definite extra

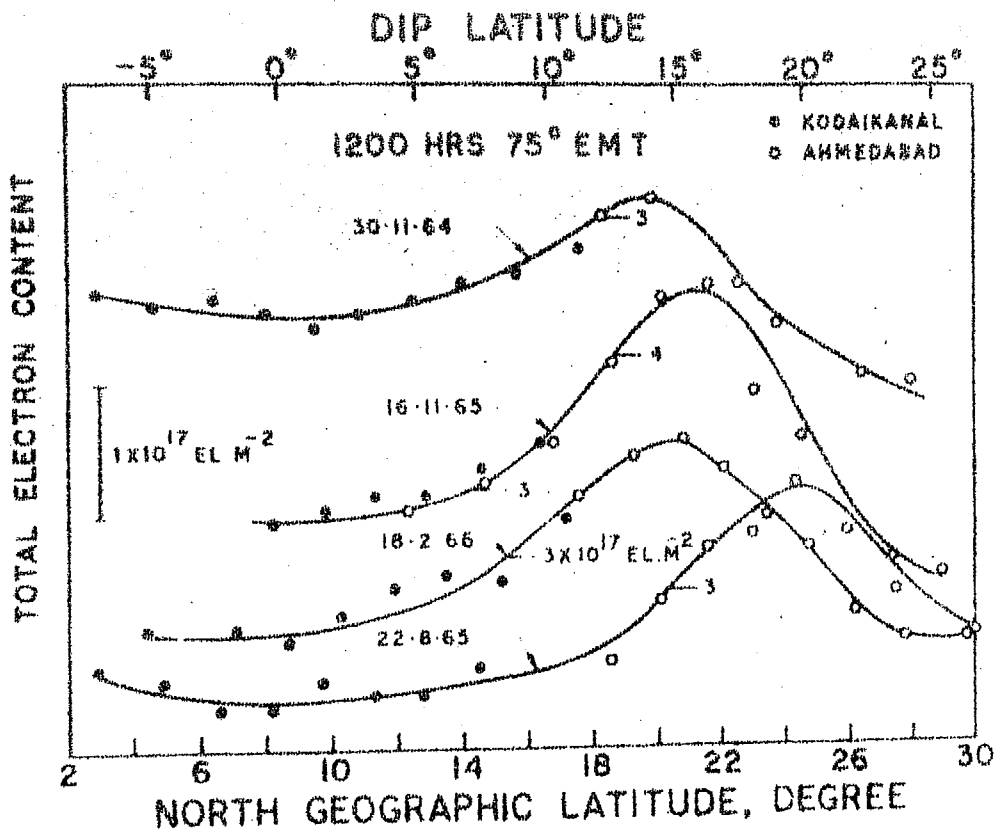


Figure 5.2 : Typical latitudinal profiles of TEC near noon indicating the equatorial anomaly in TEC in its latitudinal variation.

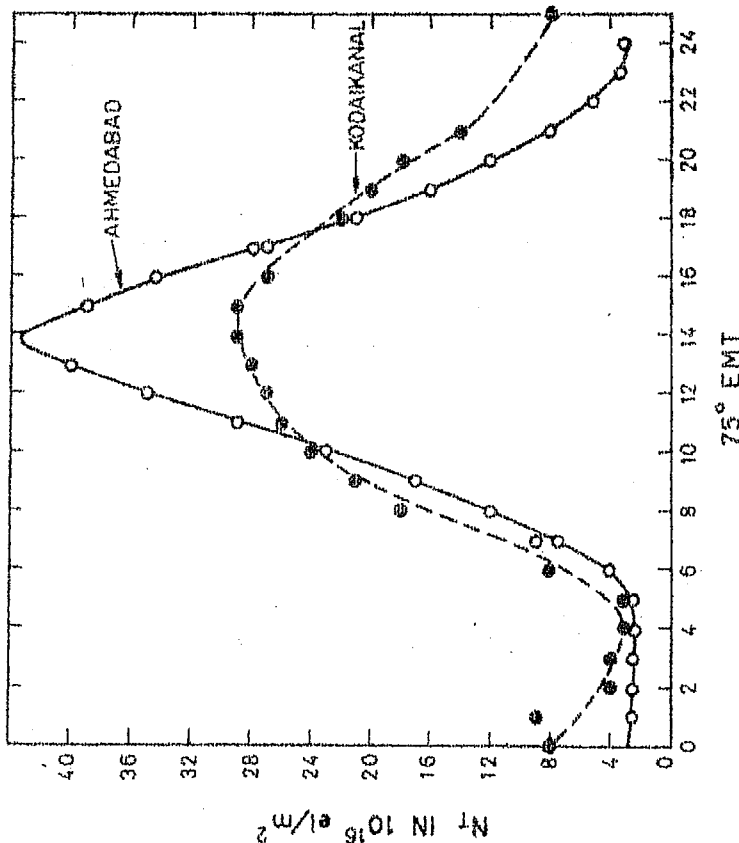


Figure 5.3 : Daily variation of TEC (marked as NP in the figure) at Ahmedabad compared with that at Kodaikanal. Note the extra ionization at Ahmedabad between 11 and 16 hrs.

ionization at Ahmedabad as compared to Kodaikanal. This extra ionization cannot be accounted for by increased production at Ahmedabad although the part played by neutral density anomaly (Hedin and Mayr 1973) cannot be ruled out. The difference in area between the two curves between 10 hr and 18 hr LT is indication of the influx of ionization at Ahmedabad by diffusion from dip equator. Thus the presence of the latitudinal anomaly in TEC is established and further investigations of the latitudinal variation of TEC is presented in the next section by combining the observations from Kodaikanal and Ahmedabad.

5.2.3 Contours of total electron content in equinoxes

For passes having more than 30° maximum elevation, at every minute during the pass, the total electron content corresponding to the sub-ionospheric point is computed using the single frequency total rotations formula. The passes of BE-B satellite whose orbital inclination was 79.69° only are used for this study to eliminate any local time variation during the pass. A fixed height of 1000 km is chosen throughout the analysis. The ionospheric height for the computation of \bar{M} is taken as 400 km for Kodaikanal and 350 km for Ahmedabad. Combining the data from Ahmedabad and Kodaikanal latitudinal profiles of TEC from 10°S to 25°N dip latitude are obtained. Care is taken to see that in the overlapping region the data from the two stations are matched reasonably well. Wherever the QT point is not clearly identifiable the closely spaced frequency method using 40 and 41

MHz is employed.

The data are then grouped into low (1964-66) and high (1967-69) sunspot epochs. Each epoch is again classified into Winter (November, December, January, February), Summer (May, June, July, August) and Equinoxes (March, April, September, October) seasons. For each season TEC values from passes around each full hour of LT (e.g. passes between 0731 to 0830 LT being taken as 0800 LT) are averaged out for every two degrees of latitude from 0° to 30° N geographic latitude. Any pass with abnormal variation of TEC was discarded from the analysis. No attempt is made to distinguish between quiet and disturbed days. Thus a mean latitudinal profile for each hour of each season for low and high solar activity periods is obtained. These TEC values at every two degrees of latitude are plotted against local time and contours of constant electron content are derived for each season of low and high solar activity. These are shown in Figures 5.4 through 5.6 for equinox, winter and summer respectively. On the lefthand side the contours for low solar activity and on the right handside those for high solar activity are plotted in these figures. Referring to the contours in equinox (Figure 5.4) the latitudinal peak is centred around 15° N dip latitude in low sunspot years while the peak is shifted to about 20° N in high sunspot years. The peak TEC in high sunspot years is 1.8 times that in low sunspot years. Diurnally, the peak is formed between 13-14 hrs LT in both high and low solar activity epochs.

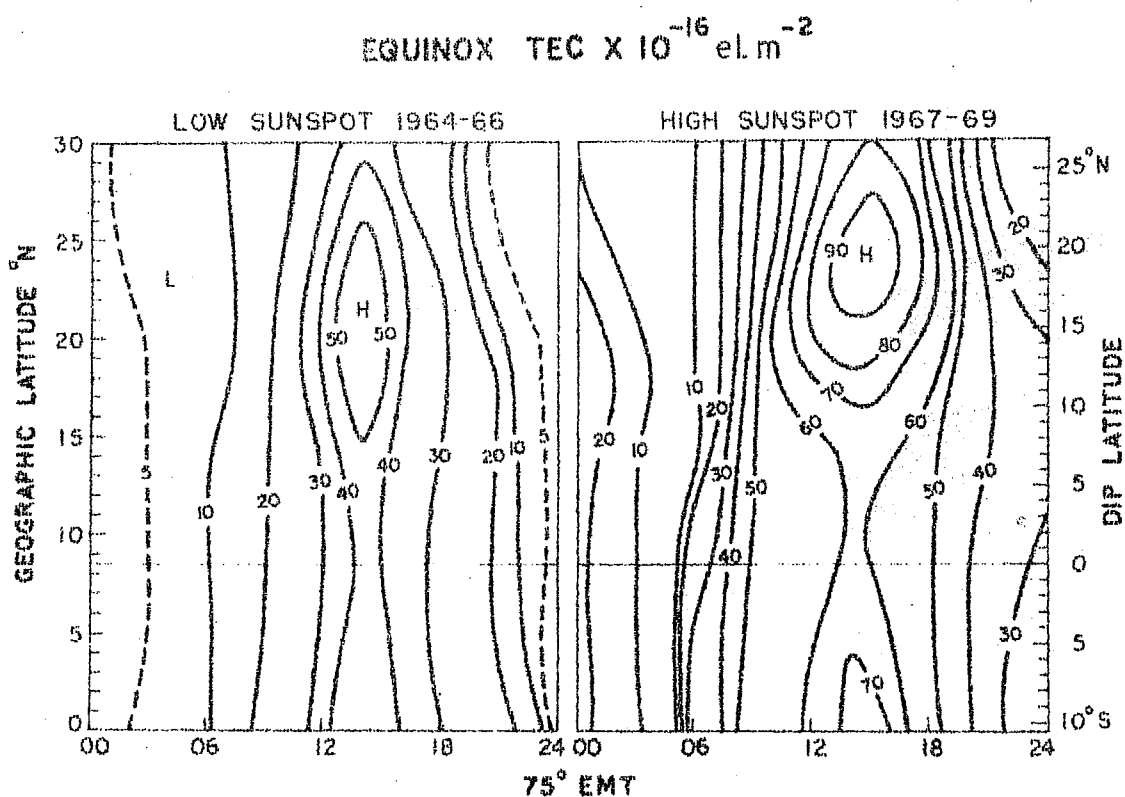


Figure 5.4 : Contours of TEC on a grid of time vs. latitude during equinox season of low (1964-66) and high (1967-69) solar activity epochs.

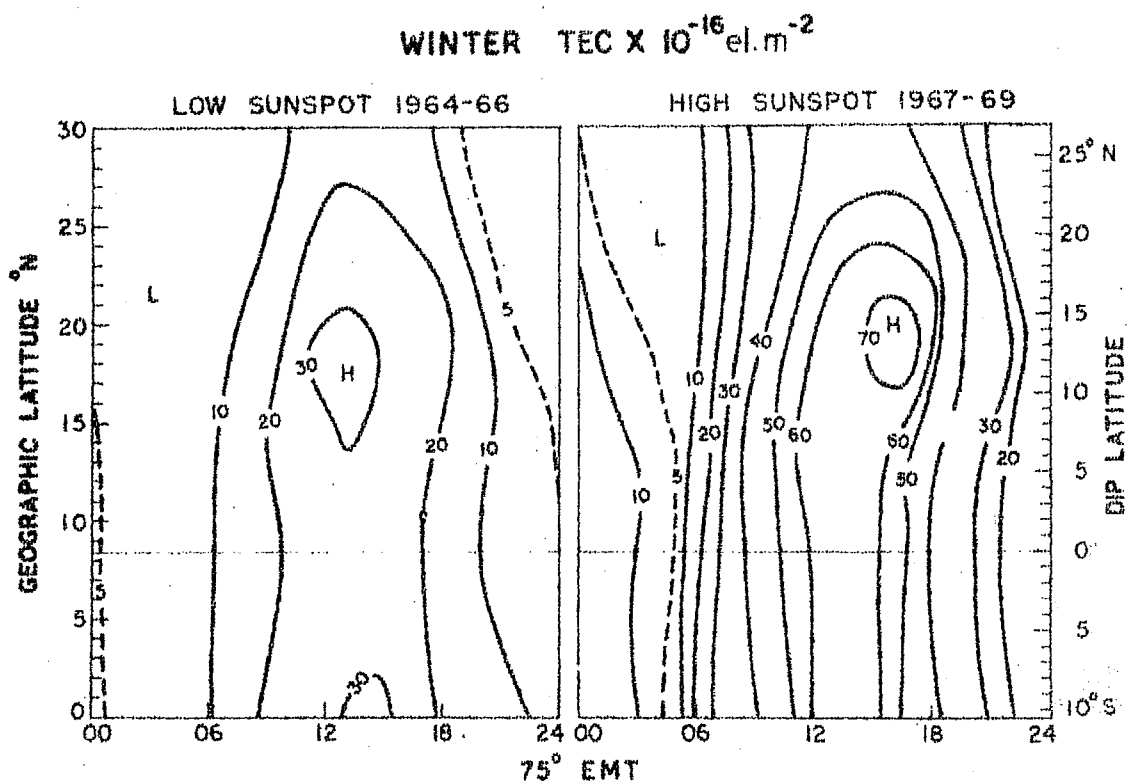


Figure 5.5 : Contours of TEC on a grid of time vs. latitude during winter season of low (1964-66) and high (1967-69) solar activity epochs.

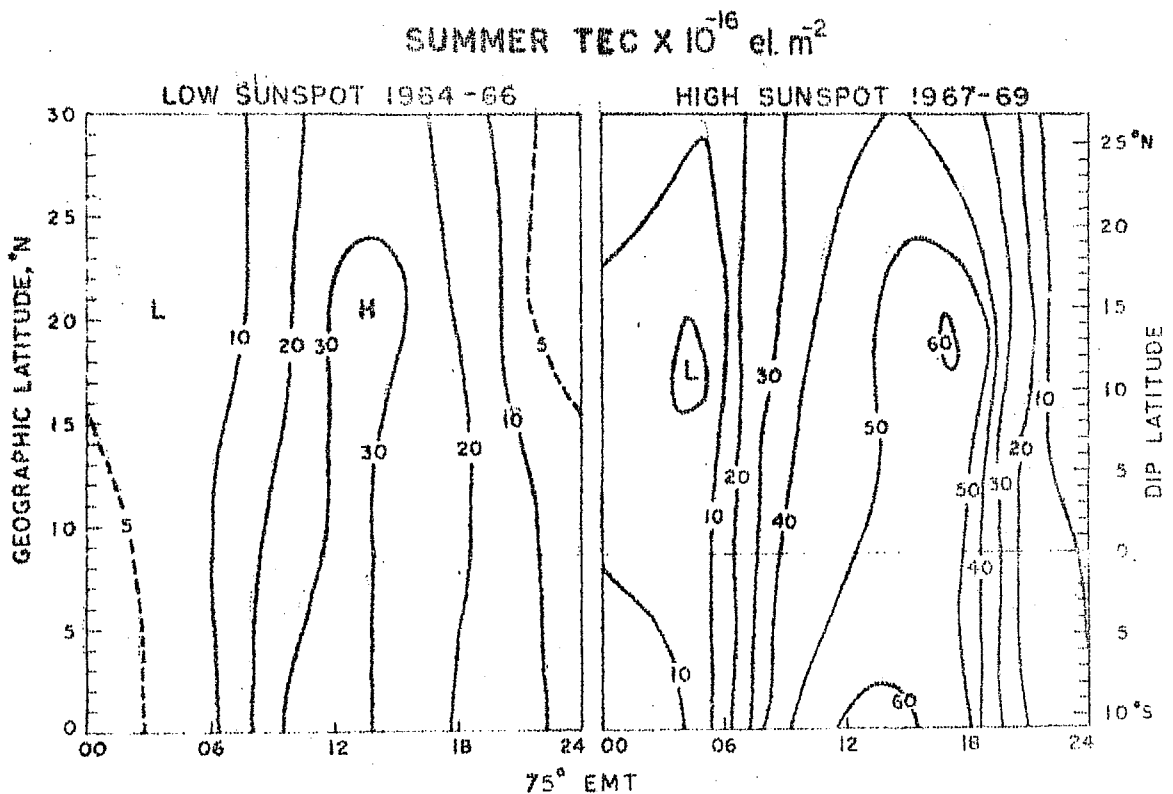


Figure 5.6 : Contours of TEC on a grid of time vs. latitude during summer season of low (1964-66) and high (1967-69) solar activity epochs.

5.2.4 Contours of TEC in winter

In Figure 5.5, the winter contours show peak TEC almost at the same dip latitude of 12°N in low and high sunspot years. While the diurnal peak is around 13 hr LT during low sunspot, it is delayed to 15-16 hr in high sunspot years. High sunspot winter TEC values are more than double that of low sunspot years.

5.2.5 Contours of TEC in summer

The summer contours in Figure 5.6 show that the latitudinal peak is broadened in low sunspot years compared to that in high sunspot years. The peak is formed around $12-13^{\circ}\text{N}$ dip latitude in both epochs. The diurnal peak develops earlier in low sunspots (13 hr LT) while it is delayed to 16-17 hr LT in high sunspot years. The high sunspot peak TEC is double that of low sunspot years.

5.3 Comparison of latitudinal variation of TEC and f_oF_2

5.3.1 Contours of f_oF_2 in equinoxes

In order to compare the latitudinal variation of TEC and N_{max} , the contours of f_oF_2 derived by Sanatani (1968) are reproduced here in Figures 5.7 through 5.9 for similar solar activity periods and corresponding seasons. The equinox contours in Figure 5.7 show peak values of f_oF_2 around 16°N dip latitude in low and high sunspot periods. Diurnally, the peaks are formed around 15-16 hr LT in both epochs. Thus there is a time

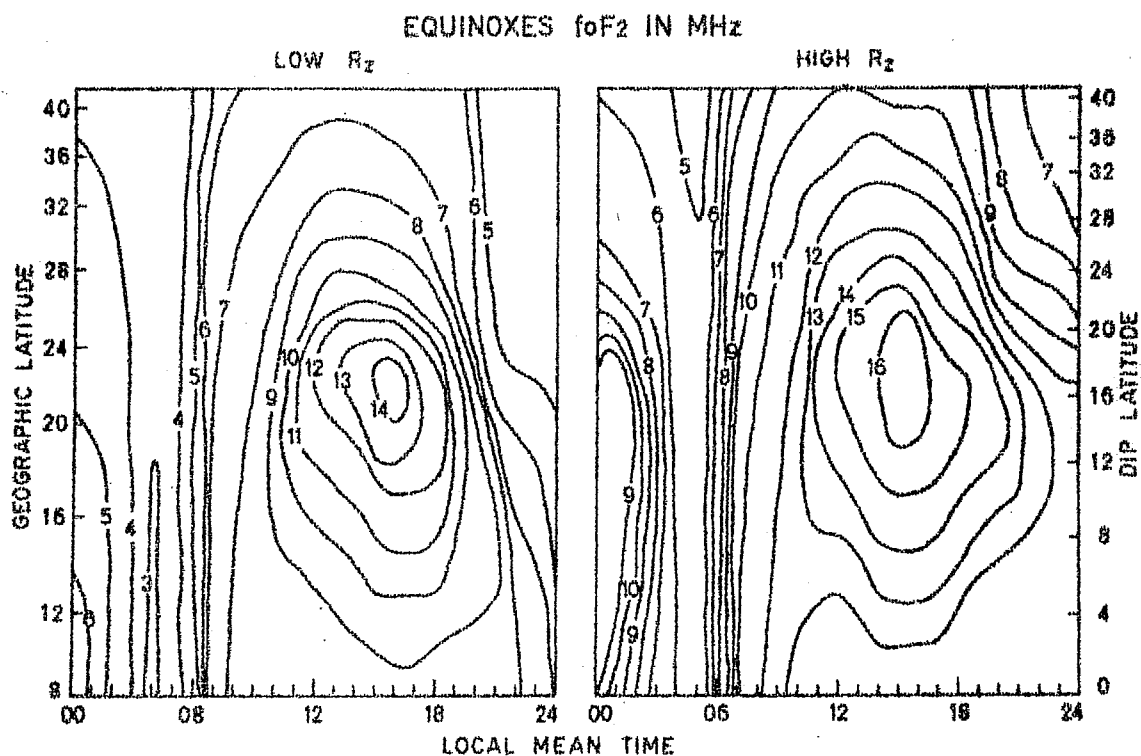


Figure 5.7 : Contours of foF2 on a grid of local time vs. dip latitude for equinox season for low and high solar activity conditions.

WINTER 10E2 IN MHz

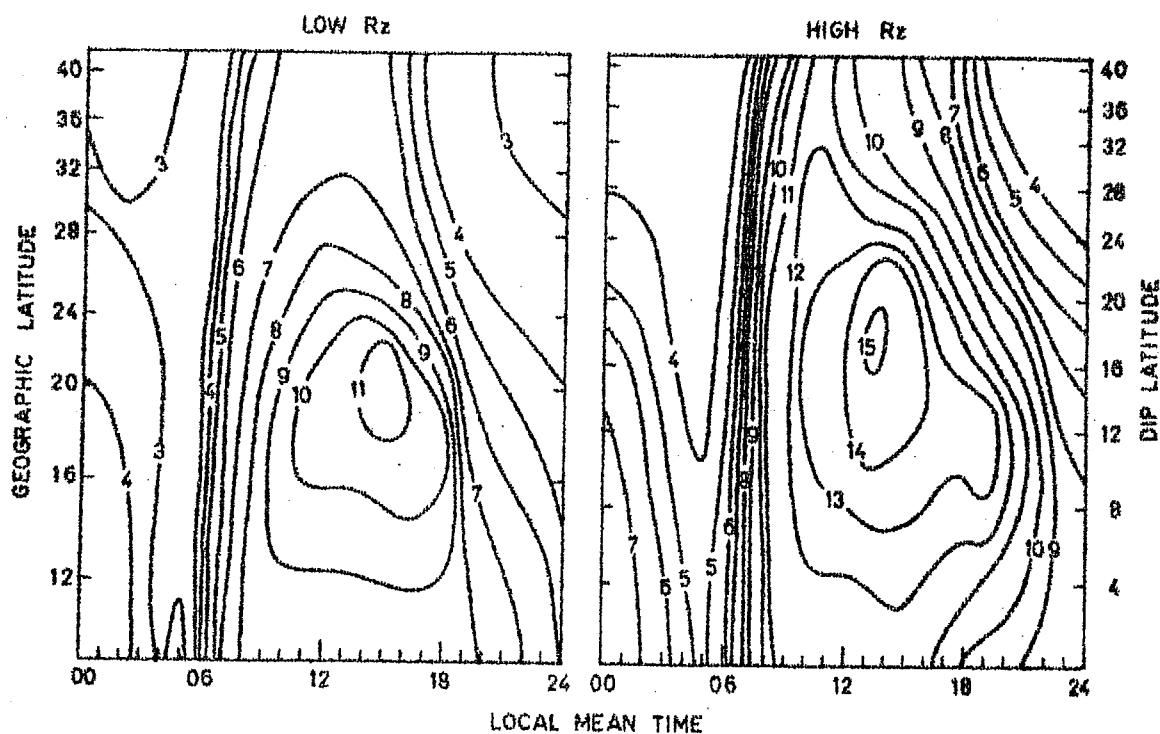


Figure 5.8 : Contours of f_oF_2 on a grid of local time vs. dip latitude for winter season for low and high solar activity conditions.

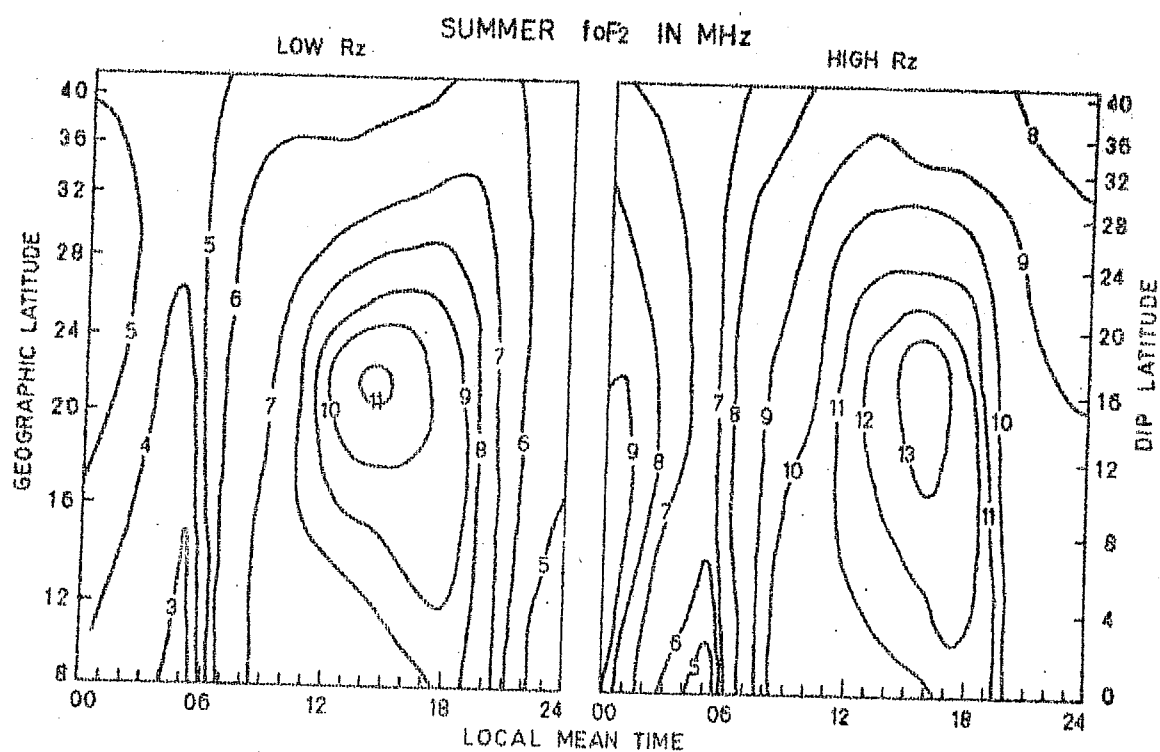


Figure 5.9 : Contours of f_oF_2 on a grid of local time vs. dip latitude for summer season for low and high solar activity conditions.

lag of about 2 hrs in the diurnal development of the equatorial anomaly in f_oF_2 compared to that in TEC in low sunspot years. However, in high sunspot years they develop almost at the same time.

5.3.2 Contours of foF2 in winter

Figure 5.8 shows the winter contours of f_oF_2 . The latitudinal peak occurs at about 14° and 18° dip latitude respectively in low and high sunspot years. The peak develops earlier in high sunspot years (13-14 hr LT) as compared to low sunspot years (15-16 hr LT).

5.3.3 Contours of foF2 in summer

Contours of f_oF_2 for summer months are shown in Figure 5.9. Peak f_oF_2 occurs around 16° dip latitude in low and high sunspot years and around 14-15 hr LT in low and 15-16 hr LT in high sunspot years.

Thus the general features of the latitudinal variation of TEC and f_oF_2 are more or less similar. The obvious difference is that TEC maximises 1-2 hrs earlier in low sunspot years than N_{\max} .

5.4 Latitudinal diurnal variation of peak TEC

To bring out the latitudinal variation of TEC in the different seasons more clearly TEC at the time of diurnal peak is plotted against latitude in Figure 5.10 for low and high solar

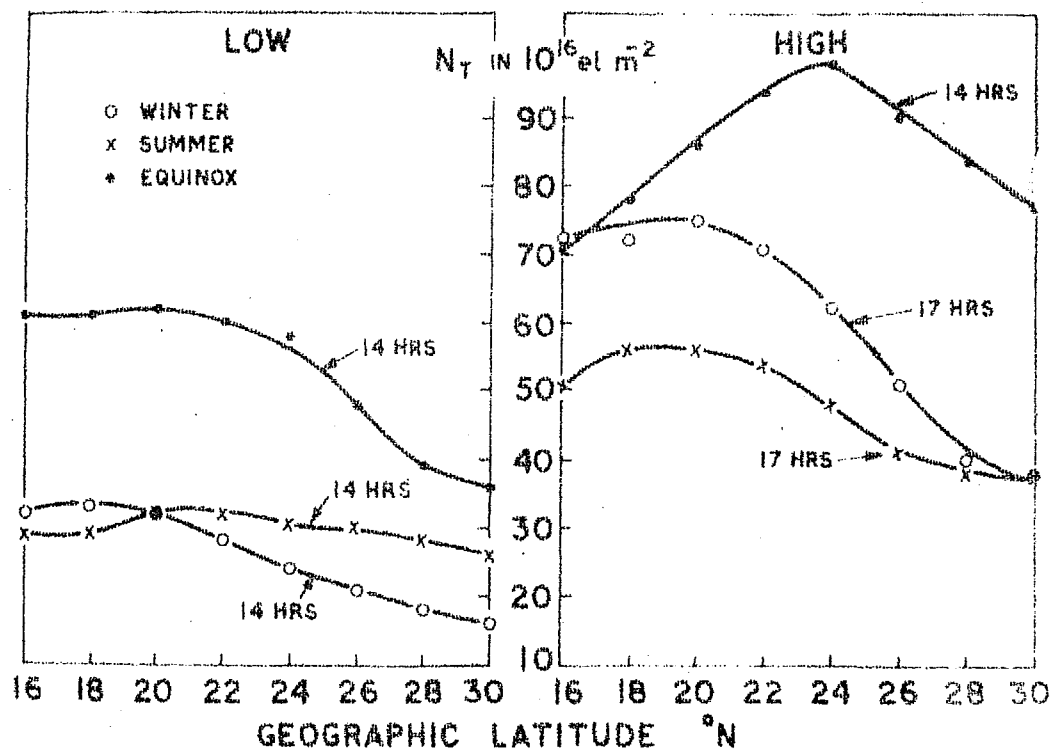
LATITUDINAL VARIATION OF N_T AT TIME OF DIURNAL PEAK

Figure 5.10 : Latitudinal variation of TEC (marked as N_T in figure) at the time of diurnal peak for equinox, winter and summer seasons of low and high solar activity conditions.

activity separately. It is found that the anomaly develops into a broad peak around 14°N dip latitude in low sunspot in all seasons. In high sunspots the picture is however different. The peaks are farthest in equinox (19°N dip latitude) and closest to the equator in summer (12° dip latitude).

In Figure 5.11, the diurnal variation of TEC at the latitudinal peak is shown. In low sunspot years the winter and summer values of TEC are almost same indicating a semiannual variation of TEC. In high sunspot years the winter values of TEC are about $1\frac{1}{2}$ times larger than that in summer indicating the presence of a winter anomaly in TEC similar to the one in f_oF_2 . Whereas in low sunspot years the diurnal maximum is reached around 13-14 hr in all seasons, in high sunspot years the peak is delayed to 16-17 hr in summer and winter while it remains around 13 hr in equinoxes.

5.5 Latitudinal variation of equivalent slab-thickness

From the above contours of TEC and f_oF_2 contours of slab-thickness $\tau = \frac{N_T}{N_m}$ have been derived. These are plotted as contours over a grid of local time vs latitude in Figure 5.12 for equinox winter and summer of low and high solar activity. τ attains large values around noon and smaller values at night. τ is larger near the dip equator and around 20°N dip latitude. The midday τ values are around 250-300 km in winter, 350 km in summer and 400 km in equinox. There is a tendency for τ to increase with solar activity.

DIURNAL VARIATION OF N_T NEAR LATITUDINAL PEAK

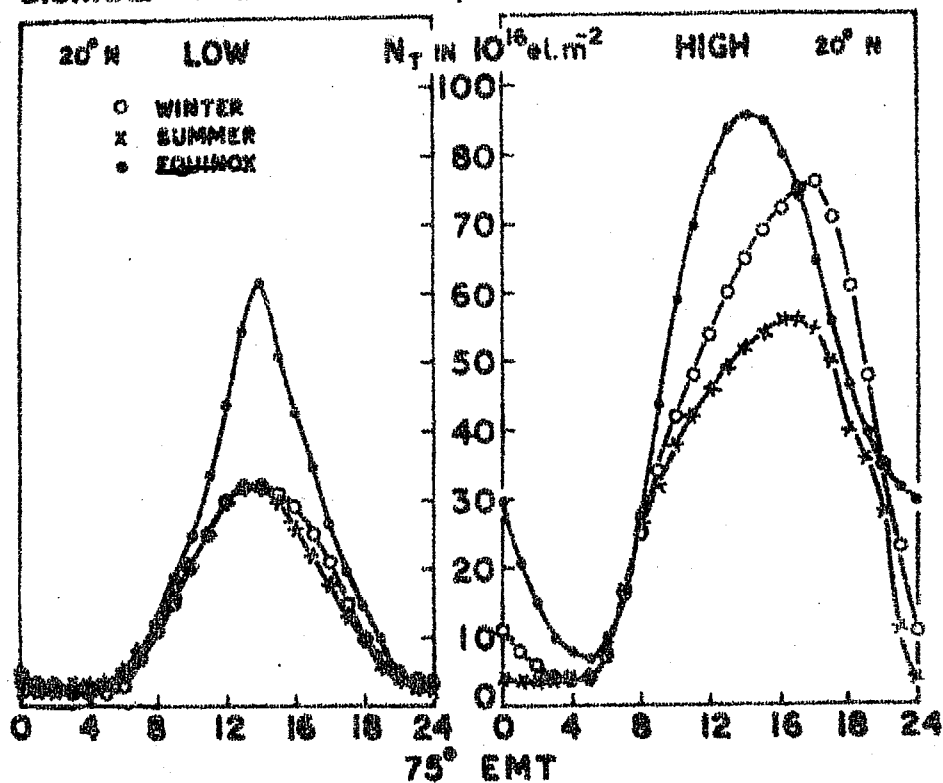


Figure 5.11 : Daily variation of TEC near the latitudinal peak for equinox, winter and summer seasons of low and high solar activity period.

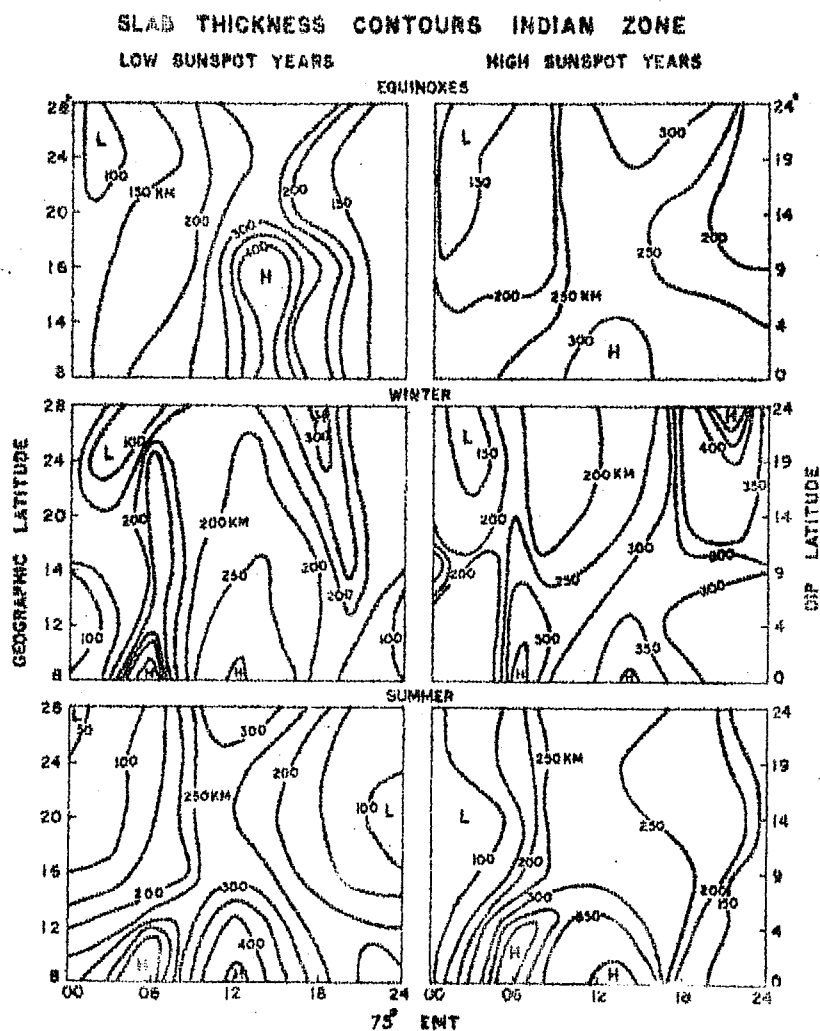


Figure 5.12 : Contours of Equivalent slab thickness on a grid of local time vs. latitude for equinox, winter and summer seasons of low and high solar activity conditions.

Slab-thickness has been used by a number of workers as an index of temperature (Hibberd and Ross 1965, Bhonsle et al. 1965, Yeh and Flaherty 1966 and Titheridge 1970). But the exact relationship between slab-thickness and temperature depends on the model used. In a hybrid model with Chapman distribution for the bottomside and diffusion transport model for the topside the slab-thickness depends on the electron to ion temperature ratio (Yeh and Flaherty 1966). Titheridge (1970) ascertains that the slab-thickness depends only on the neutral temperature and not on the plasma temperature. In general τ contours derived, follow the diurnal temperature curve.

5.6 Association of the equatorial anomaly in TEC with the equatorial electrojet strength

Two unique features of the equatorial ionosphere are the equatorial F_2 region anomaly and the equatorial electrojet. Both are controlled by the dynamo electric fields set up in this region. So an interrelationship between the two phenomena is expected. In the present work, the dependence of the equatorial anomaly in TEC on the electrojet strength is investigated using simultaneous data of TEC recorded at Kodaikanal and Ahmedabad from the satellite BE-B during the years 1964-69.

Latitudinal profiles of total electron content in the range 0° to 30° N geographic latitude by analyzing the Faraday rotation of 40 or 41 MHz signals recorded simultaneously at

Kodaikanal and Ahmedabad are obtained. Only the data from the polar orbiting satellite BE-B are used. The total rotations formula is used to obtain TEC at every minute during each pass having more than 30° peak elevation. However, near the QT region a differential formula is used. The mean field height is chosen as 350 km for Ahmedabad and 400 km for Kodaikanal. A fixed satellite height of 1000 km is used.

5.6.1 Comparison of latitudinal variation of TEC on pairs of strong and weak electrojet days

Having established the presence of the latitudinal anomaly in this section a comparison of the latitudinal variation of TEC on pairs of strong and weak electrojet days is made. Thus a pair of strong and weak electrojet days on quiet magnetic conditions are chosen viz 9 November 1965 (strong) and 29 October 1965 (weak). The Horizontal Force magnetogram at Kodaikanal is used to assess the days for the strength of the electrojet. In Figure 5.13 the latitudinal variations of TEC on such pairs of days on quiet, disturbed and strong magnetic conditions are shown. The horizontal force magnetograms are also reproduced to feel the electrojet strength on these days. We see that the whole latitudinal profile is reversed on weak electrojet days with TEC at equator more than that at tropical latitudes. The latitudes indicated in figure are geographic latitudes. The crosses refer to observations from Kodaikanal and circles those from Ahmedabad. The reversal of the latitudinal profile of TEC is seen on disturbed and stormy magnetic conditions too (refer the

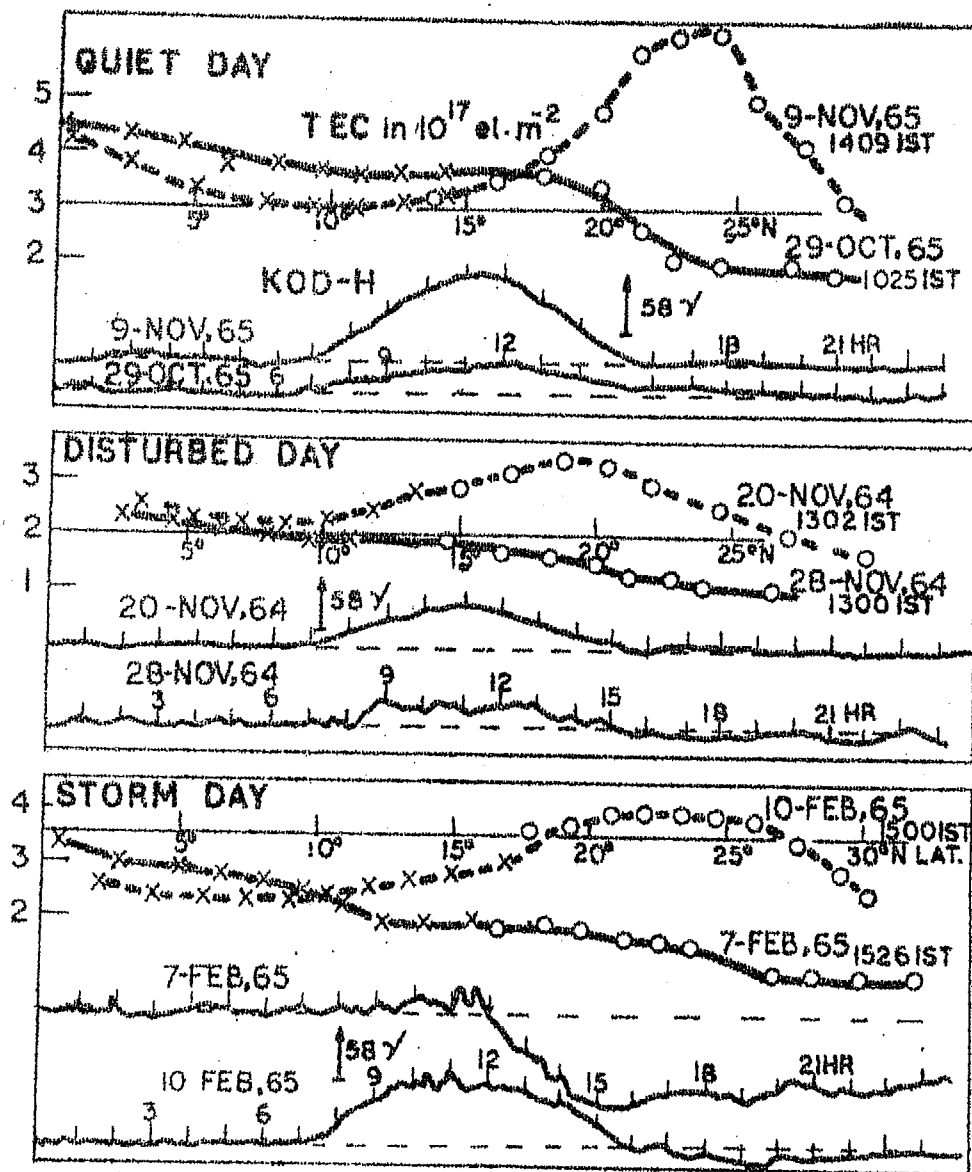


Figure 5.13 : Latitudinal variation of TEC on typical pairs of strong and weak electrojet days for magnetically quiet, disturbed and strong conditions. The H magnetograms on the corresponding days are also reproduced. 'X' indicates observations from Kodaikanal and 'O' that from Ahmedabad.

curves for 20th and 28th November 1964 and 10th and 7th February 1965). Thus the phenomenon of reversal of latitudinal TEC profiles on weak electrojet days or in otherwards the electrojet control of latitudinal variation of TEC is established. Therefore in subsequent sections a detailed investigation of electrojet control of equatorial anomaly is attempted.

5.6.2 Diurnal development of equatorial anomaly in TEC

The latitudinal profiles are classified into groups corresponding to 0-23 hrs LT (e.g. passes between 0930 and 1029 falling in the group for 1000 hr LT). From each such latitudinal profile, the following indices of the equatorial anomaly are scaled : (a) the dip latitude (Φ) of the anomaly peak, (b) the normalised depth (d) of the anomaly defined as

$$d \% = \frac{N_T(\text{peak}) - N_t(\text{dip equator})}{N_t(\text{dip equator})} \times 100$$

and (c) the strength of the anomaly $S = \Phi \times d$. For the electrojet strength the index Sd_I is obtained by subtracting the H values at a non-equatorial station (in the present case Alibag) from that at the equatorial station (Kodaikanal) both lying in the same longitude.

$$\text{Thus } Sd_I = H_t(\text{Kod}) - H_t(\text{ALB}) + \bar{H}(\text{ALB})$$

Sd_I at t hours is defined as $Sd_I(t) - Sd_I$ meaned over 00-04 hrs LT. $Sd_I(t)$, t varying from 00-23 hrs LT has been computed for each day having a latitudinal profile for TEC.

This index is a very realistic index of electrojet strength and

is not contaminated by magnetic disturbance effects (Kane 1973).

The mean position of the anomaly peak has been computed for the different hours from the grouped latitudinal profiles. The diurnal development of the equatorial anomaly is studied by plotting the dip latitude of the peak against IST hours. The result is shown in Figure 5.14. At 0900 hr IST, the anomaly peak is at 8° dip latitude and starts moving away from the equator. At about 1300 hr IST the anomaly peak reaches its maximum northward extent of about 15° dip latitude thereafter returning towards the equator. The anomaly persists till about 17-18 hr IST at about 12° dip latitude.

5.6.3 Time lag between anomaly and electrojet

The correlation between dip latitude of anomaly at t hours and the electrojet strength index at $(t - \Delta t)$ hrs, where Δt is a preassigned time shift has been calculated, for various time shift of 1, 2, 3....hrs. In Figure 5.15 the correlation coefficient is plotted against the time shift. It is found that maximum correlation of about 0.7 exists for a time shift of 2-3 hrs, thereafter the correlation falling rapidly.

5.6.4 Correlation between anomaly parameters and electrojet

As the anomaly is found to be fairly strong between 1100 - 1700 hrs LT from Figure 5.16 next, the correlation between the different anomaly parameters at t hours and the electrojet index $\Delta Sd_I(t - 2)$ hrs is studied t varying from 1100 - 1700 hrs.

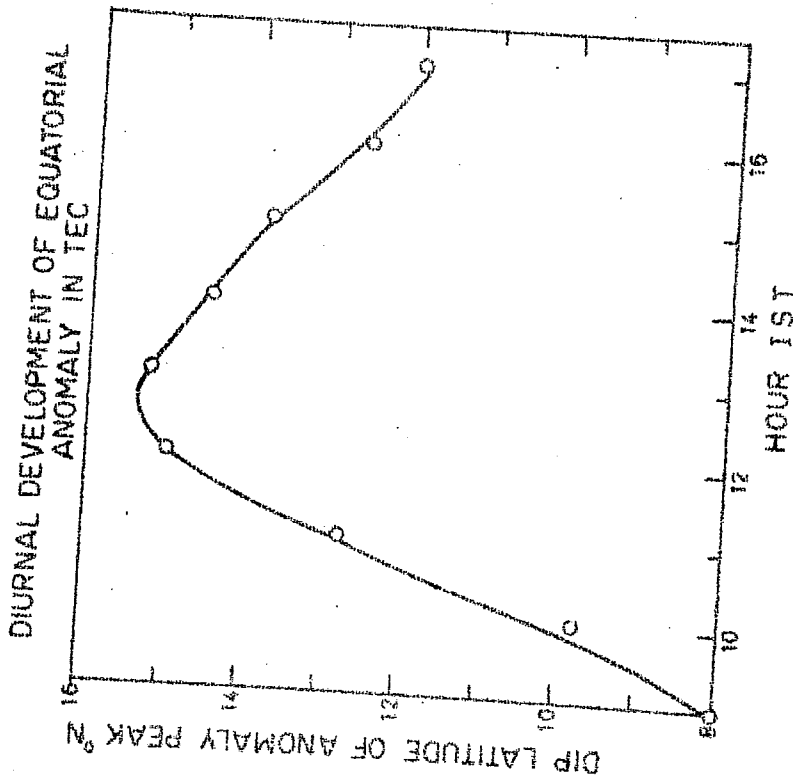


Figure 5.14 : Diurnal development of equatorial anomaly in TEC in its latitudinal variation.

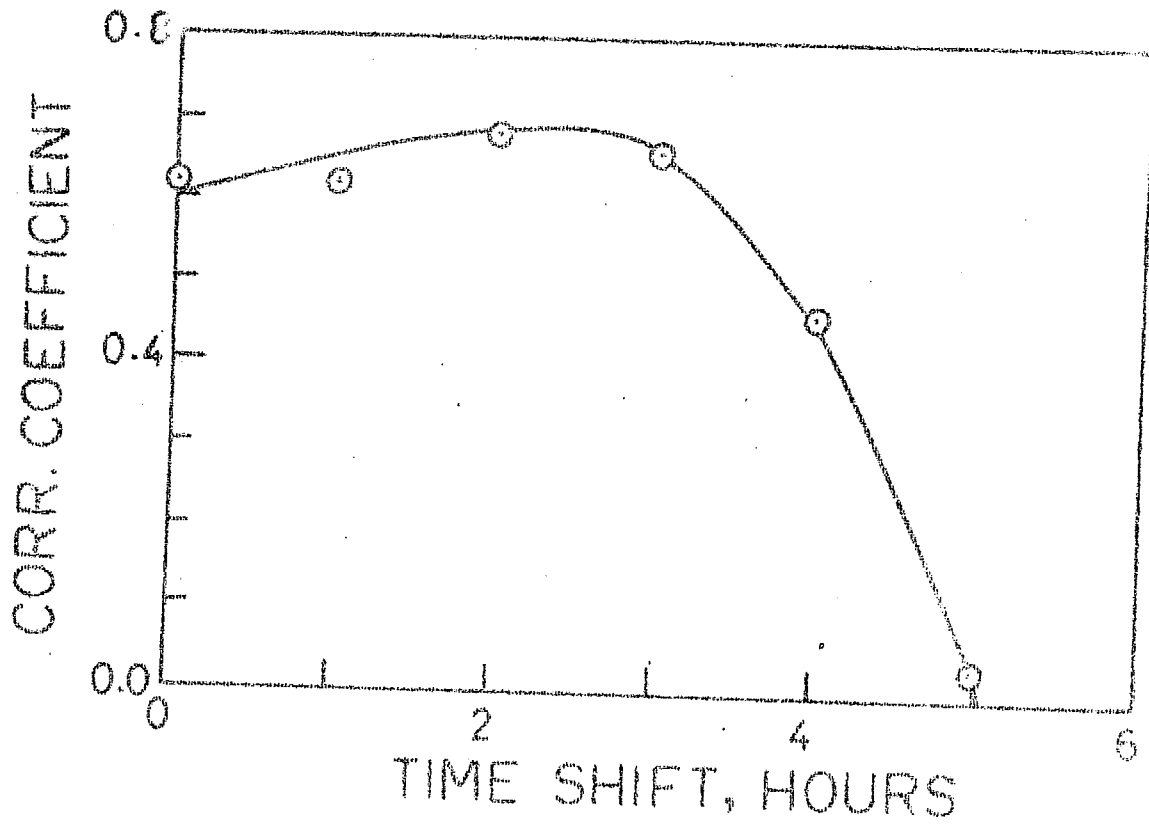


Figure 5.15 : Correlation between electrojet parameters and equatorial anomaly parameters the latter lagging by different time shifts shown in the abscissa.

CORRELATION BETWEEN ANOMALY PARAMETERS AND ELECTROJET STRENGTH

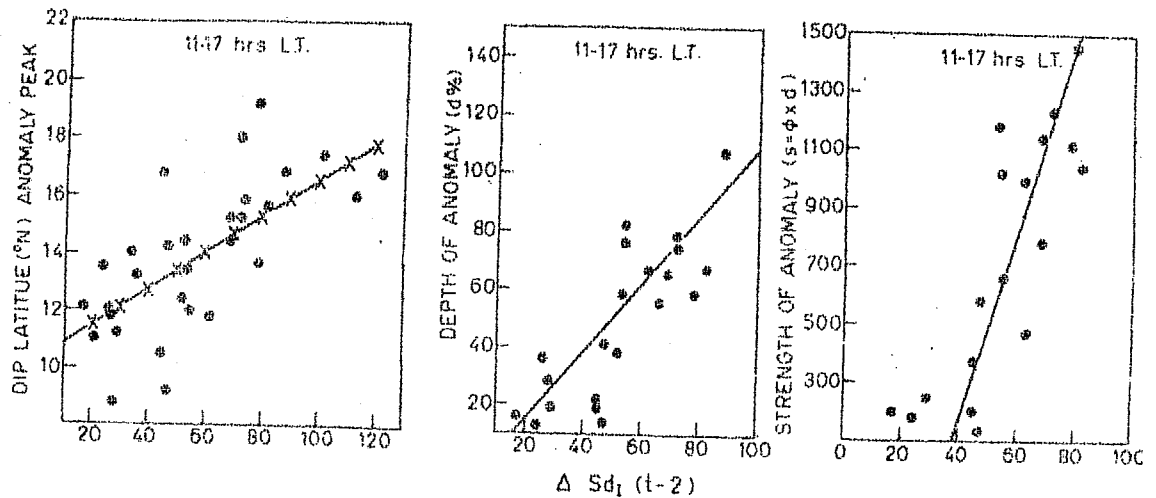


Figure 5.16 : Variation of dip latitude, ϕ , of the anomaly peak (left), the normalised depth, d , (middle), and the strength $S = \phi \times d$ (right) of the anomaly with equatorial electrojet strength two hours prior to the anomaly.

The variation of the dip latitude (ϕ), the depth ($d\%$) and the strength $S = \phi \times d$ with the electrojet index $Sd_I(t-2)$, the latter lagging by 2 hrs are plotted as a scatter plot in Figure 5.16. The best fitting least square regression lines for the observed points are also shown in the diagram. It is found that good correlation (0.68) exists between ϕ and $Sd_I(t-2)$; 0.63 between d and $Sd_I(t-2)$ and 0.48 between S and $Sd_I(t-2)$. These results indicate that the equatorial anomaly is strongly controlled by electrojet currents.

The present results show the anomaly in TEC maximising around 1400 hr and the anomaly lagging by about 2 hrs behind the electrojet. The E region currents are known to maximise before 1200 hr thus causing maximum electrojet intensity at this time.

5.7 Discussion of the results

5.7.1 Latitudinal variation of TEC

The present work brings out the existence of the equatorial anomaly in the latitudinal variation of TEC, similar to the one in f_oF_2 . Titheridge and Smith (1969) using the observations of TEC from Rarotonga had studied the latitudinal variation of TEC in the southern hemisphere. Similar latitudinal anomaly was seen by them. Mendonca et al. (1970) presented contours of TEC for different seasons using the Faraday rotation data at Brazil, again evidencing the equatorial anomaly. Golton and Walker (1971) using the data of Hong Kong have studied the

latitude variation of TEC in northern hemisphere. However, there are quantitative differences between northern and southern hemisphere. In southern hemisphere the anomaly peak is around 10° dip latitude moving southward in summer and northward in winter by about 5° of dip angle. On other hand the northern peak is around 15° dip latitude in summer and winter while it is around 20° in equinoxes. This indicates a north-south asymmetry in the sense that the northern peak is farther away from the dip equator than the southern peak. They have also discussed the diurnal development of the anomaly. It first starts at a dip angle of about 10° at 10 hr LT and attains its maximum extent around 14-15 hrs LT and disappears by midnight. The general diurnal behaviour in the northern hemisphere is similar but it seems to disappear early and the time of maximum development of the anomaly is seasonally dependent.

Titheridge and Smith (1969) observed that there is a short transition at 21°S in winter and 23°S in summer from approximately constant electron content at medium latitude to rapidly decreasing content near the equator. Das Gupta and Basu (1971) have studied the development of equatorial anomaly on quiet and disturbed days separately. They found a decrease of the anomaly on disturbed days. This was attributed to weak electrodynamic drift at equator on disturbed days. Walker and Ma (1972) have investigated the influence of solar flux on the latitude variation of TEC. They found TEC maximises one hour after h_{max} reaches maximum. Latitude of the crest and h_{max} are positively correlated with

daily solar flux.

Two points of particular interest are the continuance of equatorial anomaly after 17 hr LT and subsidiary enhancement at least in summer near Nairobi after 21 hr LT (Hunter and Webster 1965, Legg et al. 1967 and Jayendran and O'Brien 1969).

According to Thomas and Lyon (1963) and Rao (1962) the trough in f_oF_2 persists at the geomagnetic equator till 0200 hr or more at sunspot maximum although it disappears around 2000-2100 hr at sunspot minimum (Rastogi 1959, Lyon and Thomas, 1963 and Lockwood and Nelms 1964). Sawada and Shibata (1961) and Rao (1962) find that this anomaly, unlike the East African total electron content, lasts throughout a large part in night. Others observe an early disappearance of the total electron content anomaly at night (Rufenech et al. 1968, Basu and Das Gupta 1967 and Tyagi and Mitra 1970). There is undoubtedly a longitudinal effect that merits further study (Rastogi 1959, 1960, Thomas and Lyon 1963 and Thomas 1968). For example Thomas and Lyon (1963) find that the anomaly in f_oF_2 persists longer and is larger in African sector than in the American sector with a pronounced asymmetry in distribution around the dip equator, except at equinoxes, associated with the relative position of dip and geographic equator. The contribution of the topside to the total content is 2 - 4 times at night so that changes in total content should be strongly indicative of variations in the topside (King et al. 1967). Mulkowa (1969) finds that the southern crest of the anomaly moves

at the rate of 1.3° per hour from 0600 to 1600 hrs LT which is in good agreement with other work (Rastogi 1959 and King 1969).

Earlier work on the distribution of electron content with latitude in Brazil (de Mendonca 1965) was thought to show both the Brazilian magnetic anomaly and the equatorial anomaly. More recent work (de Mendonca et al. 1969) does not show any marked effect of the Brazilian anomaly on total content and suggest that the earlier result was due to 'starfish' detonation.

5.7.2 Latitudinal variation of slab-thickness

Slab-thickness defined as $\tau = \frac{N_T}{N_m}$ has been used by a number of workers as an index of temperature (Bhonsle et al. 1965, Hibberd and Ross 1966), Yeh and Flaherty 1966 and Titheridge (1973b). Yeh and Flaherty (1966) have derived empirical relation between $\frac{T_e}{T_i}$ ratio and slab-thickness for a hybrid model with Chapman type bottomside and diffusion transport topside.

Titheridge (1973b) holds that slab-thickness depends on the scale height of ionizable constituent and the scale height of loss processes both of which are hence dependent on neutral temperature. Therefore slab-thickness indicates neutral temperature. Furnan and Prasad (1973) hold the view that slab-thickness is neither a measure of neutral temperature nor of $\frac{T_e}{T_i}$ ratio. According to Chapman isothermal ionosphere theory slab-thickness was shown to be equal to $4.15 H$ (Wright 1960).

The departure of from the value $4.15 H$ is indicative of the deviation from diffusive equilibrium as measured by $\frac{D}{H^2} - \beta$ where

H is the neutral scale height, D is the diffusion coefficient and the photochemical loss coefficient.

As the f_oF_2 contours are difficult to derive in the absence of a large net work of ionospheric sounding stations, contours of τ have not been presented before. Contours of τ derived in this study follow the diurnal temperature curve with minimum values of τ at night and large values around noon. τ seems to be larger at the equator than at tropical latitudes. There is a tendency to show presunrise peaks in τ in low solar activity period. τ has larger values in equinoxes than in solstices. There is a tendency for increase of τ with solar activity. These features indicate the dependence of τ on temperature.

5.7.3 Dependence of equatorial anomaly on electrojet strength

Two unique features of magnetic equatorial latitudes are the equatorial electrojet current in the E-region and the equatorial anomaly in the F-region. Both are controlled by the electric fields set up in the dynamo region of the ionosphere. So it is natural that the two phenomena are well correlated. The electrojet strength should depend on the conductivity of equatorial ionospheric E-region and the electric fields driving the current. The present study shows that the anomaly maximises around 14 hr LT and therefore the anomaly lags by about 2 hrs behind the electrojet which is known to maximise between 11 - 12 hrs LT.

The equatorial anomaly is well explained as due to the vertical drift of F-region ionization under the $\vec{E} \times \vec{B}$ drift over the magnetic equator and its subsequent downward diffusion along the magnetic lines of force. The time of maximisation of the anomaly will therefore depend on the time of maximum electric field, the time taken for vertical drift and the diffusion time of the electrons from equator to tropical latitudes. The time taken by F-region plasma for vertical drift with drift velocities of 20-30 m/sec and the subsequent diffusion time are well discussed in literature. Baxter and Kendall (1968) have theoretically computed this time constant to $2\frac{1}{4}$ hours. The calculations of Sterling et al. (1969) distinguish between an early $\vec{E} \times \vec{B}$ drift i.e. the drift maximising around noon and late drift i.e. drift maximising after noon. In both cases they find the anomaly peak to be formed around 14° dip latitude. But the late drift case does not reproduce the observed noon bite-out in the diurnal variation of $N_m F_2$, the maximum electron density in F-region. This leads to the conclusion that what is actually existing is the early drift viz., drift maximising around noon. They also observe that the controlling factor in the position of the latitudinal peak is the electrodynamic drift while the time of maximum development of the anomaly is controlled by the diffusion velocities. The present analyses show that in high sunspot years the peak is delayed by $\frac{1}{2}$ to 1 hour as compared to low sunspot years which is due to the solar activity changes of neutral densities. The anomaly is found to maximise

around 1500 hr LT on average. This indicates an average time lag by about 3 hours between the electrojet and anomaly maximisation. This agrees well with our observations of 2 to 3 hours time lag.

It is also expected that increasing electrojet strength will lead to increased vertical drifts which in turn will create anomaly peaks farther away from the dip equator. Thus the correlation between dip latitude (ϕ) of anomaly peak and electrojet strength can be interpreted as due to increased vertical drifts. The parameter d will also be larger for higher electrojet strengths since lifting to a higher altitude leads to increased gradients and hence increased diffusion. This in turn increases the depth of the anomaly.

Equatorial anomaly in the latitudinal variation of TEC maximises around 1400 hr LT, thus having a time lag of about 2 hours between electrojet strength and anomaly. This time lag agrees well with the theoretically estimated diffusion time. The anomaly strength is well correlated with equatorial electrojet strength. These results tend to conclude that the equatorial anomaly in TEC is mainly the manifestation of vertical electrodynamic drift and ambipolar diffusion of ionization, although the role played by neutral density anomaly (Hedin and Mayr 1973) cannot be ignored.

C H A P T E R - VI

INTEGRATED PRODUCTION AND EFFECTIVE LOSS RATES IN THE IONOSPHERE

6.1 Introduction

There have been in the past two different hypothesis for the rate of production of electrons in the F region. In both it is supposed that electrons are produced by photo-ionization of atmospheric constituents. The two different suggestions were concerned with explaining why an F_2 layer is formed above and distinct from the F_1 layer below. In one hypothesis it is assumed that the peak of electrons in the F_2 layer is located near the peak of production of electrons and that a second and independent peak of production is responsible lower down for the F_1 layer. Both the layers are supposed to be similar to the classical Chapman layer.

On the other hypothesis the peaks of electron density in the F_2 and F_1 layers are supposed to be produced by the same incident radiation acting on the same atmospheric constituent. The peak of electron production is supposed to be near the level of the F_1 layer, but the rate of electron loss decreases upward so rapidly above that level that a second peak of electron density is formed and constitutes the F_2 layer. This suggestion was first made by Bradbury (1938) and has later been repeated by several other workers. Later investigations have proved that

Bradbury's hypothesis is the realistic one and is self consistent.

Several attempts have been made to deduce the electron production rate in the ionosphere. Ratcliffe et al. (1956) studied the electron density at the peak of the F_1 layer near noon at a number of different stations and obtained the production function as a function of F_1 layer recombination coefficient and mean sunspot number. The balance between electron production rate, loss rate and movements decides the electron density at any level. The loss rate is generally small at hours around sunrise time. Unless the atmospheric composition in the F layer changes rapidly at sunrise, the loss rate will remain small until the electron density has increased appreciably. The initial rate of increase of ionization at sunrise therefore depends primarily on the rate of production of electrons. This result has been used by Rishbeth and Setty (1961) to determine the production rate, q , at the peak of the F layer at sunrise, and hence to calculate the production rate q_0 for an overhead sun.

King and Lawden (1962) determined the production rate at noon in summer, from the shape of the electron density profile in the $F_1 - F_2$ transition region.

In the above discussed methods of measuring the production rate from fixed levels, the neglect of vertical motions and transport processes will be contaminating the results. This drawback can be avoided if Total Electron Content data is used to deduce the production rate as this parameter is independent of

vertical movements within a column. Therefore a detailed analysis of the time behaviour of electron content (or Faraday rotation) during a period near sunrise can yield both the height integrated production rate at sunrise and F_2 region loss coefficient. Working in these directions, Taylor (1965) used a lunar radar to determine the changes in TEC during 13 days in summer and 8 days in winter. Garriott and Smith (1965) using TEC data obtained from the geostationary satellite Syncom 3 derived the integrated production rate for an overhead sun. Following similar lines, from the diurnal curves of TEC obtained from the low orbiting beacon satellite data of Faraday rotation it is attempted to deduce average production and loss functions, in this chapter.

Coming to the loss processes, several attempts (Appleton 1937, Seaton 1947, Baral and Mitra 1950) have been made in the past to determine the rate of electron loss at different heights in the F-region. But it is now known that these results were vitiated by the occurrence of transport effects. After sunset, the electron density in the F-region decreases through the combined effects of recombination and diffusion. Under these conditions, the electron density decays at an effective loss rate β' which is independent of height, or in other words the layer settles to shape preserving solutions. If the actual loss coefficient β at any height is proportional to $\exp(-h/H)$ where H is the scale height of the ionizable gas, then the

effective loss coefficient is equal to the value of β at the peak of the layer (Martyn 1956 and Duncan 1956). If β is proportional to $\exp(-2h/H)$ (which is probably closer to the true variation the effective loss coefficient is equal to the value of β near the bottom of the F layer (Dungey 1956). In either case, the effective loss coefficient can be computed from the rate of decay of TEC after sunset. This principle is used in this chapter to deduce the effective loss rate following the work of Titheridge (1966) and Smith (1968).

6.2 Integrated production rate

6.2.1 Method of calculation of integrated production rate

In the sunrise period, for $95^\circ > \chi > 87^\circ$ (where χ is the solar zenith angle) the rate of production of ion electron pairs in the ionosphere is substantially larger than the rate of loss of electrons. An accurate measurement of variation of TEC vs time in this interval permits the production rate for an overhead sun to be deduced.

For a single constituent isothermal atmosphere, exposed to ultraviolet radiation of only one wavelength, the rate of production of ion electron pairs is given by the well known Chapman production formula

$$q = q_0 \exp [1 - z - e^{-z} \operatorname{ch}(\chi, H)] \quad (61)$$

In this equation the reduced height

$$z = \int \frac{dh}{H} = \frac{h - h_0}{H} \quad (6.2)$$

q_0 and h_0 are constants, H , the scale height $Ch(\chi, H)$ the Chapman function which replaces $\sec \chi$ in problems involving spherical geometry. More precisely, this function depends on the ratio of H to the geocentric radius of the ionospheric layer. Equation (6.1) is readily integrated with respect to height, h , to obtain the total production rate for the whole ionospheric layer:

$$Q = \int_{-\infty}^{\infty} q(H) dz = \frac{q_0 e H}{Ch(\chi, H)} = \frac{Q_0}{Ch(\chi, H)} \quad (6.3)$$

where Q_0 is the integrated production rate for an overhead sun.

This equation may be related to the electron content measurements through the continuity equation for electrons

$$\frac{\partial N}{\partial t} = q - L(N) - \text{div}(N\mathbf{v}) \quad (6.4)$$

in which L is the loss rate, N is the electron density and \mathbf{v} the drift velocity produced by diffusion, electrostatic or other forces. We next assume that horizontal gradients are sufficiently small that only vertical derivatives, $\frac{\partial}{\partial z}$, are important in the divergence expression. Then, when equation (6.4) is integrated over all heights, the divergence terms drop out, since $N \approx 0$ at both low and very high altitudes. Physically this means that although electrons may move in altitude, their integrated number remains unchanged. Performing this integration gives

$$\frac{d}{dt} \int_{-\infty}^{\infty} N dh = \int_{-\infty}^{\infty} q dh - \int_{-\infty}^{\infty} L dh \quad (6.5)$$

At sunrise as the loss term is much smaller than the production function equation (6.5) may be approximated to

$$\frac{d}{dt}(N_T) = Q = \frac{Q_0}{Ch(X, H)} \quad (6.6)$$

N_T being the vertical Total Electron Content. Thus an accurate measurement of the rate of increase of TEC at sunrise will yield a measure of the integrated production rate.

It is seen from the diurnal plots of TEC described in previous Chapters, that the rate of increase of electron content at sunrise period is remarkably steady, so also the decay rate of TEC after sunset. Hence by measuring the slope of TEC vs time curve at sunrise Q_0 can be deduced. To illustrate this fact in Figures 6.1 through 6.3 we have shown typical TEC vs time plots representing equinox, winter and summer seasons, where straight lines could be fitted between the observed points indicating the linear variation of TEC with time at these times.

6.2.2 Variation of production rate with season

The measured TEC at Ahmedabad have been plotted versus time for the period 1964 through 1969 separately for northbound and southbound passes of BE-B and BE-C. Hence four series of diurnal curves each series containing 10 - 12 diurnal curves are obtained. From these curves straight lines are fitted

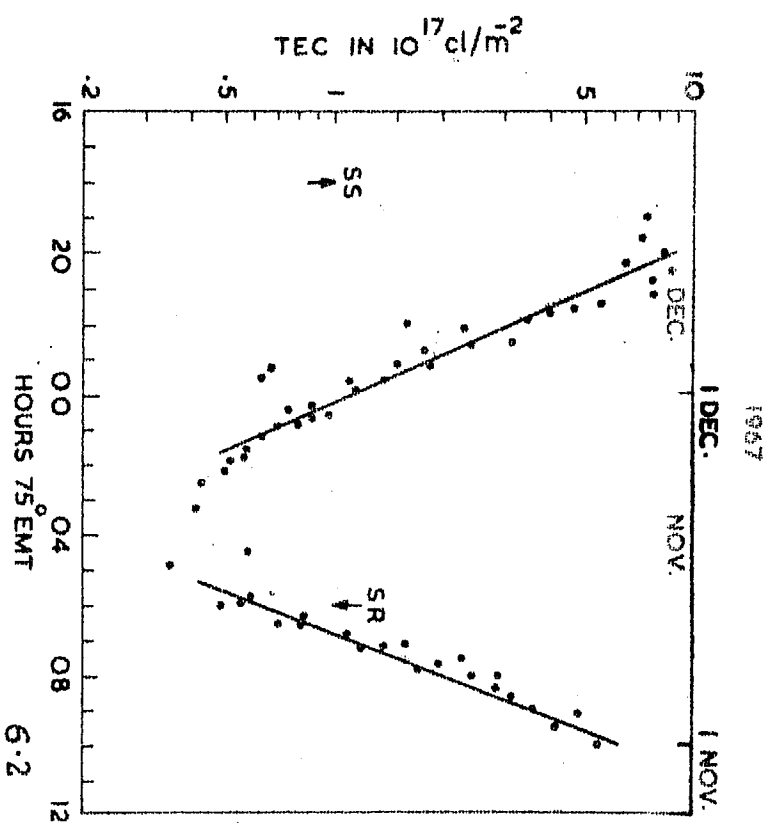
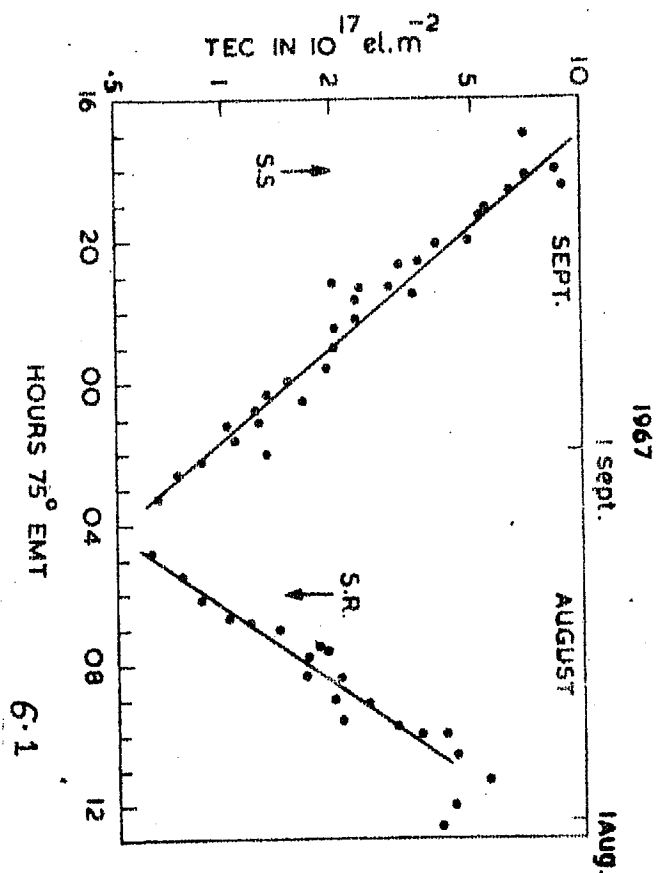
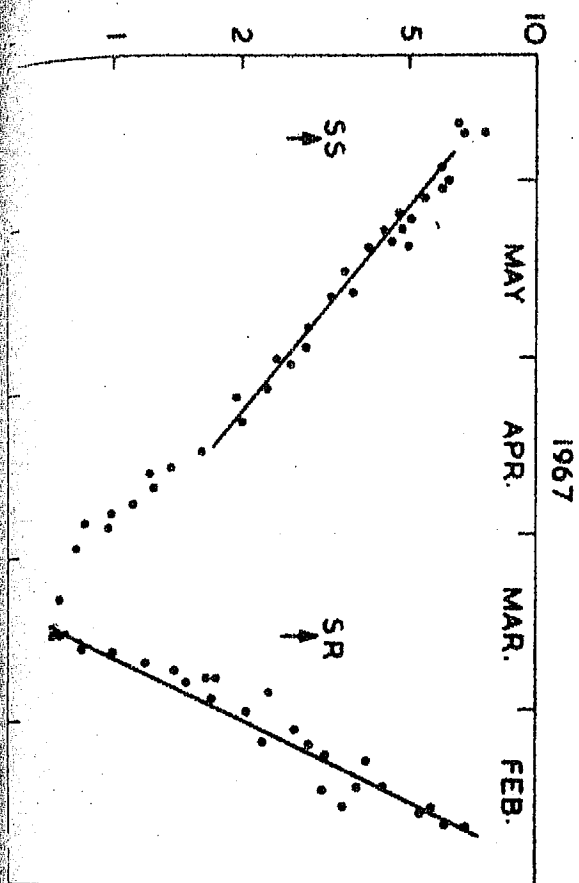


Figure 6.1 : Variation of TEC with time at sunrise and sunset periods showing the linear part for equinoxes.

Figure 6.2 : Same as Figure 6.1 for Winter.

Figure 6.3 : Same as Figure 6.1 for Summer.

TEC IN $10^{17} \text{ el.m}^{-2}$



through the observed points at sunrise and sunset portions. From the sunrise portions, the rate of increase of TEC and hence the production rate is calculated which corresponds to the months falling at each sunrise period. A value of 15, appropriate for $\chi = 90$ and $H = 50$ km, has been used for $Ch(\chi, H)$. The values of Q_0 so obtained for each month are plotted against the corresponding month to study the seasonal variation of integrated production rate. These results are shown in Figure 6.4. The production rate shows a semiannual variation with equinoxial peaks and solstitial minima for all the years 1965 through 1967. There is a general trend of increase of the mean production level with progress of years 1965 to 1967, thus indicating the solar cycle trend.

6.2.3 Solar cycle variation of production rate

In order to study the dependence of the integrated production rate on solar activity the data has been divided into three conventional seasons. The published TEC data from Delhi are also plotted as diurnal curves, they are also used to obtain the production rate. The production rates thus calculated have been plotted in Figure 6.5 against the mean 10.7 cm solar flux value for the period of observation, separately for the different seasons and the two stations. A linear increase of production rate with solar flux above a threshold of about 75 flux units is evident. The production rate increases fastest with 10.7 cm flux during winter at Ahmedabad and slowest during summer at Delhi.

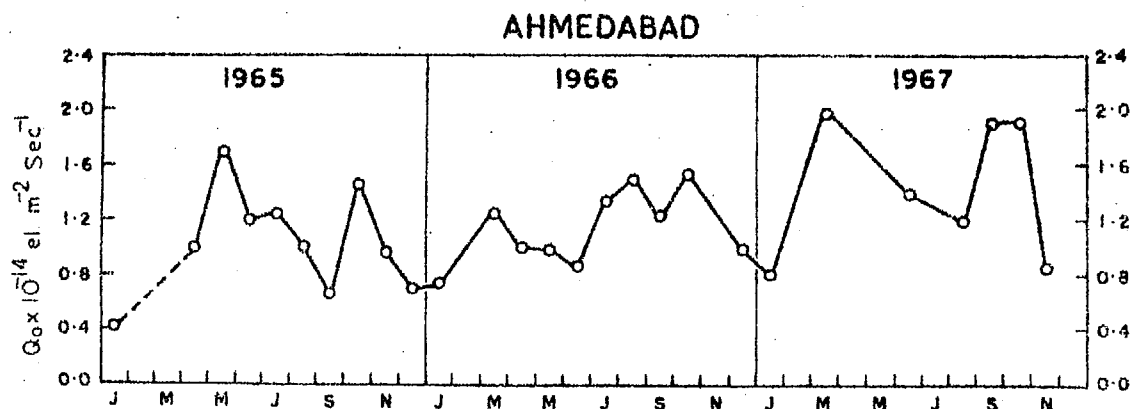


Figure 6.4 : Seasonal variation of integrated production rate for the period 1964 through 1967, showing semiannuual variation.

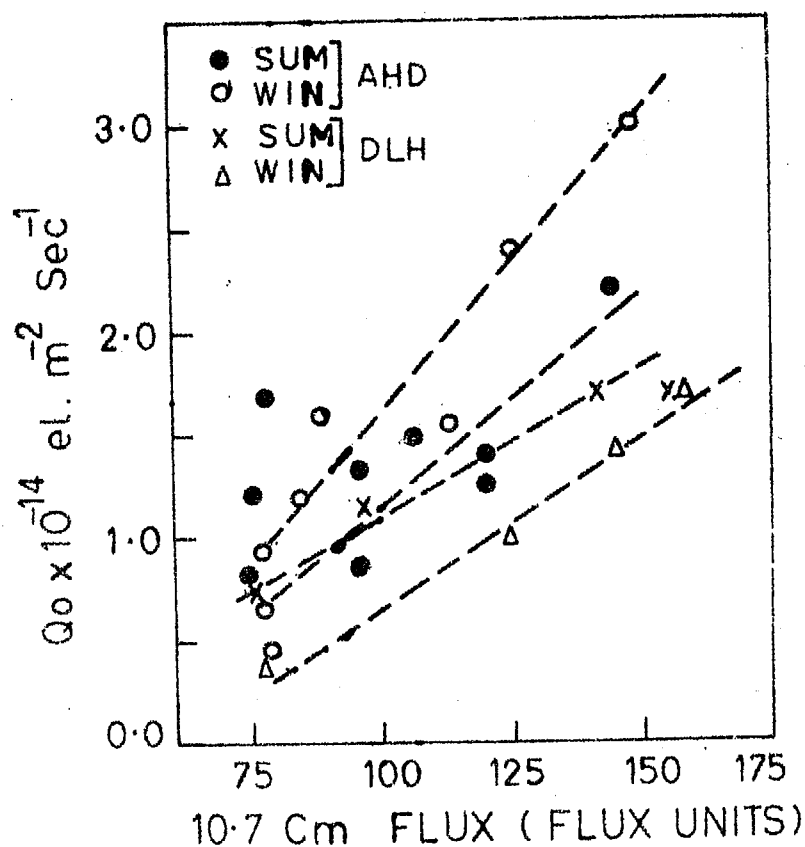


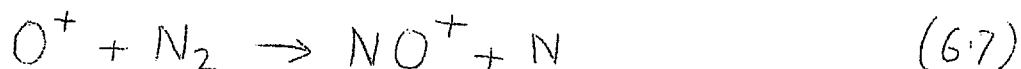
Figure 6.5 : Variation of integrated production rate at Ahmedabad and Delhi for winter and summer seasons with 10.7 cm solar flux.

The absolute production level also is found to be largest at Ahmedabad during winter. This in turn is a manifestation of the seasonal anomaly, in the sense that the rate of increase of TEC at sunrise is fastest in winter than in summer.

6.3 Effective loss rate (β')

6.3.1 Method of calculation of β'

The O^+ ions produced at sunrise are known to recombine with electrons through the two step process



It is probable that an ion atom interchange reaction involving O_2 rather than N_2 is also important (Ferguson, 1967). But the scale heights of O_2 and N_2 are sufficiently near so that the analysis is not greatly affected by neglecting the O_2 reaction. In regions such as near the F layer peak, where O^+ is virtually the only ion present reaction (6.8) must proceed so rapidly compared to reaction (6.7) that the rate of reaction (6.7) determines the overall loss rate. Loss is then governed by the familiar attachment-like expression

$$l = \beta N \quad (6.9)$$

After sunrise, the shape of the layer does not change appreciably and hence the electron density decays with an effective loss rate β' which is independent of height. Then the rate of change of

TEC after sunset will be given by

$$\frac{\partial N_T}{\partial t} = Q - \beta' N_T \quad (6.10)$$

The integrated production rate β' should be approximately same at sunset and at sunrise. The effective loss rate at sunset can then be written as

$$\beta' = \left\{ \left(\frac{\partial N_T}{\partial t} \right)_{\text{Sunrise}} - \left(\frac{\partial N_T}{\partial t} \right)_{\text{Sunset}} \right\} / N_T (\text{Sunset}) \quad (6.11)$$

Assuming that the production of ionization due to solar ultra-violet radiation has ceased after sunset equation (6.10) can be rewritten as

$$\frac{\partial N_T}{\partial t} = -\beta' N_T \quad (6.12)$$

which can be solved as

$$(N_T)_t = (N_T)_0 \exp(-\beta' t) \quad (6.13)$$

If we define $t_{\frac{1}{2}}$ as the time taken by N_T to decay to half its initial value (or half life), we can write

$$\beta' = \frac{0.693}{t_{\frac{1}{2}}} \quad (6.14)$$

Using this equation (6.14) β' is computed from the after sunset portion of each diurnal curve for the northbound and southbound passes of BE-B and BE-C.

6.3.2 Variation of effective loss rate with season

The effective loss rates (β') computed from equation 6.14 are plotted in Figure 6.6 against the months averaged for

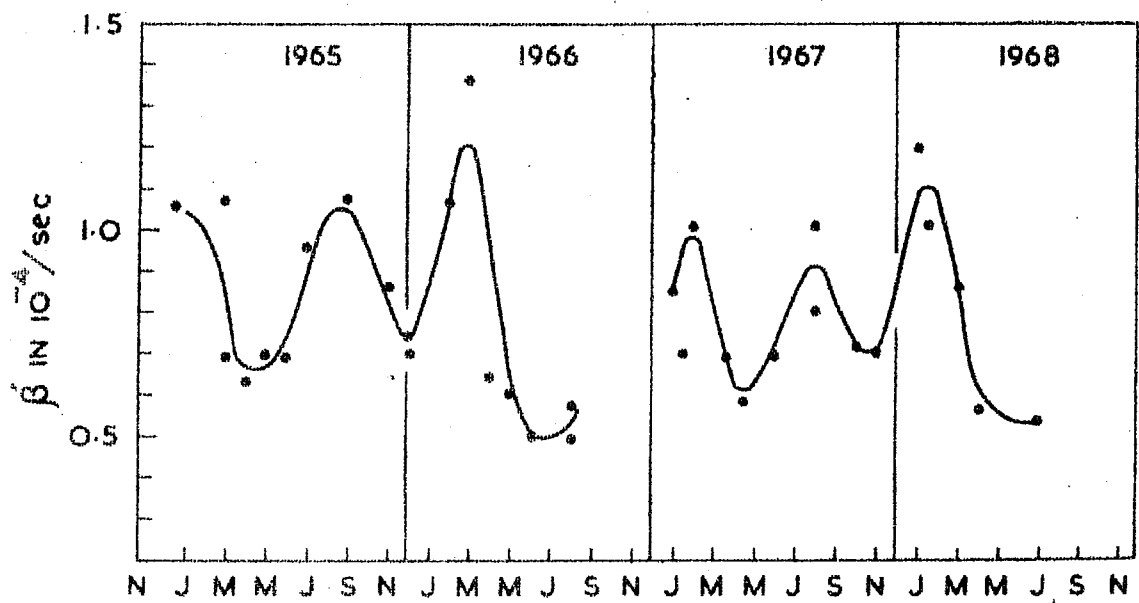


Figure 6.6 : Seasonal variation of effective loss rate for the period 1965 through 1968.

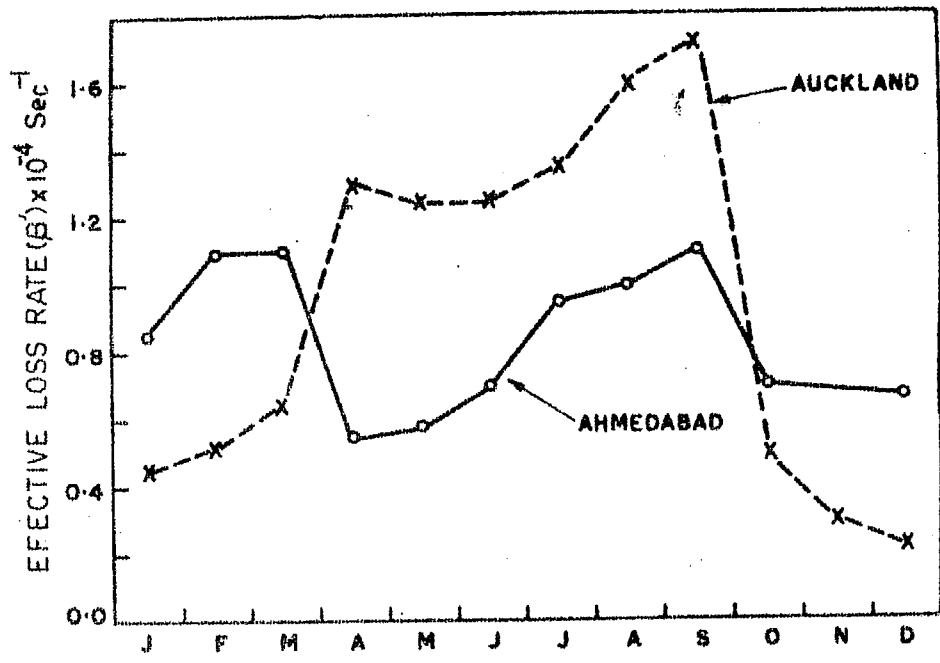


Figure 6.7 : Comparison of seasonal variation of obtained in the present study and by Titheridge (1966).

the years 1965-1968. There is a semiannual trend in the loss rate with maximum values occurring in February-March and again in August-September months, and minimum values around April.

To account for the production that may still be taking place after sunset, Titheridge (1966) has modified the loss rate formula. Assuming the production rate to be same at sunrise and sunset, the effective loss rate at sunset can be represented by equation (6.11). Using this equation and the data of Faraday rotation obtained from geostationary satellite at Auckland (36°S) Titheridge (1966) has computed the loss rate for Auckland. His results are also reproduced in Figure 6.7 together with ours. The phase shift between these two curves could be due to the hemispherical differences in local season. There seems to be general similarity in the seasonal variation of at the two places.

6.4 Discussion of the results

6.4.1 Production rate

The present study throws some light on the behaviour of integrated production and effective loss rates in the ionosphere. It must be mentioned that the diurnal curves obtained from low orbiting satellites are affected by day to day variabilities and only very average picture can be obtained. Still, comparison with the results obtained from geostationary satellite by other

workers, shows fairly good agreement.

Taylor (1965) used lunar radar to determine the changes in TEC during sunrise for 13 days in summer and 8 days in winter. He obtained an integrated production rate of about $1.0 (\pm 0.4) \times 10^{14}$ el/m²/sec in summer and $2.4 \pm 0.4 \times 10^{14}$ in winter at a mean sunspot number of 100. Garriott and Smith (1965) using the data of Faraday rotation from the geostationary satellite Syncom 3 recorded at Hawaii and Stanford also calculated the production rate arriving at similar results. Titheridge (1966) using the same satellite data computed the integrated production rate at Auckland and came out with minimum production rate in summer (November-December) of 0.5×10^{14} el/m²/sec and about 1.5×10^{14} el/m²/sec in equinoxes. Smith (1968), again with geostationary satellite data obtained daily values of $Q_{90}(O^+)$ i.e. production rate for a zenith angle of 90° assuming one component atmosphere of O only. On the average he obtained values of 1.7×10^{13} el/m²/sec for a two year period 1965-66. He did not obtain any significant seasonal variation even after correcting for the production due to N₂. This is contrary to our results as well as that of Garriott and Smith (1965) and Titheridge (1966).

Any significant seasonal variation in the relative concentration of O and N₂ in the F region would be expected to produce a seasonal variation in the production rate. Mayr and Mahajan (1971) have reported a semiannual variation in O/N₂ ratio with equinoxial peaks and solstitial minima with an amplitude

of about 1:1.5. These semiannual changes in the neutral composition should be able to explain the semiannual variation of production rate and also the semiannual variation of TEC reported in Chapter IV.

A clear solar activity dependence of Q_o has been evidenced in the present study. Some justification for using 10.7 cm flux as an index for solar activity rather than R_z is necessary. It is well known that radiation in the band $165 < \lambda < 911$ is mainly responsible for production of ionization in the F region. Neupert et al. (1964) using data from the OSO1 satellite observed a strong correlation between solar flux in 170-300 Å part of EUV spectrum and the solar radio flux at 10.7 cm. Presumably there is some correlation between 10.7 cm solar flux and total EUV photon flux between 165 and 911 Å.

The integrated production rate Q_o is related to the peak production rate q_o in the ionosphere through the equation.

$$Q_o = e H q_o \quad (6.15)$$

Ratcliffe et al. (1956) studied the electron density at the peak of the F_1 layer near noon at a number of different stations and obtained the mean result

$$\frac{q_o}{\alpha} = 5.0 [1 + 0.016R] \times 10^{22-6} \text{ m}^{-3} \quad (6.16)$$

where R is the mean sunspot number and α the F_1 layer recombination coefficient, of order $10^{-14} \text{ m}^3/\text{sec}$. Calculations of q_o based on the present value of Q_o agree with the value of

Ratcliffe et al. (1956) for similar solar activity conditions. Rishbeth and Setty (1961) studied the rate of change of electron density at fixed heights in the ionosphere at sunrise and obtained a solar cycle variation of Q_o similar again to that obtained by Ratcliffe et al. (1956). King and Lawden (1962) determined the production rate at noon in summer from the shape of electron density profile in the F_1 - F_2 transition region and obtained same sunspot cycle variation of Q_o as obtained by Ratcliffe et al. (1956). Titheridge (1966) obtained a solar cycle variation of Q_o using Syncom 3 data of TEC of the same order as obtained by earlier workers using ionogram data. Smith (1968) studied the correlation between $Q_{90}(O^+)$ and solar flux at 10.7 cm after a 30 days running mean has been subtracted out. He found a significant, though not large, correlation between the two. Walker (1971) has reported linear increase of integrated production rate for an overhead sun, Q_o , with sunspot number R (for $R \geq 50$) according to the equation.

$$Q_o = 8.55(1.3 + 0.01R)10^{13} / \text{cm}^2 / \text{sec} \quad (6.17)$$

All the above results support our present observation of linear increase of Q_o with 10.7 cm solar flux.

6.4.2 Effective loss rate

A semianual variation in the loss rate is also seen in the present study. Rishbeth (1964) determined the effective loss rate from the rate of decay of electron density at the peak of

F layer in the first few hours after sunset. He obtained mean results for Slough (52°N) and Watheroo (30°S) of about $0.4 \times 10^{-4} \text{ sec}^{-1}$ in summer and 1.2×10^{-4} in winter. Our results give values of β' about $0.5 \times 10^{-4} \text{ sec}^{-1}$ in summer and $1.1 \times 10^{-4} \text{ sec}^{-1}$ in winter. This shows a good agreement. Titheridge (1966) obtained a value of β' of $0.47 \times 10^{-4} \text{ sec}^{-1}$ in summer and $1.17 \times 10^{-4} \text{ sec}^{-1}$ in winter at Auckland. Thus it is seen that the loss rate calculated from Total content as well as from fixed heights on near the peak agree well each other. This means the loss rate is independent of height and that the layer takes up a shape preserving form. Seasonal variation in the effective loss rate has also been found by Titheridge (1966) and Walker (1971) agreeing with the present results.

If the loss rate that is found after sunset had persisted throughout the night, the electron content would have fallen by a factor of 10 to 40 in about 6 hours. But in practice this fall is greatly reduced and one sees that many times the electron content is steady during the night. This can be explained as due to a very small loss rate than what is observed at sunset or due to some extra production sources, which maintain the nighttime ionosphere. The loss rate may be reduced by vertical movement of the layer to a region of low loss rate. The extra production sources could be downward diffusion from the protonosphere and charged particle flux which produces ionization. Thus the measurement of the loss rate at night is of great importance in judging the relative importance of the above said processes in maintaining nighttime and winter polar ionosphere.

C H A P T E R - V I I

IONOSPHERIC SCINTILLATIONS OF RADIO SIGNALS

7.1 Introduction

The random fluctuations in the amplitude and phase of trans-ionospheric signals because of the diffraction of these signals at the ionospheric irregularity screen are known as scintillations. The study of such scintillations of signals transmitted by artificial satellites or of radio star signals gives information about the physical nature and scattering mechanisms of these irregularities. Another area where these data are essential is for the designing of any satellite radio communication systems.

Global Morphological study of the occurrence of scintillations have been carried out by Aarons et al. (1971), Pope (1974) and Aarons (1975). On average there is an equatorial belt of high scintillation of $\pm 20^\circ$ in width, then a region of weak scintillations in middle latitudes and again a high latitude high scintillation region extending from about 60° to the poles. Scintillation is mainly a nighttime phenomenon and is affected by solar and magnetic activities and is seasonally dependent.

Early studies of scintillations were carried out at middle and high latitudes using radio star signals traversing the ionosphere. These studies have indicated a high degree of

correlation between nighttime scintillations and spread F (Wild and Roberts 1956 and Booker 1958). With the advent of artificial earth satellites scintillation studies were extended to all latitudes. In middle latitudes again a positive correlation was found between scintillation and spread F (Yeh and Swenson 1959, Beynon and Jones 1964 and McClure 1964). At equatorial latitudes, Kent (1961) observed that scintillation is a nighttime phenomenon and its behaviour was very similar to spread F. Singleton and Lynch (1962) and Koster (1972) also observed the same. Bhargava (1964) studied the radio star scintillation at Kodaikanal and Chandra and Rastogi (1974) using satellite signal scintillations at 40 MHz at Thumba also established a positive correlation between scintillation and spread F. Thus scintillation is confirmed to be mainly a nighttime phenomenon associated with spread F irregularities. In this chapter a study of the occurrence of scintillation, the nocturnal and seasonal variation of scintillation activity and the latitudinal extent of low latitude irregularity belt is made using the scintillation data of 40 and 41 MHz signals recorded at Ahmedabad during the years 1964 through 1968.

There has been evidence for the occurrence of daytime scintillations at high and middle latitudes. Chivers and Greenhow (1959) have observed that there is a large contribution at auroral latitudes to radio star scintillations from field aligned irregularities in the E region. Bolton et al. (1953), Dueno (1956)

and Munro (1966) also associated daytime high latitude scintillations with sporadic E irregularities. McClure (1964) has estimated the height of scintillation causing irregularities using a three station triangulation technique and found that irregularities causing daytime scintillations are around 100 km altitude at a middle latitude site. He also attributed these to Es irregularities. Larons and Whitney (1968) again at two mid latitude observatories have concluded that summer daytime scintillations during periods of low magnetic activity are associated with Es patches of 300 - 600 km width with high critical frequency.

Coming to equatorial and low latitudes, Singleton and Lynch (1962) have not found any significant correlation between scintillations and f_oE_s at Brisbane (20°N). Koster and Wright (1963) have observed an unusually regular type of daytime scintillations, which were closely related to disturbances in the equatorial electrojet. Bhargava (1964) could not identify any genuine daytime scintillations at Kodaikanal in radio star transmissions. Nevertheless, Ramakrishnan (1967) has reported correlation of scintillation with Es at Ahmedabad. Most recent observations of 40, 140 and 360 MHz scintillations at Ootacamund from the ATS-6 satellite transmissions have evidenced quite strong daytime scintillations at all these three frequencies which seems to obey the inverse frequency dependence of scintillation strength. This indicates that the thin screen weak or single

scattering mechanism is valid at daytime which in turn gives the inference that daytime scintillations are due to thin Es patches which are known to have very small vertical extents of the order of 1-2 km. It may also be mentioned ~~at~~ this context that the above observations (viz at Ootacamund using ATS-6) also evidenced that nighttime scintillations often violate the frequency law thereby indicating that nighttime scintillations are due to a thick belt (vertical extent about 100 km) of spread F irregularities (Deshpande et al. 1976).

Report from Comsat stations (Taur 1973) indicate microwave scintillations and Whitney et al. (1973) observed scintillations in the 4-6 GHz band at equator. L band scintillations greater than 1 db were observed at Peru (Sessions 1972). Thus the scintillation activity is strong even upto L band frequencies at equator. Under this state of affairs a detailed study of scintillation at equatorial and low latitudes is essential at as high frequencies and as many frequencies as possible.

7.2 Seasonal variation of scintillation occurrence

Scintillations were observed mainly on nighttime passes. Passes having scintillation for the whole or part of the passes were analysed to study scintillation phenomenon. Nighttime and daytime scintillations were studied separately. A cursory examination of the data showed that scintillations were more frequent in low solar activity years 1964 and 1966 compared to

the high solar activity years 1967 and 1968. On each pass showing scintillations, the time of onset and disappearance of the scintillations were first noted. From this the sub-satellite latitude and longitude for the start and end of scintillation could be read off from the refined world maps for the satellites supplied by NASA. Knowing the sub-satellite points the sub-ionospheric point for an ionospheric height of 350 km where the F layer irregularities are supposed to be concentrated were computed. Thus, an estimate of the latitudinal extent of the irregularity region was obtained. It must be noted that in many passes an abrupt scintillation boundary was seen showing clear Faraday fades on one side of this transition and random amplitude fluctuations marking the Faraday fades on other side of this transition. These are indicative of the boundary of the low latitude scintillation belt at around 20-30° geographic latitude.

From each pass having scintillation a mean scintillation index was scaled defined as

$$S.I = \frac{P_{max} - P_{min}}{P_{max} + P_{min}} \quad (7.1)$$

where P_{max} and P_{min} are the maximum and minimum excursions made by the signal amplitude.

During the period 1964 November through 1968 December about 560 nighttime passes showing scintillations were observed. These were grouped into different months and the number of passes

with scintillation seen in each month were plotted against the month for each year. This result is shown in Figure 7.1. In the upper right of the diagram, the mean seasonal variation obtained by combining the data of all the years is plotted. It is seen that the number of cases in the low sunspot year 1965 is much more than the number of cases in the years 1967 or 1968 indicating an inverse relationship of scintillation occurrence on solar activity. Further, in any particular year the number of passes with scintillation is much more in the summer months of May, June, July and August than the other months, thus showing a summer maximum in the occurrence of scintillations. In the average annual curve also, scintillation is most pronounced in the summer months.

7.3 Nocturnal variation of scintillation

Having confirmed the summer maximum of scintillation occurrence, the summer data is subjected to more detailed analysis to study the nocturnal variation of scintillation activity. All the nighttime summer scintillation data are grouped into different hourly intervals from 18 hr LT to 06 hr LT. The number of scintillation occurrence in each time group is plotted against the hour to obtain the nocturnal variation of scintillation occurrence. The results are shown in Figure 7.2. It is seen that the occurrence of scintillation increases steadily from about 18 hr LT upto about 22 hr LT after which there is a decrease of scintillation activity till about 01 hr. Again a

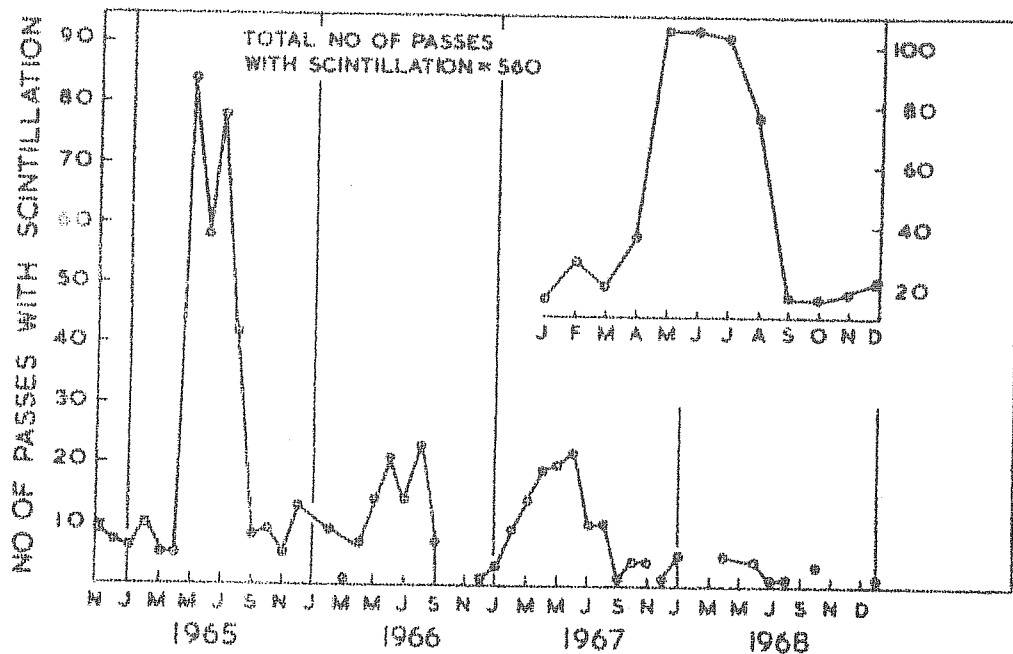


Figure 7.1 : Seasonal variation of scintillation occurrence for each year separately for all the years put together (upper right diagram)

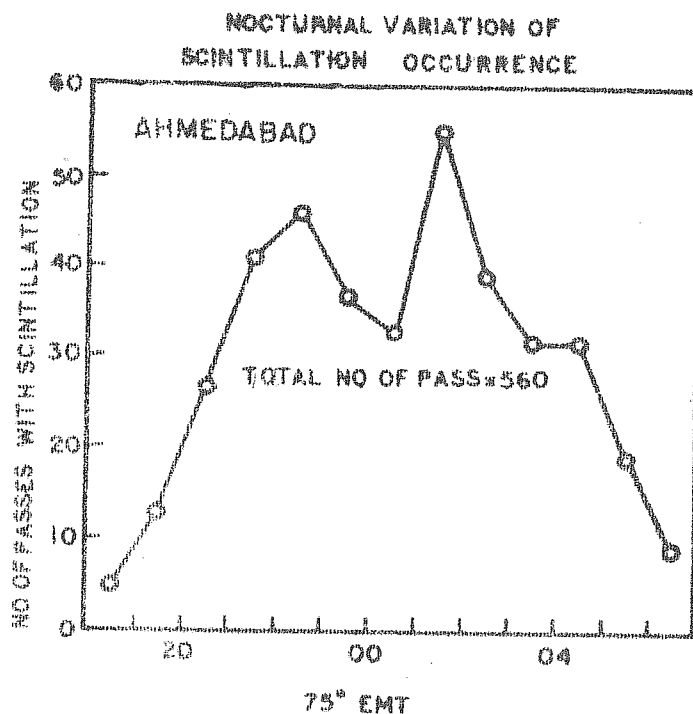


Figure 7.2 : Nocturnal variation of scintillation occurrence.

second peak of scintillation occurrence around 02 hr LT is seen after which the scintillation occurrence falls. Thus two peaks of scintillation occurrence one in the pre midnight portion and the other in the post midnight time separated by a valley of low occurrence around midnight is seen during summer months.

Next, it is attempted to study the depth of the scintillations. For this, the scintillation index defined in equation (7.1) is used to calculate the scintillation index (S.I). The value of scintillation index scaled from each nighttime pass is grouped into different hourly groups from 18 hr LT to 06 hr LT. The mean scintillation index for each hourly group is then calculated and plotted against time. These results of nocturnal variation of scintillation index are shown in Figure 7.3 for equinox winter and summer months separately. The annual mean nocturnal variation of S.I. is also shown in the Figure. The general tendency of these curves in any season to show a dip in scintillation index around midnight and a double peak structure one in the pre midnight and the other in post midnight period. This picture is true for all the seasons although there are some differences in the position and size of these peaks in different seasons. Hence on the annual average picture also the same structure is seen.

7.4 Latitudinal variation of scintillation

It has already been said in Chapter V that the best advantage of low orbiting satellites is to study the spatial

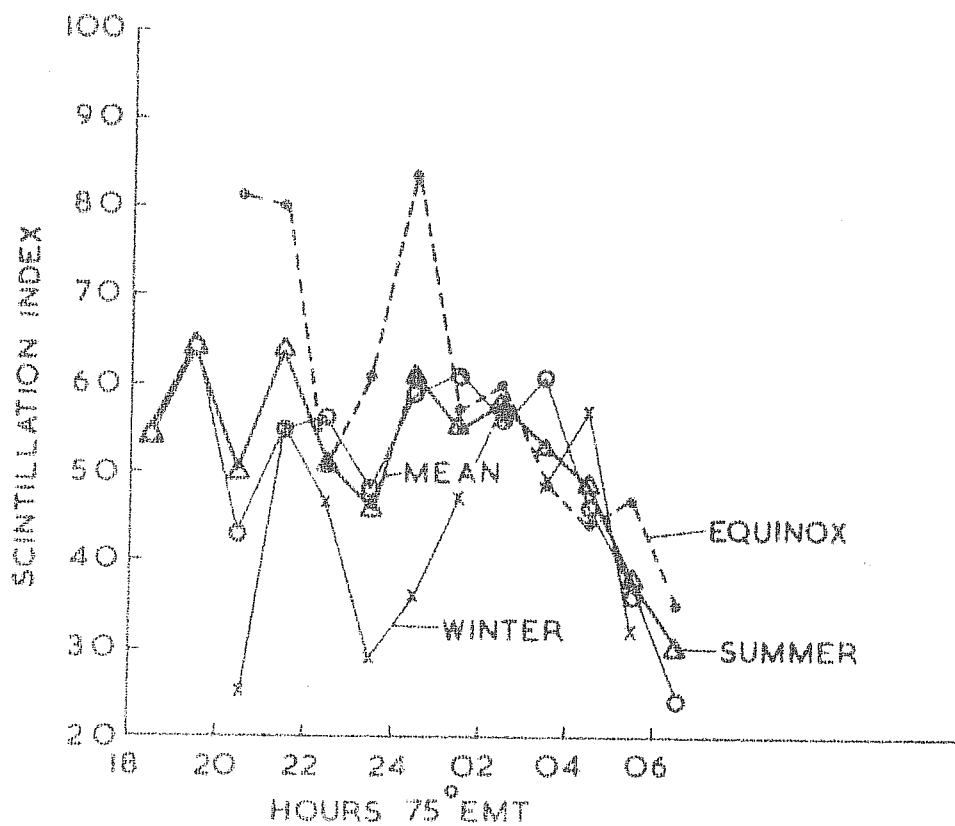


Figure 7.3 : Nocturnal variation of scintillation index at Ahmedabad.

variation of ionospheric phenomena. Hence, in each pass, a section of the irregularity belt is scanned by the ray path from the satellite to the observer. If this ray path happens to pass through the boundary between high scintillating and relatively scintillation free zones, an abrupt boundary in the record will be noticed indicating this transition. Such abrupt boundaries are often noticed and the sub-ionospheric latitude corresponding to this boundary is found to be on average between 20 and 30°N geographic latitude. This gives an indication of the upper boundary of low latitude irregularity belt.

Often it is not possible to identify such abrupt boundaries but scintillation will be observed throughout the extent of the pass. For such passes the scintillation index was scaled every 30 seconds during the pass and the sub-ionospheric latitude corresponding to these points calculated. Putting together all the nighttime scintillating passes in summer months an examination of the latitude variation of the scintillation index is made. These results are shown in Figure 7.4. Although there is not much variation in the scintillation index with latitude, at a latitude of about 28°N we see that S.I. is greatly reduced from a value of 63% to about 50%, thereafter upto about 32°N latitude scintillation index remains low at about 50%. This transition may be again indicative of the upper boundary of low latitude irregularity belt.

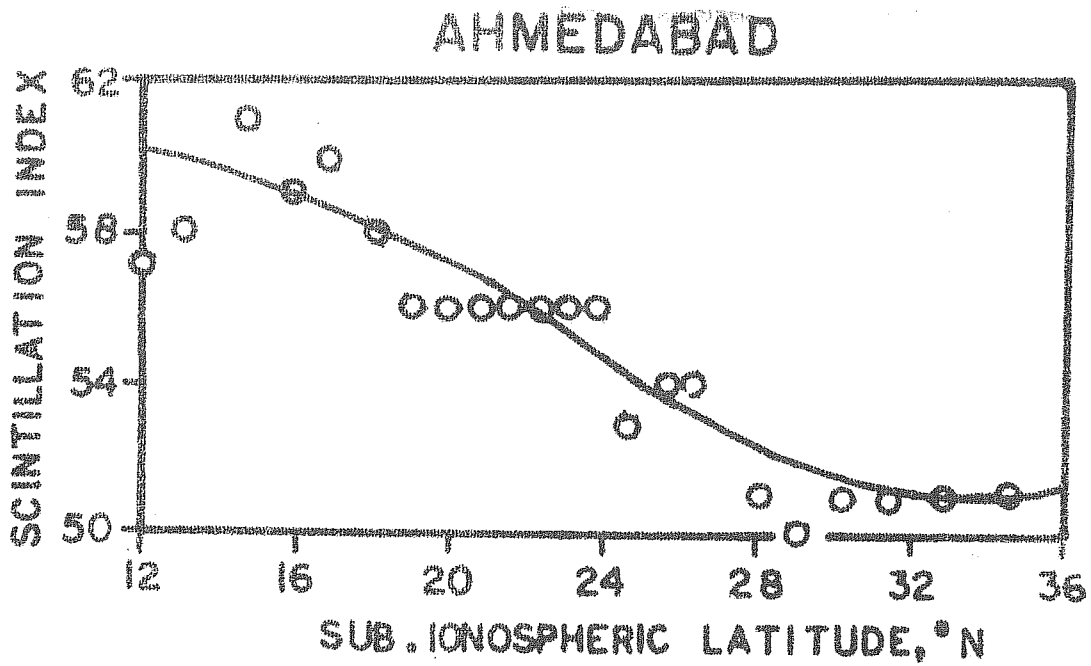


Figure 7.4 : Latitudinal variation of scintillation index.

7.5 Dependence of scintillation on sporadic E

As mentioned in the introduction, there is not much evidence for the association between scintillation in the daytime and sporadic E irregularities, whereas at auroral and high latitudes daytime scintillations are known to be caused by Es irregularities. Therefore an attempt was made to correlate the daytime scintillation activity with sporadic E irregularities. Most of the daytime scintillations were seen on summer months and blanketing type of sporadic E is common at tropical latitudes in summer. Therefore a relationship between the two is sought. Daytime scintillations are distinct from the nighttime ones in that daytime scintillations are of patchy type with about one degree in latitudinal extent or about 100 km horizontal dimension. An example of this type of scintillation patch during daytime is seen from Figure 7.5. The figure shows a pass of the satellite BE-C on 6 May 1965 at about 0930 75° EMT. The sub-ionospheric latitude for an ionospheric height of 100 km is also indicated in the figure. We see that a patch of strong scintillation extending in latitude from about 23.5 to 23.7°N is seen, outside which extent the Faraday fades are very clear. The ionograms taken at Ahmedabad (23°N) at 0915, 0930 and 0945 hr are also shown in the figure. It is seen that strong Es patches with critical frequency of about 7 MHz and at least two reflections are seen in these ionograms. The F region, expectedly is quite smooth. This indicates that the scintillations of the satellite signals at 40 and 41 MHz are caused by the Es-b irregularities.

6-MAY, 1965

0915

0930

0945

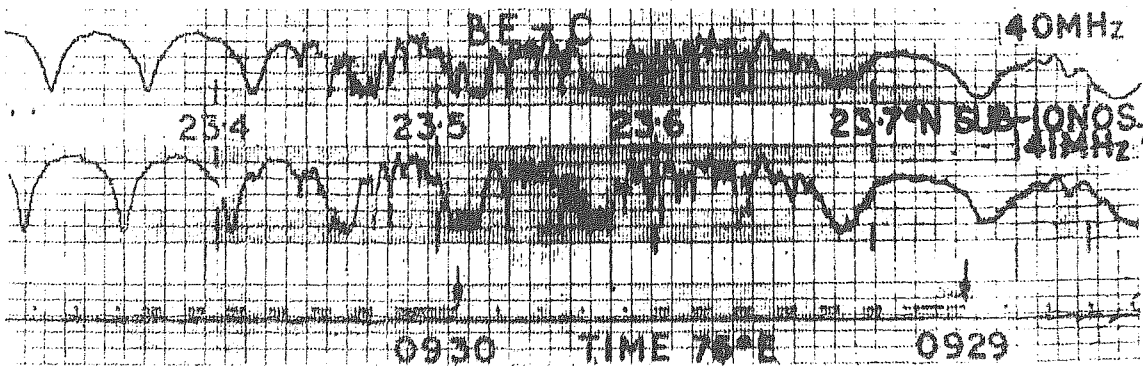
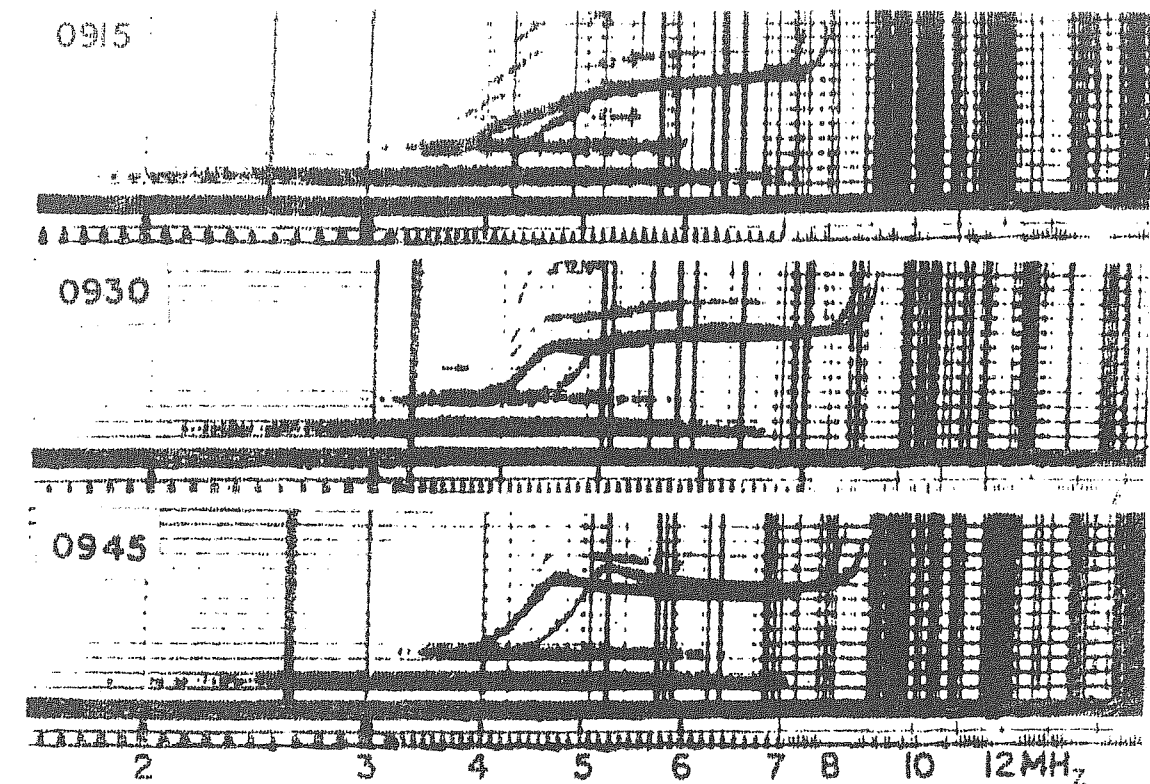


Figure 7.5 : Example of a daytime patch of scintillation at 40 and 41 MHz signals from BE-C satellite on 6 May 1965 caused by the blanketing Es seen in the ionograms at Ahmedabad on the top of the diagram.

Another example of similar patchy type scintillations caused by Es-b irregularities of critical frequency greater than 15 MHz on the 40 and 41 MHz transmissions from satellite BB-B on 25 May 1965 is shown in Figure 7.6. The above two examples indicate effectiveness of E region irregularities in causing satellite signal scintillations.

To understand the dependence of scintillation strength on the intensity of the Es irregularities, the critical frequency (f_oE_s) of the Es trace as seen on the actual ionograms at the nearest time of satellite pass is scaled. A plot of S.I. against f_oE_s is made in Figure 7.7. A good linear relationship between the two is obtained with a scintillation index of about 30% at 4 MHz increasing to 100% for an f_oE_s value of 16 MHz. This indicates that stronger the irregularity amplitude in the Es patch larger the scintillation index.

7.6 Discussion of the results

The conclusions from the above investigation may be summarised as follows. Scintillation activity is more frequent during summer months and low solar activity period. Nocturnal variation of scintillation occurrence as well as S.I. shows a dip around midnight with two peaks one in the pre midnight and the other in the post midnight period. The latitudinal extent of the low latitude irregularity belt is at least upto 28°N latitude (geographic). Sporadic E patches of blanketing type are effective in causing daytime scintillations and the strength

25-MAY, 1965

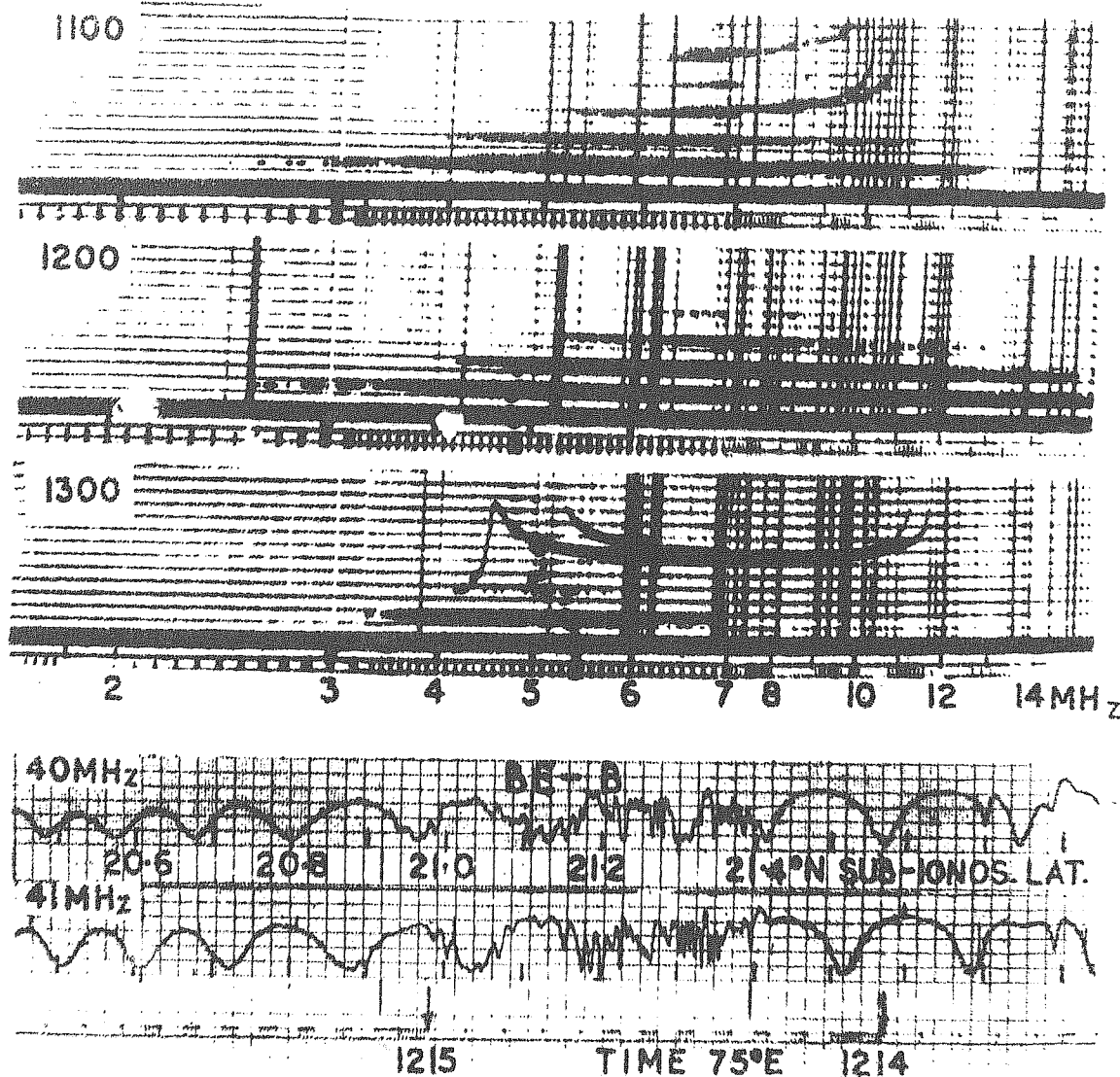


Figure 7.6 : Example of daytime scintillations caused by Es-b irregularities on 25 May 1965.

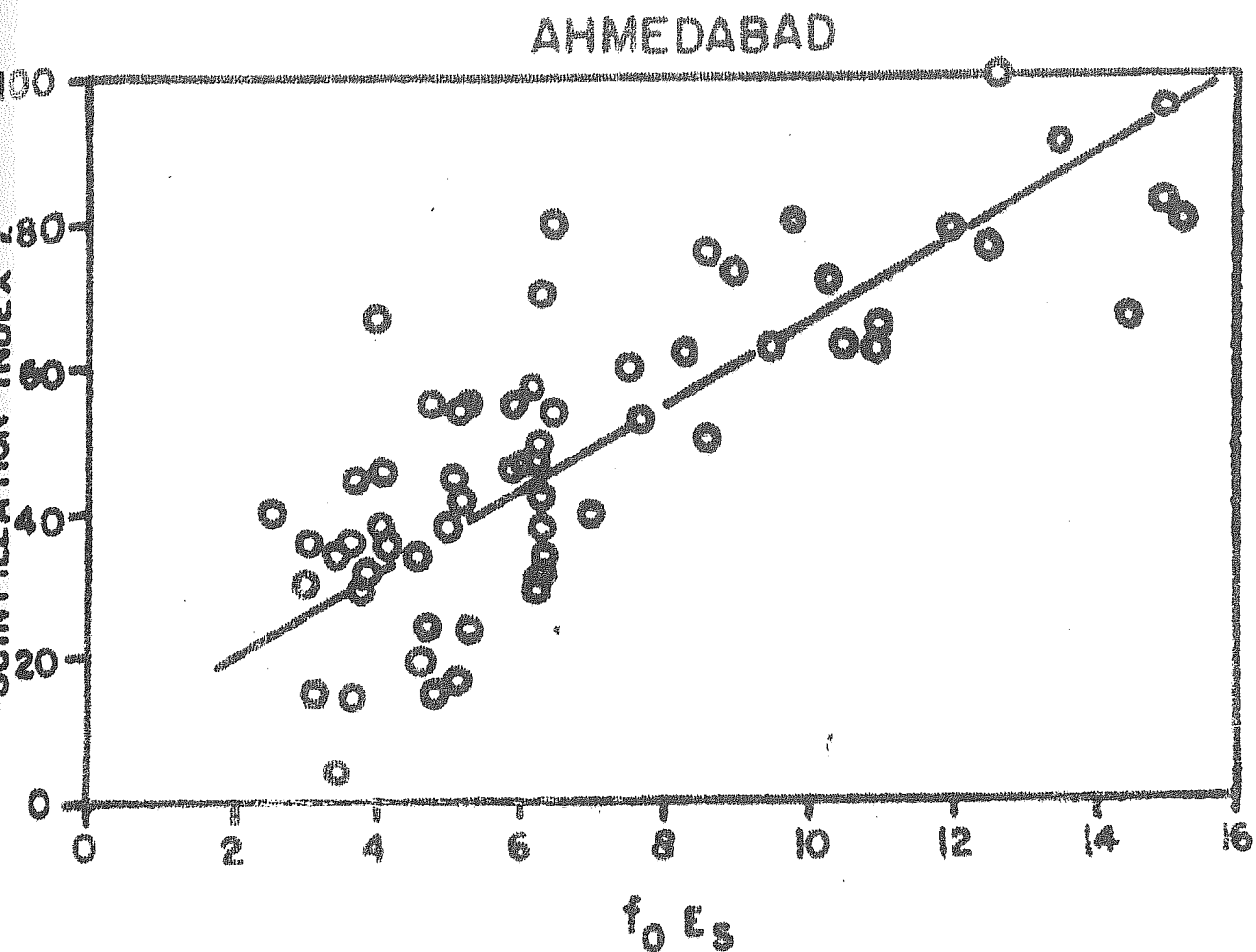


Figure 7.7 : Dependence of scintillation index (S.I) on critical frequency of Es ($f_o E_s$)

of scintillation linearly increases with the critical frequency of Es layer.

As regards the seasonal pattern of scintillations, there are significant longitudinal differences. Long series of observations of ATS-3 at Huancayo (Hawkins and Mullen 1974) has shown that scintillation occurrence is maximum in equinoxes; but the November to January occurrence is also comparable to the equinoctial occurrence in some years. It should also be noted that Laur (1973) found maxima in February, March, April and in September, October and November. The above are in VHF and still higher frequency range and hence may be showing high occurrence in the northern summer solstice due to saturation effects of the receiving set up where relatively low signal to noise levels persist and hence scintillation fades close to noise levels will be observed. Comparing with the results of Koster (1968) at Legon (African zone) and Chatterjee et al. (1974) at Huancayo using 41 MHz transmissions of BE-B and BE-C satellites it is found that a principally semiannual periodicity is seen at Legon while at Huancayo, a superposition of annual and semiannual periodicities, the annual one predominating, is visible. Our results favour a clear annual periodicity with summer maximum. In Indian zone Bhar et al. (1970) using 20 and 40 MHz signals from BE-B and BE-C again found a seasonal variation with summer maxima and winter minima. It seems that the relative position and separation between the geographic and

of scintillation linearly increases with the critical frequency of Es layer.

As regards the seasonal pattern of scintillations, there are significant longitudinal differences. Long series of observations of ATS-3 at Huancayo (Hawkins and Mullen 1974) has shown that scintillation occurrence is maximum in equinoxes; but the November to January occurrence is also comparable to the equinoxial occurrence in some years. It should also be noted that Taur (1973) found maxima in February, March, April and in September, October and November. The above are in VHF and still higher frequency range and hence may be showing high occurrence in the northern summer solstice due to saturation effects of the receiving set up where relatively low signal to noise levels persist and hence scintillation fades close to noise levels will be observed. Comparing with the results of Koster (1968) at Legon (African zone) and Chatterjee et al. (1974) at Huancayo using 41 MHz transmissions of BE-B and BE-C satellites it is found that a principally semianual periodicity is seen at Legon while at Huancayo, a superposition of annual and semianual periodicities, the annual one predominating, is visible. Our results favour a clear annual periodicity with summer maximum. In Indian zone Bhar et al. (1970) using 20 and 40 MHz signals from BE-B and BE-C again found a seasonal variation with summer maxima and winter minima. It seems that the relative position and separation between the geographic and

magnetic equators play a part in the seasonal pattern. Wherever the two coincide, equinoctial peaks seem to be occurring.

Coming to the nocturnal variation of scintillation occurrence, Koster (1968) has reported a single peak around midnight at Legon, Ghana. At Huancayo, Chatterjee et al. (1974) reported a double peaked structure with a pre midnight and post midnight peak in scintillation occurrence. Aarons (1975) has shown that at Huancayo at 5.4 MHz transmission from LES-6 satellite scintillation shows before midnight peak in both quiet and disturbed days while on the scintillation occurrence shows a second peak after mid night only on disturbed days. Basu et al. (1975) using INTELSAT 2F2 observation at Calcutta have shown there are two distinct types of scintillations, one occurring mostly in the post midnight period and associated with spread F the other mainly in the afternoon sunset period and associated with Es. As we have not distinguished between quiet and disturbed days in this study, the occurrence of pre midnight and post midnight peaks in scintillation occurrence seems to be in agreement with observations at other low latitudes.

The northern boundary of the irregularity belt as seen from our results is about 28°N geographic which will correspond to a dip of about (38°N). This is in agreement with the observation of Chandra and Rastogi (1974) from the analysis of BE-B and BE-C passes recorded at Thumba, that the latitudinal width of the irregularity belt is about 1000 km centred on a dip of 5° . Sinclair and Kelleher (1969) have estimated the width of

equatorial irregularity belt from BE-B and BE-C data from 3 stations in Africa situated between 0.6°S and 21.2°S dip latitudes. They were able to observe only the southern half of the belt. They found that on average the scintillation belt has a width of about 32° of magnetic latitude. Observations of Chatterjee et al. (1974) indicate a width of only about 11° for the belt at Huancayo using similar technique.

A close association between scintillation and spread F is known to exist and is proved for Indian equatorial region by comparison with ionosonde and BE-B and BE-C data at Thumba by Chandra and Rastogi (1974). Therefore it would also be worth comparing the width estimated from spread F observations. Skinner and Wright (1957) and later Wright (1959) reported on the basis of their observations in Africa that the equatorial spread F belt is confined roughly between $\pm 20^{\circ}$ magnetic latitude. For American zone Knecht and Schlitt (1958) made a preliminary estimate using IGY data of a chain of stations across the equator and found the belt extends $\pm 5^{\circ}$ magnetic latitude. This narrow width was disproved by a fuller analysis by Singleton (1960) who found the belt extends to $\pm 20^{\circ}$ magnetic latitude. Shimazaki (1959) using a global survey found that under sunspot maximum conditions the width of the belt is $\pm 20^{\circ}$ geomagnetic latitudes. Lyon et al. (1960) examined the data on a zonal basis and found that the average extension of the belt is $\pm 30^{\circ}$ magnetic latitude. The belt was also observed by topside sounder satellites (Calvert and Schmidt, 1964) at a value of $\pm 30^{\circ}$

geomagnetic latitude has been reported.

The values of the width given by different authors are not directly comparable as width depends on several factors and some kind of prior standardisation is required. The factors are local time, season, sunspot activity, magnetic activity reference level of occurrence at which width is estimated (half occurrence, 5% occurrence etc) and the unit (degree of dipole latitude, dip latitude etc). Furthermore, a very close chain of stations were operating only for a very short duration during IGY. Therefore the width estimates by low orbiting satellites are to be considered more reliable. It appears that most estimates using spread F index favour a width of $\pm 20^\circ$ magnetic latitudes as the average limits of the belt (Elkins 1970). However, Lyon et al. (1960) observed that the width of the belt is about 26° in J months in Afro-Indian zone while it is only about 8° in American zone. These observations are confirmed by our estimate of the boundary of the belt at about 28° geographic latitude or about 25° dip latitude.

The present study also indicates the distinction between scintillations produced by spread F irregularities and Es irregularities.

Based on the observations of microwave scintillations Wernick and Liu (1974) have theoretically found that a thick irregularity screen of 200 km vertical extent with electron

density irregularities 20% of the background density will explain the observed results. The frequency dependence of scintillations at 4 and 6 GHz also supports this view.

For the generation of the equatorial scintillation causing irregularities Beer (1973) have postulated spatial resonance mechanism where the vertical and horizontal components of the ionization's velocity match respectively with the vertical and horizontal phase velocities of atmospheric gravity waves. This will set up a plasma instability which grows and hence accounted for irregularities ranging from a few metres to several kilometres in size.

C H A P T E R - V I I I

APPLICATIONS OF BEACON SATELLITE MEASUREMENTS

8.1 Introduction

Beacon signals transmitted from satellites can be considered as electro magnetic waves with essentially constant amplitude, frequency and polarization. The expression coherent means that two beacon signals are emitted from a satellite in such a way that their phase relation is constant with time at the antenna (or is at least varying only very slowly compared to the phase changes observed at the location of the receiver, originating from the changes in the intervening ionospheric and tropospheric medium).

Two types of Beacon Satellites can be used (a) Low orbiting satellites (most data are from satellites in nearly circular orbits with an altitude around 1000 km) and (b) Geostationary satellites (better geosynchronous satellites with small eccentricity and small orbital inclination). Since geostationary satellites are available for beacon measurements, more data have been derived from the observations of this type of satellites. The advantage of geostationary satellites is obvious. It is possible from each station to observe continuously under stable geometric conditions and with very good time resolution. Disadvantage is that one station alone cannot give spatial resolution. Problems arise because of geographic

application in the wider sense of the term - the use of data derived from beacon measurements in ionospheric research - is excluded.

8.2 Direct application of beacon measurements

Direct applications of beacon satellite measurements are used to derive geometrical relations between signal source (satellite and receiver). The interlaying medium affects the signal parameters and through these the accuracy of the results. It is not possible to separate the geometrical influence and the influence of the medium (ionosphere, troposphere) but a careful choice of the beacon frequencies and the application of the knowledge we already have of the characteristics of the medium will help evaluate the relative contributions. The beacon observations can be applied in two ways (1) Tracking of satellites - determination of the orbit of the satellite when the position of the receiver is known (2) Position finding (determination of the position of the receiving station when the orbit of the satellite is known). Position finding is applied for navigation (e.g. commercial use of the USNNSS) and for geodetic problems. The importance of the latter use is increasing because the accuracy obtained with Doppler system is comparable with the accuracy of Laser ranging if the ionosphere is quiet and if the influence of the ionosphere is carefully taken into account.

For many purposes it is necessary to use corrections for the influence of the ionosphere. The best way to get the

appropriate corrections is to measure the ionospheric contribution to the signal parameters observed. In the case of phase measurements it is possible to use automatic compensation for the first order ionospheric influence if the satellite has two coherent beacons with widely spaced frequencies. The first order ionospheric influence in all signal parameters is proportional to the slant electron content.

8.3 Application of beacon methods in space research

Space probes are necessarily linked to ground via radio waves. Therefore it is an obvious idea to use communication carriers (or special radio beacons) for scientific investigations of the plasma between the space probe and the ground station. The main characteristic which can be investigated is again the electron content from the space probe to ground station. In most cases it is necessary to subtract the contribution of the ionosphere of the earth.

To give a few examples: Beacon measurements have been used or will be used in near future to study the interplanetary plasma, the solar corona and the ionosphere of planets.

8.4 Application of satellite beacon data in the construction of engineering parameters

Data on the behaviour of the ionosphere are needed whenever satellites are used. Communication systems are among the most important technical applications of satellites. Therefore Engineering parameters derived from beacon satellite observations

are normally tailored to the needs of communication links using satellites.

In most cases details of the electron density profile are not of interest because the first order contributions of the ionosphere to all signal parameters is proportional to the slant electron content from the ground to the satellite. Therefore the electron content is the basis from which engineering parameters are derived.

Among others, the following information useful for the planning and construction of engineering systems can be derived from electron content data:

- state of ionosphere (disturbed or undisturbed)
- occurrence of magnetically disturbed conditions
- dependence on solar activity
- range of electron content values under quiet and disturbed conditions
- mean values, extreme values, probability that a given value is exceeded
- rate of change of electron content
- mean latitude dependence of electron content
- horizontal gradients of electron content mean and extreme values.

8.5 Application of scintillations data

It is at least equally important to characterize the quality of reception of transmissions in respect of occurrence of

irregular fluctuations (scintillations). The frequency dependence of scintillations, the amplitude of the fluctuations which are to be expected at various conditions, the geographic distribution of scintillation occurrence the correlation of scintillation occurrence with solar and geomagnetic activity give the basic material for the derivation of engineering parameters which are very important for all systems using radio links through the ionosphere.

From scintillation data one can derive the following information:

- probability of scintillation occurrence in a given region and for a given frequency
- severity of scintillation in amplitude and phase
- probability that a given value of amplitude or phase deviation is exceeded
- time dependence of scintillation occurrence
- probability that scintillations occur at a given time in a given region and for a given frequency.

A number of alternatives such as going to VHF band where the effect of scintillation is small, to use frequency diversity, to use space diversity and to use coded communications have been suggested to overcome the effect of ionospheric scintillations. Each of these has its own advantages and disadvantages in different applications.

8.6 Computation of engineering parameters from the results of present studies

8.6.1 Method of computation

Some of the engineering parameters such as range error, phase deviation, group delay and differential phase shift between the centre frequency and the different frequencies in a band are computed in this section using as the main input the electron content obtained from the present investigations. The contours of TEC presented in Chapter V for different seasons and solar activity conditions are used to obtain the vertical columnar electron content at important cities like Delhi, Ahmedabad, Calcutta, Bombay and Madras in India. Typically we have assumed a geostationary satellite to be positioned at 35°E (representing ATS-6) and computed the elevation angles from the above cities for this satellite. The contours of constant elevation angle on a grid of latitude vs. longitude is shown in Figure 8.1. From these contours the zenith angle at the ionospheric point for these stations is derived. These are used to obtain the slant electron content at these locations when observed from ATS-6. This slant TEC becomes the basic input for the computation of engineering parameters.

8.6.2 Theory of computation of engineering parameters

(a) Range error

The time delay of a signal propagating through the ionosphere is given by

ANGLE OF ELEVATION OF ATS-6 STATIONED AT 35° EAST

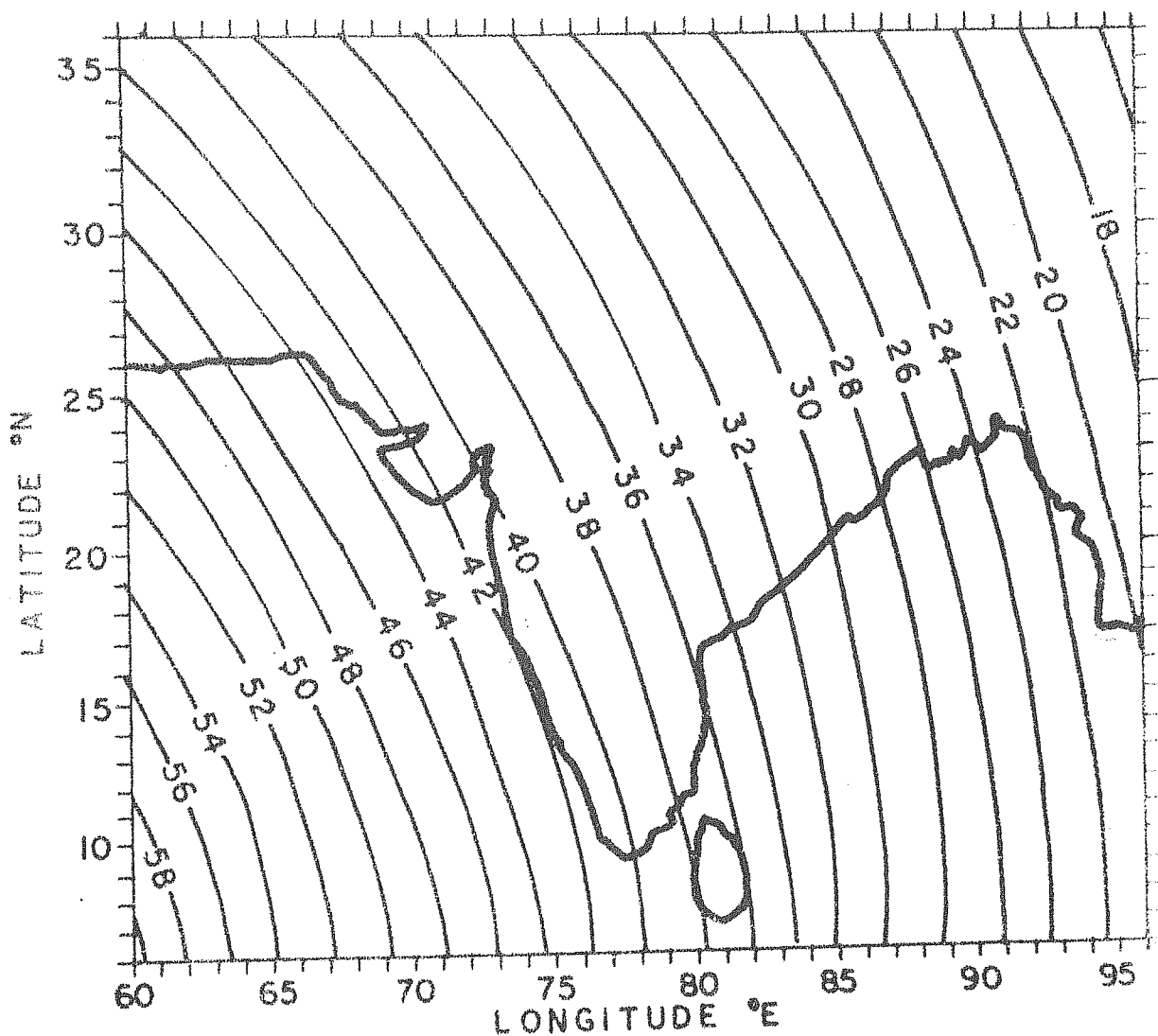


Figure 8.1 : Contours of elevation angle of ATS-6 (at 35°E) over a grid of latitude versus longitude for Indian zone.

$$t = \int_p \frac{ds}{v_g} = \int \frac{ds}{c\mu} \quad (8.1)$$

where ds is an element of path, c velocity of light in vacuum, μ refractive index of the ionosphere at the element ds and \int_p denotes that the integration is performed along the optical path. If we assume a straight line propagation then

$$\int_g ds = R \quad (8.2)$$

where R is the true range and \int_g denotes the integration is performed along the geometric path. An apparent range R' can be defined as the distance resulting from multiplying the observed time delay by the speed of light, i.e.

$$R' = ct \quad (8.3)$$

The error caused by assuming that the apparent range is actually the true range, i.e. by disregarding the ionospheric effect, is

$$\Delta R = R' - R = \int_p \frac{ds}{\mu} - \int_g ds \quad (8.4)$$

The ionospheric refractive index can be expressed as a power series in terms of angular frequency (ω) of the radio wave and under quasi-longitudinal propagation conditions, as

$$\mu = 1 - \frac{\omega_p^2}{2\omega^2} \pm \frac{\omega_c \omega_p^2}{2\omega^3} - \frac{\omega_p^4}{8\omega^4} + \quad (8.5)$$

where ω_p is the angular plasma frequency and ω_c the electron angular gyrofrequency due to the longitudinal component of the geomagnetic field.

We can then express the range error in kilometres by the equation

$$\Delta R = \int_p \left(1 - \frac{\omega_p^2}{2\omega^2} - \frac{\omega_p^2}{8\omega^4} \right) ds - \int_g ds \quad (8.6)$$

Equation (8.5) can be approximated to the first order to get

$$\mu = 1 - \frac{\omega_p^2}{2\omega^2} \quad (8.7)$$

under the valid assumption, ω_p and $\omega_c \ll \omega$, then the range error becomes

$$\Delta R = \frac{40.3}{f^2} \int N ds = 40.3 \frac{\langle \sec \chi \rangle}{f^2} \int N dh \quad (8.8)$$

The quantity $\int N dh$ is the vertical columnar electron content and $\langle \sec \chi \rangle$ is the zenith angle at the mean field height.

(b) Relative phase distortion

The net phase change across the frequency band of a wide band signal is due to two effects. These are the reduction in phase path length and the group delay. Both these can be converted to electrical phase at the appropriate frequency.

The change in phase path length can be written as

$$\Delta S = - \int_0^s (\mu - 1) ds = \frac{e^2}{2\epsilon_0 m \omega^2} \int_0^s N ds \quad (8.9)$$

where ω is the angular frequency of the wave in question.

Equation (8.9) indicates that the phase path length relative to the free space is reduced due to ionospheric electrons directly

as the total electron content along the ray path. This change in phase path can be converted to the phase difference

$$d\phi = \frac{2\pi}{\lambda} \Delta s \quad (8.10)$$

Now the differential phase shift between a frequency f and the central frequency f_c of a band can be written as

$$\Delta\phi = d\phi \Delta f \left(\frac{1}{f} - \frac{1}{f_c} \right) \quad (8.11)$$

where Δf is the band width.

(c) Group delay

If μ' is the group refractive index the incremental group path length relative to the free space path can be written as

$$\Delta s' = \int_0^s (\mu' - 1) ds \approx \int_0^s (1 - \mu) ds = -\Delta s \quad (8.12)$$

This can be expressed as a time delay as

$$dt = \frac{\Delta s'}{c}$$

Therefore the relative group delay at a frequency f with respect to the central frequency is

$$\Delta t = \frac{e^2}{2\epsilon_0 mc} \left(\frac{1}{f^2} - \frac{1}{f_c^2} \right) \int N ds \quad (8.13)$$

(d) Faraday rotation

If a plane polarized wave traverses through the ionosphere, its plane of polarization rotates through a quantity

$$\Omega = \frac{k}{f^2} \bar{M} N_T \quad (8.14)$$

where $k = .0297$, \bar{M} is the magnetic field factor and N_T , the TEC. This rotation of plane of polarization will appear again as a phase change.

8.6.3 Results of a computation of engineering parameters

The basic input for the computation of engineering parameters (Equations 8.8, 8.11, 8.13 and 8.14) for the stations Trivandrum, Madras, Bombay, Ahmedabad, Calcutta, Delhi and Kashmir are the TEC values at these stations derived from the contours of TEC obtained in Chapter V. The contours of elevation angle when a geostationary satellite is stationed at 35°E are also calculated. Knowing these all the propagation parameters except equation (8.14) can be calculated. Calculation of Faraday rotation requires \bar{M} values. These have been computed by our programme and used to derive the Faraday rotation at the upper UHF band. Other parameters are evaluated by calculating the slant electron content.

The results are shown in the form of tables. The frequency range selected is from 800 - 900 MHz with a central frequency 850 MHz. This frequency band has been chosen as it is band used for satellite TV in the SITE experiment.

Tyagi et al.(1972) have calculated the errors in the range and elevation angle due to Ionospheric and Tropospheric refraction effects at Delhi as a function of zenith angle of the object whose position is to be fixed. Calla (1971) has calculated the

relative phase distortion, which is made up of the phase path delay and group path delay, in the 100 MHz communication band between 790 and 890 MHz. He used an assumed electron content of 10^{17} el/m². The present calculations using the actually measured electron content for appropriate season and solar activity conditions and taking into account the slant electron content with appropriate elevation angles should give a more realistic estimate of the propagation effects.

With the advances in the field of radio communication, the geostationary satellites are being made to play a major role for Telephone communication and Television transmissions. As the demand on number of channels increases the bandwidth of the transmissions has also to be increased. With increase of bandwidth the propagation through the ionosphere gets affected in terms of phase dispersion. In a wideband signal, the relative phase dispersion of the various frequency components of a signal can become quite large, causing distortion of the signal and television pictures.

It is therefore expected that the present calculations will be useful in estimating the various propagation effects due to actual ionosphere.

In the tables that follow the following abbreviations are used: AHD - Ahmedabad; CLT - Calcutta, DELR1 and DELR2 - Range error at 150 and 400 MHz respectively and DELPHI1 and DELPHI2 - Phase error at 150 and 400 MHz respectively.

STATION	SEASON	EPOCH	FREQ. (MHZ)	RANGE ERROR (METRES)	PHASE ERROR (RADIAN)	GROUP DELAY (NA.SEC)	DIFFL. PHASE SHIFT (RADIAN)	FARADAY ROTATION (RADIAN)
CELHI	SUMMER	HIGRZ	750	52.235	130.588	0.039	15.459	1.319
DELHI	SUMMER	HIGRZ	760	50.870	128.870	0.034	13.730	1.284
DELHI	SUMMER	HIGRZ	770	49.557	127.195	0.030	12.046	1.251
DELHI	SUMMER	HIGRZ	780	48.294	125.565	0.026	10.405	1.219
DELHI	SUMMER	HIGRZ	790	47.080	123.976	0.022	8.806	1.189
DELHI	SUMMER	HIGRZ	800	45.910	122.426	0.018	7.247	1.159
DELHI	SUMMER	HIGRZ	810	44.783	120.915	0.014	5.726	1.131
CELHI	SUMMER	HIGRZ	820	43.698	119.440	0.010	4.242	1.103
DELHI	SUMMER	HIGRZ	830	42.651	118.001	0.007	2.794	1.077
DELHI	SUMMER	HIGRZ	840	41.642	116.597	0.003	1.380	1.051
DELHI	SUMMER	HIGRZ	850	40.668	115.225	0.000	0.000	1.027
DELHI	SUMMER	HIGRZ	860	39.727	113.885	-0.003	-1.348	1.003
DELHI	SUMMER	HIGRZ	870	38.819	112.576	-0.006	-2.665	0.980
CELHI	SUMMER	HIGRZ	880	37.942	111.297	-0.009	-3.952	0.958
DELHI	SUMMER	HIGRZ	890	37.094	110.046	-0.012	-5.211	0.936
DELHI	SUMMER	HIGRZ	900	36.275	108.824	-0.015	-6.441	0.916

CELHI SUMMER HIGRZ DELR1= 1305.88 DELR2= 183.64 DELPHI1= 652.94 DELPHI2= 244.85

STATION	SEASON	EPOCH	FREQ. (MHZ)	RANGE ERROR (METRES)	PHASE ERROR (RADIAN)	GROUP DELAY (NA.SEC)	DIFFL. PHASE SHIFT (RADIAN)	FARADAY ROTATION (RADIAN)
DELHI	SUMMER	LOWRZ	750	35.673	89.182	0.026	10.558	0.901
DELHI	SUMMER	LOWRZ	760	34.740	88.009	0.023	9.377	0.877
DELHI	SUMMER	LOWRZ	770	33.844	86.866	0.020	8.227	0.854
DELHI	SUMMER	LOWRZ	780	32.982	85.752	0.017	7.106	0.833
DELHI	SUMMER	LOWRZ	790	32.152	84.667	0.015	6.014	0.812
DELHI	SUMMER	LOWRZ	800	31.353	83.608	0.012	4.949	0.792
DELHI	SUMMER	LOWRZ	810	30.584	82.576	0.009	3.910	0.772
DELHI	SUMMER	LOWRZ	820	29.842	81.569	0.007	2.897	0.753
DELHI	SUMMER	LOWRZ	830	29.128	80.586	0.005	1.908	0.735
DELHI	SUMMER	LOWRZ	840	28.438	79.627	0.002	0.943	0.718
DELHI	SUMMER	LOWRZ	850	27.773	78.690	0.000	0.000	0.701
DELHI	SUMMER	LOWRZ	860	27.131	77.775	-0.002	-0.921	0.685
DELHI	SUMMER	LOWRZ	870	26.511	76.881	-0.004	-1.820	0.669
DELHI	SUMMER	LOWRZ	880	25.912	76.008	-0.006	-2.699	0.654
DELHI	SUMMER	LOWRZ	890	25.333	75.154	-0.008	-3.559	0.640
DELHI	SUMMER	LOWRZ	900	24.773	74.318	-0.010	-4.399	0.625
DELHI	SUMMER	LOWRZ	DELRI=	DELRI=	DELRI=	DELPHI1=	DELPHI2=	167.22

STATION	SEASON	EPOCH	FREQ. (MHZ)	RANGE ERROR (METRES)	PHASE ERROR (RADIAN)	GROUP DELAY (NA.SEC)	DIFFL. PHASE SHIFT (RADIAN)	FARADAY ROTATION (RADIAN)
CELHI	WINTER	HIGRZ	750	57.331	143.328	0.043	16.968	1.447
DELHI	WINTER	HIGRZ	760	55.833	141.442	0.038	15.070	1.409
DELHI	WINTER	HIGRZ	770	54.392	139.606	0.033	13.221	1.373
DELHI	WINTER	HIGRZ	780	53.006	137.816	0.028	11.421	1.338
CELHI	WINTER	HIGRZ	790	51.673	136.071	0.024	9.665	1.304
DELHI	WINTER	HIGRZ	800	50.389	134.370	0.019	7.954	1.272
DELHI	WINTER	HIGRZ	810	49.152	132.712	0.015	6.284	1.241
DELHI	WINTER	HIGRZ	820	47.961	131.093	0.011	4.656	1.211
DELHI	WINTER	HIGRZ	830	46.812	129.514	0.007	3.067	1.182
DELHI	WINTER	HIGRZ	840	45.704	127.972	0.004	1.515	1.154
DELHI	WINTER	HIGRZ	850	44.635	126.466	0.000	0.000	1.127
DELHI	WINTER	HIGRZ	860	43.603	124.996	-0.003	-1.480	1.101
DELHI	WINTER	HIGRZ	870	42.607	123.559	-0.007	-2.925	1.076
DELHI	WINTER	HIGRZ	880	41.644	122.155	-0.010	-4.338	1.051
CELHI	WINTER	HIGRZ	890	40.713	120.782	-0.013	-5.719	1.028
DELHI	WINTER	HIGRZ	900	39.814	119.440	-0.016	-7.070	1.005
DELHI	WINTER	HIGRZ	DELRI= 1433.28	DELRI= 201.56	DELPHI= 716.64	DELPHI2= 268.74		

STATION	SEASON	EPOCH	FREQ. (MHZ)	RANGE ERROR (METRES)	PHASE ERROR (RADIAN)	GROUP DELAY (NA.SEC)	DIFFL. PHASE SHIFT (RADIAN)	FARADAY ROTATION (RADIAN)
DELHI	WINTER	LOWRZ	750	25.481	63.701	0.019	7.541	0.643
DELHI	WINTER	LOWRZ	760	24.814	62.863	0.017	6.698	0.626
DELHI	WINTER	LOWRZ	770	24.174	62.047	0.015	5.876	0.610
DELHI	WINTER	LOWRZ	780	23.558	61.251	0.012	5.076	0.595
DELHI	WINTER	LOWRZ	790	22.966	60.476	0.010	4.296	0.580
DELHI	WINTER	LOWRZ	800	22.395	59.720	0.009	3.535	0.565
DELHI	WINTER	LOWRZ	810	21.846	58.983	0.007	2.793	0.551
DELHI	WINTER	LOWRZ	820	21.316	58.264	0.005	2.069	0.538
DELHI	WINTER	LOWRZ	830	20.805	57.562	0.003	1.363	0.525
DELHI	WINTER	LOWRZ	840	20.313	56.876	0.002	0.673	0.513
DELHI	WINTER	LOWRZ	850	19.838	56.207	0.000	0.000	0.501
DELHI	WINTER	LOWRZ	860	19.379	55.554	-0.002	-0.658	0.489
DELHI	WINTER	LOWRZ	870	18.936	54.915	-0.003	-1.300	0.478
DELHI	WINTER	LOWRZ	880	18.508	54.291	-0.004	-1.928	0.467
DELHI	WINTER	LOWRZ	890	18.095	53.681	-0.006	-2.542	0.457
DELHI	WINTER	LOWRZ	900	17.695	53.085	-0.007	-3.142	0.447
DELHI	WINTER	LOWRZ	DELRI= 637.01	DELRI2= 89.58	DELPHI1= 318.51	DELPHI2= 119.44		

STATION	SEASON	EPOCH	FREQ. (MHZ)	RANGE ERROR (METRES)	PHASE ERROR (RADIAN)	GROUP DELAY (NA.SEC)	DIFFL. PHASE SHIFT (RADIAN)	FARADAY ROTATION (RADIAN)
DELHI	EQUINOX	HIGRZ	750	112.115	280.286	0.083	33.181	2.830
DELHI	EQUINOX	HIGRZ	760	109.184	276.598	0.073	29.470	2.756
DELHI	EQUINOX	HIGRZ	770	106.366	273.006	0.064	25.855	2.685
DELHI	EQUINOX	HIGRZ	780	103.656	269.506	0.055	22.333	2.617
DELHI	EQUINOX	HIGRZ	790	101.049	266.095	0.046	18.901	2.551
DELHI	EQUINOX	HIGRZ	800	98.538	262.769	0.038	15.554	2.488
DELHI	EQUINOX	HIGRZ	810	96.120	259.524	0.030	12.289	2.427
DELHI	EQUINOX	HIGRZ	820	93.790	256.360	0.022	9.105	2.368
DELHI	EQUINOX	HIGRZ	830	91.544	253.271	0.014	5.997	2.311
DELHI	EQUINOX	HIGRZ	840	89.377	250.256	0.007	2.963	2.256
DELHI	EQUINOX	HIGRZ	850	87.287	247.312	0.000	0.000	2.204
DELHI	EQUINOX	HIGRZ	860	85.269	244.436	-0.007	-2.893	2.153
DELHI	EQUINOX	HIGRZ	870	83.320	241.627	-0.013	-5.720	2.103
DELHI	EQUINOX	HIGRZ	880	81.437	238.881	-0.020	-8.483	2.056
DELHI	EQUINOX	HIGRZ	890	79.617	236.197	-0.026	-11.184	2.010
DELHI	EQUINOX	HIGRZ	900	77.858	233.572	-0.032	-13.825	1.966

DELHI EQUINOX HIGRZ DELR1= 2802.86 DELR2= 394.15 DELPHI1= 1401.43 DELPHI2= 525.54

STATION	SEASON	EPOCH	FREQ. (MHZ)	RANGE ERROR (METRES)	PHASE ERROR (RADIAN)	GROUP DELAY (NA.SEC)	DIFFL. PHASE SHIFT (RADIAN)	FARADAY ROTATION (RADIAN)
DELHI	EQUINOX	LOWRZ	750	53.509	123.773	0.040	15.836	1.351
DELHI	EQUINOX	LOWRZ	760	52.110	132.013	0.035	14.065	1.316
DELHI	EQUINOX	LOWRZ	770	50.766	130.298	0.031	12.340	1.282
DELHI	EQUINOX	LOWRZ	780	49.472	128.628	0.026	10.659	1.249
DELHI	EQUINOX	LOWRZ	790	48.228	127.000	0.022	9.021	1.218
DELHI	EQUINOX	LOWRZ	800	47.030	125.412	0.018	7.423	1.187
DELHI	EQUINOX	LOWRZ	810	45.876	123.864	0.014	5.865	1.158
DELHI	EQUINOX	LOWRZ	820	44.764	122.354	0.010	4.345	1.130
DELHI	EQUINOX	LOWRZ	830	43.691	120.879	0.007	2.862	1.103
DELHI	EQUINOX	LOWRZ	840	42.657	119.440	0.003	1.414	1.077
DELHI	EQUINOX	LOWRZ	850	41.660	118.035	0.000	0.000	1.052
DELHI	EQUINOX	LOWRZ	860	40.696	116.663	-0.003	-1.381	1.027
DELHI	EQUINOX	LOWRZ	870	39.766	115.322	-0.006	-2.730	1.004
DELHI	EQUINOX	LOWRZ	880	38.868	114.011	-0.009	-4.049	0.981
DELHI	EQUINOX	LOWRZ	890	37.999	112.730	-0.012	-5.338	0.959
DELHI	EQUINOX	LOWRZ	900	37.159	111.478	-0.015	-6.598	0.938
DELHI	EQUINOX	LOWRZ	DELRI= 1337.73	DELRI= 188.12	DELPHI1= 668.87	DELPHI2= 250.82		

STATION	SEASON	EPOCH	FREQ. (MHZ)	RANGE ERROR (METRES)	PHASE ERROR (RADIAN)	GROUP DELAY (NA.SEC)	DIFFL. PHASE SHIFT (RADIAN)	FARADAY ROTATION (RADIAN)
CLT	SUMMER	HIGRZ	750	83.246	208.115	0.062	24.637	1.607
CLT	SUMMER	HIGRZ	760	81.070	205.377	0.055	21.882	1.565
CLT	SUMMER	HIGRZ	770	78.978	202.710	0.048	19.198	1.525
CLT	SUMMER	HIGRZ	780	76.966	200.111	0.041	16.583	1.486
CLT	SUMMER	HIGRZ	790	75.030	197.578	0.034	14.034	1.448
CLT	SUMMER	HIGRZ	800	73.166	195.108	0.028	11.549	1.412
CLT	SUMMER	HIGRZ	810	71.370	192.699	0.022	9.125	1.378
CLT	SUMMER	HIGRZ	820	69.640	190.350	0.016	6.760	1.344
CLT	SUMMER	HIGRZ	830	67.972	188.056	0.011	4.453	1.312
CLT	SUMMER	HIGRZ	840	66.363	185.817	0.005	2.200	1.281
CLT	SUMMER	HIGRZ	850	64.811	183.631	0.000	0.000	1.251
CLT	SUMMER	HIGRZ	860	63.313	181.496	-0.005	-2.148	1.222
CLT	SUMMER	HIGRZ	870	61.866	179.410	-0.010	-4.247	1.194
CLT	SUMMER	HIGRZ	880	60.468	177.371	-0.015	-6.299	1.167
CLT	SUMMER	HIGRZ	890	59.116	175.378	-0.019	-8.304	1.141
CLT	SUMMER	HIGRZ	900	57.810	173.430	-0.023	-10.265	1.116
CLT	SUMMER	HIGRZ	DELRI= 2081.15	DELRI= 292.66	DELPHI= 1040.58	DELPHI2= 390.22		

STATION	SEASON	EPOCH	FREQ. (MHZ)	RANGE ERROR (METRES)	PHASE ERROR (RADIAN)	GROUP DELAY (NA.SEC)	DIFFL. PHASE SHIFT (RADIAN)	FARADAY ROTATION (RADIAN)
CLT	SUMMER	LOWRZ	750	50.262	125.655	0.037	14.875	0.970
CLT	SUMMER	LOWRZ	760	48.948	124.001	0.035	13.212	0.945
CLT	SUMMER	LOWRZ	770	47.685	122.391	0.029	11.591	0.921
CLT	SUMMER	LOWRZ	780	46.470	120.822	0.025	10.012	0.897
CLT	SUMMER	LOWRZ	790	45.301	119.292	0.021	8.473	0.875
CLT	SUMMER	LOWRZ	800	44.175	117.801	0.017	6.973	0.853
CLT	SUMMER	LOWRZ	810	43.091	116.347	0.013	5.509	0.832
CLT	SUMMER	LOWRZ	820	42.047	114.928	0.010	4.082	0.812
CLT	SUMMER	LOWRZ	830	41.040	113.543	0.006	2.688	0.792
CLT	SUMMER	LOWRZ	840	40.069	112.192	0.003	1.328	0.774
CLT	SUMMER	LOWRZ	850	39.131	110.872	0.000	0.000	0.755
CLT	SUMMER	LOWRZ	860	38.227	109.583	-0.003	-1.297	0.738
CLT	SUMMER	LOWRZ	870	37.353	108.323	-0.006	-2.565	0.721
CLT	SUMMER	LOWRZ	880	36.509	107.092	-0.009	-3.803	0.705
CLT	SUMMER	LOWRZ	890	35.693	105.889	-0.012	-5.014	0.689
CLT	SUMMER	LOWRZ	900	34.904	104.712	-0.014	-6.198	0.674
CLT	SUMMER	LOWRZ	DELRI= 1256.54	DELRI= 176.70	DELPHI1= 628.27	DELPHI2= 235.60		

STATION	SEASON	EPOCH	FREQ. (MHZ)	RANGE ERROR (METRES)	PHASE ERROR (RADIAN)	GROUP DELAY (NA.SEC)	DIFFL. PHASE SHIFT (RADIAN)	FARADAY ROTATION (RADIAN)
CLT	WINTER	HIGRZ	750	108.377	270.942	0.081	32.075	2.092
CLT	WINTER	HIGRZ	760	105.544	267.377	0.071	28.487	2.038
CLT	WINTER	HIGRZ	770	102.820	263.905	0.062	24.993	1.985
CLT	WINTER	HIGRZ	780	100.201	260.521	0.053	21.589	1.934
CLT	WINTER	HIGRZ	790	97.680	257.224	0.045	18.271	1.886
CLT	WINTER	HIGRZ	800	95.253	254.009	0.036	15.035	1.839
CLT	WINTER	HIGRZ	810	92.916	250.873	0.029	11.880	1.794
CLT	WINTER	HIGRZ	820	90.664	247.813	0.021	8.801	1.750
CLT	WINTER	HIGRZ	830	88.492	244.828	0.014	5.797	1.708
CLT	WINTER	HIGRZ	840	86.398	241.913	0.007	2.864	1.668
CLT	WINTER	HIGRZ	850	84.377	239.067	0.000	0.000	1.629
CLT	WINTER	HIGRZ	860	82.426	236.287	-0.007	-2.797	1.591
CLT	WINTER	HIGRZ	870	80.542	233.571	-0.013	-5.530	1.555
CLT	WINTER	HIGRZ	880	78.722	230.917	-0.019	-8.200	1.520
CLT	WINTER	HIGRZ	890	76.963	228.323	-0.025	-10.811	1.486
CLT	WINTER	HIGRZ	900	75.262	225.786	-0.031	-13.364	1.453
CLT	WINTER	HIGRZ	DELRI= 2709.42	DELRI= 381.01	DELPHI1= 1354.71	DELPHI2= 508.02		

STATION	SEASON	EPOCH	FREQ. (MHZ)	RANGE ERROR (METRES)	PHASE ERROR (RADIAN)	GROUP DELAY (NA.SEC)	DIFFL. PHASE SHIFT (RADIAN)	FARADAY ROTATION (RADIAN)
CLT	WINTER	LOWRZ	750	39.267	98.168	0.029	11.621	0.758
CLT	WINTER	LOWRZ	760	38.240	96.876	0.026	10.322	0.738
CLT	WINTER	LOWRZ	770	37.254	95.618	0.022	9.056	0.719
CLT	WINTER	LOWRZ	780	36.305	94.392	0.019	7.822	0.701
CLT	WINTER	LOWRZ	790	35.391	93.197	0.016	6.620	0.683
CLT	WINTER	LOWRZ	800	34.512	92.032	0.013	5.448	0.666
CLT	WINTER	LOWRZ	810	33.665	90.896	0.010	4.304	0.650
CLT	WINTER	LOWRZ	820	32.849	89.787	0.008	3.189	0.634
CLT	WINTER	LOWRZ	830	32.062	88.706	0.005	2.100	0.619
CLT	WINTER	LOWRZ	840	31.304	87.650	0.002	1.038	0.604
CLT	WINTER	LOWRZ	850	30.571	86.619	0.000	0.000	0.590
CLT	WINTER	LOWRZ	860	29.864	85.611	-0.002	-1.013	0.577
CLT	WINTER	LOWRZ	870	29.182	84.627	-0.005	-2.004	0.563
CLT	WINTER	LOWRZ	880	28.522	83.666	-0.007	-2.971	0.551
CLT	WINTER	LOWRZ	890	27.885	82.726	-0.009	-3.917	0.538
CLT	WINTER	LOWRZ	900	27.269	81.806	-0.011	-4.842	0.526
CLT	WINTER	LOWRZ	DELRI= 981.68	DEL2= 138.05	DELPHI1= 490.84	DELPHI2= 184.06		

STATION	SEASON	EPOCH	FREQ. (MHZ)	RANGE ERROR (METRES)	PHASE ERROR (RADIAN)	GROUP DELAY (NA.SEC)	DIFFL. PHASE SHIFT (RADIAN)	FARADAY ROTATION (RADIAN)
CLT	EQUINOX	HIGRZ	750	149.215	373.037	0.111	44.161	2.881
CLT	EQUINOX	HIGRZ	760	145.314	368.128	0.098	39.222	2.805
CLT	EQUINOX	HIGRZ	770	141.564	363.348	0.085	34.411	2.733
CLT	EQUINOX	HIGRZ	780	137.958	358.689	0.073	29.724	2.663
CLT	EQUINOX	HIGRZ	790	134.487	354.149	0.061	25.155	2.596
CLT	EQUINOX	HIGRZ	800	131.146	349.722	0.050	20.701	2.532
CLT	EQUINOX	HIGRZ	810	127.928	345.405	0.039	16.356	2.470
CLT	EQUINOX	HIGRZ	820	124.827	341.192	0.029	12.118	2.410
CLT	EQUINOX	HIGRZ	830	121.837	337.082	0.019	7.981	2.352
CLT	EQUINOX	HIGRZ	840	118.953	333.069	0.009	3.943	2.296
CLT	EQUINOX	HIGRZ	850	116.171	329.150	0.000	0.001	2.243
CLT	EQUINOX	HIGRZ	860	113.485	325.323	-0.009	-3.851	2.191
CLT	EQUINOX	HIGRZ	870	110.891	321.584	-0.018	-7.613	2.141
CLT	EQUINOX	HIGRZ	880	108.385	317.929	-0.026	-11.291	2.092
CLT	EQUINOX	HIGRZ	890	105.963	314.357	-0.034	-14.885	2.046
CLT	EQUINOX	HIGRZ	900	103.622	310.865	-0.042	-18.400	2.000
CLT	EQUINOX	HIGRZ	DELRI= 3730.37	DELRI= 524.58	DELRI= 1865.18	DELRI= 699.44		

STATION	SEASON	EPOCH	FREQ. (MHZ)	RANGE ERROR (METRES)	PHASE ERROR (RADIAN)	GROUP DELAY (NA.SEC)	DIFFL. PHASE SHIFT (RADIAN)	FARADAY ROTATION (RADIAN)
CLT	EQUINOX	LOWRZ	750	98.953	247.382	0.074	29.286	1.910
CLT	EQUINOX	LOWRZ	760	96.366	244.127	0.065	26.010	1.860
CLT	EQUINOX	LOWRZ	770	93.879	240.957	0.056	22.820	1.812
CLT	EQUINOX	LOWRZ	780	91.488	237.868	0.048	19.712	1.766
CLT	EQUINOX	LOWRZ	790	89.186	234.857	0.041	16.682	1.722
CLT	EQUINOX	LOWRZ	800	86.970	231.921	0.033	13.728	1.679
CLT	EQUINOX	LOWRZ	810	84.836	229.058	0.026	10.847	1.638
CLT	EQUINOX	LOWRZ	820	82.780	226.264	0.019	8.036	1.598
CLT	EQUINOX	LOWRZ	830	80.797	223.538	0.013	5.293	1.560
CLT	EQUINOX	LOWRZ	840	78.885	220.877	0.006	2.615	1.523
CLT	EQUINOX	LOWRZ	850	77.040	218.279	0.000	0.000	1.487
CLT	EQUINOX	LOWRZ	860	75.258	215.741	-0.006	-2.554	1.453
CLT	EQUINOX	LOWRZ	870	73.538	213.261	-0.012	-5.049	1.420
CLT	EQUINOX	LOWRZ	880	71.877	210.838	-0.017	-7.487	1.388
CLT	EQUINOX	LOWRZ	890	70.270	208.469	-0.023	-9.871	1.357
CLT	EQUINOX	LOWRZ	900	68.718	206.152	-0.028	-12.202	1.327
CLT	EQUINOX	LOWRZ	DEL R1= 2473.82	DEL R2= 347.88	DEL PH1= 1236.91	DEL PH2= 463.84		

STATION	SEASON	EPOCH	FREQ. (MHZ)	RANGE ERROR (METRES)	PHASE ERROR (RADIAN)	GROUP DELAY (NA.SEC)	DIFFL. PHASE SHIFT (RADIAN)	FARADAY ROTATION (RADIAN)
AHC	SUMMER	HIGRZ	750	58.711	146.778	0.044	17.376	1.090
AHC	SUMMER	HIGRZ	760	57.177	144.847	0.038	15.433	1.061
AHC	SUMMER	HIGRZ	770	55.701	142.966	0.034	13.540	1.034
AHC	SUMMER	HIGRZ	780	54.282	141.133	0.029	11.695	1.008
AHC	SUMMER	HIGRZ	790	52.917	139.347	0.024	9.898	0.982
AHC	SUMMER	HIGRZ	800	51.602	137.605	0.020	8.145	0.958
AHC	SUMMER	HIGRZ	810	50.336	135.906	0.016	6.436	0.934
AHC	SUMMER	HIGRZ	820	49.115	134.249	0.011	4.768	0.912
AHC	SUMMER	HIGRZ	830	47.939	132.631	0.007	3.140	0.890
AHC	SUMMER	HIGRZ	840	46.804	131.052	0.004	1.552	0.869
AHC	SUMMER	HIGRZ	850	45.710	129.511	0.000	0.000	0.848
AHC	SUMMER	HIGRZ	860	44.653	128.005	-0.004	-1.515	0.829
AHC	SUMMER	HIGRZ	870	43.632	126.533	-0.007	-2.996	0.810
AHC	SUMMER	HIGRZ	880	42.646	125.096	-0.010	-4.442	0.792
AHC	SUMMER	HIGRZ	890	41.693	123.690	-0.013	-5.857	0.774
AHC	SUMMER	HIGRZ	900	40.772	122.316	-0.017	-7.240	0.757
AHC	SUMMER	HIGRZ	DEL R1= 1467.78	DEL R2= 206.41	DEL PH1= 733.89	DEL PH2= 275.21		

STATION	SEASON	EPOCH	FREQ. (MHZ)	RANGE ERROR (METRES)	PHASE ERROR (RADIAN)	GROUP DELAY (NA.SEC)	DIFFL. PHASE SHIFT (RADIAN)	FARADAY ROTATION (RADIAN)
AHC	SUMMER	LOWRZ	750	35.448	88.621	0.026	10.491	0.658
AHC	SUMMER	LOWRZ	760	34.522	87.455	0.023	9.318	0.641
AHC	SUMMER	LOWRZ	770	33.631	86.319	0.020	8.175	0.624
AHC	SUMMER	LOWRZ	780	32.774	85.213	0.017	7.061	0.608
AHC	SUMMER	LOWRZ	790	31.950	84.134	0.015	5.976	0.593
AHC	SUMMER	LOWRZ	800	31.156	83.082	0.012	4.918	0.578
AHC	SUMMER	LOWRZ	810	30.391	82.057	0.009	3.886	0.564
AHC	SUMMER	LOWRZ	820	29.655	81.056	0.007	2.879	0.550
AHC	SUMMER	LOWRZ	830	28.944	80.079	0.005	1.896	0.537
AHC	SUMMER	LOWRZ	840	28.259	79.126	0.002	0.937	0.525
AHC	SUMMER	LOWRZ	850	27.598	78.195	0.000	0.000	0.512
AHC	SUMMER	LOWRZ	860	26.960	77.286	-0.002	-0.915	0.500
AHC	SUMMER	LOWRZ	870	26.344	76.398	-0.004	-1.809	0.489
AHC	SUMMER	LOWRZ	880	25.749	75.529	-0.006	-2.682	0.478
AHC	SUMMER	LOWRZ	890	25.173	74.681	-0.008	-3.536	0.467
AHC	SUMMER	LOWRZ	900	24.617	73.851	-0.010	-4.371	0.457
AHC	SUMMER	LOWRZ	DEL1= 886.21	DEL2= 124.62	DELPH1= 443.10	DELPH2= 166.16		

STATION	SEASON	EPOCH	FREQ. (MHZ)	RANGE ERROR (METRES)	PHASE ERROR (RADIAN)	GROUP DELAY (NA.SEC)	DIFFL. PHASE SHIFT (RADIAN)	FARADAY ROTATION (RADIAN)
AHC	WINTER	HIGRZ	750	76.436	191.089	0.057	22.622	1.419
AHC	WINTER	HIGRZ	760	74.437	188.575	0.050	20.092	1.382
AHC	WINTER	HIGRZ	770	72.516	186.126	0.044	17.627	1.346
AHC	WINTER	HIGRZ	780	70.669	183.739	0.037	15.226	1.312
AHC	WINTER	HIGRZ	790	68.891	181.414	0.031	12.886	1.279
AHC	WINTER	HIGRZ	800	67.180	179.146	0.026	10.604	1.247
AHC	WINTER	HIGRZ	810	65.531	176.934	0.020	8.379	1.216
AHC	WINTER	HIGRZ	820	63.943	174.777	0.015	6.207	1.187
AHC	WINTER	HIGRZ	830	62.411	172.671	0.010	4.086	1.159
AHC	WINTER	HIGRZ	840	60.934	170.615	0.005	2.020	1.131
AHC	WINTER	HIGRZ	850	59.509	168.608	0.000	0.000	1.105
AHC	WINTER	HIGRZ	860	58.133	166.648	-0.005	-1.973	1.079
AHC	WINTER	HIGRZ	870	56.804	164.732	-0.009	-3.900	1.054
AHC	WINTER	HIGRZ	880	55.521	162.860	-0.013	-5.784	1.031
AHC	WINTER	HIGRZ	890	54.280	161.030	-0.018	-7.625	1.008
AHC	WINTER	HIGRZ	900	53.080	159.241	-0.022	-9.425	0.985
AHC	WINTER	HIGRZ	DELRI= 1910.89	DELRI2= 268.72	DELPHI1= 955.44	DELPHI2= 358.29		

STATION	SEASON	EPOCH	FREQ. (MHZ)	RANGE ERROR (METRES)	PHASE ERROR (RADIAN)	GROUP DELAY (NA.SEC)	DIFFL. PHASE SHIFT (RADIAN)	FARADAY ROTATION (RADIAN)
AHD	WINTER	LOWRZ	750	27.694	69.235	0.021	8.196	0.514
AHD	WINTER	LOWRZ	760	26.970	68.324	0.018	7.280	0.501
AHC	WINTER	LOWRZ	770	26.274	67.437	0.016	6.387	0.488
AHD	WINTER	LOWRZ	780	25.605	66.572	0.014	5.517	0.475
AHD	WINTER	LOWRZ	790	24.961	65.730	0.011	4.669	0.463
AHD	WINTER	LOWRZ	800	24.341	64.908	0.009	3.842	0.452
AHD	WINTER	LOWRZ	810	23.743	64.107	0.007	3.036	0.441
AHC	WINTER	LOWRZ	820	23.168	63.325	0.005	2.249	0.430
AHD	WINTER	LOWRZ	830	22.613	62.562	0.004	1.481	0.420
AHC	WINTER	LOWRZ	840	22.078	61.817	0.002	0.732	0.410
AHD	WINTER	LOWRZ	850	21.561	61.090	0.000	0.000	0.400
AHC	WINTER	LOWRZ	860	21.063	60.380	-0.002	-0.715	0.391
AHD	WINTER	LOWRZ	870	20.581	59.686	-0.003	-1.413	0.382
AHC	WINTER	LOWRZ	880	20.116	59.007	-0.005	-2.096	0.373
AHD	WINTER	LOWRZ	890	19.667	58.344	-0.006	-2.763	0.365
AHC	WINTER	LOWRZ	900	19.232	57.696	-0.008	-3.415	0.357
AHD	WINTER	LOWRZ	DELRI= 692.35	DELRI2= 97.36	DELPHI1= 346.18	DELPHI2= 129.82		

STATION	SEASON	EPOCH	FREQ. (MHZ)	RANGE ERROR (METRES)	PHASE ERROR (RADIAN)	GROUP DELAY (NA.SEC)	DIFFL. PHASE SHIFT (RADIAN)	FARADAY ROTATION (RADIAN)
AHC	EQUINOX	HIGRZ	750	105.237	263.094	0.078	31.146	1.953
AHC	EQUINOX	HIGRZ	760	102.486	259.632	0.069	27.662	1.902
AHC	EQUINOX	HIGRZ	770	99.842	256.260	0.060	24.269	1.853
AHC	EQUINOX	HIGRZ	780	97.298	252.975	0.052	20.964	1.806
AHC	EQUINOX	HIGRZ	790	94.850	249.772	0.043	17.741	1.761
AHC	EQUINOX	HIGRZ	800	92.494	246.650	0.035	14.600	1.717
AHC	EQUINOX	HIGRZ	810	90.224	243.605	0.028	11.536	1.675
AHC	EQUINOX	HIGRZ	820	88.037	240.635	0.020	8.546	1.634
AHC	EQUINOX	HIGRZ	830	85.929	237.735	0.013	5.629	1.595
AHC	EQUINOX	HIGRZ	840	83.895	234.905	0.007	2.781	1.557
AHC	EQUINOX	HIGRZ	850	81.932	232.142	0.000	0.000	1.521
AHC	EQUINOX	HIGRZ	860	80.038	229.442	-0.006	-2.716	1.486
AHC	EQUINOX	HIGRZ	870	78.209	226.805	-0.012	-5.370	1.452
AHC	EQUINOX	HIGRZ	880	76.441	224.228	-0.018	-7.963	1.419
AHC	EQUINOX	HIGRZ	890	74.733	221.709	-0.024	-10.498	1.387
AHC	EQUINOX	HIGRZ	900	73.082	219.245	-0.030	-12.977	1.357
AHC	EQUINOX	HIGRZ	DELRI= 2630.94	DELRI= 369.98	DELPHI1= 1315.47	DELPHI2= 493.30		

STATION	SEASON	EPOCH	FREQ. (MHZ)	RANGE ERROR (METRES)	PHASE ERROR (RADIAN)	GROUP DELAY (NA.SEC)	DIFFL. PHASE SHIFT (RADIAN)	FARADAY ROTATION (RADIAN)
AHC	EQUINOX	LOWRZ	750	69.789	174.473	0.052	20.654	1.295
AHD	EQUINOX	LOWRZ	760	67.965	172.177	0.046	18.344	1.262
AHC	EQUINOX	LOWRZ	770	66.211	169.941	0.040	16.094	1.229
AHC	EQUINOX	LOWRZ	780	64.524	167.762	0.034	13.902	1.198
AHC	EQUINOX	LOWRZ	790	62.901	165.639	0.029	11.765	1.168
AHC	EQUINOX	LOWRZ	800	61.338	163.568	0.023	9.682	1.139
AHD	EQUINOX	LOWRZ	810	59.833	161.549	0.018	7.650	1.111
AHC	EQUINOX	LOWRZ	820	58.382	159.579	0.014	5.668	1.084
AHD	EQUINOX	LOWRZ	830	56.984	157.656	0.009	3.733	1.058
AHC	EQUINOX	LOWRZ	840	55.635	155.779	0.004	1.844	1.033
AHC	EQUINOX	LOWRZ	850	54.334	153.947	0.000	0.000	1.009
AHC	EQUINOX	LOWRZ	860	53.078	152.157	-0.004	-1.801	0.985
AHD	EQUINOX	LOWRZ	870	51.865	150.408	-0.008	-3.561	0.963
AHC	EQUINOX	LOWRZ	880	50.693	148.698	-0.012	-5.281	0.941
AHD	EQUINOX	LOWRZ	890	49.560	147.028	-0.016	-6.962	0.920
AHD	EQUINOX	LOWRZ	900	48.465	145.394	-0.020	-8.606	0.900

AHD EQUINOX LOWRZ DELR1= 1744.72 DELR2= 245.35 DELPHI1= 872.36 DELPHI2= 327.14

STATION	SEASON	EPOCH	FREQ. (MHZ)	RANGE ERROR (METRES)	PHASE ERROR (RADIAN)	GROUP DELAY (NA.SEC)	DIFFL. PHASE SHIFT (RADIAN)	FARADAY ROTATION (RADIAN)
BOMBAY	SUMMER	HIGRZ	750	55.739	139.348	0.041	16.496	0.828
BOMBAY	SUMMER	HIGRZ	760	54.282	137.514	0.037	14.651	0.806
BOMBAY	SUMMER	HIGRZ	770	52.881	135.728	0.032	12.854	0.785
BOMBAY	SUMMER	HIGRZ	780	51.534	133.988	0.027	11.103	0.765
BOMBAY	SUMMER	HIGRZ	790	50.238	132.292	0.023	9.397	0.746
BOMBAY	SUMMER	HIGRZ	800	48.989	130.638	0.019	7.733	0.727
BOMBAY	SUMMER	HIGRZ	810	47.787	129.026	0.015	6.110	0.710
BOMBAY	SUMMER	HIGRZ	820	46.629	127.452	0.011	4.527	0.692
BOMBAY	SUMMER	HIGRZ	830	45.512	125.917	0.007	2.981	0.676
BOMBAY	SUMMER	HIGRZ	840	44.435	124.418	0.003	1.473	0.660
BOMBAY	SUMMER	HIGRZ	850	43.396	122.954	0.000	0.000	0.644
BOMBAY	SUMMER	HIGRZ	860	42.392	121.524	-0.003	-1.438	0.630
BOMBAY	SUMMER	HIGRZ	870	41.423	120.127	-0.007	-2.844	0.615
BOMBAY	SUMMER	HIGRZ	880	40.487	118.762	-0.010	-4.218	0.601
BOMBAY	SUMMER	HIGRZ	890	39.583	117.428	-0.013	-5.560	0.588
BOMBAY	SUMMER	HIGRZ	900	38.708	116.123	-0.016	-6.873	0.575
BOMBAY	SUMMER	HIGRZ	DELRI= 1393.47	DELRI= 195.96	DELRI= 696.74	DELRI= 261.28		

STATION	SEASON	EPOCH	FREQ. (MHZ)	RANGE ERROR (METRES)	PHASE ERROR (RADIAN)	GROUP DELAY (NA.SEC)	DIFFL. PHASE SHIFT (RADIAN)	FARADAY ROTATION (RADIAN)
BOMBAY	SUMMER	LOWRZ	750	32.514	81.286	0.024	9.623	0.483
BOMBAY	SUMMER	LOWRZ	760	31.664	80.217	0.021	8.547	0.470
BOMBAY	SUMMER	LOWRZ	770	30.847	79.175	0.019	7.498	0.458
BOMBAY	SUMMER	LOWRZ	780	30.061	78.160	0.016	6.477	0.446
BOMBAY	SUMMER	LOWRZ	790	29.305	77.170	0.013	5.481	0.435
BOMBAY	SUMMER	LOWRZ	800	28.577	76.206	0.011	4.511	0.424
BOMBAY	SUMMER	LOWRZ	810	27.876	75.265	0.009	3.564	0.414
BOMBAY	SUMMER	LOWRZ	820	27.200	74.347	0.006	2.640	0.404
BOMBAY	SUMMER	LOWRZ	830	26.549	73.451	0.004	1.739	0.394
BOMBAY	SUMMER	LOWRZ	840	25.920	72.577	0.002	0.859	0.385
BOMBAY	SUMMER	LOWRZ	850	25.314	71.723	0.000	0.000	0.376
BOMBAY	SUMMER	LOWRZ	860	24.729	70.889	-0.002	-0.839	0.367
BOMBAY	SUMMER	LOWRZ	870	24.164	70.074	-0.004	-1.659	0.359
BOMBAY	SUMMER	LOWRZ	880	23.618	69.278	-0.006	-2.460	0.351
BOMBAY	SUMMER	LOWRZ	890	23.090	68.500	-0.007	-3.244	0.343
BOMBAY	SUMMER	LOWRZ	900	22.580	67.739	-0.009	-4.009	0.335

BOMBAY SUMMER LOWRZ DELR1= 812.86 DELR2= 114.31 DELPHI1= 406.43 DELPHI2= 152.41

STATION	SEASON	EPOCH	FREQ. (MHZ)	RANGE ERROR (METRES)	PHASE ERROR (RADIAN)	GROUP DELAY (NA.SEC)	DIFFL. PHASE SHIFT (RADIAN)	FARADAY ROTATION (RADIAN)
BOMBAY	WINTER	HIGRZ	750	65.029	162.572	0.048	19.246	0.966
BOMBAY	WINTER	HIGRZ	760	63.329	160.433	0.043	17.093	0.940
BOMBAY	WINTER	HIGRZ	770	61.695	158.350	0.037	14.997	0.916
BOMBAY	WINTER	HIGRZ	780	60.123	156.319	0.032	12.954	0.893
BOMBAY	WINTER	HIGRZ	790	58.610	154.341	0.027	10.963	0.870
BOMBAY	WINTER	HIGRZ	800	57.154	152.412	0.022	9.022	0.849
BOMBAY	WINTER	HIGRZ	810	55.752	150.530	0.017	7.128	0.828
BOMBAY	WINTER	HIGRZ	820	54.400	148.694	0.013	5.281	0.808
BOMBAY	WINTER	HIGRZ	830	53.097	146.903	0.008	3.478	0.788
BOMBAY	WINTER	HIGRZ	840	51.841	145.154	0.004	1.719	0.770
BOMBAY	WINTER	HIGRZ	850	50.628	143.446	0.000	0.000	0.752
BOMBAY	WINTER	HIGRZ	860	49.458	141.778	-0.004	-1.678	0.734
BOMBAY	WINTER	HIGRZ	870	48.327	140.149	-0.008	-3.318	0.718
BOMBAY	WINTER	HIGRZ	880	47.235	138.556	-0.011	-4.920	0.701
BOMBAY	WINTER	HIGRZ	890	46.180	136.999	-0.015	-6.487	0.686
BOMBAY	WINTER	HIGRZ	900	45.159	135.477	-0.018	-8.019	0.671

BOMBAY WINTER HIGRZ DELR1= 1625.72 DELR2= 228.62 DELPHI1= 812.86 DELPHI2= 304.82

STATION	SEASON	EPOCH	FREQ. (MHZ)	RANGE ERROR (METRES)	PHASE ERROR (RADIAN)	GROUP DELAY (NA.SEC)	DIFFL. PHASE SHIFT (RADIAN)	FARADAY ROTATION (RADIAN)
BOMBAY	WINTER	LOWRZ	750	32.514	81.286	0.024	9.623	0.483
BOMBAY	WINTER	LOWRZ	760	31.664	80.217	0.021	8.547	0.470
BOMBAY	WINTER	LOWRZ	770	30.847	79.175	0.019	7.498	0.458
BOMBAY	WINTER	LOWRZ	780	30.061	78.160	0.016	6.477	0.446
BOMBAY	WINTER	LOWRZ	790	29.305	77.170	0.013	5.481	0.435
BOMBAY	WINTER	LOWRZ	800	28.577	76.206	0.011	4.511	0.424
BOMBAY	WINTER	LOWRZ	810	27.876	75.265	0.009	3.564	0.414
BOMBAY	WINTER	LOWRZ	820	27.200	74.347	0.006	2.640	0.404
BOMBAY	WINTER	LOWRZ	830	26.549	73.451	0.004	1.739	0.394
BOMBAY	WINTER	LOWRZ	840	25.920	72.577	0.002	0.859	0.385
BOMBAY	WINTER	LOWRZ	850	25.314	71.723	0.000	0.000	0.376
BOMBAY	WINTER	LOWRZ	860	24.729	70.889	-0.002	-0.839	0.367
BOMBAY	WINTER	LOWRZ	870	24.164	70.074	-0.004	-1.659	0.359
BOMBAY	WINTER	LOWRZ	880	23.618	69.278	-0.006	-2.460	0.351
BOMBAY	WINTER	LOWRZ	890	23.090	68.500	-0.007	-3.244	0.343
BOMBAY	WINTER	LOWRZ	900	22.580	67.739	-0.009	-4.009	0.335
BOMBAY	WINTER	LOWRZ	DELRI=	812.86	DELRI2=	114.31	DELPHI1=	406.43
							DELPHI2=	152.41

STATION	SEASON	EPOCH	FREQ. (MHZ)	RANGE ERROR (METRES)	PHASE ERROR (RADIAN)	GROUP DELAY (NA.SEC)	DIFFL. PHASE SHIFT (RADIAN)	FARADAY ROTATION (RADIAN)
BOMBAY	EQUINOX	HIGRZ	750	74.319	185.797	0.055	21.995	1.104
BOMBAY	EQUINOX	HIGRZ	760	72.376	183.352	0.049	19.535	1.075
BOMBAY	EQUINOX	HIGRZ	770	70.508	180.971	0.042	17.139	1.047
BOMBAY	EQUINOX	HIGRZ	780	68.712	178.651	0.036	14.804	1.020
BOMBAY	EQUINOX	HIGRZ	790	66.983	176.390	0.031	12.529	0.995
BOMBAY	EQUINOX	HIGRZ	800	65.319	174.185	0.025	10.310	0.970
BOMBAY	EQUINOX	HIGRZ	810	63.716	172.034	0.020	8.146	0.946
BOMBAY	EQUINOX	HIGRZ	820	62.172	169.936	0.014	6.035	0.923
BOMBAY	EQUINOX	HIGRZ	830	60.683	167.889	0.009	3.975	0.901
BOMBAY	EQUINOX	HIGRZ	840	59.247	165.890	0.005	1.964	0.880
BOMBAY	EQUINOX	HIGRZ	850	57.861	163.939	0.000	0.000	0.859
BOMBAY	EQUINOX	HIGRZ	860	56.523	162.032	-0.004	-1.918	0.839
BOMBAY	EQUINOX	HIGRZ	870	55.231	160.170	-0.009	-3.792	0.820
BOMBAY	EQUINOX	HIGRZ	880	53.983	158.350	-0.013	-5.623	0.802
BOMBAY	EQUINOX	HIGRZ	890	52.777	156.571	-0.017	-7.414	0.784
BOMBAY	EQUINOX	HIGRZ	900	51.610	154.831	-0.021	-9.164	0.766

BOMBAY EQUINOX HIGRZ DELR1= 1857.97 DELR2= 261.28 DELPH11= 928.98 DELPH12= 348.37

STATION	SEASON	EPOCH	FREQ. (MHZ)	RANGE ERROR (METRES)	PHASE ERROR (RADIAN)	GROUP DELAY (NA.SEC)	DIFFL. PHASE SHIFT (RADIAN)	FARADAY ROTATION (RADIAN)
BOMBAY	EQUINOX	LOWRZ	750	46.449	116.123	0.035	13.747	0.690
BOMBAY	EQUINOX	LOWRZ	760	45.235	114.595	0.030	12.209	0.672
BOMBAY	EQUINOX	LOWRZ	770	44.068	113.107	0.027	10.712	0.654
BOMBAY	EQUINOX	LOWRZ	780	42.945	111.657	0.023	9.253	0.638
BOMBAY	EQUINOX	LOWRZ	790	41.865	110.243	0.019	7.831	0.622
BOMBAY	EQUINOX	LOWRZ	800	40.825	108.865	0.016	6.444	0.606
BOMBAY	EQUINOX	LOWRZ	810	39.823	107.521	0.012	5.092	0.591
BOMBAY	EQUINOX	LOWRZ	820	38.857	106.210	0.009	3.772	0.577
BOMBAY	EQUINOX	LOWRZ	830	37.927	104.931	0.006	2.485	0.563
BOMBAY	EQUINOX	LOWRZ	840	37.029	103.681	0.003	1.228	0.550
BOMBAY	EQUINOX	LOWRZ	850	36.163	102.462	0.000	0.000	0.537
BOMBAY	EQUINOX	LOWRZ	860	35.327	101.270	-0.003	-1.199	0.525
BOMBAY	EQUINOX	LOWRZ	870	34.519	100.106	-0.006	-2.370	0.513
BOMBAY	EQUINOX	LOWRZ	880	33.739	98.969	-0.008	-3.515	0.501
BOMBAY	EQUINOX	LOWRZ	890	32.985	97.857	-0.011	-4.634	0.490
BOMBAY	EQUINOX	LOWRZ	900	32.257	96.769	-0.013	-5.728	0.479
BOMBAY	EQUINOX	LOWRZ	DEL R1= 1161.23	DEL R2= 163.30	DELPHI1= 580.61	DELPHI2= 217.73		

STATION	SEASON	EPOCH	FREQ. (MHZ)	RANGE ERROR (METRES)	PHASE ERROR (RADIAN)	GROUP DELAY (NA. SEC)	DIFFL. PHASE SHIFT (RADIAN)	FARADAY ROTATION (RADIAN)
MADRAS	SUMMER	HIGRZ	750	54.439	136.098	0.040	16.112	0.404
MADRAS	SUMMER	HIGRZ	760	53.016	134.308	0.036	14.310	0.394
MADRAS	SUMMER	HIGRZ	770	51.648	132.563	0.031	12.555	0.383
MADRAS	SUMMER	HIGRZ	780	50.332	130.864	0.027	10.844	0.374
MADRAS	SUMMER	HIGRZ	790	49.066	129.207	0.022	9.178	0.364
MADRAS	SUMMER	HIGRZ	800	47.847	127.592	0.018	7.552	0.355
MADRAS	SUMMER	HIGRZ	810	46.673	126.017	0.014	5.967	0.347
MADRAS	SUMMER	HIGRZ	820	45.542	124.480	0.011	4.421	0.338
MADRAS	SUMMER	HIGRZ	830	44.451	122.981	0.007	2.912	0.330
MADRAS	SUMMER	HIGRZ	840	43.399	121.517	0.003	1.439	0.322
MADRAS	SUMMER	HIGRZ	850	42.384	120.087	0.000	0.000	0.315
MADRAS	SUMMER	HIGRZ	860	41.404	118.691	-0.003	-1.405	0.307
MADRAS	SUMMER	HIGRZ	870	40.457	117.326	-0.006	-2.778	0.300
MADRAS	SUMMER	HIGRZ	880	39.543	115.993	-0.010	-4.119	0.294
MADRAS	SUMMER	HIGRZ	890	38.660	114.690	-0.012	-5.431	0.287
MADRAS	SUMMER	HIGRZ	900	37.805	113.416	-0.015	-6.713	0.281
MADRAS	SUMMER	HIGRZ	DELRI= 1360.98	DELRI= 191.39	DELPHI1= 680.49	DELPHI2= 255.18		

STATION	SEASON	EPOCH	FREQ. (MHZ)	RANGE ERROR (METRES)	PHASE ERROR (RADIAN)	GROUP DELAY (NA.SEC)	DIFFL. PHASE SHIFT (RADIAN)	FARADAY ROTATION (RADIAN)
MADRAS	SUMMER	LOWRZ	750	39.054	97.636	0.029	11.558	0.290
MADRAS	SUMMER	LOWRZ	760	38.033	96.351	0.026	10.266	0.282
MADRAS	SUMMER	LOWRZ	770	37.052	95.100	0.022	9.007	0.275
MADRAS	SUMMER	LOWRZ	780	36.108	93.881	0.019	7.780	0.268
MADRAS	SUMMER	LOWRZ	790	35.200	92.692	0.016	6.584	0.261
MADRAS	SUMMER	LOWRZ	800	34.325	91.534	0.013	5.418	0.255
MADRAS	SUMMER	LOWRZ	810	33.483	90.404	0.010	4.281	0.249
MADRAS	SUMMER	LOWRZ	820	32.671	89.301	0.008	3.172	0.243
MADRAS	SUMMER	LOWRZ	830	31.889	88.225	0.005	2.089	0.237
MADRAS	SUMMER	LOWRZ	840	31.134	87.175	0.002	1.032	0.231
MADRAS	SUMMER	LOWRZ	850	30.406	86.149	0.000	0.000	0.226
MADRAS	SUMMER	LOWRZ	860	29.703	85.148	-0.002	-1.008	0.221
MADRAS	SUMMER	LOWRZ	870	29.024	84.169	-0.005	-1.993	0.216
MADRAS	SUMMER	LOWRZ	880	28.368	83.212	-0.007	-2.955	0.211
MADRAS	SUMMER	LOWRZ	890	27.734	82.278	-0.009	-3.896	0.206
MADRAS	SUMMER	LOWRZ	900	27.121	81.363	-0.011	-4.816	0.201

MADRAS SUMMER LOWRZ DELR1= 976.36 DELR2= 137.30 DELPH1= 488.18 DELPH2= 183.07

STATION	SEASON	EPOCH	FREQ. (MHZ)	RANGE ERROR (METRES)	PHASE ERROR (RADIAN)	GROUP DELAY (NA.SEC)	DIFFL. PHASE SHIFT (RADIAN)	FARADAY ROTATION (RADIAN)
MACRAS	WINTER	HIGRZ	750	76.925	192.313	0.057	22.766	0.571
MADRAS	WINTER	HIGRZ	760	74.914	189.783	0.050	20.220	0.556
MACRAS	WINTER	HIGRZ	770	72.981	187.318	0.044	17.740	0.542
MACRAS	WINTER	HIGRZ	780	71.122	184.916	0.038	15.324	0.528
MACRAS	WINTER	HIGRZ	790	69.333	182.576	0.032	12.968	0.515
MACRAS	WINTER	HIGRZ	800	67.610	180.294	0.026	10.672	0.502
MACRAS	WINTER	HIGRZ	810	65.951	178.068	0.020	8.432	0.490
MACRAS	WINTER	HIGRZ	820	64.352	175.896	0.015	6.247	0.478
MACRAS	WINTER	HIGRZ	830	62.811	173.777	0.010	4.115	0.466
MACRAS	WINTER	HIGRZ	840	61.324	171.708	0.005	2.033	0.455
MACRAS	WINTER	HIGRZ	850	59.890	169.688	0.000	0.000	0.445
MACRAS	WINTER	HIGRZ	860	58.505	167.715	-0.005	-1.985	0.434
MACRAS	WINTER	HIGRZ	870	57.168	165.787	-0.009	-3.925	0.424
MACRAS	WINTER	HIGRZ	880	55.876	163.903	-0.013	-5.821	0.415
MACRAS	WINTER	HIGRZ	890	54.628	162.062	-0.018	-7.674	0.406
MACRAS	WINTER	HIGRZ	900	53.420	160.261	-0.022	-9.486	0.397
MACRAS	WINTER	HIGRZ	DELRI= 1923.13	DELRI= 270.44	DELPHI= 961.56	DELPHI2= 360.59		

STATION	SEASON	EPOCH	FREQ. (MHZ)	RANGE ERROR (METRES)	PHASE ERROR (RADIAN)	GROUP DELAY (NA.SEC)	DIFFL. PHASE SHIFT (RADIAN)	FARADAY ROTATION (RADIAN)
MADRAS	WINTER	LOWRZ	750	30.770	76.925	0.023	9.107	0.228
MADRAS	WINTER	LOWRZ	760	29.966	75.913	0.020	8.088	0.222
MADRAS	WINTER	LOWRZ	770	29.192	74.927	0.018	7.096	0.217
MADRAS	WINTER	LOWRZ	780	28.449	73.967	0.015	6.129	0.211
MADRAS	WINTER	LOWRZ	790	27.733	73.030	0.013	5.187	0.206
MADRAS	WINTER	LOWRZ	800	27.044	72.117	0.010	4.269	0.201
MADRAS	WINTER	LOWRZ	810	26.380	71.227	0.008	3.373	0.196
MADRAS	WINTER	LOWRZ	820	25.741	70.358	0.006	2.499	0.191
MADRAS	WINTER	LOWRZ	830	25.124	69.511	0.004	1.646	0.187
MADRAS	WINTER	LOWRZ	840	24.530	68.683	0.002	0.813	0.182
MADRAS	WINTER	LOWRZ	850	23.956	67.875	0.000	0.000	0.178
MADRAS	WINTER	LOWRZ	860	23.402	67.086	-0.002	-0.794	0.174
MADRAS	WINTER	LOWRZ	870	22.867	66.315	-0.004	-1.570	0.170
MADRAS	WINTER	LOWRZ	880	22.350	65.561	-0.005	-2.328	0.166
MADRAS	WINTER	LOWRZ	890	21.851	64.825	-0.007	-3.069	0.162
MADRAS	WINTER	LOWRZ	900	21.368	64.104	-0.009	-3.794	0.159
MADRAS	WINTER	LOWRZ	DELRI= 769.25	DELRI2= 108.18	DELPHI1= 384.63	DELPHI2= 144.23		

STATION	SEASON	EPOCH	FREQ. (MHZ)	RANGE ERROR (METRES)	PHASE ERROR (RADIAN)	GROUP DELAY (NA.SEC)	DIFFL. PHASE SHIFT (RADIAN)	FARADAY ROTATION (RADIAN)
MADRAS	EQUINOX	HIGRZ	750	75.742	189.354	0.056	22.416	0.562
MADRAS	EQUINOX	HIGRZ	760	73.762	186.863	0.050	19.909	0.548
MADRAS	EQUINOX	HIGRZ	770	71.858	184.436	0.043	17.467	0.534
MADRAS	EQUINOX	HIGRZ	780	70.028	182.072	0.037	15.088	0.520
MADRAS	EQUINOX	HIGRZ	790	68.266	179.767	0.031	12.769	0.507
MADRAS	EQUINOX	HIGRZ	800	66.570	177.520	0.025	10.508	0.494
MADRAS	EQUINOX	HIGRZ	810	64.936	175.328	0.020	8.302	0.482
MADRAS	EQUINOX	HIGRZ	820	63.362	173.190	0.015	6.151	0.470
MADRAS	EQUINOX	HIGRZ	830	61.845	171.104	0.010	4.051	0.459
MADRAS	EQUINOX	HIGRZ	840	60.381	169.067	0.005	2.002	0.448
MADRAS	EQUINOX	HIGRZ	850	58.969	167.078	0.000	0.000	0.438
MADRAS	EQUINOX	HIGRZ	860	57.605	165.135	-0.005	-1.955	0.428
MADRAS	EQUINOX	HIGRZ	870	56.289	163.237	-0.009	-3.865	0.418
MADRAS	EQUINOX	HIGRZ	880	55.017	161.382	-0.013	-5.731	0.408
MADRAS	EQUINOX	HIGRZ	890	53.787	159.569	-0.017	-7.556	0.399
MADRAS	EQUINOX	HIGRZ	900	52.599	157.796	-0.021	-9.340	0.391
MADRAS	EQUINOX	HIGRZ	DELRI= 1893.54	DELRI= 266.28	DELRI= 946.77	DELRI= 355.04		

STATION	SEASON	EPOCH	FREQ. (MHZ)	RANGE ERROR (METRES)	PHASE ERROR (RADIAN)	GROUP DELAY (NA.SEC)	DIFFL. PHASE SHIFT (RADIAN)	FARADAY ROTATION (RADIAN)
MADRAS	EQUINOX	LOWRZ	750	54.439	136.098	0.040	16.112	0.404
MADRAS	EQUINOX	LOWRZ	760	53.016	134.308	0.036	14.310	0.394
MADRAS	EQUINOX	LOWRZ	770	51.648	132.563	0.031	12.555	0.383
MADRAS	EQUINOX	LOWRZ	780	50.332	130.864	0.027	10.844	0.374
MADRAS	EQUINOX	LOWRZ	790	49.066	129.207	0.022	9.178	0.364
MADRAS	EQUINOX	LOWRZ	800	47.847	127.592	0.018	7.552	0.355
MADRAS	EQUINOX	LOWRZ	810	46.673	126.017	0.014	5.967	0.347
MADRAS	EQUINOX	LOWRZ	820	45.542	124.480	0.011	4.421	0.338
MADRAS	EQUINOX	LOWRZ	830	44.451	122.981	0.007	2.912	0.330
MADRAS	EQUINOX	LOWRZ	840	43.399	121.517	0.003	1.439	0.322
MADRAS	EQUINOX	LOWRZ	850	42.384	120.087	0.000	0.000	0.315
MADRAS	EQUINOX	LOWRZ	860	41.404	118.691	-0.003	-1.405	0.307
MADRAS	EQUINOX	LOWRZ	870	40.457	117.326	-0.006	-2.778	0.300
MADRAS	EQUINOX	LOWRZ	880	39.543	115.993	-0.010	-4.119	0.294
MADRAS	EQUINOX	LOWRZ	890	38.660	114.690	-0.012	-5.431	0.287
MADRAS	EQUINOX	LOWRZ	900	37.805	113.416	-0.015	-6.713	0.281

MADRAS EQUINOX LOWRZ DELR1= 1360.98 DELR2= 191.39 DELPHI1= 680.49 DELPHI2= 255.18

CHAPTER - IX

UPWARD MOVING IONOSPHERIC IRREGULARITIES

18 AUGUST 1953

9.1 Introduction

Regular ionospheric soundings close to the magnetic equator in India were started in October 1964 with the installation of a C_4 ionosonde at Thumba (magnetic latitude $0.3^\circ S$). Soundings were made once every hour for the first two years but have been more frequent and at every 15 minute interval since January 1967. The examination of these more frequent ionograms soon led Rastogi (1970) to the discovery of a new transient phenomenon which seems to be peculiar to magnetic equatorial ionosphere only. This new type of ionospheric irregularity came to be known as kinks because of their appearance on the virtual height frequency trace as a sharp discontinuity.

Figure 9.1 shows the ionograms recorded on 18 August 1953 at Kodaikanal when such a kink was noticed. At 0815 hr the ionogram shows normal E_s , F_1 and F_2 layers. At 0830 hr there is a sharp thin stratification at about 330 km virtual height. At 0845 hr this stratification (kink) is at about 350 km although the critical frequency has not changed appreciably. At 0900 hr both the frequency and height at which the kink appears have increased. At 0915 hr the kink is above $f_o F_1$ at 6.7 MHz and 440 km. The movement on both the frequency and virtual height continues and by 1000 hr the kink is near $f_o F_2$.

KODAIKANAL 18 AUGUST 1953

VIRTUAL HEIGHT IN KM

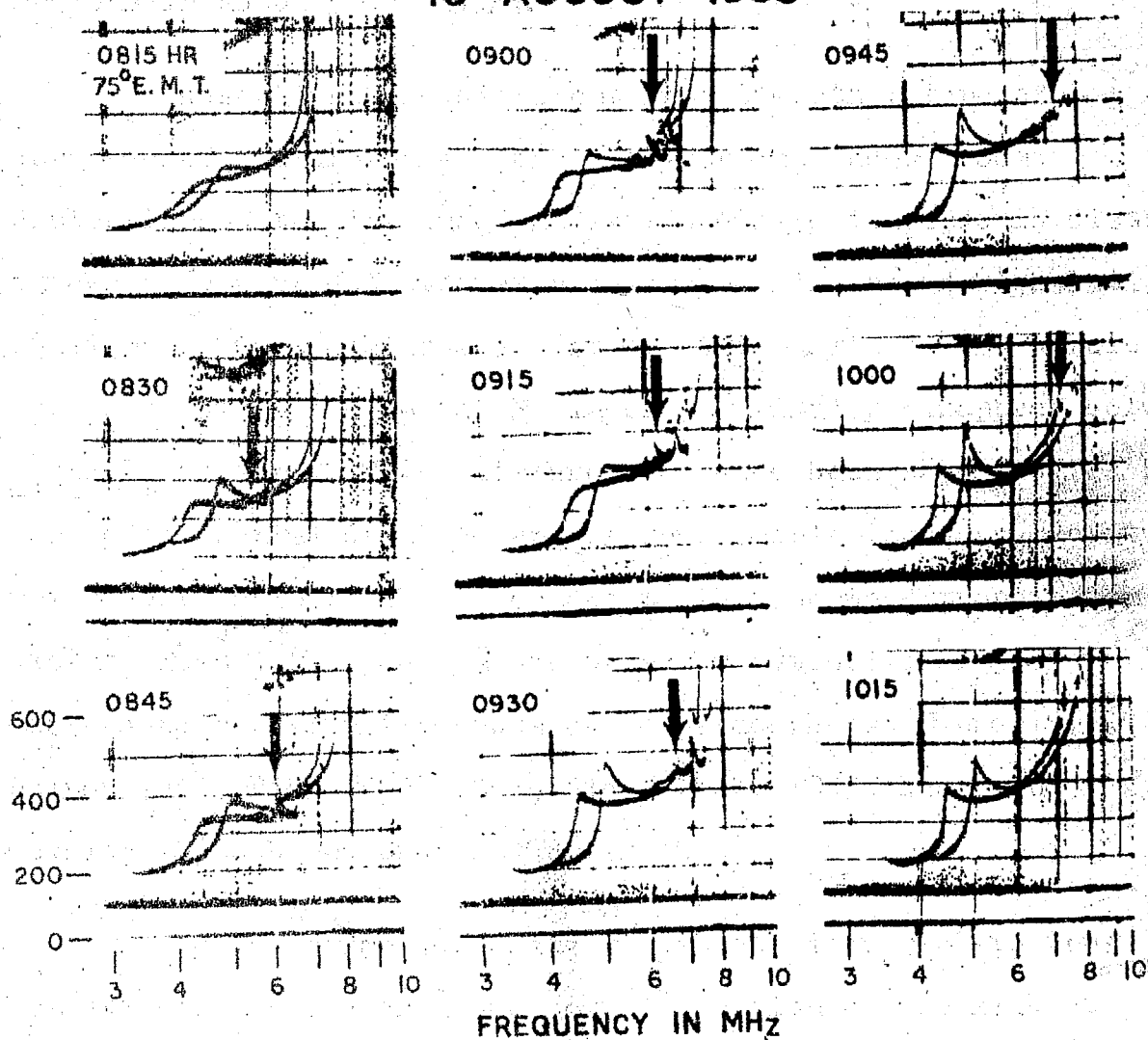


Figure 9.1 : Sequence of ionograms at Kodaikanal on 18 August 1953, showing the kinks (marked by the arrow)

The above described discontinuity seems to be the signature of a new type of ionospheric disturbance which originates in the E-region and moves up through the F_1 and F_2 regions in about a few hours.

These kinks are different from the other type of ionospheric disturbances seen at higher latitudes. Some distortions noted in ionograms as travelling ionospheric disturbances have been detected at a number of middle and high latitude stations. These disturbances start at F_2 critical frequencies move down the trace to the F_1 layer and finally disappear between E and F_1 regions. These disturbances have been suggested to be due to horizontal displacement of wave fronts (such as gravity waves) with a forward tilt or due to the downward propagation of disturbances like hydromagnetic waves or meteoritic impact disturbances originating outside the atmosphere (Munro 1948, Beynon 1948, Bibl 1952, 1953, Bibl et al. 1955, Munro and Heisler 1956a,b and Bibl and Rawer 1959).

The ionograms depicting kinks were converted to true height profiles and from the actual position of the kink at different times, its vertical velocity was computed. This comes out to be about 16 m/sec. This is much smaller than those observed in TIDs or other wave motions. The lifetime of these kinks (~ 4 hrs) is also much larger than those of TIDs.

Having thus confirmed that these are a new class of ionospheric irregularities their occurrence at another equatorial

station, Kodaikanal, in the same longitude zone was investigated by Rastogi (1971). These kinks have been found to occur mostly in summer months. Their occurrence was found to be closely associated with horizontal F-region drifts, occurrence of intermediate cusp between F_1 and F_2 layers, bite-out effects on f_oF_2 and rise of h_pF_2 , all these being pronounced around 1000 hr LT. Subsequently these kinks have been observed at other equatorial stations viz., Fort Archambault (dip lat. 1.5°S), Ouagadougou (dip lat. 4.5°N) by Faynot et al. (1971), Huancayo (dip lat 1°N) by Rastogi (1972), Chimbote (dip lat. 3°N), Natal (dip lat. 0°), Djibouti (dip lat. 3°N) and Jicamarca (dip lat 1°N) by Rastogi (1973).

Thus it is confirmed that these kinks occur only in the dip equatorial region confined to a belt of $\pm 3^\circ$ latitude. It is to be noted that these kinks are quite different from the lunar stratifications observed at some equatorial stations Huancayo, Kodaikanal and Talara (Gautier et al. 1951, Bhargava and Saha 1967 and Shapley 1970). The equatorial F_2 layer is lifted up very rapidly for a few hours after sunrise. This rapid rise sometimes causes an additional stratification which is often known as G layer (Rivault 1950). A sequence of ionograms showing the G layer at Kodaikanal on 4 April 1964 are reproduced in Figure 9.2. The ionogram at 1000 75° EMT is quite normal $h'F_2 = 380$ km and $h_pF_2 = 420$ km. At 1015 LT although f_oF_2 has not changed much, $h'F_2$ increases to about 400 km and h_pF_2

KODAIKANAL 4 APRIL 1964

220

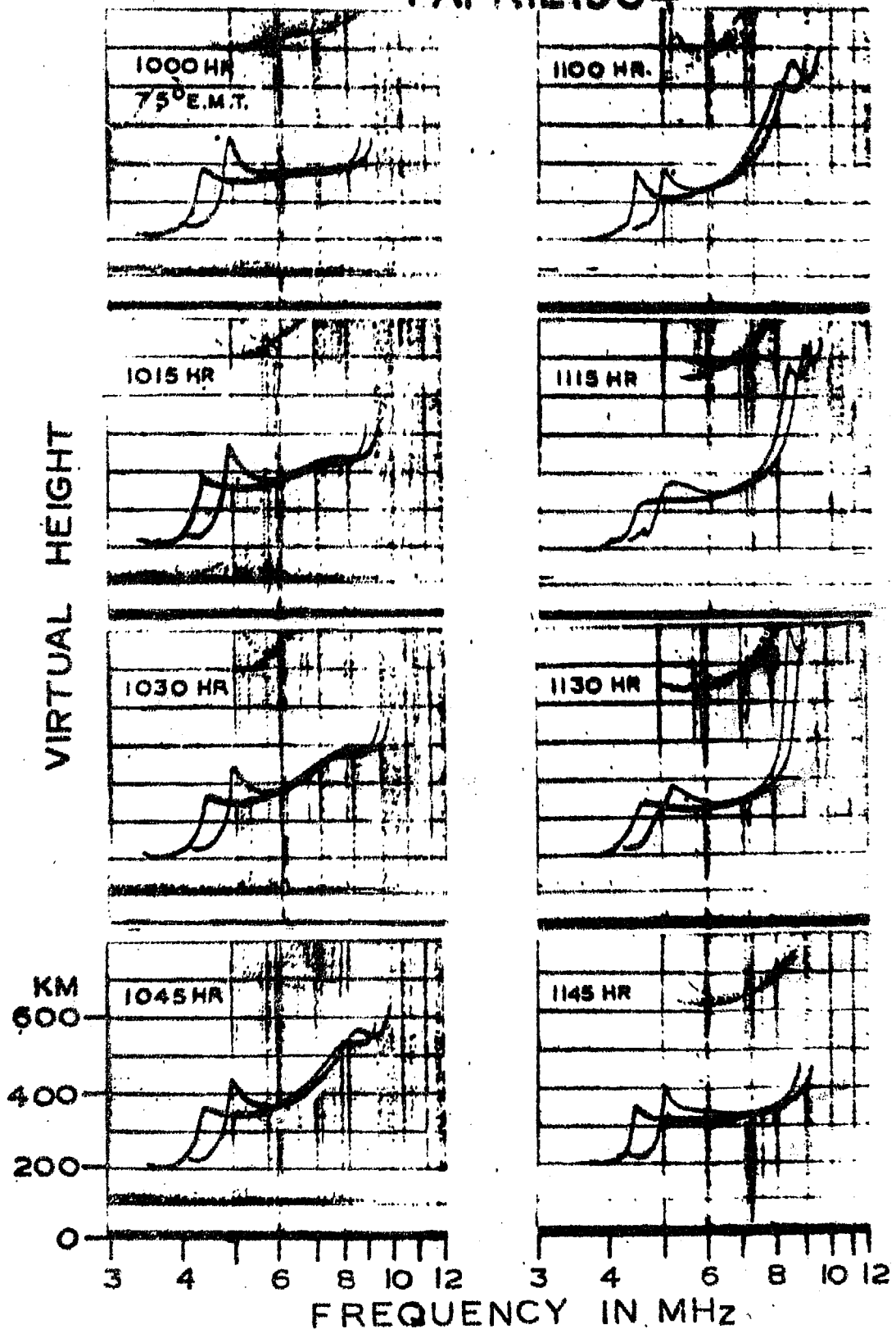


Figure 9.2 : Sequence of ionograms at Kodaikanal on 4 April 1964 showing G layer cusps.

has increased much more to about 450 km. A small discontinuous change in $h'(f)$ is also seen. At 1045 a clear cusp is seen close to f_oF_2 , h_pF_2 now being more than 550 km. This additional cusp is generally referred to as G layer. The G layer is seen on the ionograms till about 1130 when it goes above the F_2 peak and a thick F_2 region with decreased f_oF_2 is left behind. The irregularity referred to as kink is a completely different phenomenon than G layer.

It is to be noted that the kinks indicate a definite extra-ionization and are distinguishable from the E_s irregularities, which blanket the refraction from upper layers. On each ionogram the discontinuity can be clearly seen on the ordinary as well as extraordinary traces. Further, whenever second order traces are seen within the height range of the ionogram, the height of the irregularity in the second order trace is exactly double that in the first order trace. This confirms that this is not due to any off vertical reflections in which case the height of the second order trace will be less than twice the height of first order trace.

On many occasions kinks are seen simultaneously with G layer thus avoiding the confusion between the two. This is evident from Figure 9.3 in which a sequence of ionograms at Kodaikanal on 3 April 1964 are reproduced. At 0830 and 0845 75° EMT the upper portion of the trace is distorted due to the uplifting of the F layer. At 0915, 0930 and 0945 LT one can see the additional G layer cusp. At 0830 a small distortion is seen at a

KODAIKANAL 3 APRIL 1964

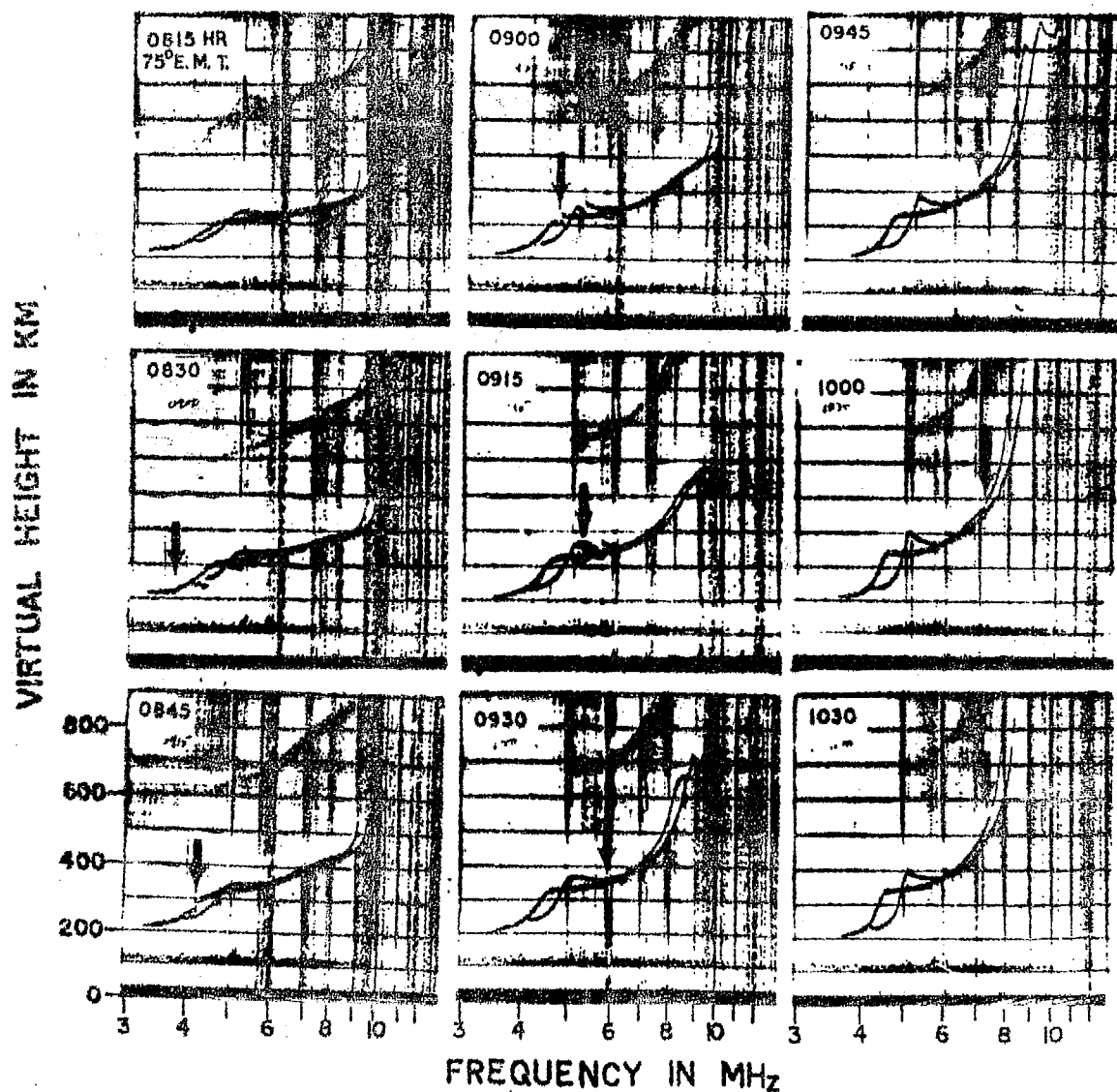


Figure 9.3 : Sequence of ionograms at Kodaikanal on 3 April 1964 showing simultaneous occurrence of kinks and G layer.

virtual height of about 220 km which is marked in the figure by an arrow. This kink moves up with time; at 0915, 0930 and 0945 kink and G layer cusps are simultaneously seen. The G layer has disappeared at 0945 but the kink still persists till 1030. The above picture confirms that kink and G layer are two independent phenomena and they can coexist or occur separately.

9.2 Analysis and results

A detailed analysis of the occurrence of kinks at Kodaikanal from 1958-64 was carried out, and the results are evident from the paper 'On the Occurrence and Vertical Movements of Kink at Kodaikanal ' by K.Narayana Iyer and R.G.Rastogi published in J. Geophys. Res., 79, 209, 1974. A reprint of this paper is attached.

Further, the longitudinal differences in the occurrence and vertical movement of these kinks were studied by using the ionograms at Huancayo, Natal and Kodaikanal. These results are discussed in the paper 'Vertical Drift Calculations from Upward Moving Ionospheric Irregularities (Kinks) over the Magnetic Equator' by K.N.Iyer and R.G.Rastogi published in Ind. J. Radio and Space Physics, , 4, 6, 1975. A reprint of this paper is also attached.

C H A P T E R - X

GEOMAGNETIC H FIELD AT LOW LATITUDES

10.1 Introduction

The study of solar daily variation of the geomagnetic components has attracted many workers since the beginning of this branch of science. The daily variation of the geomagnetic field has been attributed to the ionospheric dynamo currents (Schuster 1908 and Chapman 1919). Significant seasonal variations are seen in these field components and different sources have been suggested for these variations (Vestine 1954, McIntosh 1959, Price 1963 and Currie 1966).

The geomagnetic data at low latitudes are of special importance because, within a narrow belt of $4^\circ - 5^\circ$ centred over the magnetic dip equator, the daily variation of geomagnetic H field on quiet days, $rS_q(H)$, is abnormally large compared with other observatories in the low latitude region but outside this belt. This large $S_q(H)$ variation has been due to large ionospheric currents in the dynamo region over the dip equator and has been named as 'Equatorial Electrojet' by Chapman (1951). This excess current is now explained in terms of the enhanced electrical conductivity in that region which in turn is due to the inhibition of vertical Hall currents by the vertical Hall polarisation field resulting in extra conductivity in the E-W direction. The enhancement of the currents does not continue

till the night time due to the depletion of E layer ionisation (Chapman and Raja Rao 1965). way of representing the low latitude ionospheric currents is to consider the currents to be due to the normal S_q current extrapolated from the tropical latitudes over which is added another current system which is entirely due to the electrojet (Forbush and Casaverde 1961 and Onwumechilli 1967).

Recently Rastogi (1975) has suggested that the observed variation of the H field at ground in the electrojet region is due to the superimposition of two current systems one which is associated with world wide S_q and flows always eastward at a height of about 107 km ; another simultaneous current at about 100 km which may flow eastward or westward. At low latitudes, the horizontal component is the major part of the total field and the vertical component is significantly affected by the geological and geographic surroundings of the station. Therefore at present we have studied only the horizontal component of the geomagnetic field.

One of the oldest and foremost geomagnetic observatories at low latitudes is at Huancayo, Peru operating since 1922. Further, the observatories at Huancayo, Yauca, Chimbote, Chiclayo, Talara and Fuquene which were operating at IGY-IGC period provided one of the best chain of geomagnetic observatories at low latitudes. Still, the geomagnetic observatories in India only have provided the geomagnetic data over a period of more

than a solar cycle simultaneously at three stations within the electrojet belt (Trivandrum, Kodaikanal and Annamalainagar) and two stations outside the belt (Hyderabad and Alibag). The period of our present study is from 1958 to 1972. The coordinates of the low latitude geomagnetic observatories used in this study are given in Table 10.1.

Table 10.1

Stations used in the study and their coordinates

Station	Magnetic dip	Geographic	
		Longitude	Latitude
Addis Ababa	0.8° S	39.0° E	9.0° N
Alibag	24.5° N	72.9° E	18.6° N
Annamalainagar	5.2° N	79.7° E	11.4° N
Huancayo	2.0° N	75.0° W	12.0° S
Kodaikanal	3.4° N	77.5° E	10.2° N
Trivandrum	0.6° S	77.0° E	8.5° N

10.2 Solar daily variation of H near the equator in different longitudes

First we compare the annual average daily variation of H on five International Quiet days of each month at stations close to the dip equator but in different longitudes. In Figure 10.1 we have shown the yearly average $S_q(H)$ variations at Huancayo (dip 2° N), Addis Ababa (dip 0.4° S) and at Trivandrum (dip 0.6° S).

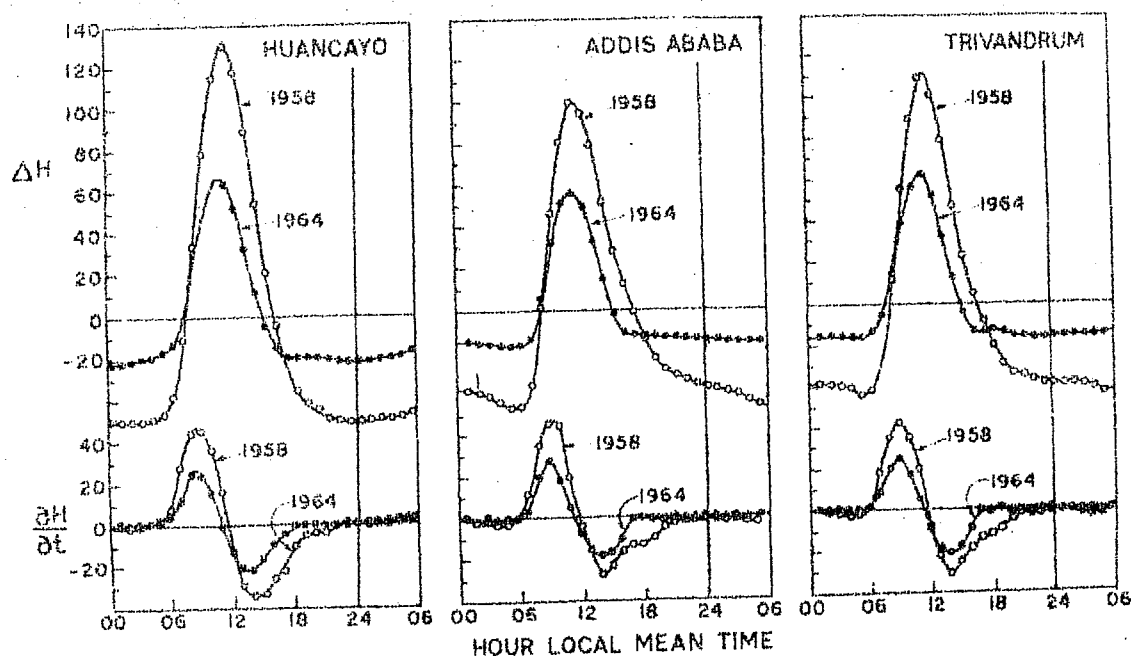


Figure 10.1 : Yearly average daily variation of H field as well as the rate of change of H field ($\frac{\partial H}{\partial t}$) at Huancayo, Addis Ababa and Trivandrum for low (1964) and high (1958) solar activity periods.

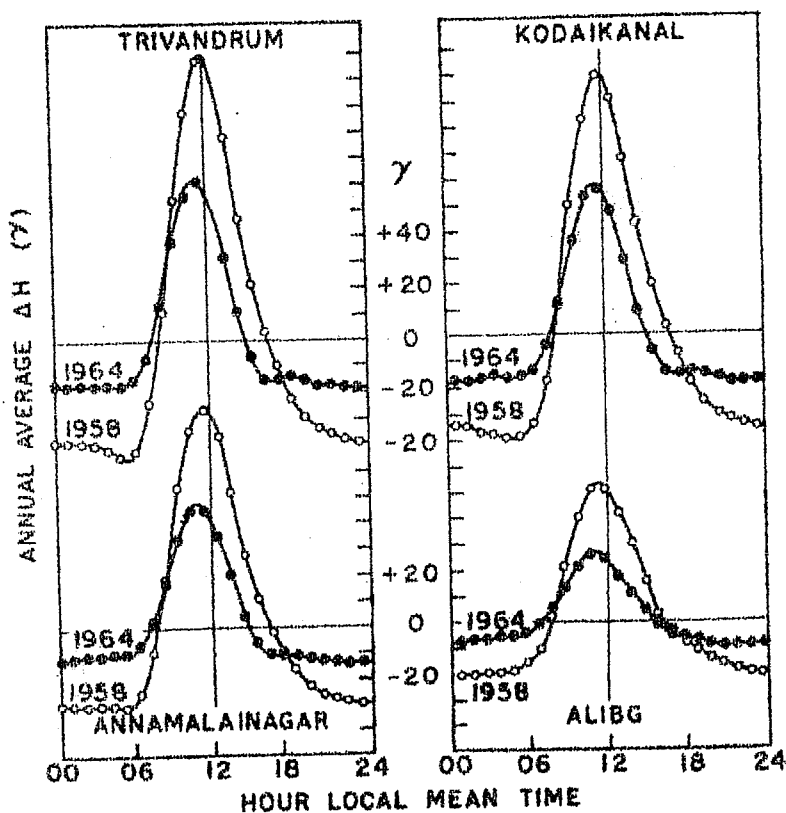


Figure 10.2 : Annual average daily variation of H field for the stations Trivandrum, Kodaikanal, Annamalaiagar and Alibag during the years 1964 and 1958.

for the low sunspot year 1964 and for the high sunspot year 1958. In the diagram $\Delta H = H_t - \bar{H}$ is the hourly mean value for time t and H is the average value for all the hours. The time derivative of the H field $\partial H / \partial t$ is also plotted in Figure 10.1 which shows more explicitly the position of the maximum of H field during the day time.

Referring to the curves for the year 1964, $S_q(H)$ at these stations started increasing shortly before 0600 LT with the rising of sun at E layer heights, reached its maximum at about 1100 LT, returned to the nighttime value at 1600 LT and the value of H remained constant throughout most of the night. In the high sunspot year 1958 there was a depression of H before sunrise at Trivandrum and Addis Ababa. This feature had been earlier noted by Gouin and Mayaud (1967) and was suggested to be due to counter-electrojet currents in the early morning hours. After 0600 LT the value of H continued to increase reaching a maximum at about 1200 LT, i.e. the peak is delayed by about an hour in 1958 as compared to that in 1964. During the high sunspot year the decrease continued till about midnight at Huancayo, and almost till 0600 LT at Addis Ababa and Trivandrum. The gradient $\partial H / \partial t$ shows a maximum positive around 0800-0900 LT and a maximum negative around 1300-1400 LT with the zero crossing between 1100 and 1200 LT. A closer scrutiny shows that the zero crossing of $\partial H / \partial t$ or the time of maximum H occurs at about 1600 LT during low sunspot year (1964) while it remains at significantly non zero value upto 2100 LT during high sunspot

year (1958). This clearly indicates that the H field in the equatorial electrojet region comes to the base level immediately after sunset during low sunspot years while it continues to decrease throughout the night during high sunspot years.

To show the latitudinal dependence of this morning and evening decrease of the H field the yearly average variation of H for the station Trivandrum (dip 0.6°S), Kodaikanal (dip 3.4°N), Annamalainagar (dip 5.2°N) and Alibag (dip 24.5°N) are shown in Figure 10.2 for 1958 and 1964. For all these stations, the nighttime value remains fairly steady in the quiet sun year 1964 while the decrease of H field continues after sunset till about midnight for all these stations in the high sunspot year 1958. It may be noted from the figure that the rate of decrease of H field after sunset is more at Trivandrum and progressively decreases as the latitude increases. The pre sunrise decrease of the field below the nighttime level is conspicuous at Trivandrum and Kodaikanal while it is almost absent at Annamalainagar and Alibag. Also for the quiet sun year this pre sunrise decrease is almost non existent for all these stations. This decrease of the H field after sunset could be due to currents set up at higher heights since it is seen at all stations. The pre sunrise dip in H should be ionospheric phenomenon connected with the equatorial electrojet.

10.3 Diurnal variation of H field at low latitudes

To study critically the variation of S_q field with solar activity and its dependence on latitude, we have harmonically

analysed the quiet day H field (after applying non-cyclic correction) averaged for the International Quiet days of each year over a period 1958-1972 for all the Indian stations Trivandrum, Kodaikanal, Annamalaiagar and Alibag. The amplitudes and phases (local time of maxima) for the first four harmonics are studied. Figure 10.3 shows a plot of the amplitude of the different harmonics against the year on the left side and the time of maxima of the different harmonics plotted against the corresponding year on the right side. The diagram also shows the ratio of the amplitude of the two harmonics i.e. C_1/C_2 as well as the difference in the phases of the two harmonics i.e. $T_1 - T_2$. It is to be noted that the scales of the amplitude of the third and fourth harmonics are magnified by two and five times respectively for the sake of clarity.

The amplitude of diurnal component C_1 shows a very clear solar cycle variation being maximum around 1958 and again around 1968-70. The solar cycle dependence was less marked in the higher harmonic C_2 and to a lesser extent still in C_3 while it is ~~slwst~~ uncertain for C_4 . The magnitude of the ratio C_1/C_2 ranges from 1.8 to 2.3 during maximum sunspot years and 1.5 to 1.8 during minimum sunspot years. Although the diurnal as well as semidiurnal component is progressively larger towards the equator the ratio of C_1/C_2 is lowest for Trivandrum and highest for Alibag. Thus it may be concluded that the contribution of semi-diurnal component to the daily variation is most significant at a station near the dip equator.

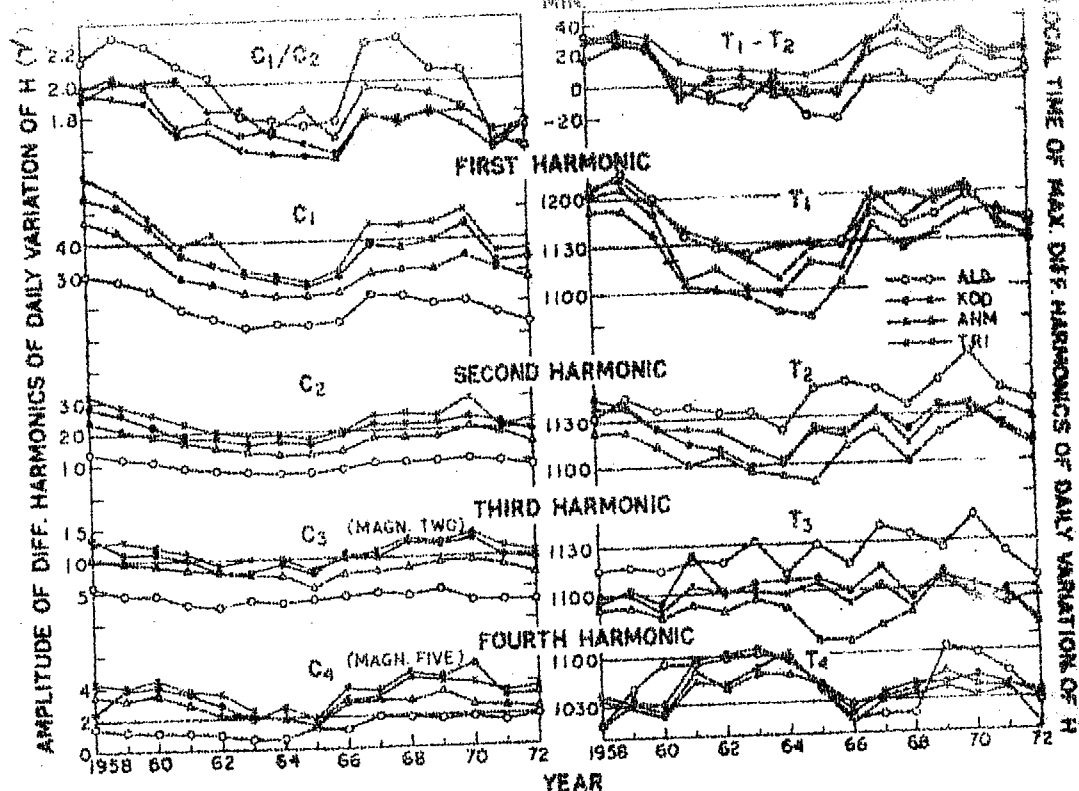


Figure 10.3 : Amplitudes C_1, C_2, C_3 and C_4 of the first 4 harmonics and their times of maximum T_1, T_2, T_3 and T_4 of the daily variation of H field for the four Indian stations plotted against the year. Note that the amplitudes and times of maximum are higher in 1958 and 1969 than in 1964.

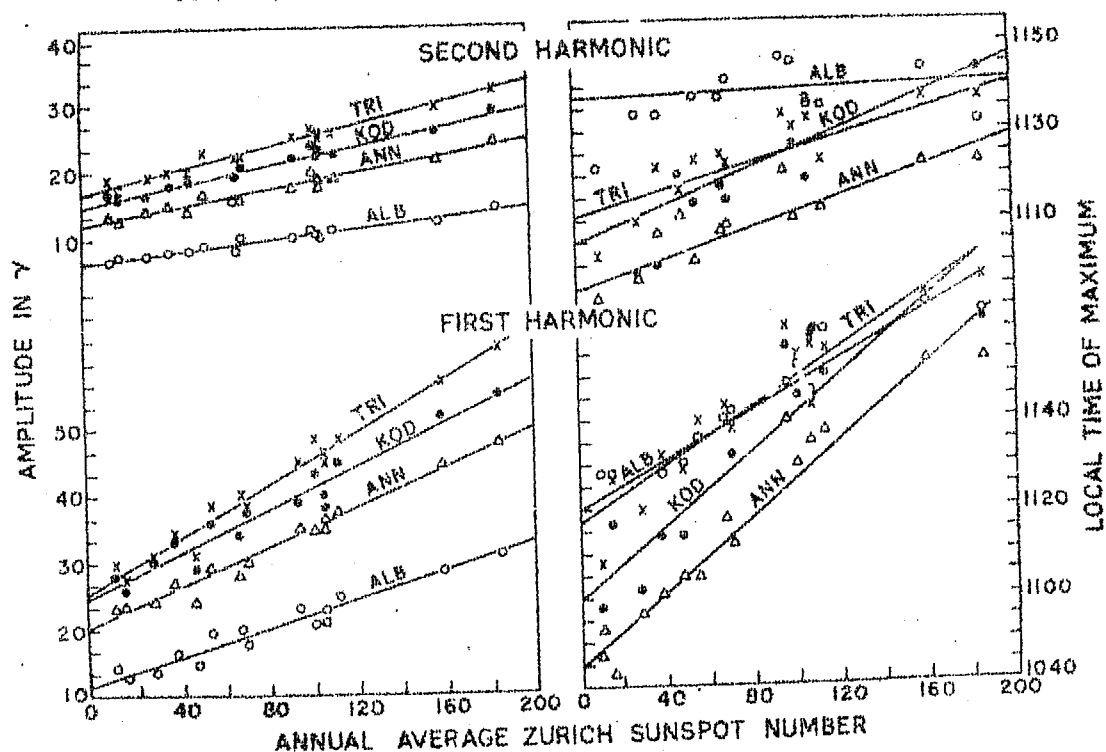


Figure 10.4 : Amplitudes and Times of maximum of the diurnal and semidiurnal component of the daily variation of H at the four Indian stations as a function of Zurich sunspot number.

The phase T_1 shows a prominent effect of the solar activity. The diurnal component of H had reached a maximum value after 1200 LT in the year 1958 and 1959 but between 1100 and 1130 LT during the years around 1964. The phase T_2 also shows similar trend with solar cycle but to a lesser extent. The difference $T_1 - T_2$ is of the order of half an hour during high sunspot years and practically zero during low sunspot years. It is further to be noted that both the diurnal as well as semidiurnal component reaches maximum value earlier at low latitudes than at Alibag. The time of maximum of the third and fourth harmonic components of the daily variation seems to be erratic and thus shows uncertain dependence on solar cycle.

To bring out the latitudinal dependence of the amplitudes and time of maxima of the different harmonics and their solar cycle variation more clearly, we have plotted in Figure 10.4 on the left side the amplitudes of the first two harmonics against the annual mean zurich sunspot number (R_z) of each of the years 1958-1972. On the right side of the diagram the time of maxima of the two harmonics are also plotted against R_z . The least square regression lines of the form $C = a + bR_z$ and $T = a' + b'R_z$ for each of these stations are also drawn. The coefficients of the equations of these lines are given in Table 10.2. It is clear from the figure that the amplitude of both the first and second harmonic components show a significant linear relationship with sunspot number. A perusal of Table 10.2 shows that the values of 'a' as well as 'b' for the first and

Table 10.2

The diurnal and the semi-diurnal amplitude (C_1 and C_2) and phase (T_1 and T_2) of annual daily variation of H field as a function of annual mean zurich sunspot number according to the equation $C = a + b R_z$ or $T = a' + b' R_z$

	Amplitude		Phase	
	First Harmonic C_1 a b $(b/a) \times 10^4$	Second Harmonic C_2 a b $(b/a) \times 10^4$	First Harmonic T_1 a' b' $(hr LT)$	Second Harmonic T_2 a' b' $(hr LT)$
Trivandrum	25.7 0.194 75.0	17.0 0.077 45.3	11.25 0.56	11.2 0.25
Kodaikanal	25.0 0.157 62.8	15.0 0.069 46.0	11.00 0.71	11.8 0.36
Annamalainagar	20.5 0.145 70.7	12.3 0.058 47.1	10.73 0.71	10.91 0.29
Alibab	11.7 0.103 88.0	6.5 0.040 60.0	11.33 0.47	11.63 0.03

second harmonics are largest for Trivandrum and decreases with increasing latitude of the station. The large value of b at the magnetic equator could be due to the large inherent value of ' a ' near the magnetic equator. Therefore we have examined the ratio (b/a) which represents the sensitivity of the field to sunspot activity normalized to zero sunspot field. It is seen that the coefficient b/a is practically the same at electrojet stations and is slightly less than the corresponding value for Alibag. This indicates that the proportional changes of H field are the same at the electrojet stations.

Referring to the variation of the time of maximum of the H field with sunspot number one finds a very clear linear relationship for the first harmonic, T_1 and to a much less extent for the second harmonic T_2 . It is significant that the increases of T_1 and T_2 are much smaller for the non-equatorial station Alibag as compared to that for the equatorial stations Trivandrum, Kodaikanal and Annamalainagar. The time T_1 at Annamalainagar, for example, changes from 1045 LT for zero R_z to about 1210 LT for an R_z of 180. At Alibag T_1 is 1115 LT for $R_z=2$ and it is 1215 LT for $R_z=180$.

To further understand the seasonal effects of the solar cycle variation we have calculated the harmonic coefficients for the amplitude and phases of the first two harmonics separately for each of the seasons viz., D-months (November, December, January, February), J-months (May, June, July, August) and E-months (March, April, September, October). The coefficients of the

linear regression lines for each season are tabulated in Table 10.3. Looking at table 10.3 it is seen that for the station Alibag, the amplitude of both the diurnal and semidiurnal component is maximum in J-months (summer) and least in D-months (winter). Thus it follows basically the solar zenith angle variation with season. At the equatorial stations Trivandrum, Kodaikanal and Annamalainagar, the coefficients are larger in summer and winter but the largest amplitudes occur during the equinoctial months. This equinoctial peak of the amplitude of daily variation seems to accentuate with R_z as evidenced by higher value of 'b' for the equinoctial months.

10.4 Seasonal variation of the $S_q(H)$ field

Another parameter to study the maximum ionospheric currents during the course of a day is the so called daily range of H field. One of the most suitable definitions of the daily range has been given by Chapman and Raja Rao (1965) as the maximum value around noon minus the mean value over 0000, 0100, 0200 and 2200, 2300 and 2400 hrs LT for any particular day and is denoted as $rS_q(H)$. This range is computed from the monthly mean $S_q(H)$ variation for each of the months of the years 1958-1972 for the stations, Trivandrum, Kodaikanal, Annamalainagar and Alibag. In Figure 10.5 are plotted the month to month variation of $rS_q(H)$ for all the above Indian stations. Twelve months' running average is also superposed on the corresponding curves of $rS_q(H)$. At the lower part of the diagram, the monthly mean value of R_z as well as twelve months running mean of R_z is

Table 10.3

Variation with zurich sunspot number (R_z) of the amplitude (C) and phase (T) of the diurnal (first harmonic) and semi-diurnal (second harmonic) variations of H field at low-latitude stations for different seasons: $C = a + b R_z$ or $T = a' + b' R_z$

	First harmonic			Second harmonic		
	Amplitude a	b	Phase a' LT b' LT	Amplitude a	b	Phase a' LT b' LT
Trivandrum						
D-Months	22.8	0.18	11.5	0.003	11.5	0.003
J-Months	25.9	0.17	11.0	0.006	11.0	0.006
E-Months	30.8	0.22	11.2	0.004	11.2	0.004
Kodaikanal						
D-Months	21.1	0.14	10.8	0.007	10.8	0.007
J-Months	24.3	0.16	11.1	0.007	11.1	0.007
E-Months	28.4	0.20	11.6	0.008	11.6	0.008
Annamalainagar						
D-Months	18.0	0.13	11.1	0.005	11.1	0.005
J-Months	20.9	0.13	10.6	0.007	10.6	0.007
E-Months	23.2	0.17	10.7	0.006	10.7	0.006
Alibag						
D-Months	11.5	0.08	10.8	0.006	10.8	0.006
J-Months	14.0	0.10	11.3	0.003	11.3	0.003
E-Months	12.7	0.11	11.2	0.005	11.2	0.005

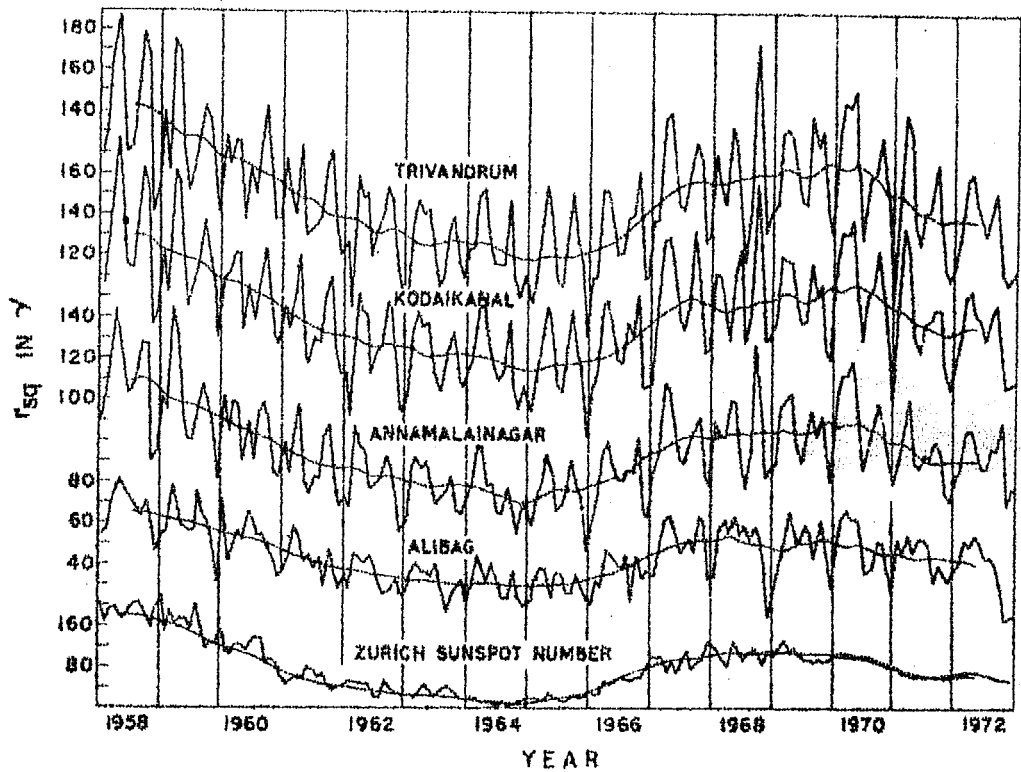


Figure 10.5 : Semianual variation of the monthly mean daily range of H field $rSq(H)$ for the years 1958-1972 at the four Indian stations. The 12 months' running mean is also indicated. Variation of monthly mean Zurich sunspot number and its 12 months' running mean is also shown.

plotted for comparison.

It may be seen from Figure 10.5 that for the equatorial stations, Trivandrum, Kodaikanal and Annamalainagar two peaks of $rS_q(H)$ are seen for each year around the vernal and autumn equinoxes. At Alibag the yearly variations seem to have a single peak during summer months. To show this more clearly in Figure 10.6 we have plotted the deviations of $rS_q(H)$ from the twelve months' running mean for each month averaged over the year 1958-1972. A significant semiannual component with maxima around March and September (equinoxes) is again seen for all the equatorial stations Trivandrum, Kodaikanal and Annamalainagar but there is no definite semiannual component at Alibag. The amplitudes of these components are more in high than in low sunspot years.

The deviations of $rS_q(H)$ from the twelve months' running mean (the solar cycle effect thus being removed) are subjected to harmonic analysis and a significant semiannual component again obtained. In order to study the effect of solar activity on this daily range, the annual mean daily range is plotted against sunspot number for each of the stations. This is shown in Figure 10.7. The best fitted strength line equations between the annual mean daily range $rS_q(H)$ and the zurich mean sunspot number (R_z) are for

$$\text{Trivandrum, } rS_q(H) = 67.54 + 0.40 R_z$$

$$\text{Kodaikanal, } rS_q(H) = 63.40 + 0.35 R_z$$

$$\text{Annamalainagar, } rS_q(H) = 50.72 + 0.31 R_z$$

$$\text{Alibag, } rS_q(H) = 27.94 + 0.21 R_z$$

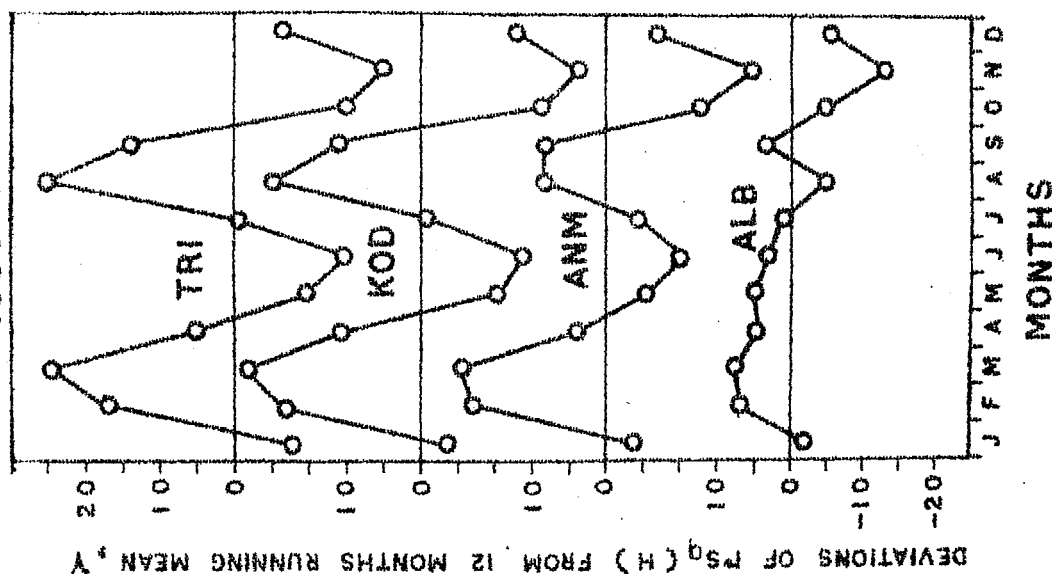


Figure 10.6 : Seasonal variation of $rSq(H)$ averaged for 1958-72 at the four Indian stations. Note the equinoctial maxima and solstitial minima at the equatorial stations while rather irregular variation is given at Alibag.

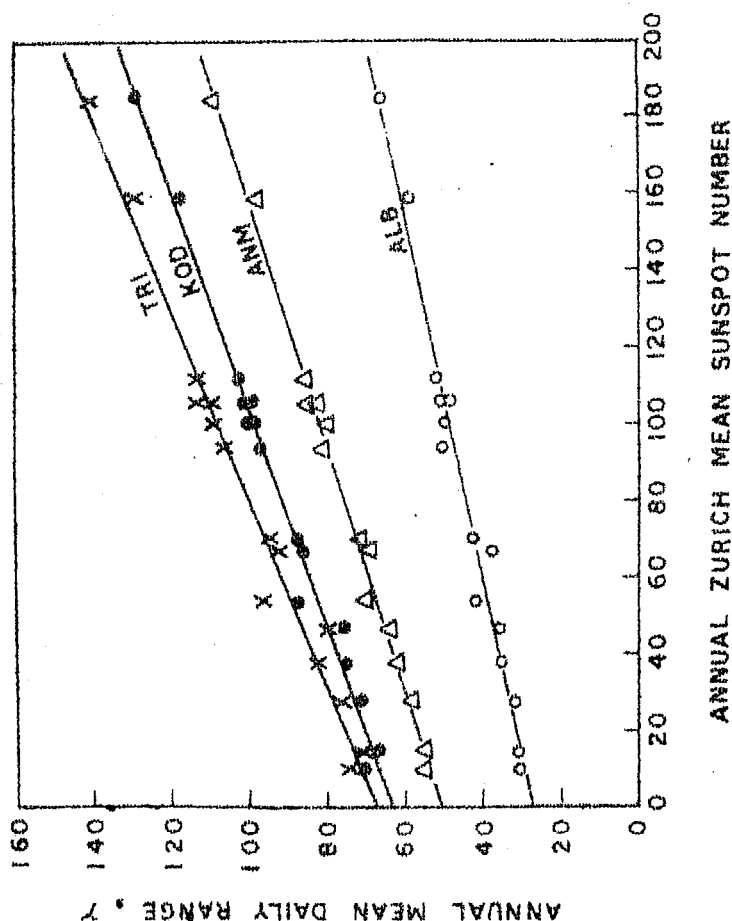


Figure 10.7 : Annual mean daily range of H field plotted annual mean Zurich sunspot number.

From Figure 10.7 it can be seen that the slope of the line is largest for Trivandrum and smallest for Alibag, which can be confirmed from the values of b being 0.40 for Trivandrum and only 0.21 for Alibag. As expected, the values of ' a ' i.e. the range for zero sunspot number progressively increases from Alibag to Trivandrum. To better understand the seasonal variation of the diurnal range, the coefficients ' a ' and ' b ' have been computed for each month of the year for Kodaikanal and are plotted against the corresponding months in Figure 10.8. The range for zero sunspot, ' a ' shows a semiannual variation being maximum in March-April and again in September. The sensitivity ' b ' also shows semiannual variation with maximum in equinoxes.

10.5 Interrelationship between the annual and daily variations of electrojet current

To study the effect of the yearly average solar daily range of H (or the sunspot number) on the annual and semiannual variations we have plotted in Figure 10.9 the amplitudes of annual and semiannual variations at different stations against the corresponding yearly mean $rS_q(H)$. It is seen from the diagram that the points in the annual component plot are quite scattered indicating the absence of any relation between the yearly component of H and the yearly mean $rS_q(H)$ or the yearly mean R_z . In the semiannual plot, the points are aligned along a single straightline indicating that the semiannual amplitude of H is proportional to the average $rS_q(H)$. The semiannual variation in H is most prominent in high sunspot years for any station.

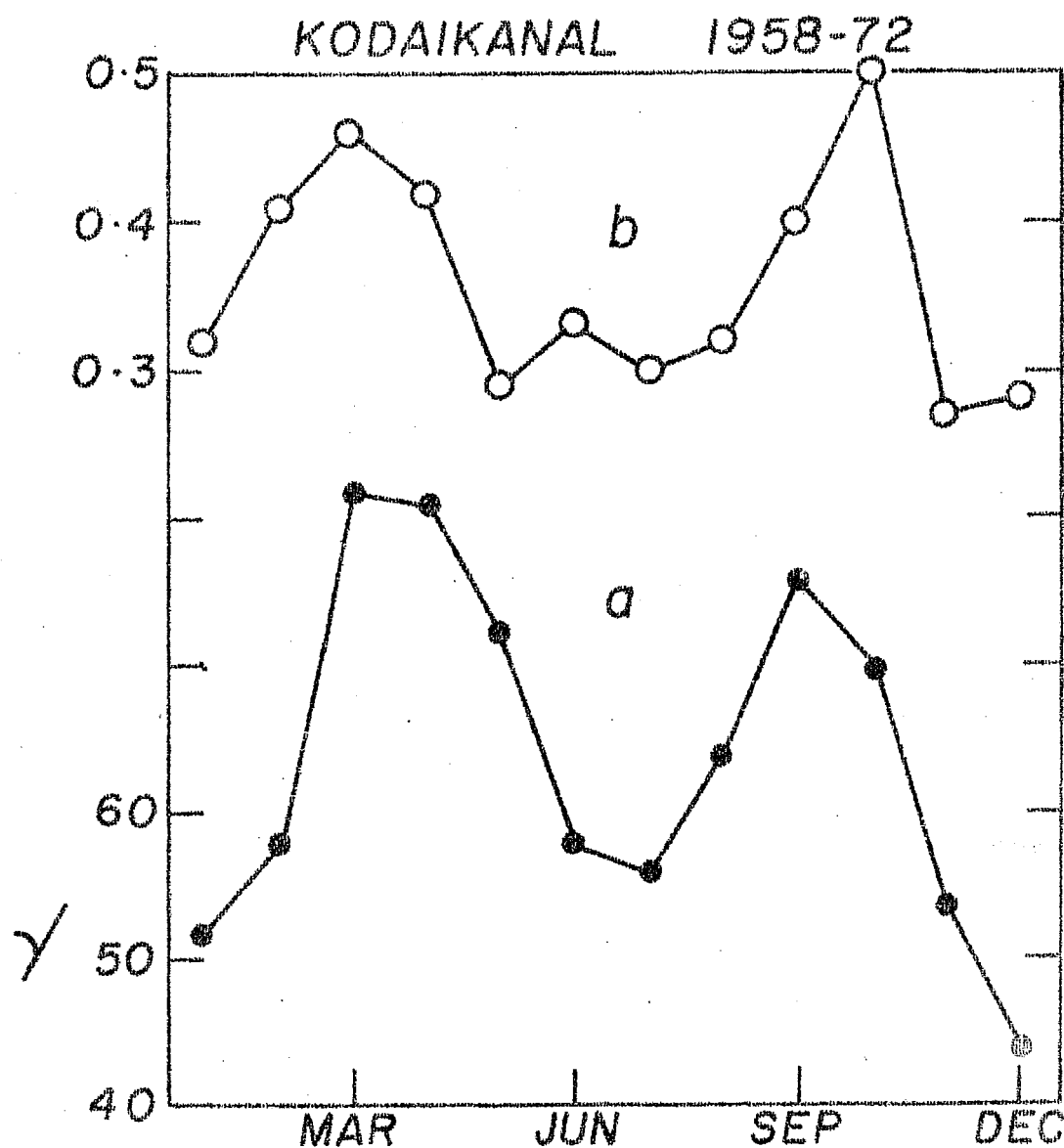


Figure 10.8 : Month to month variation of the coefficients 'a' and 'b' for Kodaikanal in the equation $rSo(H) = a + bkz$. Note the semiannuual variation shown by 'a' and 'b'.

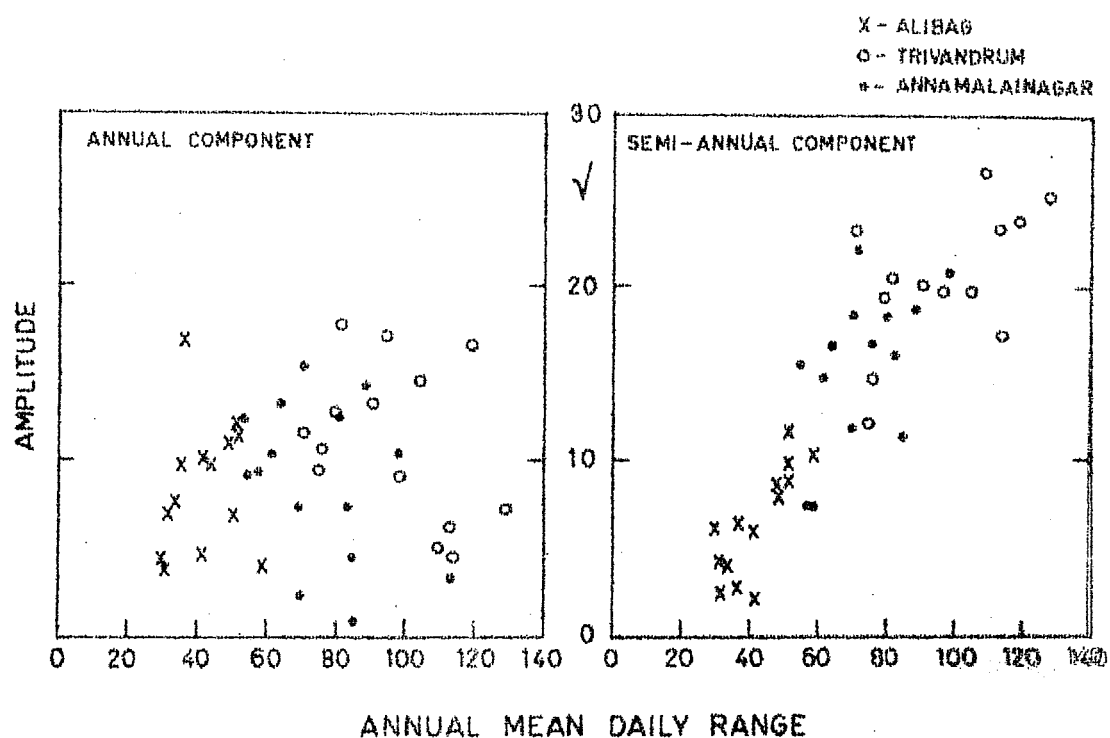


Figure 10.9 : Variation of the amplitude of the annual and the semiannual component of H for different stations with annual mean daily range.

We now study the latitudinal variation of the amplitude of the annual and the semiannual variation of $rS_q(H)$. For any particular station, the values of these different components were normalised to the corresponding values at Trivandrum i.e. almost to the dip equator value. Figure 10.10 shows the latitudinal variation of these normalised components. The vertical flags indicate the standard deviation on averaging over the years 1958-1972. It is seen that the curve for the amplitude of semiannual component vs dip latitude is very similar to the $rS_q(H)$ vs dip latitude curve. No such systematic latitudinal variation of the annual component is evident in the diagram. Thus it may be concluded that the semiannual variation in H at low latitude is very much associated with the electrojet itself.

10.6 Effect of geomagnetic disturbance on the solar daily range of H field

Of late there has been a renewed interest in the daily range ΔH of the geomagnetic H field particularly with the development of magnetospheric physics. The solar daily variation of the H field at low latitudes on quiet days is attributed to the S_q currents. The daily variation range H is amplified in a narrow belt of $\pm 3^\circ$ centred around dip equator because of the enhanced W-E conductivity and the resultant additional electrojet current in this zone (Chapman 1951a). Many authors have used the definition $\Delta H = H_{\max} - H_{\min}$ where H_{\max} and H_{\min} are the maximum and minimum instantaneous values of the H field during the day. The properties of such a range

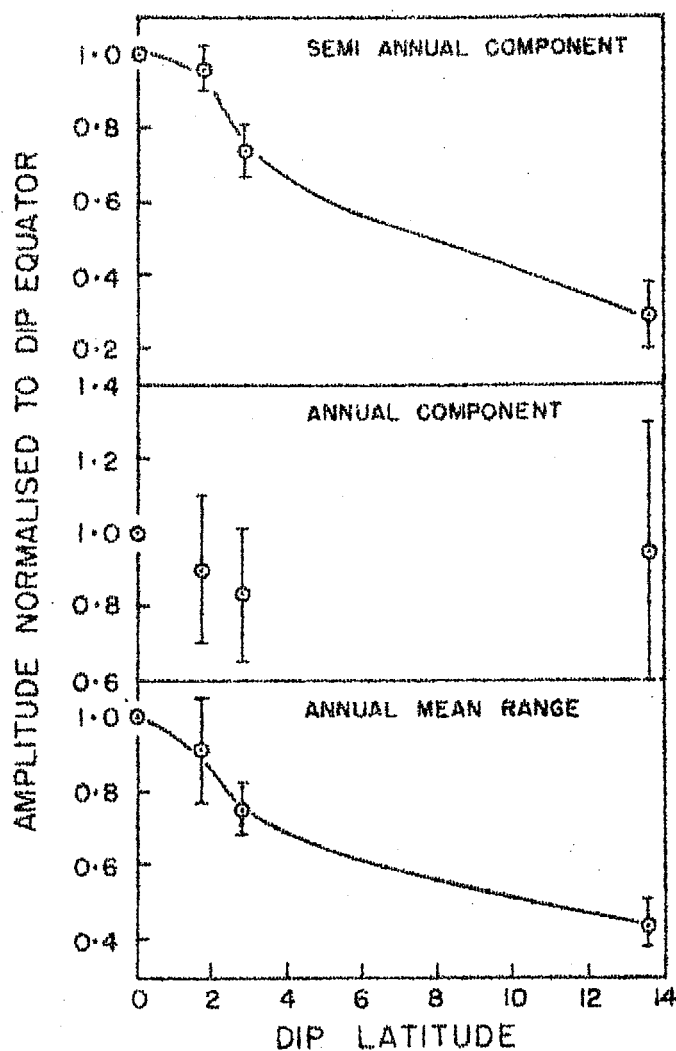


Figure 10.10 : Dependence of the annual mean range, annual and semiannual components of $rSq(H)$ on the dip latitude.

are obviously different on quiet and disturbed days. On quiet days the minimum occurs at night while on disturbed days it could occur at any time during the day or night depending on the disturbance. On such days the above definition can lead to erroneous conclusions. Especially after the suggestion of Sarabhai and Nair (1969) that large H ranges are due to decreases of nighttime field rather than due to increase of daytime field, and that this decrease is due to magnetospheric currents, there has been a revived interest in the nature and location of the currents responsible for the changes in H.

Various criteria have been used to define the solar daily range of H by different authors. Chapman and Raja Rao (1965) have discussed the comparative merits of some of these and have recommended a definition of diurnal range S derived from the mean hourly values of the H field. For a particular day it is equal to the highest mean hourly value minus the hourly value averaged over 0000 - 0300 hrs and 2100 - 2400 hrs. Many observatories publish in their monthly bulletins the range R defined as the maximum instantaneous value - minimum instantaneous value of H for each day. Sarabhai and Nair (1969), Hutton (1970) and Kane (1971) have studied the variation of H_{\max} and H_{\min} in relation to the daily range. In the following, the relative effects of geomagnetic disturbance on the ranges of H field defined by $\Delta H(R)$ and $\Delta H(S)$ are studied.

Kane (1971) showed that H values are positively correlated with H_{\max} and negatively correlated with H_{\min} and suggested that both increases as well as decreases contribute to large ΔH values at low latitudes. Misra (1972) has shown that changes in ΔH as defined by $H_{\max} - H_{\min}$ are due to both increase of H_{\max} and decrease of H_{\min} , while the range defined as the difference between the mean daytime and mean nighttime value is contributed by changes in the daytime value only.

10.7 Daily range of H on quiet and disturbed days

We have taken the published hourly values of H at Alibag and Trivandrum for the years 1964 and 1965. The range in H has been calculated for the five international quiet days of all months using the following two definitions :

$$\Delta H(R) = H_{\max} - H_{\min} \quad (\text{instantaneous values}) \quad (10.1)$$

$$\Delta H(S) = H_{\text{midday}} - H_{\text{night}} \quad (\text{mean hourly values}) \quad (10.2)$$

where H_{midday} is the highest mean hourly value between 1100 and 1300 hrs and H_{night} is the hourly averaged value over the period 0000 - 0300 and 2100 - 2400 hrs. Similarly the process is repeated for the five international disturbed days of each month in 1964 and 1965. The ranges are then grouped into 0 - 9 γ , 10 - 19 γ , 20 - 29 γ etc. and the corresponding mean values of H_{\max} and H_{\min} for each of these groups are evaluated separately for quiet and disturbed days.

Figure 10.11 shows a plot of H_{\max} and H_{\min} against the range $\Delta H(R)$ defined according to equation (10.1). It is evident that on quiet as well as disturbed days H_{\max} shows an increase with increasing value of $H(R)$, while H_{\min} remains almost steady on quiet days; on disturbed days H_{\min} seems to be negatively correlated with $\Delta H(R)$. This indicates that on quiet days variations in $\Delta H(R)$ are due to an increase in daytime value as a result of the ionospheric currents and not due to changes in H_{\min} . On the contrary, $\Delta H(R)$ is composed of an increase in daytime value as also a decrease in nighttime value for disturbed days. The variations of H_{\max} and H_{\min} are similar for both the stations Alibag and Trivandrum. The decrease in nighttime value on disturbed days could be due to currents flowing in a direction opposite to that of S_q currents at large heights, possibly at magnetospheric heights, so that they affect both the stations similarly.

Alternately, if we define the range as given by equation (10.2) and plot the corresponding values of H_{midday} and H_{night} against the range $\Delta H(S)$ the results will be as in Figure 10.12. It is seen that on quiet as well as on disturbed days H_{midday} shows an increase with $\Delta H(S)$ while H_{night} remains fairly constant with $\Delta H(S)$ both on quiet as well as disturbed days. Therefore, there is negligible contribution from H_{night} to the observed changes in $\Delta H(S)$ on quiet and disturbed days.

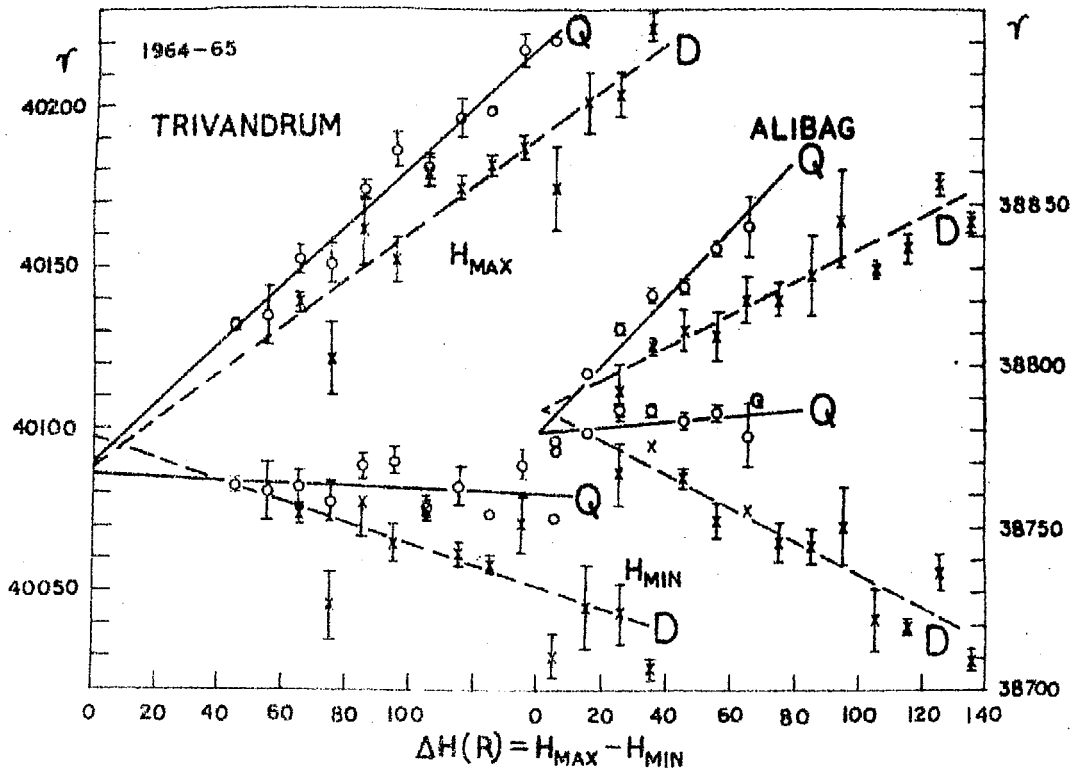


Figure 10.11 Variation of H_{\max} and H_{\min} with the range $\Delta H(R)$ for quiet (Q) and disturbed (D) days at Trivandrum and Alibag.

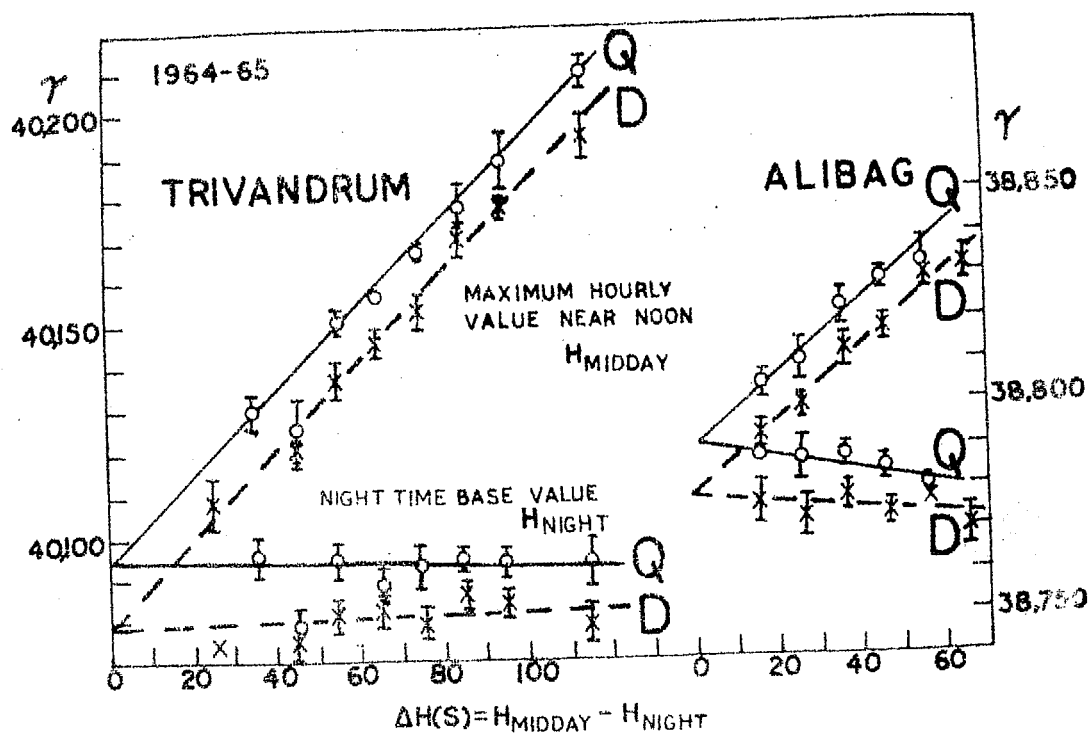


Figure 10.12 : H_{midday} and H_{night} plotted against the range $\Delta H(S)$ for quiet (Q) and disturbed (D) days at Trivandrum and Alibag.

The variation of H_{midday} with the range $\Delta H(S)$ can be described by the following best-fitted straight line equations:

For quiet days

$$\begin{aligned} \text{at Trivandrum } H_{\text{midday}} &= [40097 + 1.00 \Delta H(S)] \gamma \\ \text{at Alibag } H_{\text{midday}} &= [38791 + 0.82 \Delta H(S)] \gamma \end{aligned} \quad (10.3)$$

For disturbed days

$$\begin{aligned} \text{at Trivandrum } H_{\text{midday}} &= [40079 + 1.03 \Delta H(S)] \gamma \\ \text{at Alibag } H_{\text{midday}} &= [38778 + 0.90 \Delta H(S)] \gamma \end{aligned} \quad (10.4)$$

H_{night} remains fairly constant with $\Delta H(S)$ on quiet as well as on disturbed days for both the stations.

The variation of H_{max} and H_{min} with $\Delta H(R)$ can be represented by the following best-fitted least square straight line equations:

For quiet days

$$\begin{aligned} \text{at Trivandrum } H_{\text{max}} &= [40090 + 0.91 \Delta H(R)] \gamma \\ \text{at Trivandrum } H_{\text{min}} &= [40086 - 0.04 \Delta H(R)] \gamma \\ \text{at Alibag } H_{\text{max}} &= [38785 + 0.49 \Delta H(R)] \gamma \\ \text{at Alibag } H_{\text{min}} &= [38778 + 0.08 \Delta H(R)] \gamma \end{aligned} \quad (10.5)$$

For disturbed days

$$\begin{aligned} \text{at Trivandrum } H_{\text{max}} &= [40087 + 0.73 \Delta H(R)] \gamma \\ \text{at Trivandrum } H_{\text{min}} &= [40097 - 0.33 \Delta H(R)] \gamma \\ \text{at Alibag } H_{\text{max}} &= [38779 + 1.04 \Delta H(R)] \gamma \\ \text{at Alibag } H_{\text{min}} &= [38786 - 0.51 \Delta H(R)] \gamma \end{aligned} \quad (10.6)$$

This suggests that while the range $\Delta H(S)$ is hardly affected by magnetic disturbance, $\Delta H(R)$ is greatly affected by

the degree of magnetic disturbance. The apparent discrepancies in similar studies by different authors are due to the different definitions of the range in H . It is concluded that for any comparative studies of geomagnetic H field range with other geophysical parameters at low latitudes, the definition of the range should be quite clear and preferably the range $\Delta H(S)$ should be used.

10.8 Discussion of the results and conclusions

According to the classical dynamo theory, the diurnal variation of H on a quiet day is due to the currents flowing in the E region of the ionosphere; hence changes in the amplitude or phase of the diurnal variation of H should be through changes in this current system. The integrated current in the dynamo region can be expressed as products of the Cowling conductivity (σ_3) and the eastward electric field (E_y). In other terms it can be expressed as the product between the electron number density N_e , the electronic charge e and the westward electron drift velocity v . The electron density N_e is known to be maximum very close to noontime whereas the E region drift velocities are maximum around 0900-1000 LT (Rastogi et al. 1966 and Balsley 1973). The conductivity being basically a function of electron density will also be maximum very close to noon. The electric field E_y arises from the ionospheric winds due to the solar and lunar tidal forces and the solar heating of the ionosphere and hence its maximum could deviate appreciably from

the noontime. Of these, the electron density and solar heating vary diurnally while the tidal forces are significantly semi-diurnal. The amplitude of the diurnal component is higher than the corresponding value of the semi-diurnal component for any of the stations. However, the ratio of C_1/C_2 (refer Figure 10.3 and Table 10.1) is largest for Alibag and smallest for Trivandrum. In other words the solar heating and ion-production are important causes of $S_q(H)$ at all latitudes but at stations near the dip equator the semi-diurnal tidal forces become increasingly important for the daily variation of the H field. It has been shown by Rastogi (1963,1964) that the lunar tidal oscillations in equatorial electrojet currents are greatly enhanced at stations under the equatorial electrojet belt. The magnitude of the $S_q(H)$ should therefore be largely controlled by the intensity of ionization in the E region or in other words by the solar ultra-violet radiation flux. A measure of the radiation flux or intensity of ionization, is the character figure of the E region $(f_oE)^4/\cos \chi$. Appleton and Naismith (1939) showed that the E region character figure for Slough was minimum during solar minimum and maximum for solar maximum. They indicated that the E region ionization and conductivity varied by 50 to 60 per cent through the solar cycle, of the same order as the magnitude of the daily magnetic variation. Allen (1948) obtained the relation $(f_oE)^4 = 1 + 0.097 R$ averaged for a number of stations. Ratcliffe and Weekes (1960) have represented the linear relationship between the intensity of ionizing radiation q_o (proportional to $(f_oE)^4/\cos \chi$)

and sunspot number as

$$q_0 = 180 (1 + kR) \text{ cm}^{-3} \text{ sec}^{-1} \quad (10.7)$$

where the constant $k \times 10^4$ varies from 70 to 95. Yacob and Prabhavalkar (1965) obtained the value of $b/a \times 10^4$ as 74 in their relation between the amplitude C_1 of the diurnal component of $S_q(H)$ at Alibag and R_z expressed as

$$C_1 = a (1 + \frac{b}{a} R_z) \quad (10.8)$$

Since the values of k and $\frac{b}{a}$ are in the same order as that obtained by Allen (1948) and Ratcliffe and Weeks (1960), they concluded that the increase of the amplitude of the diurnal component is due to an increase of ionisation intensity with R_z . From our study (Table 10.1) it may be found that we get values of $\frac{b}{a} \times 10^4$ ranging from 63 to 88. This also confirms the view that the increase of the magnitude of daily magnetic variation with R_z must be due to increase of the ionization density.

One of the explanations which we suggest for the maximum of $rS_q(H)$ to be well before noon is that the current being a product of N_e , e and v would maximise somewhere between the time of maximum of N_e and v . The electron density reaches its maximum close to noon while v (or hence the electric field) maximises near 0900-1000 LT. Therefore it is appropriate that the product is maximum around 1000LT. With increasing R_z , N_e is known to increase by 50% or more whereas the electron drift velocity does not show any change and even shows rather a

decrease (Rastogi et al. 1966). Thus the product of N_e and v should shift to a later time near noon in high sunspot years.

Yacob and Prabhavalkar (1965) have suggested the shift of the time of maximum of $rS_q(H)$ as due to the "sluggishness" of the E layer. It may be pointed out that the magnitude of "sluggishness" is given by $\frac{1}{2\alpha N}$ (Appleton, 1953) where N is the electron density at the time of maximum electron production (near noon) and α the recombination coefficient. The magnitude of this relaxation time is only a few minutes and hence the time shift in the time of maximum is too large to be accounted for by the suggestion of Yacob and Prabhavalkar (1965).

Another plausible cause for the time lag was suggested by Yacob and Rao (1966) as due to the contamination of $S_q(H)$ even on very quiet days by the residual geomagnetic disturbance effect. They found that the maximum in the diurnal component of $SD(H)$ occurs one hour later, for an increase of R_z by 100. The directions of change of the time of maximum of $SD(H)$ and $S_q(H)$ are the same. Thus they concluded that an interference between $SD(H)$ diurnal wave and $S_q(H)$ diurnal wave can shift the time of maxima of the $S_q(H)$ wave unless the similar phase changes in both are due to some common sources. This effect too seems to be too small for quiet days.

The seasonal variations of the range of $rS_q(H)$ may be examined in the light of the axial and equinoctial hypotheses. According to the axial theory (Cortie, 1912) the earth by virtue

of its highest heliocentric latitudes of 7.2° on March 5 and September 7, is on these days in its optimum position with respect to the radial flow of the solar plasma from sunspot zones. This could account for the equinoctial maxima of magnetic variations. According to the alternative theory i.e. 'equinoctial hypothesis' of Bartels (1932) and McIntosh (1959) a semi-annual increase in magnetic activity is expected due to the varying angle between the geomagnetic axis of the earth and the sun earth line, as a result of the rotation of the earth about the sun. The maximum magnetic activity according to this theory should occur near March 21 and September 23. Since the dates of maximum magnetic activity differ only by 16 days between the two theories it is impossible to show whether the maximum is due to asymmetries in solar wind or due to varying angle between geomagnetic axis and the ecliptic. At least roughly the equinoctial maxima seen in the semi-annual variation of $rS_q(H)$ in the present study could be explained by the above theories. From power spectral analysis of 74 years mean daily values of H at Alibag, Bhargava and Yacob (1970) and Bhargava (1972) have found maxima of semi-annual component near March 21 and September 23 supporting the equinoctial hypothesis. The depression in H close to March 5 and September 7 suggests an axial effect also.

Boller and Stolov (1970) have attributed the semi-annual variation of geomagnetic activity to the variation of the Kelvin-Helmholtz instability at the magnetopause boundary due to the seasonal changes in the orientation of the geomagnetic dipole

axis with respect to solar wind flow. The development of magnetospheric physics in the past decade has shown that in addition to the ionospheric S_q current system there are at least three current systems which are external to the earth's surface and persist during solar quiet conditions. They are the magnetopause or boundary current, the neutral sheet current and the ring current. The rotation of the earth under such current systems should produce a daily variation in the earth's surface magnetic field (Mead, 1964). Olson (1970a) has calculated the contribution of these magnetospheric current systems to the earth's magnetic field and found that it is not larger than 10γ , when the currents induced within the earth are also considered. He also explains the peak field at 1130 hr LT by the solar wind direction being about 8° west of optical sun (Hundhausen et al. 1969).

Olson (1970b) has postulated a single current system flowing on the magnetopause capable of explaining the daily semi-annual and annual variations. This current system is caused by the deflection of protons and electrons in the solar wind at the magnetopause boundary. The earth's rotation axis is inclined at 23° to the perpendicular to the ecliptic plane while the geomagnetic dipole axis is separated from the rotation axis by over 11° . Therefore, the angle between the dipole axis and the direction of solar wind is continuously changing through the year. Since this current system depends on this angle the strength and form of the current system are expected to show

seasonal dependence. It was found by Olson (1970b) that this single current system is exactly similar in form to S_q current though it cannot explain the magnitude of the H variation observed on ground. Therefore, it would be reasonable to believe that at least the S_q current system is modulated by the magnetopause current which will explain the seasonal dependence of the diurnal $S_q(H)$ variation and the semi-annual variation of the daily range in H.

Currie (1966) proposed a ring current origin probably situated at about three earth radii for the semiannual line in the power spectrum of H variation. From the amplitudes, coherence and phase observations he inferred that the annual and semi-annual variations have different generating mechanisms.

Vestine (1954) invoked the influence of meridional ionospheric winds blowing from summer to the winter hemisphere in explaining the annual variation.

Russel and McPherron (1973) proposed a new explanation for the semi-annual variation of geomagnetic activity that it is caused by a semi-annual modulation of the effective southward components of the interplanetary magnetic field, because of the varying probability throughout the year of a southward component of the geomagnetic field as seen by the magnetosphere. This arises from the changing orientation between the solar equatorial coordinate system in which the interplanetary field is ordered.

Their model also assumes that northward interplanetary fields are non-interacting. Again we invoke here the mechanism of the electron drift speed controlling the semi-annual variation of $rS_q(H)$. Ionospheric drift measurements at Thumba (dip $0.6^\circ S$) and at Ahmedabad (dip $34^\circ N$) indicate that the drifts speed maximise in equinoxes at Thumba suggesting a semi-annual variation of drift speed near the magnetic equator whereas the drift speeds at Ahmedabad maximise in summer showing an annual variation at non-equatorial latitudes (Chandra et al. 1971). This suggests that the predominant semi-annual variation of $rS_q(H)$ at the equatorial stations and significant annual variation at the non-equatorial station Alibag could be related to the corresponding variations of drift speed.

Harmonic analysis of the annual mean daily variation of geomagnetic H field at low latitudes in the Indian zone shows a significant diurnal and semi-diurnal component, the diurnal variation having its peaks around 1130 LT. The amplitudes of diurnal and semi-diurnal component linearly increase with sunspot number. The times of maximum of the diurnal and semi-diurnal component are delayed by about half an hour in high sunspot years as compared to low sunspot years. The amplitudes decrease with latitudes away from the dip equator.

Harmonic analysis of the monthly mean diurnal range for quiet days, $rS_q(H)$, shows a significant semiannual variation

for the electrojet stations - Trivandrum, Kodaikanal and Annamalainagar, but a predominantly annual component for Alibag, a station outside the electrojet. The amplitude of the semi-annual component is linearly related to the annual mean daily range and increases linearly with sunspot number R_z .

The dependence of amplitude of the diurnal component with R_z is due to enhanced E-region ionization with increasing R_z while the delay in the time of maximum is suggested to be due to the changes in the E-region electric fields driving the ionospheric currents.

The annual and semi-annual variations of $rs_q(H)$ may be related to the corresponding variations of horizontal electron drift speeds.

C H A P T E R - X I

SUMMARY AND CONCLUSIONS

In this thesis study of the Ionospheric Total Electron Content at equatorial and low latitudes derived from Faraday Rotation of beacon signals at 40 and 41 MHz signals from BE-B and BE-C satellites is presented. A study of the Geomagnetic H field variations at low latitude is also included. Other ionospheric parameters that can be derived from TEC and ionosonde data such as slab-thickness of the ionosphere, topside to bottomside content ratio, integrated production rate, effective loss rate and satellite signal scintillations associated with spread F and sporadic E are also investigated.

A unique feature of this study is that the ionosonde data recorded at the same place as the Faraday rotation recording station are used. For studying the latitudinal variation of TEC data recorded at two stations with an overlapping zone in between are used.

The main conclusions that can be drawn are:

(i) Total Electron Content at the magnetic equator does not show the noon bite-out seen in f_oF_2 .

(ii) At non-equatorial latitudes the daily variation of TEC and f_oF_2 are similar.

(iii) Latitudinal variation of TEC does show the equatorial anomaly with peak TEC about 15-20° dip latitude, which again is seasonally dependent.

(iv) Daily maximum TEC shows a semiannual variation while daily minimum TEC shows rather an annual variation at tropical station Ahmedabad. But at the magnetic equator both seem to show semiannual variation.

(v) TEC increases with 10.7 cm solar flux in all seasons and at both equatorial and low latitude stations.

(vi) Slab-thickness follows the diurnal temperature curve. Increase of slab-thickness with 10.7 cm solar flux seen at Ahmedabad is absent at the equatorial station Kodaikanal.

(vii) Integrated production rate has a semiannual variation with equinoctial peaks and increases with solar flux.

(viii) Effective loss rate also has a seasonal variation with larger values in equinoxes than in solstices.

(ix) Equatorial scintillation belt extends at least upto 28° N geographic latitude; scintillation index tends to increase towards the equator.

(x) Daytime scintillation can be caused by intense blanketing sporadic E patches of width about 300 km. Daytime scintillation strength is directly proportional to $f_o E_s$.

(xi) Daily variation of H at low latitudes has a predominant diurnal component, the amplitude of which increases with solar activity and the diurnal maximum is delayed with the progress of solar activity.

(xii) The daily range of H field shows a significant semi-annual component at magnetic equatorial stations and annual component at non-equatorial station. This semi-annual component is more directly related to the annual mean range or solar activity while the annual component is rather unrelated to solar activity.

(xiii) Upward moving ionospheric irregularities (kinks) move under the $E \times B$ drift with velocities $\sim 20-40$ m/sec.

(xiv) These kinks are representative of ionospheric irregularities, probably due to accumulation of metallic ions over the equator by equatorward neutral winds or gravity waves.

REFERENCES

- Aarons J. and Whitney H.E. (1968) Planet. Space Sci., 16, 21.
- Aarons J., Whitney H.E. and Allen R.S. (1971) Proc. IEE., 59, 159.
- Aarons J. (1975) Proc. Beacon Satellite Investigations of the Ionosphere Structure and ATS-6 Data, Nov. 1974, 1, 184.
- Abur Robb M.F.K. (1969) Planet. Space Sci., 17, 1269.
- Abur Robb M.F.K. and Windle D.W. (1969) Planet. Space Sci., 17, 96.
- Allen C.W. (1968) Terr. Magn. Atmos. Elec., 53, 433.
- Anderson D.N. (1971) NCAR Co-operative Thesis No.24, University of Colorado.
- Appleton E.V. and Barnett M.A.F. (1925) Nature (London), 115, 333.
- Appleton E.V. and Naismith R. (1935) Proc. Roy. Soc., A150, 685.
- Appleton E.V. (1937) Proc. Roy. Soc., A162, 451.
- Appleton E.V. and Naismith R. (1939) Phil. Mag., 27, 144.
- Appleton E.V. (1946) Nature, 157, 691.
- Appleton E.V. (1953) J. Atmos. Terr. Phys., 3, 282.
- Appleton E.V. (1954) J. Atmos. Terr. Phys., 5, 348.
- Baker W.B. and Martyn D.F. (1953) Phil. Trans. Roy. Soc., A246, 281.
- Bandopadhyay P. (1970) Planet. Space Sci., 18, 129.
- Baral S.S. and Mitra A.P. (1950) J. Atmos. Terr. Phys., 6, 95.
- Bartels J. (1932) Terr. Magn. Atmos. Elec., 37, 1.
- Basu S. and Das Gupta A. (1968) J. Geophys. Res., 73, 5599.
- Basu Sunanda and Basu S. (1969) J. Geophys. Res., 74, 6502.

- Basu Sunanda and Basu S. (1971) J. Geophys. Res., 76, 5337.
- Basu S., Guhathakurta B.K., (1975) Proc. Beacon Satellite
Bhattacharyya G.N. and Investigations Ionosphere
Das Gupta A. Structure and ATS-6 Data,
November 1974, 1, 210.
- Baxter R.G. (1964) J. Atmos. Terr. Phys., 26, 711.
- Baxter R.G. and Kendall P.C (1968) Proc. Roy. Soc., A304, 171.
- Beer T. (1973) Planet. Space Sci., 21, 297.
- Berkner L.V. and Wells W.H. (1934) Terr. Magn. Atmos. Elec., 39, 215.
- Beynon W.J.G. (1948) Nature, (London), 162, 887.
- Beynon W.J.G. and (1964) J. Atmos. Terr. Phys., 26, 1175.
Jones E.S.O.
- Bhar J.N., Das Gupta A., (1970) Radio Sci., 5, 939.
and Basu S.
- Bhargava B.N. (1964) J. Inst. Telecom. Engrs., 10, 404.
- Bhargava B.N. and Saha A.K. (1967) Memoris of the Kodaikanal
Observatory - an atlas of
Ionograms, plates 8-9, pub. by
Manager of Publications,
Govt. of India Press, New Delhi.
- Bhargava B.N. and (1970) J. Atmos. Terr. Phys., 32, 1489.
Yacob A.
- Bhargava B.N. (1972) Planet. Space Sci., 20, 423.
- Bhonsle R.V., da Rosa A.V., (1965) Radio Sci., 69D, 929.
and Garriott O.K.
- Bibl K. (1952) C.R. Acad. Sci. Paris, 235, 734.
- Bibl K. (1953) Zeit. Fur. Geophysik, 19, 136.
- Bibl K., Harnischmacher E. (1955) Physics of the Ionosphere,
and Rawer K. Physical Soc. London, p.113.
- Bibl K. and Rawer K. (1959) J. Geophys. Res., 64, 2232.
- Blackband W.T. (1960) J. Geophys. Res., 65, 1987.
- Blumle L.J. (1962) J. Geophys. Res., 67, 4609.
- Boller B.R. and Stolov H.L. (1970) J. Geophys. Res., 75, 6073.

- Bolton J.G., Slee O.B. and Stanley G.J. (1953) Austr. J. Phys., 26, 1175.
- Booker H.G. (1958) Proc. IRE 46, 298.
- N.E. (1938) Terr. Magn. Atmos. Elec., 43, 55.
- E.N. and Ross W.J. (1951) Proc. Roy. Soc., A207, 251.
- Bramley E.N. (1953) Proc. Roy. Soc., A220, 39.
- Bramley E.N. and Peart M. (1964) J. Geophys. Res., 69, 609.
- Bramley E.N. and Young M. (1968) J. Atmos. Terr. Phys., 30, 99.
- Breit G. and Tuve M.A. (1925) Nature (London), 116, 357.
- Browne I.C., Evans J.V., Hargreaves J.K. and Murray W.A.S. (1956) Proc. Phys. Soc., B69, 901.
- Budden K.G. (1954) Rep. Cambridge Conf. Ionos. Phys., Phys. Soc., London, p.332.
- Burkard O. (1954) Z. Geophys., 20, 51.
- Calla O.P.N. (1971) J. Inst. Telecom. Engrs., 17, 160.
- Calvert W. and Schmidt C.W. (1964) J. Geophys. Res., 69, 1839.
- Chance P. (1972) Scientific Report No.56, University of the West Indies, Kingston, Jamaica.
- Chandra H., Misra R.K. and Rastogi R.G. (1971) Planet. Space Sci., 19, 1487.
- Chandra H., Rajaram G., and Rastogi R.G. (1973) Ind. J. Radio Space Phys., 2, 243.
- Chandra H. and Rastogi R.G. (1974) Curr. Sci., 43, 567.
- Chandra S. and Goldberg R.A. (1964) J. Geophys. Res., 69, 3187.
- Chapman S. (1919) Phil. Trans. Roy. Soc., London, 219A, 1.
- Chapman S. (1931) Proc. Phys. Soc. (London), 43, 26.

- Chapman S. and Bartels J. (1940) Geomagnetism, Oxford Clarendon Press.
- Chapman S. (1948) Terr. Magn. Atmos. Elec., 53, 247.
- Chapman S. (1951) Proc. Phys. Soc. (London), B64, 833.
- Chapman S. (1951a) Arch. Meteorol. Geophys. u. Biopotential A4, 368.
- Chapman S. (1956) Nuovo Cimento, 10(4), 1385.
- Chapman S. and Raja Rao K.S. (1965) J. Atmos. Terr. Phys., 27, 559.
- Chatterjee S.K.,
Bandopadhyay A.K.,
Guhathakurta B.K. and
Bandopadhyay P. (1974) Ann. de Geophys., 30, 329.
- Chicccacci P.F. (1972) Physics of the Upper Atmosphere, ed. F. Verniani, Editrici Compositori, Bologna, p.139.
- Chivers H.J.A. and
Greenhow J.S. (1959) J. Atmos. Terr. Phys., 17, 1.
- Cortie A.L. (1912) Monthly Not. Roy. Astron. Soc., 73, 52.
- Currie R.G. (1966) J. Geophys. Res., 71, 4579.
- da Rosa A.V. and Smith F.L. (1967) J. Geophys. Res., 72, 1829.
- Das Gupta A. and Basu S. (1971) Ind. J. Pure. Appl. Phys., 9, 509.
- Davies M.J. and da Rosa A.V. (1969) J. Geophys. Res., 74, 5721.
- Davies T.N., Burrows K. and
Stolarik J.D. (1967) J. Geophys. Res., 72, 1845.
- de Mendonca F. (1965) Space Res., 2, 687.
- de Mendonca F., Kantor I.J. and
Clemesha B. (1969) Radio Sci., 4, 823.
- Deshpande M.R., Rastogi R.G.,
Vats H.O., Davies K.,
Grubb R.N. and Jones J.E. (1976) Pramana (in press)
- Dieminger W.,
Shodel J.P.,
Schmidt G. and
Hartmann G.K. (1970) J. Atmos. Terr. Phys., 32, 1615.

- Dueno B. (1956) J. Geophys. Res., 61, 535.
- Duncan R.A. (1956) Austr. J. Phys., 9, 436.
- Duncan R.A. (1960) J. Atmos. Terr. Phys., 18, 89.
- Dunford E. (1967) J. Atmos. Terr. Phys., 29, 1489.
- Dungey J.W. (1959) J. Atmos. Terr. Phys., 9, 90.
- Egedal J. (1947) Terr. Magn. Atmos. Elec., 52, 449.
- Egedal J. (1948) Nature (London), 161, 443.
- Elkins T.J. and Slack F.F. (1969) J. Atmos. Terr. Phys., 31, 421.
- Elkins T.J. (1970) Special Report No.106, p.19, AFCRL.
- Evans J.V. and Taylor G.N. (1961) Proc. Roy. Soc., A263, 189.
- Eyfrig R. (1962) J. Geophys. Res., 67, 1678.
- Farley D.T. (1966) Electron Density Profiles in Ionosphere and Exosphere, ed. Frihagen, p.466.
- Faynot J.M., Vila P. and Walter J. (1971) J. Atmos. Terr. Phys., 33, 1621.
- Ferguson E.E. (1967) Rev. Geophys., 5, 305.
- Forbush S.E. and Casavarde M. (1961) Carnegie Inst. Washington, Publ. 620, 140.
- Furman D.R. and Prasad S.S. (1973) J. Geophys. Res., 78, 5837.
- Garriott O.K. (1960) J. Geophys. Res., 65, 1139.
- Garriott O.K. and Smith F.L. (1965) Planet. Space Sci., 13, 839.
- Garriott O.K., Smith F.L. and Yuen P.C. (1965) Planet. Space Sci., 13, 829.
- Garriott O.K., da Rosa A.V., Davies M.J. and Villard O.G. (1967) J. Geophys. Res., 72, 6099.

- Gautier T.M., Knetch R.W. and McNish A.G. (1951) Proc. Second Meet. Mixed Commission Ionosphere, Brussels, p.100.
- Golton E. and Walker G.O. (1971) J. Atmos. Terr. Phys., 33, 1.
- Goodman J.M. (1966) J. Geophys. Res., 71, 985.
- Goodman J.M. (1968) Planet. Space Sci., 16, 951.
- Gouin P. and Mayaud P.N. (1967) Ann. de Geophys., 23, 41.
- Hanson W.B. and Moffett R.J. (1966) J. Geophys. Res., 71, 5559.
- Harish Chandra and Rastogi R.G. (1971) J. Inst. Telecom. Engrs., 17, 207.
- Hawkins G. and Mullen (1974) A.F.C.R.L. TR-74-0160.
- Hedin A.E. and Mayr H.G. (1973) J. Geophys. Res., 78, 1688.
- Hibberd F.H. and Ross W.J. (1966) J. Geophys. Res., 71, 2243.
- Hirono M. (1950a) J. Geomag. Geoelect., 2, 1.
- Hirono M. (1950b) J. Geomag. Geoelec., 2, 113.
- Hirono M. (1952) J. Geomag. Geoelec., 4, 7.
- Hudson R.M. (1969) Planet. Space Sci., 17, 1045.
- Handhauson A.J., Bame S.J. and Asbridge J.R. (1969) J. Geophys. Res., 74, 2799.
- Hunter A.N. and Webster A.R. (1965) Proc. Second Int. Symp. Equat. Aeron., 152, Sao Jose dos Campos, Sao Polo, Brazil.
- Hutton R. (1970) Ann. de Geophys., 26, 927.
- Iyer K.N. and Rastogi R.G. (1975) Ind. J. Radio Space Phys., 4, 6.
- Jayendran R. and O'Brien (1969) J. Atmos. Terr. Phys., 31, 555.
- Jensen D.C. and Cain J.C. (1962) J. Geophys. Res., 67, 3568.
- Jonathan Mass (1966) Radio Sci., 1, 1137.
- Jones H.S. and Melotte P.F. (1953) Monthly Not. Roy. Astr. Soc. Geophys. Suppl., 6, 409.
- Kane R.P. (1971) J. Geophys. Res., 76, 8199.

- Kane R.P. (1973) Proc. Ind. Acad. Sci., 78A, 149.
- Kent G.S. (1961) J. Atmos. Terr. Phys., 16, 10.
- Kersley L. and Taylor G.N. (1974) J. Atmos. Terr. Phys., 36, 93.
- King Hele D.G. (1964) Theory of Satellite Orbits in an Atmosphere, London, Butterworths.
- King G.A.M. and Lawden M.D. (1962) J. Atmos. Terr. Phys., 24, 565.
- King J.W., Olatunji E.O., Eccles D. and Newman W.S. (1967) J. Atmos. Terr. Phys., 29, 1391.
- King J.W. (1969) Ann. IQSY 5, 131, MIT Press.
- Klobuchar J.A. and Allen R.S. (1970) AFCRL Report No.8.
- Koster J.R. and Wright R.W. (1963) Radio Astronomical and Satellite Studies of Atmosphere, North Holland, p.114.
- Koster J.R. (1966) Ann. de Geophys., 22, 435.
- Koster J.R. (1968) Progress Report No.8, Contract No.F-61052-67, C 0027, AFCRL.
- Koster J.R. (1972) Planet. Space Sci., 20, 1997.
- Ketch R.W. and Schlitt D.W. (1958) N.B.S. Report No.5587.
- Legg A.J., King J.W. and Precce D.M. (1967) J. Atmos. Terr. Phys., 29, 1397.
- Little C.G. and Lawrence R.S. (1960) Space Res., 1, 340.
- Lockwood G.E.K. and Nelms G.L. (1964) J. Atmos. Terr. Phys., 26, 569.
- Lyon A.J., Skinner N.J. and Wright R.W.H. (1960) J. Atmos. Terr. Phys., 19, 145.
- Lyon A.J. and Thomas L. (1963) J. Atmos. Terr. Phys., 25, 373.
- Lyon A.J. (1965) Rept. Equatorial Aeron. ed. F. de Mendonca, C.T.A., Brazil 129.

- Mac Dougall J.W. (1969) Radio Sci., 4, 805.
- Maeda H. (1955) Rep. Ionos. Res. (Japan), 9, 59.
- Maeda K., Uyeda H. and Shinkawa H. (1942) Rep. Res. Phys. Inst. Radio Waves No.1, 2.
- Maeda K. (1952) J. Geomag. Geoelec., 4, 63.
- Maeda K. and Matsumoto H. (1962) Rep. Ionos. Space Res.(Japan), 16, 1.
- Martyn D.F. (1947) Proc. Roy. Soc., A190, 273.
- Martyn D.F. (1948) Proc. Roy. Soc., A294, 429.
- Martyn D.F. (1953) Phil. Trans. Roy. Soc. (London), A246, 306.
- Martyn D.F. (1956) Austr. J. Phys., 9, 161.
- Matsushita S. (1967) Solar Quiet and Lunar Daily Variation fields in 'Physics of Geomagnetic Phenomena', Vol.1, eds.S.Matsushita and W.Campbell, Academic Press, N.Y., 301.
- Matsushita S and Campbell W. (1967) Physics of Geomagnetic Phenomena, Vol.I, Academic Press, New York.
- Matsushita S. (1968) Radio Sci., 3, 658.
- Maynard N.C. (1967) J. Geophys. Res., 72, 1863.
- McClure J.P. (1964) J. Geophys. Res., 69, 2774.
- McIntosh D.H. (1959) Phil. Trans. Roy. Soc. London, 251A, 525.
- McNish A.G. (1937) I.A.T.M.E. Bull., 10, 271.
- Mead G.D. (1964) J. Geophys. Res., 69, 1181.
- Mendillo M., Papagiannis M.D. and Klobuchar J.A. (1969) J. Atmos. Terr. Phys., 31, 1359.
- Mendillo M., Papagiannis M.D. and Klobuchar J.A. (1970) Radio Sci., 5, 895.
- Misra R.K. (1972) Curr. Sci., 41, 863.
- Mitra S.K. (1946) Nature (London), 158, 668.

- Morse P.M. and Feshbach H. (1953) Methods of Theoretical Physics, 2, Mc Graw Hill, 1325.
- Mulkowa W.N. (1969) M.Sc. Thesis, University of East Africa, University College, Nairobi, Kenya.
- Munro G.H. (1948) Nature (London), 162, 886.
- Munro G.H. and Heisler L.H. (1956a) Aust. J. Phys., 9, 343.
- Munro G.H. and Heisler L.H. (1956b) Aust. J. Phys., 9, 359.
- Munro H. (1966) Radio Sci., 1, 1186.
- Murray W.A.S. and Hargreaves J.K. (1954) Nature, 173, 944.
- Nancy Uss Crooker (1970) J. Atmos. Terr. Phys., 32, 179.
- Narayana Iyer K. and Rastogi R.G. (1974) J. Geophys. Res., 79, 209.
- Newpert W.M., Behring W.E. and Lindsay J.C. (1964) Space Res., 4, 719.
- Olatunji E.O. (1965) Rept. Equatorial Aeron. ed. F. de Mendonca, C.T.A., Brazil, 135.
- Olatunji E.O. (1967) J. Atmos. Terr. Phys., 29, 277.
- Olson W.P. (1970a) J. Geophys. Res., 75, 7244.
- Olson W.P. (1970b) Planet. Space Sci., 18, 1471.
- Onwukwe D.N. (1974) J. Atmos. Terr. Phys., 36, 1259.
- Onwumechilli C.A. and Alexander N.S. (1959) J. Atmos. Terr. Phys., 13, 222.
- Pelz D.T. and Newton G.P. (1969) J. Geophys. Res., 74, 267.
- Pope J.H. (1974) Radio Sci., 9, 675.
- Pramanik S.K. and Yegnanarayanan S. (1952) Ind. J. Met. Geophys., 3, 212.
- Pramanik S.K. and Hariharan P.S. (1953) Ind. J. Met. Geophys., 4, 353.
- Price A.T. (1963) J. Geophys. Res., 68, 6383.

- Raghavarao R. and Sivaraman M.R. (1974) Nature (London), 249, 331.
- Ramakrishnan S. (1967) Ph.D. Thesis, Kerala University.
- Rao B.C.N. (1963) J. Geophys. Res., 68, 2541.
- Rao C.S.R. (1962) J. Atmos. Terr. Phys., 24, 729.
- Rao C.S.R. and Malhotra P.L. (1964) J. Atmos. Terr. Phys., 26, 1075.
- Rastogi R.G. (1959a) J. Atmos. Terr. Phys., 14, 31.
- Rastogi R.G. (1959b) Can. J. Phys., 37, 874.
- Rastogi R.G. (1959c) J. Geophys. Res., 64, 727.
- Rastogi R.G. (1960) J. Atmos. Terr. Phys., 18, 315.
- Rastogi R.G. (1962) J. Atmos. Terr. Phys., 24, 1031.
- Rastogi R.G. and Sanatani S. (1963) J. Atmos. Terr. Phys., 25, 799.
- Rastogi R.G. (1964) J. Geophys. Res., 69, 1020.
- Rastogi R.G. (1966) J. Inst. Telecomm. Engrs., 12, 245.
- Rastogi R.G., Deshpande M.R. and Kaushika N.D. (1966) J. Atmos. Terr. Phys., 28, 137.
- Rastogi R.G. (1970) Nature (London), 225, 258.
- Rastogi R.G. (1971) Nature (London), 229, 240.
- Rastogi R.G. and Rajaram G. (1971) Ind. J. Pure Appl. Phys., 9, 531.
- Rastogi R.G. and Sharma R.P. (1971) Planet. Space Sci., 19, 505.
- Rastogi R.G. (1971) Proc. Ind. Acad. Sci., 73, 284.
- Rastogi R.G. (1972) J. Atmos. Terr. Phys., 34, 1537.
- Rastogi R.G., Sharma R.P. and Shodhan V. (1973) Planet. Space Sci., 21, 713.
- Rastogi R.G. (1973) Ann. de Geophys., 29, 421.

- Rastogi R.G. (1975) Proc. Ind. Acad. Sci., A81, 80.
- Rastogi R.G., Iyer K.N. and Bhattacharyya J.C. (1975) Curr. Sci., 44, 531.
- Ratcliffe J.A., Schmerling E.R., Setty C.S.G.K. and Thomas J.O. (1956) Phil. Trans. Roy. Soc., A248, 621.
- Ratcliffe J.A. (1959) The Magneto-ionic Theory and its Application to the Ionosphere, p.75, Cambridge University Press.
- Ratcliffe J.A. and Weeks K. (1960) Physics of the Atmosphere, ed. J.A.Ratcliffe, p.417, Academic Press, New York & London.
- Rishbeth H. and Setty C.S.G.K. (1961) J.Atmos. Terr. Phys., 20, 263.
- Rishbeth H. (1964) J. Atmos. Terr. Phys., 26, 657.
- Rishbeth H. (1974) Contemp. Phys., 14, 229.
- Rivault R. (1950) Proc. Phys. Soc., London, 68, 126.
- Ross W.J. and Blumle L.J. (1963) Proc. Int. Conf. Ionos., Inst. Phys. and the Phys. Soc., London, p.84.
- Ross W.J. (1965) J.Geophys. Res., 70, 597.
- Rufenach C.L., Nimit V.T. and Leo R.E. (1968) J. Geophys. Res., 73, 2459.
- Rush C.M. and Richmond A.D. (1973) J. Atmos. Terr. Phys., 35, 1171.
- Russel C.T. and McPheron P.L. (1973) J. Geophys. Res., 78, 92.
- Sarabhai V. and Nair K.N. (1969) Nature (London), 223, 603.
- Sastry T.S.G. (1968) J. Geophys. Res., 73, 1789.
- Sawada K. and Shibata H. (1961) J. Radio Res. Lab., Tokyo, 8(37), 219.
- Schuster S. (1908) Phil. Trans. Roy. Soc., London, 208A, 163.

- Seaton S.L. (1947) J. Met., 4, 197.
- Sessions W.P. (1972) Goddard Space Flight Center, Greenbelt, Ms. June 1972.
- Shapley A.H. (1970) Atlas of Ionograms, Report U.A.G-10, III-25, Pub. by U.S. Dept. of Commerce, ESSA, USA.
- Sinclair J. and Kelleher R.F. (1969) J. Atmos. Terr. Phys., 31, 201.
- Singleton D.G. (1960) J. Geophys. Res., 65, 3615.
- Singleton D.G. and Lynch G.J.E. (1962) J. Atmos. Terr. Phys., 24, 353.
- Skinner N.J. and Wright R.W. (1957) Proc. Phys. Soc. (London), B70, 833.
- Skinner N.J. (1966) Planet. Space Sci., 14, 1123.
- Smith III F.L. (1968) J. Geophys. Res., 73, 7385.
- Somayajulu Y.V., Tyagi T.R. and Nagi N.K. (1972) Ind. J. Radio Space Phys., 1, 62.
- Sterling D.L., Hanson W.B., Moffett R.J. and Baxter R.G. (1969) Radio Sci., 4, 1005.
- Stewart B. (1882) Encyclopedia Britanica 16, 159.
- Sugira M. and Cain J.C. (1966) J. Geophys. Res., 71, 1869.
- Sugira M. Poros D.J. (1969) J. Geophys. Res., 74, 4025.
- Swenson G.W. (1963) Cospar Information Bulletin No.15, 20.
- Tarpley J.D. (1970) Planet. Space Sci., 18, 1075.
- Taur R.R. (1973) Comsat Technical Review 3, 145.
- Taylor G.N. (1965) Planet. Space Sci., 13, 507.
- Taylor G.N. and Earnshaw R.D.S. (1970) J. Atmos. Terr. Phys., 32, 1675.
- Thiruvengadhan A. (1954) Ind. J. Met. Geophys., 5, 267.

- Thomas L. and Lyon A.J. (1963) Rep. IM54, Radio Res. Station, Slough, England.
- Thomas L. (1968) J. Atmos. Terr. Phys., 30, 1631.
- Titheridge J.E. (1966) J. Atmos. Terr. Phys., 28, 1135.
- Titheridge J.E. and Andrews M.K. (1967) Planet. Space Sci., 15, 1157.
- Titheridge J.E. (1968a) J. Geophys. Res., 73, 2985.
- Titheridge J.E. (1968b) J. Atmos. Terr. Phys., 30, 1857.
- Titheridge J.E. (1968c) J. Geophys. Res., 73, 243.
- Titheridge J.E. (1968d) J. Atmos. Terr. Phys., 30, 73.
- Titheridge J.E. and Smith W.D. (1969) Planet. Space Sci., 17, 1667.
- Titheridge J.E. (1971) J. Geophys. Res., 76, 4569.
- Titheridge J.E. (1973a) J. Atmos. Terr. Phys., 35, 981.
- Titheridge J.E. (1973b) Planet. Space Sci., 21, 1775.
- Tyagi T.R. and Somayajulu Y.V. (1966) Radio Sci., 1, 1125.
- Tyagi T.R. and Bhatnagar V.P. (1969) J. Atmos. Terr. Phys., 31, 943.
- Tyagi T.R. and Mitra A.P. (1970) J. Atmos. Terr. Phys., 32, 1807.
- Tyagi T.R. and Somayajulu Y.V. (1970) Ind. J. Pure. Appl. Phys., 8, 577.
- Tyagi T.R. and Mittal (1971) Ind. J. Pure. Appl. Phys., 9, 504.
- Tyagi T.R., Ghosh A.B., Mitra A.P. and Somayajulu Y.V. (1972) Space Res. XII, 1195.
- Untiedt J. (1967) J. Geophys. Res., 72, 5799.
- Vestine E.H. (1954) J. Geophys. Res., 59, 93.
- Walker G.O. (1971) J. Atmos. Terr. Phys., 33, 1041.
- Walker G.O. and Ma J.H.K. (1972) J. Atmos. Terr. Phys., 34, 1419.
- Walker G.O. and Ting S.D. (1972) J. Atmos. Terr. Phys., 34, 283.

- Webb H.D. (1969) J. Geophys. Res., 74, 1880.
- Wernik A.W. and Liu C.H. (1974) J. Atmos. Terr. Phys., 36, 871.
- Whitney H.E., Aarons J., (1973) Radio Sci., 7, 12.
Allen R.S. and
Seemann D.R.
- Wild J.P. and Roberts J.A. (1956) J. Atmos. Terr. Phys., 8, 55.
- Wright R.W.H. (1959) J. Geophys. Res., 64, 2203.
- Yacob A. and Prabhavalkar A.S. (1965) J. Atmos. Terr. Phys., 27, 73.
- Yacob A. and Rao D.R.K. (1966) J. Atmos. Terr. Phys., 28, 351.
- Yeboah-Amankwah D. and (1972) Planet. Space Sci., 20, 395.
Koster J.R.
- Yeh K.C. and Swenson G.W. (1959) J. Geophys. Res., 64, 2281.
- Yeh K.C. and Gonzales V.H. (1960) J. Geophys. Res., 65, 3209.
- Yeh K.C. and Swenson G.W. (1961) J. Geophys. Res., 66, 1061.
- Yeh K.C. and Flaherty B.J. (1966) J. Geophys. Res., 71, 4557.
- Young D.M.L., Yuen P.C. and (1970) Planet. Space Sci., 18, 1163.
Roelofs T.H.
- Yuen P.C. and Roelofs T.H. (1966) J. Geophys. Res., 71, 849.
- Yuen P.C. and Roelofs T.H. (1967) J. Atmos. Terr. Phys., 29, 321.

APPENDIX 1 FORTRAN PROGRAM FOR SATELLITE PREDICTION

```

//SATPR JOB ,SOLPP10,10,100
//SATPRD EXEC FORTRAN)BCD*
C ADVANCE EQUATORIAL CROSSING AND SATELLITE PREDICTIONS
C PUNCH THE VALUE OF INT AS 1 IF THE INTERMEDIATE OUTPUT IS REQD
C JEND IS THE NO. OF OBSERVATIONS FOR PART III
C NCR IS THE NO. OF COPIES REQUIRED FOR OUTPUT
C IF NCR=2, IT WILL GIVE TWO COPIES FOR OUTPUT, OTHERWISE IT WILL GIVE
C ONLY ONE COPY.
C READ CONROL CARD FOR PART III FOLLOWED BY PART III
C PART III IS TO BE PUNCHED OUT FROM THE BULLETIN RECEIVED FROM NASA
C PUNCH HEADING IN COLUMNS 27-46 OF FIRST CARD
C NLP = NO. OF LINES PER PAGE
C DIMENSION DT)45*,ET)45*,CN)45*,HH)45*,DDT)150*,CCN)150*,HHH)150*
C DIMENSION JYR)30*,JASRV)30*,JARV)30*,JMTH)30*,JID)30*
C DIMENSION IH)30,25*,ZM)30,25*,CL)30,25*,IDNT)5*
C DIMENSION KHR)45*,KIQ)45*,ZDAZ)45*,ZDEL)45*,ZSR)45*,KISH)45*,
1KISM)45*
C NLP=60
2 FORMAT)1H2*
20 BB=1.0
30 READ40,JEND,SLT,SLN,NCR,DMIN,IDNT,INT
40 FORMAT)I2,2F8.2,I2,F6.2,5A4,I2*
IF)NCR.EQ.2*GO TO 50
NCR=1
50 B=SLT/57.2958
IF)JEND.LE.45.AND.JEND.GE.1*GO TO 110
PRINT60,JEND
60 FORMAT)1X,'THE VALUE OF JEND IS OUT OF RANGE ,1 AND 45',I6*
GO TO 200
110 READ90,)DT)J*,ET)J*,CN)J*,HH)J*,J=1,JEND*
90 FORMAT)F6.2,F8.2,F10.2,F8.1*
C READ DATA CARD TO GENERATE PART II INSIDE THE MEMORY
C ISYR,MSTH AND ISD ARE YEAR,MONTH AND DATE RESPECTIVELY-
C -FROM WHICH DATE ONWARDS THE OUTPUT IS REQD
C IN IS THE NO.OF DAYS FOR WHICH THE OUTPUT IS REQD
C READ120,IYR,MTH,ID,ARV,IH)1,1*,ZM)1,1*,CL)1,1*,C,D,IN,ISYR,MSTH,
1ISD
120 FORMAT)3I3,F8.0,I3,4F10.4,4I3*
PRINT2
PRINT141
141 FORMAT) 1X,'INPUT DATA CARDS ARE AS UNDER',/*
PRINT142,JEND,SLT,SLN,NCR,DMIN,IDNT
142 FORMAT)1X,I4,2F10.2,I4,F8.2,5X,5A4/*
PRINT143,)DT)J*,ET)J*,CN)J*,HH)J*,J=1,JEND*
143 FORMAT)1X,F8.2,F10.2,F12.2,F10.1*
PRINT144,IYR,MTH,ID,ARV,IH)1,1*,ZM)1,1*,CL)1,1*,C,D,IN,ISYR,MSTH,
1ISD
144 FORMAT)1H0,3I4,F10.2,I4,4F12.4,4I5*
DDT)1*=DT)1*
CCN)1*=CN)1*
HHH)1*=HH)1*
NNN=1
JEN=JEND-1

```

```

      IF)INT. NE. 1*GO TO 170
      PRINT2
150 PRINT160, IDNT
160 FORMAT) 1X, 6X, 17HINTERMEDIATE FOR, 2X, 5A4/1H0*
      PRINT260, NNN, ET)1*, CN)1*, HH)1*
      LINE=3
170 DO280J=1, JEN
      XPM=ET)J. 1*-ET)J*
      ALT=)DT)J. 1*-DT)J**/XPM
      LAN=)CN)J. 1*-CN)J**/XPM
      SH=)HH)J. 1*-HH)J**/XPM
      IP=ET)J. 1*
      IQ=ET)J*
      N=IP-IQ
      IF)N*180, 180, 210
180 PRINT190
190 FORMAT)1X, 'PLEASE CHECK PART III WHICH IS WRONGLY PUNCHED.*
200 CALL EXIT
210 ETJ=ET)J*
      DTJ=DT)J*
      CNJ=CN)J*
      HHJ=HH)J*
      DO270K=1, N
      E=BB-ETJ
      XPM=DTJ. E*ALT
      RV=CNJ. E*ALN
      RVM=HHJ. E*SH
      NNN=NNN. 1
      IF)NNN-150*240, 240, 220
220 PRINT230
230 FORMAT)1X, 36HINTERMEDIATE IS MORE THAN 150 CARDS,,
      128H PLEASE CHECK PART III INPUT*
      GO TO 200
240 DDT)NNN*=XPM
      CCN)NNN*=RV
      HHH)NNN*=RVM
      IF)INT. NE. 1*GO TO 270
250 PRINT260, NNN, XPM, RV, RVM
260 FORMAT)1X, I4, 3F12.3*
      LINE=LINE. 1
      IF)LINE. LE. NLP*GO TO 270
      PRINT2
      PRINT160, IDNT
      LINE=3
270 BB=BB. 1. 0
280 CONTINUE
      NERR=0
      JEN=NNN-1
      JJJ=1
      MMM=1
      IF)IH)1, 1*. LE. 24. AND. IH)1, 1*. GE. 1*GO TO 360

```

```

330 PRINT340,IYR,MTH,ID,IH)1,1*
340 FORMAT)1X,'HOUR I SWRONG FOR',4I3*
    NERR=1
360 IF)ZM)1,1*.LE.60.AND.ZM)1,1*.GE.1*GO TO 400
370 PRINT380,IYR,MTH,ID,IH)1,1*,ZM)1,1*
380 FORMAT)1X,'MINUTES ARE WRONG FOR',4I5,F10.4*
    NERR=1
400 ZM)1,1*=ZM)1,1*.ADIM
    IF)IN.GE.1*GO TO 430
    PRINT420,IN
420 FORMAT)1X,'THE VALUE OF IN IS WRONG IN COLUMNS 61-63',I4*
    NERR=1
430 IF)ID*440,440,470
440 PRINT450,ID
450 FORMAT)1X,'34HINPUT DATE IS WRONG IN COLUMNS 7-9,I5*
    NERR=1
470 IF)MTH*480,480,510
480 PRINT490,MTH
490 FORMAT)1X,'35HINPUT MONTH IS WRONG IN COLUMNS 4-6,I5*
    NERR=1
510 IF)IYR*520,520,531
520 PRINT530,IYR
530 FORMAT)1X,'34HINPUT YEAR IS WRONG IN COLUMNS 1-3,I5*
    NERR=1
531 IF)ISD.GT.0*GO TO 532
    ISYR=IYR
    MSTH=MTH
    ISD=ID
    GO TO 542
532 IF)IYR-ISYR*542,536,533
533 PRINT534,IYR,MTH,ID,ISYR,MSTH,ISD
534 FORMAT)1X,'THE YEAR IS WRONG IN COLUMNS 64-66',3I5,5X,3I5*
    GO TO 200
536 IF)MTH-MSTH*542,539,537
537 PRINT538,IYR,MTH,ID,ISYR,MSTH,ISD
538 FORMAT)1X,'THE MONTH IS WRONG IN COLUMNS 67-69',3I5,5X,3I5*
    GO TO 200
539 IF)ID-ISD*542,542,540
540 PRINT541,IYR,MTH,ID,ISYR,MSTH,ISD
541 FORMAT)1X,'THE DATE IS WRONG IN COLUMNS 70-72',3I5,5X,3I5*
    GO TO 200
542 IF)NERR.EQ.1*GO TO 200
560 INN=0
    NDA=1
    CP=C
    DP=D
    LLL=1
    MMM=1
570 IF)MTH-2*580,620,580
580 GOTO)610,590,610,600,610,600,610,610,610,600,610,600,610*,MTH
590 STOP590
600 IDAY=30
    GOTO660
610 IDAY=31
    GOTO660

```

```

620 IYY=IYR/4
    IDA=IYR-IYY*4
    IF)IDA*630,640,650
630 PRINT635
635 FORMAT)1X,'STOP 630'*
    GOTO 200
640 IDAY=29
    GO TO 660
650 IDAY=28
660 GO TO )670,1020*,LLL
670 IF)ID-IDAY*680,680,440
680 IF)C*690,690,710
690 PRINT700,C,D
700 FORMAT)1X,28HTHE VALUE OF C OR D IS WRONG,14H (-VE OR ZERO),
    12F10.4*
    GO TO 200
710 IF)D*690,690,720
720 ASRV=ARV
    I=1
730 HRR=IH)NDA,I**60
    HRM=HRR.ZM)NDA,I*.C
    CL)NDA,I.1*=CL)NDA,I*.D
    IH)NDA,I.1*=HRM/60.
    HI=IH)NDA,I.1*
    ZM)NDA,I.1*=HRM-HI*60.
740 IF)CL)NDA,I.1*-360.*760,750,750
750 CL)NDA,I.1*=CL)NDA,I.1*-360.
    GO TO 740
760 IF)IH)NDA,I.1*-24*780,770,770
770 IH)NDA,I.1*=IH)NDA,I.1*-24
    GO TO 820
780 GOTO)785,910*,MMM
785 I=I.1
    ARV=ARV.1C0
    IF)I-25*730,730,790
790 PRINT800,IYR,MTH,ID,C
800 FORMAT)1X,45HNO, OF CARDS IN PART II ARE MORE THAN 25 FOR ,3I4,1X
    136HPLEASE CHECK THE VALUE OF C WHICH IS,F12.4*
    GO TO 200
820 L=I
840 IF)ID-ISD*950,850,950
830 GOTO)840,910*,JJJ
850 +F)MTH-MSTH*950,860,950
860 IF)IYR-ISYR*950,870,950
870 GOTO)880,910*,JJJ
880 PRINT2
    PRINT890,IDNT
890 FORMAT) 1X,7X,11HPART II FOR,2X,5A4/1H0*
    LINE=3
900 JJJ=2
910 JYR)NDA*=IYR
    JASRV)NDA*=ASRV
    JARV)NDA*=ARV
    JMTH)NDA*=MTH
    JID)NDA*=ID
    PRINT912,IYR,MTH,ID,ASRV,ARV
912 FORMAT)1X,3I3,2F10.3*

```

```

LINE=LINE.1
IF)LINE.LE.NLP*GO TO 5555
PRINT2
PRINT890,IDNT
LINE=3
555 GOTO)915,913*,MMM
913 NDA=NDA-1
GO TO 950
915 DO930J=1,L
PRINT940,IH)NDA,J*,ZM)NDA,J*,CL)NDA,J*
940 FORMAT)1X,I4,2F10.2*
LINE=LINE.1
IF)LINE.LE.NLP*GO TO 930
PRINT2
PRINT890,IDNT
LINE=3
930 CONTINUE
945 INN=INN.1
950 LDA=NDA
GOTO)970,960*,JJJ
960 NDA=NDA.1
970 IH)NDA,1*=IH)LDA,L.1*
O-)ND+,1Q=OM+LDA,LF1*
CL)NDA,1*=CL)LDA,L.1*
ARV=ARV.1.0
ID=ID.1
980 IF)ID-IDAY*1020,1020,990
990 ID=ID-IDAY
MTH=MTH.1
+F)MTH-12*1020,1020,1000
1000 MTH=MTH-12
IYR=IYR.1
LLL=2
GOTO570
020 IF)NDA-30*1030,1090,1090
030 IF)NDA-IN*570,570,1090
090 NDA=NDA-1
DO1400KK61,NC-
PRINT2
1100 PRINT1110,IDNT
1110 FORMAT) 1X,6X,'OUTPUT FOR',2X,5A4/1H0*
LINE=3
IDD=1
DO1390MD=1,NDA
N=JARV)MD*-JASRV)MD*.1
IYR=JYR)MD*
MTH=JMTH)MD*
ID=JID)MD*
DO1380J=1,N
IHR=IH)MD,J*
RV=ZM)MD,J*
RVM=CL)MD,J*
XPM=IHR*60

```

```

IP=XPM.RV.1.
SH=IP
TDF=SH-XPM-RV
CC=-90.
IF)RVM-)SLN-180.**1120,1130,1130
1120 RVM=SLN-360.-RVM
GO TO 1140
1130 RVM=SLN-RVM
1140 MIYR=IYR
MMTH=MTH
MID=ID
MIHR=IHR
XRV=RV
1160 KKL=0
MMC=1
DO1370I=1,JEN
SLT=RVM-)CCN)I.1*-CCN)I***TDF-CCN)I*.CCN)1*
IF)SLT*1170,1180,1180
1170 SLT=-SLT
IP=1
GO TO 1190
1180 IP=2
1190 IF)SLT-90.*1200,1370,1370
1200 DLT=)DDT)I.1*-DDT)I***TDF.DDT)I*
IF)DLT*1210,1240,1220
1210 ALT=-DLT
GO TO 1230
1220 ALT=DLT
1230 IF)ALT-90.*1240,1370,1370
1240 SLT=SLT/57.2958
DLT=DLT/57.2958
RV=)HHH)I.1*-HHH)I***TDF.HHH)I*
ALT=SIN)DLT**SIN)B*.COS)DLT**COS)B**COS)SLT*
A11=1.-ALT*ALT
IF)A11.GT.0.0*GO TO 1245
SG=0.0
GO TO 1248
1245 SG=ATAN)SQRT)A11*/ALT*
1248 SP=)RV.6334.4*)1.-ALT**/)6334.4*SIN)SG**
DEL=)ATAN)SP*-SG**57.2958
IF)DEL*1250,1260,1260
1250 IF)DEL-CC*1371,1368,1368
1260 SL=SIN)SLT*/SIN)SG**COS)DLT*
A12=1.-SL*SL
IF)A12.GT.0.0*GO TO 1265
DAZ=1.57079
GO TO 1268
1265 DAZ=ATAN)SL/SQRT)A12**
1268 DAZ=DAZ*57.2958
1270 IF)DLT-B*1280,1280,1290

```

```

1280 DAZ=180.00DAZ
      GO TO 1320
1290 DAZ=360.0-DAZ
      GO TO 1320
1300 IF)DLT-B*1310,1320,1320
1310 DAZ=180.0-DAZ
1320 SR=SQRT)RV.12668.8*)6334.4.RV**)1.0-ALT**
      RS=SH/60.
      IHR=RS
      RV=IHR
      IQ=)RS-RV**60.00.01
      IIM=IHR*60.IQ
      ISM=IIM.330
      IF)ISM-1440*1340,1330,1330
1330 ISM=ISM-1440
1340 ISH=ISM/60
      ISM=ISM-ISH*60
      KKL=KKL.1
      IF)KKL.LE.45* GO TO 1363
      PRINT1361,MIYR,MMTH,MID,MIHR,XRV
1361 FORMAT)1X,'PASS IS MORE THAN 45 MINUTES FOR',2I5*
      KKL=KKL-1
      GOTO1371
1363 IF)DEL.LT.10.0*GO TO 1365
      MMC=2.
1365 KIHR)KKL*=IHR
      KIQ)KKL*=IQ
      ZDAZ)KKL*=DAZ
      ZDEL)KKL*=DEL
      ZSR)KKL*=SR
      KISH)KKL*=ISH
      KISM)KKL*=ISM
1368 CC=DEL
1370 SH=SH.1.
1371 IF)KKL.NE.0*GO TO 1372
      PRINT1373,MIYR,MMTH,MID,MIHR,XRV
      LINE=LINE.1
      IF)LINE.LE.NLP*GO TO 1380
      GOTO )6666,6664*,IDD
6664 PRINT7778
      IDD=1
6666 PRINT2
      PRINT1110,IDNT
      LINE=3
      GO TO 1380
1372 IF)MMC.EQ.1*GO TO 1376
      PRINT1373,MIYR,MMTH,MID,MIHR,XRV
1373 FORMAT)1X,2I4,I4,I6,F10.2*
      LINE=LINE.1
      IF)LINE.LE.NLP*GO TO 6675
      GO TO )6674,6670*,IDD
6670 PRINT7778
      IDD=1
6674 PRINT2

      PRINT1110,IDNT

```

```
LINE=3
6675 DO1375MN=1,KKL
      PRINT1374,KIHR)MN*,KIQ)MN*,ZDAZ)MN*,ZDEL)MN*,ZSR)MN*,KISH)MN*,
      1KISM)MN*
1374 FORMAT)I18,I4,F12.2,F9.2,F12.2,2I5*
      LINE=LINE.1
      IF)LINE.LE.NLP*GO TO 1375
      GO TO 18888,7777*,IDD
7777 PRINT7778
7778 FORMAT)/2X,'*** INDICATES THAT THE WHOLE PASS WAS HAVING LESS TH
      1AN 10 DEGREE ELEVATION'*
      IDD=1
8888 PRINT2
      PRINT1110,IDNT
      LINE=3
1375 CONTINUE
      GO TO 1380.
1376 PRINT1377,MIYR,MMTH,MID,MIHR,XRV
1377 FORMAT)1X,3I4,I6,F10.2,12X,'***!*'
      IDD=2
1378 LINE=LINE.1
      IF)LINE.LE.NLP*GO TO 1380
      GOTO)9999,9998*,IDD
9998 PRINT7778
      IDD=1
9999 PRINT2
      PRINT1110,IDNT
      LINE=3
1380 CONTINUE
1390 CONTINUE
      GOTO)1400,1395*,IDD
1395 PRINT7778
1400 CONTINUE
1500 CALL EXIT
      END
```


APPENDIX 2 FORTRAN PROGRAM FOR COMPUTATION OF MAGNETIC FIELD FACTOR AND TOTAL ELECTRON CONTENT

```
//IYER JOB ,SOLPP10,10,20
//LATVAR EXEC FORTRAN)BCD*
```

COMPUTES MC-FACTOR FOR FARADAY ROTATIONS(IN AMP/M) AND NT.

INPUTS

FLATO,FLONO=LATITUDE AND EAST LONGITUDE OF OBSERVER (IN DEGREES).

STN1,STN2 STN3 TOGETHER STAND FOR THE NAME OF THE STATION.

J=NO.OF VALUES.

ID,IM,IY,IT=DAY,MONTH,YEAR AND STARTING TIME RESPECTIVELY

Y(I) AND Z(I)=SUB. SAT. LONGITUDE AND LATITUDE RESPECTIVELY(IN
1DEGREES).

O(I)=OMEGA=NUMBER OF FADES

HC,HS=IONOSPHERIC AND SATELLITE HEIGHT(IN KM) RESPECTIVELY.

PI=CONSTANT, ER=EARTHS RADIUS

G,H=GAUSS COEFFICIENTS.

OUTPUTS

DLONC,FLATC=SUB IONOSPHERIC POINTS, EL=ELEVATION,AZ=AZIMUTH,

SECHIC=SEC(CHI),NSR=RANGE OF THE SATELLITE, TEL=TOTAL ELECTRON CONT
AND FMC=MC. FACTOR.

FORTRAN IV COMPILATION

THIS PROGRAM CAN BE USED FOR ANY STATION.

```
DIMENSION SP)8*, CP)8*, DP)8,8*, P)8,8*, G)7,7*,CONST)8,8*,H)7,7*,
10)90*,Y)90*,Z)90*
```

```
PRINT2
```

```
LOGICAL EAST
```

```
DATA G)2,1*,G)2,2*,G)3,1*,G)3,2*,G)3,3*,G)4,1*,G)4,2*,G)4,3*,
1G)4,4*,G)5,1*,G)5,2*,G)5,3*,G)5,4*,G)5,5*,G)6,1*,G)6,2*,G)6,3*,
2G)6,4*,G)6,5*,G)6,6*,G)7,1*,G)7,2*,G)7,3*,G)7,4*,G)7,5*,G)7,6*,
3G)7,7*/24.20046,1.70885,1.91264,-4.07858,-1.06483,-2.50814,
44.94415,-1.98132,-0.51694,-3.32586,-3.60470,-1.73439,0.55768,
5-0.16266,1.29361,-2.73802,-1.54754,-0.04838,0.22083,0.05547,
6-1.55359,-0.38619,0.25560,1.70399,0.08364,0.01806,0.08873/,H)2,1*,
7H)2,2*,H)3,1*,H)3,2*,H)3,3*,H)4,1*,H)4,2*,H)4,3*,H)4,4*,H)5,1*,
8H)5,2*,H)5,3*,H)5,4*,H)5,5*,H)6,1*,H)6,2*,H)6,3*,H)6,4*,H)6,5*,
6H)6,6*,H)7,1*,H)7,2*,H)7,3*,H)7,4*,H)7,5*,H)7,6*,H)7,7*/0.00000,
1-4.61464,0.00000,2.63592,-0.12565,0.00000,1.18332,-0.32428,
20.01671,0.00000,-0.94100,0.79625,0.03422,0.11021,0.00000,-0.06334,
3-0.15915,0.36582,0.19266,-0.09693,0.00000,-0.45821,-0.69511,
4-0.27104,-0.00939,-0.08881,-0.02586/
```

```

READ8,FLATO,FLONO,HS,STN1, STN2, STN3
IHS=HS
HC=350
IHC=HC
PI=3.14159
ER=6371.2
RAD=.0174533
FLATO=FLATO*RAD
FLONO=FLONO*RAD
SLATO=SIN)FLATO*
CLATO=COS)FLATO*
RS=ER.HS
AT=1.570796-FLATO
10 READ1,J,ID,IM,IY,IT,SAT
READ7,)Y)I*,Z)I*,O)I*,I=1,J*
PRINT5,ID,IM,IY,IT,IHS,IHC,SAT
PRINT6
PRINT4
DO 185 I=1,J
305 FLONS=Y)I*
FLATS=Z)I*
FLONS=FLONS*RAD
FLATS=FLATS*RAD
TB=1.570796-FLATS
IF)FLONS.LT.0.0* FLONS=FLONS.6.283186
IF)FLONO.LT.0.0* FLONO=FLONO.6.283186
30 DL=FLONO-FLONS
DLONOS=ABS)DL*
IF)DLONOS.GT.PI* DLONOS=6.283186-DLONOS
40 SDL=SIN)DLONOS*
CDL=COS)DLONOS*
SLATS=SIN)FLATS*
CLATS=COS)FLATS*
CDOS=SLATO*SLATS.CLATO*CLATS*CDL
SDOS=SQRT)1.-CDOS**2*
SR=SQRT)ER**2.RS**2-2.*ER*RS*CDOS*
CSEL=SDOS*RS/SR
SNEL=SQRT)1.-CSEL**2*
EL=ATAN)SNEL/CSEL*
EL=EL/RAD
A=ATAN)SDOS/CDOS*
SS=)A.AT.TB*/2.
SNAZ=SQRT) )SIN)SS-AT**SIN)SS-A**/ )SIN)AT**SIN)A***
CSAZ=SQRT)1.-SNAZ**2*
AZ=ATAN)SNAZ/CSAZ**2
IF)DL*50,50,45
45 AZ=6.283186-AZ
50 AZ=AZ/RAD
SCHIC=ER*RS*SDOS/ )SR* )ER.HC**
CCHIC=SQRT)1.-SCHIC**2*
CHIC=ATAN)SCHIC/CCHIC*

```

```

TAN=SIN)CHIC*/COS)CHIC*
SECHIC=1/CCHIC
SGAMA=CLATS*SDL/SDOS
CGAMA=)SLATS-CDOS*SLATO*/)SDOS*CLATO*
SCHIO=)RS**SDOS/SR
CCHIO=SQRT)1.-SCHIO**2*
CDOC=CCHIO*CCHIC.SCHIO*SCHIC
SDOC=SQRT)1.-CDOC**2*
SLATC=SLATO*CDOC.CLATO*SDOC*CGAMA
CLATC=SQRT)1.-SLATC**2*
FLATC=ATAN)SLATC/CLATC*
SDLONC=SDOC*SGAMA/CLATC
CDLONC=SQRT)1.-SDLONC**2*
DLONC=ATAN)SDLONC/CDLONC*
SENA=CLATO*SGAMA/CLATC
COSA=)SLATO-CDOC*SLATC*/)SDOC*CLATC*
EAST=.FALSE.
IF)FLONO.LT.FLONS*EAST=.TRUE.
IF)ABS)DL*.GT.PI*EAST=.NOT.EAST
IF)EAST*GOTO80
75 DLONC=FLONO-DLONC
   GOT092
80 DLONC=FLONO.DLONC
   IF)DLONC.GT.PI*DLONC=DLONC-6.283186
92 DO95N=2,7
   FN=N
   DO95M=1,N
   P)M,N*=0.
   DP)M,N*=0.
   FM=M-1
95 CONST)N,M*=)FN-2.***2-FM**2*/))2.*FN-3.**2.*FN-5.**
   CONST)2,2*=0.
   P)1,1*=1.
   DP)1,1*=0.
   SP)1*=0
   CP)1*=1.
   SP)2*=SIN)DLONC*
   CP)2*=COS)DLONC*
   S=CLATC
   C=SLATC
   DO100M=3,7
   SP)M*=SP)2**CP)M-1*.CP)2**SP)M-1*
100 CP)M*=CP)2**CP)M-1*-SP)2**SP)M-1*
   AOR=ER/ER.HC*
   AR=AOR**2
   BT=0.
   BR=0.
   BP=0
   DO130N=2,7
   AR=AR*AOR
   FN=N
   DO130M=1,N
   FM=M-1

```

```

      IF)M=N*110,105,110
105  P)N,N*=S*P)N-1,N-1*
      DP)N,N*=S*DP)N-1,N-1*.C*P)N-1,N-1*
      GOTO125
110  IF)N-2*120,115,120
115  P)2,M*=C*P)1,M*
      DP)2,M*=C*DP)1,M*-S*P)1,M*
      GOTO125
120  P)N,M*=C*P)N-1,M*-CONST)N,M**P)N-2,M*
      DP)N,M*=C*DP)N-1,M*-S*P)N-1,M*-CONST)N,M**DP)N-2,M*
125  PAR=P)N,M**AR
      TEMP=G)N,M**CP)M*.H)N,M**SP)M*
      BT=BT+TEMP*DP)N,M**AR
      BP=BP-(G)N,M**SP)M*-H)N,M**CP)M***FM*PAR
130  BR=BR-TEMP*PAR
      BP=BP/S
      BB=SQRT)BT*BT+BP*BP+BR*BR*
      BH=SQRT)BT*BT+BP*BP*
      IF)EAST*COSFD=COSA*BT+SENA*BP
      IF).NOT.EAST*COSFD=COSA*BT-SENA*BP
155  X=COSFD*TAN+BR
      FMC=-X
      FLATC=FLATC/RAD
      DLONC=DLONC/RAD
      NSR=SR
165  TEL=(1.69*O)I**/FMC
180  TEL=ABS)TEL*
      PRINT3,Y)I*,Z)I*,DLONC,FLATC,TEL,EL,AZ,FMC,O)I*,SECHIC,NSR
185  CONTINUE
      GOTO10
1  FORMAT)5I5,A5*
2  FORMAT)1H2*
3  FORMAT)1X,4F10.2,F10.3,2F10.1,F10.3,2F10.2,I10*
4  FORMAT)1H0,6X,4HSLON,6X,4HSLAT,6X,4HILON,6X,4HILAT,7X,2HNT,7X,
   14HELEV,6X,4HAZIM,5X,5HM.FAC,5X,5HOMEGA,5X,5HSECHI,5X,5HRANGE*
5  FORMAT)1H0,5HDATE=,3I5,10X,5HTIME=,I5,10X,11HSAT+HEIGHT=,I6,2HKM,
   110X,11HION+HEIGHT=,I5,2HKM,5X,A5*
6  FORMAT)1H0,6X,13HSUB SATELLITE,7X,14HSUB IONOSPHERE*
7  FORMAT)2F5.2,F5.0,3A4*
8  FORMAT)15F5.2*
END

```

**ON THE OCCURRENCE AND VERTICAL MOVEMENT OF
KINK AT KODAIKANAL ***

K. NARAYANA IYER and R. G. RASTOGI

Physical Research Laboratory

Ahmedabad-9 (India)

and

Indian Institute of Astrophysics

Kodaikanal (India)

PHYSICAL RESEARCH LABORATORY

AHMEDABAD-380009, INDIA.

ON THE OCCURRENCE AND VERTICAL MOVEMENT OF KINK AT KODAIKANAL *

K. NARAYANA IYER and R. G. RASTOGI

Physical Research Laboratory
Ahmedabad-9 (India)

and

Indian Institute of Astrophysics
Kodaikanal (India)

ABSTRACT

The occurrence of ionospheric irregularities observed as sharp discontinuities (kinks) on the ionograms and moving upward with time at Kodaikanal have been studied for a period covering high, medium and low solar activity conditions. These kinks are most common during the summer season and during the morning (0900 LT) and evening (1500 LT). The vertical velocities of these irregularities obtained by true height analysis of the ionograms lie in the range 10-40 m/sec. The velocity shows a minimum around noon with no significant solar cycle dependence. One of the possible causes for the generation of these irregularities is suggested to be the accumulation of metallic ions over the equator by equatorward neutral winds or gravity waves and their uplift to be due to the $E \times B$ drift.

INTRODUCTION

The equatorial ionosphere is known to have properties very different from those of the ionosphere at middle latitudes. The first abnormality, detected by *Seaton* and *Berkner* (1939), was that the daily variation of f_oF_2 at Huancayo, close to the magnetic equator, shows two maxima, one in the morning and the other in the evening with a bite-out during midday. *Appleton* (1946) noted that the latitudinal variation of f_oF_2 at noon shows a trough over the magnetic equator and two maxima at magnetic latitudes around $20^\circ N$ and $20^\circ S$. The height of peak ionisation at an equatorial station shows a very large increase around midday hours in low sunspot years, this rise continues till the sunset hours during high sunspot years (*Rastogi*, 1971a). These abnormal features of the low-latitude ionosphere have been explained by the so-called Fountain Effect, namely that the ionosphere over the magnetic equator is lifted upwards by the $E \times B$ force with simultaneous movements away from the equator roughly along the lines of force

(*Martyn*, 1947, *Rastogi*, 1959, *Duncan*, 1960, *Bramley*, and *Peart*, 1965, *Moffett* and *Hanson*, 1965). The expected vertical drift of ionisation over the magnetic equator has been confirmed by the backscatter observations at Jicamarca by *Woodman* and *Hagfors* (1969).

Some distortions noted in ionogram recordings known as travelling ionospheric disturbances have been detected at a number of middle and high latitude stations. These disturbances start at the F_2 critical frequencies, move along the trace down to the F_1 layer and disappear between E and F-regions. These disturbances have been suggested to be due to horizontal displacement of wave front with a forward tilt or due to the downward propagation of disturbances originating outside the atmosphere (*Munro*, 1948, *Beynon*, 1948, *Bibl*, 1952, 1953, *Bibl et al.*, 1955, *Munro* and *Heisler*, 1956a, b, *Bibl* and *Rawer*, 1959).

Shortly after the commencement of ionospheric recordings at Thumba (dip. lat. $0.3^\circ S$), which is very

close to the magnetic equator in Indian zone, a new type of upward moving ionospheric irregularities was noted by *Rastogi*, 1970). These disturbances, called by him 'kinks', appear as an intermediate layer between E and F-region and move upward through the whole F-region with the progress of time. Subsequently these kinks have been observed at other equatorial stations, namely Kodaikanal (dip. lat. 1.7°N) by *Rastogi* (1971b), Fort Archambault (dip. lat. 1.5°S), Ouagadougou (dip. lat. 4.5°N) by *Faynot et al* (1971), Huancayo (dip. lat. 1°N) by *Rastogi* (1972), Chimbote (dip. lat. 3°N), Natal (dip. lat. 0°), Djibouti (dip. lat. 3°N), Jicamarca (dip. lat. 1°N) by *Rastogi* (1973).

The present article describes the characteristics of kinks observed in the ionograms of Kodaikanal and the upward drift velocity computed from the temporal variation of the height of the kink for years of low, medium and high solar activity.

CHARACTERISTICS OF IRREGULARITIES SEEN ON THE IONOGRAMS

Lunar stratifications have been noted at some equatorial stations; Huancayo, Kodaikanal and Talara (*Gautier et al.*, 1951; *Bhargava and Saha*, 1967; *Shapley*, 1967). KODAIKANAL
1-MAY, 1952

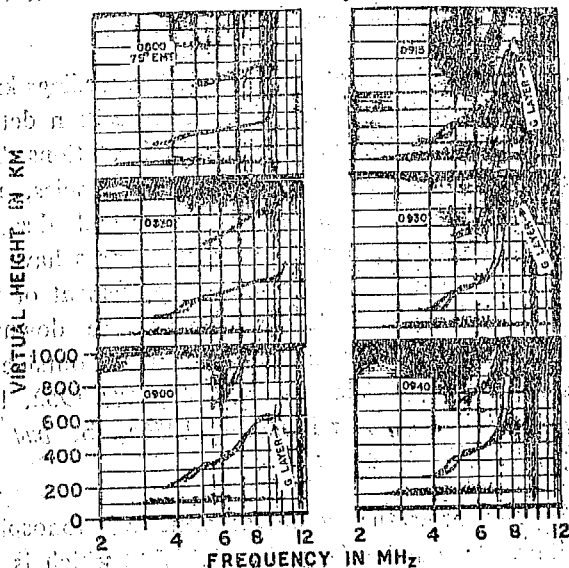


Fig. 1

A sequence of ionograms on 1 May, 1952 showing the occurrence of G layer at Kodaikanal. The cusp corresponding to G layer is marked with an arrow.

1970). The equatorial F_2 layer is lifted up very rapidly for a few hours after sunrise. This rapid rise sometimes causes an additional layer which is often referred to as the G layer (*Rivault*, 1950).

A sequence of ionograms showing the G layer at Kodaikanal on 1 May 1952 is reproduced in Fig. 1. The ionogram at 0800 LT is quite normal, $h'F_2 = 280$ kms, while $h_pF_2 = 330$ kms. At 0830 LT, although f_0F_2 has not changed much, $h'F_2$ increases to 300 km. and h_pF_2 has increased much more, to about 400 km. A small discontinuous change in $h'(f)$ trace is also seen. At 0900 LT a clear cusp is seen close to f_0F_2 , h_pF_2 now being more than 550 km. This layer is generally referred to as the G layer. The G layer is seen on ionograms till about 0930 LT, when it goes above the peak of F_2 , and a thick F_2 region with decreased f_0F_2 is left behind at 0940 LT.

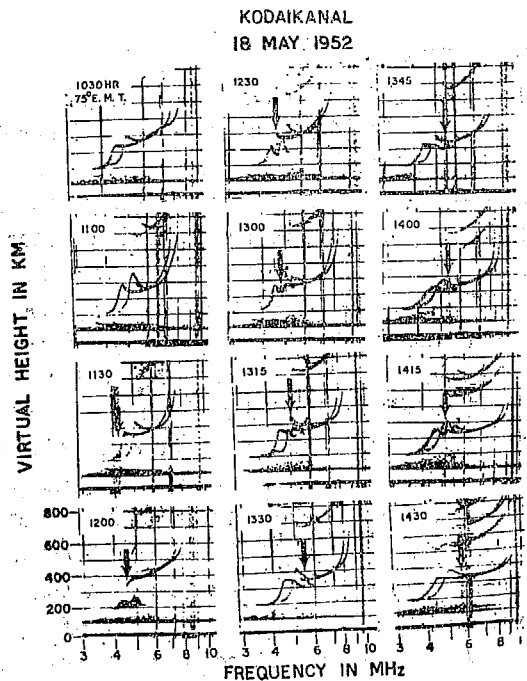


Fig. 2

A sequence of ionograms on 18 May, 1952 showing the occurrence of kink at Kodaikanal indicated by an arrow in the diagram. Note the frequency and the height of the kink increases progressively with time.

The irregularity referred to as a kink is a completely different phenomenon. This is evident from Fig. 2 in which an example of the occurrence of kink at Kadaikanal as seen from ionograms is reproduced, for 18 May 1952. At 1030 LT one can see the normal q type of sporadic E and the F₂ layer is distorted due to the uplifting of ionisation. At 1100 LT and 1130 LT one can see very intense ionisation at about 120 km which is transparent to the upper reflections. At 1200 LT this intense E₂ ionisation disappears and a discontinuity or a ledge is formed on the F₁ trace. At subsequent ionograms this discontinuity continues to steadily rise in both the virtual height and the frequency.

It is to be noted that these kinks indicate a definite extra ionisation and are distinguishable from the E_s irregularities, which blanket the reflections from upper layers. On each of the ionograms the irregularity can be clearly seen on both the ordinary and extra-ordinary traces. Further, whenever second order traces are visible within the height range of the ionogram, the height of the irregularity in the second order trace is exactly double that on the first order trace, indicating that it is not due to any off-vertical reflection, in which case the height of the kink in the second order trace will be less than twice the height of the first order trace.

On many occasions kinks are seen simultaneously with the G layer. This is evident from Fig. 3 in which a sequence of ionograms at Kodaikanal for 1 May 1964 and 13 Feb. 1964 are reproduced. At 0930 and 0945 LT the upper portion of the trace is distorted due to the uplifting of the layer. At 1000 LT and 1015 LT one can see the additional G layer cusp. At 1030 LT a small distortion of the trace is seen at a virtual height of about 420 km, which is marked in the figure as a kink. On 13 Feb. 1964 the kink starts at about 1530 LT. At 1600 LT and 1630 LT the kink and the G layer are simultaneously present. The G layer has disappeared at 1700 LT but the kink still persists till 1700 LT.

METHOD OF ANALYSIS

Ionograms at Kodaikanal are recorded on a regular basis every 15 minutes. On all the events when kinks

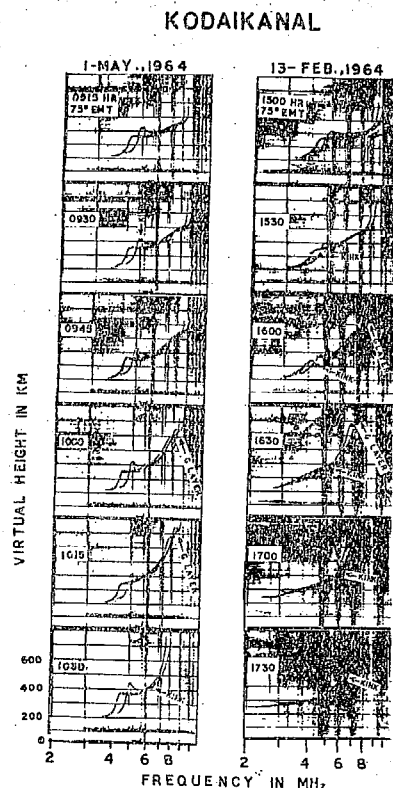


Fig. 3

A sequence of ionograms at Kodaikanal for 1 May, 1964 on the left-side and 13 Feb. 1964 on the right-side of the diagram. Note that the kink and G layer can occur simultaneously.

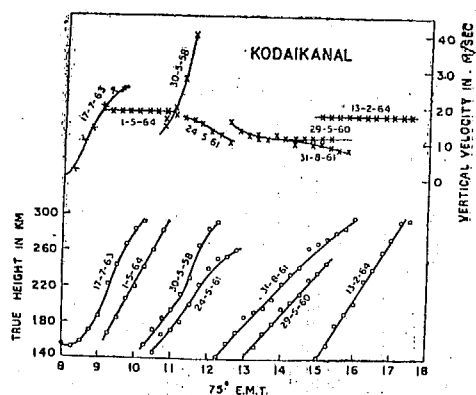


Fig. 4

Typical plots of the variation with time of true height and velocity of kink at Kodaikanal occurring at different times of the day. Figure shows kinks with constant velocity (13 Feb. 1964), kinks with increasing velocity (30 May 1958) and with decreasing velocity (24 May 1961) with height.

are observed on the ionograms, the true height of these kinks was computed using the method of *Doupnik and Schmerling* (1965). From the variation of the true height with time one gets the velocity of upward drift. In Fig. 4 are reproduced the true height variation of some of the events, and the vertical velocity component derived from it is shown in the upper part of the diagram. In the original paper of *Rastogi* (1970) he has shown that the true height of the kink increases linearly with time and thereby concluded that the upward drift velocity in the F region is independent of height. Later analysis had indicated that at height below 180 km the magnitude of velocity is significantly reduced. Further the velocities during sunset time are much smaller than during the pre-noon hours. This diagram shows that although in many cases the velocities are constant there are instances when the velocity does increase with height. From a general examination of the data it is found that the kink occurs mostly between 180 and 240 km. On some cases the kink is seen to move right from the E layer to the top of the F₂ peak.

DIURNAL VARIATION OF THE OCCURRENCE OF KINKS

In Fig. 5 are shown the number of days on which kinks are observed in the Kodaikanal ionograms as

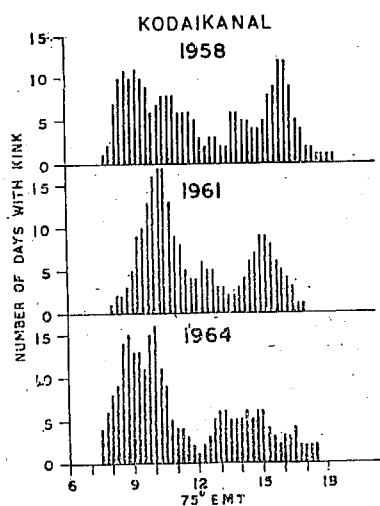


Fig. 5

Histograms showing the occurrence pattern of kink at Kodaikanal with time for the years 1958, 1961 and 1964. Figure shows two peaks one in the morning and the other in the evening with a dip around midday.

function of the time of the day at intervals of 15 minutes. A particular event may be seen in a number of successive ionograms. The diagram shows that kinks are most frequent during the forenoon hours around 0900 LT and in the evening hours around 1500 LT with a dip around noon. The evening peak seems to be much stronger in the high sunspot years and occurs at slightly later time.

SEASONAL VARIATION OF OCCURRENCE OF KINKS

Fig. 6 shows the percentage occurrence of kinks for different months of the year 1964, 1961 and 1958. One

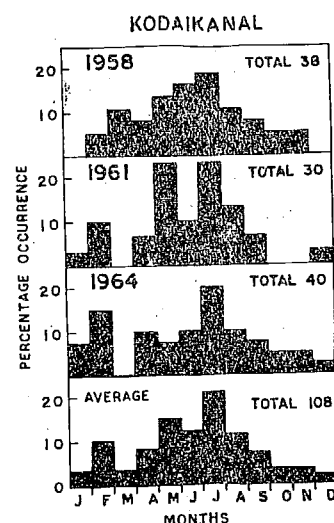


Fig. 6

Histograms showing the seasonal variation of the occurrence of kinks at Kodaikanal for the years 1958, 1961 and 1964 and average of all these three years is also shown.

can see that kinks are observed on roughly 30 to 40 days in any year. Seasonally kinks are seen to occur mostly during the summer months and their occurrence is least during winter months for any of the years.

DISTRIBUTION OF VERTICAL VELOCITY IN THE F-REGION

In Fig. 7 are shown the histograms of the magnitude of the vertical drift velocity for different years. The velocity for any solar activity condition ranges from 10-40 m/sec. The average velocity for any of the years lies between 17 and 19 m/sec, the mean velocity being

16.5 m/sec. in low sunspot years and 18.8 m/sec in high

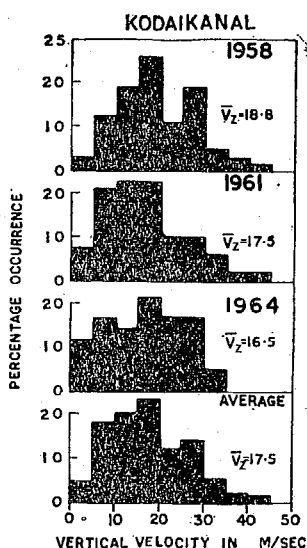


Fig. 7

Velocity distribution of kinks at Kodaikanal for the years 1958, 1961 and 1964 and averaged for these three years. The mean velocities (V_z) are also indicated in the figure.

sunspot years. The diurnal variation of the drift velocity is shown in Fig. 8. There appears to be a minimum in

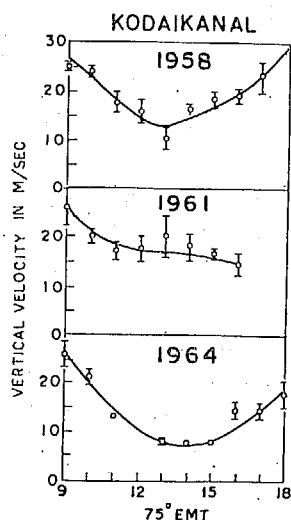


Fig. 8

Variation of vertical velocity of kinks at Kodaikanal with time of the day for the years 1958, 1961 and 1964. Increases of velocity towards the morning and evening hours with a dip around midday is seen.

the velocity around 1300 LT, the magnitude being around 8 m/sec during low sunspot years and 12 m/sec during high sunspot years. There is a tendency for the velocity to increase towards the early hours as well as later hours from midday. Whether there is a maximum of velocity cannot be determined from the present observations because kinks are rarely seen before 0800 LT and after 1800 LT. Velocities are computed for different groups of heights and the average drift velocities for different height groups of the kinks are shown in Fig. 9. Taken as a whole, the average velocity slightly increases with height between the height range of 120 to 260 km.

DISCUSSION

The analysis reveals some of the features of these upward travelling disturbances. *Rastogi* (1971b) had found that the morning peak of occurrence of kinks coincided fairly well in time with the peak in F-region horizontal drift at Thumba, the maximum in height of

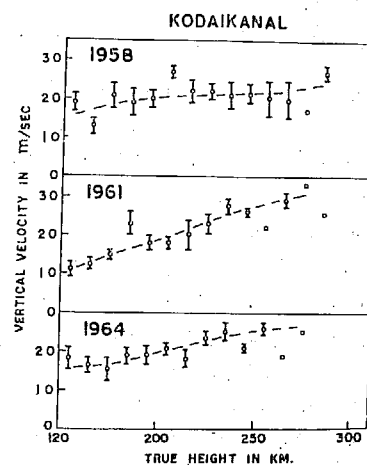


Fig. 9

Vertical velocity plotted against true height of the kink. Note the slight tendency for the velocity to increase with height in the height range of 120 to 260 km.

peak F₂ ionisation, and the depression in f₀F₂. He had also suggested that the upward movement of kinks represented the vertical drift velocity. The upward movement of these irregularities could be explained in terms of the E×B drift in the equatorial ionosphere. The electric fields in the E-region at low latitudes are mapped into

the F-region via the highly conducting field lines. During the daytime, the eastward electric field interacting with the northward magnetic field would move the F₂ layer ionisation in the vertical direction. *Balsley and Woodman* (1969) and *Woodman* (1970) have reported the results of vertical drift measurements at Jicamarca using the backscatter technique. They have found that the velocities are upward by day and downward by night. The velocities they obtain are widely variable over a range (10–40 m/sec) as large as the velocity itself. The order of magnitude of the velocity they measured and obtained from our present study are in good agreement. The upward moving kinks are also seen only in daylight hours. *Balsley and Woodman* (1969) have found that the velocity does not vary much with height in the altitude range of 200–700 km. But our results seem to favour a slight increase of velocity with height in the altitude range of 120–260 km. The observed velocities are such that it rules out the possibility of magnetohydrodynamic wave motion being responsible for the movement of these irregularities, as suggested by *Akasofu* (1956).

These irregularities are seen for a long period of about 3–4 hours. This suggests that they must be extra-ionisation possibly due to metallic ions having low loss rates. *Hanson et al.*, (1972) have shown the existence of metallic ions in the equatorial F-region from the Ogo observations. Fe⁺ ions of mass number 56 fit best their experimental data. They have calculated the distribution, layer shape and vertical velocity of these ions. The velocity they derived is of the same order as ours. They have argued that if there exists a geographically uniform source of Fe⁺ ions below 100 km, these ions will be raised to 160 km height, which is the boundary for the collisional domain, by the strong polarisation fields in the equatorial electrojet. Since the equatorial electrojet itself is a narrow belt, the mechanism could be operative only in a narrow belt around the equator. In fact, *Rastogi* (1973) has shown the kinks are observed only in a latitude belt of $\pm 6^\circ$ centred around dip equator. Once the ions are raised above the collisional domain they will be lifted up by the electromagnetic drift. *Untiedt* (1967) has shown that the usual method of calculating the dynamo current system with

no vertical currents fails at the equator. The vertical polarisation field at the equator also gives rise to vertical currents. It is the ion velocity associated with these currents that help the metallic ions to escape from the source region below 100 km. On several occasions mass spectrometers have detected the presence of Fe⁺ ions in the E_s layer at about 95 km (*Narcisi*, 1968). Equatorward neutral winds or a varying chemical source induced by gravity waves could be possible candidates responsible for the accumulation of metallic ions over the equator.

SUMMARY AND CONCLUSIONS

The occurrence pattern and vertical velocity of ionospheric irregularities seen as kinks on the ionograms are studied for the station Kodaikanal for the years 1958, 1961 and 1964 covering a period of high, medium and low solar activity. The main conclusions may be enumerated as follows:

1. Kinks are different from the additional cusp of ionization in F₂ region which is generally known as G layer. Kinks are seen only at equatorial regions and only during the daytime hours.
2. Kinks are the manifestation of a sharp thin layer of ionisation created in the ambient electron density distribution of the E and F-regions.
3. The daily variation of occurrence of F-region kinks shows two maxima, in the morning and evening hours.
4. The variation of average velocity with time of day also shows a dip around noon with increasing values towards morning and evening hours.
5. Kinks are more frequent in summer than in winter months.
6. The upward velocity of the kinks is considered to represent the vertical drift velocity of the F-region and its magnitude ranges from 10 to 40 m/sec.
7. There is no significant solar cycle effect in the vertical drift velocity in the F-region.
8. These kinks are suggested to be due to the accumulation of long-lasting metallic ions, probably Fe⁺ over the magnetic equator by the equatorward neutral winds or gravity waves, with subsequent upward motion because of the $E \times B$ drift.

ACKNOWLEDGEMENTS

The authors are pleased to express their thanks to Professor K. R. Ramanathan for his keen interest and encouragement in the collaborative work between the Physical Research Laboratory and the Indian Institute of Astrophysics. Grateful thanks are also due to Dr. M. K. Vainu Bappu, Dr. J. C. Bhattacharyya and other staff of Indian Institute of Astrophysics for the kind hospitality and facilities provided during the authors' stay at

Kodaikanal. Grateful thanks are also due to Dr. T. E. Van Zandt for critical discussions and suggestions. Thanks are also due to all the members of the Ionospheric Group at PRL especially to Dr. Harish Chandra, Dr. (Mrs.) Girija Rajaram and Dr. R. P. Sharma for their assistance and discussions at various stages of the work. One of the authors (K.N. I) is thankful to the Ministry of Education, Government of India for providing him a research scholarship.

REFERENCES

- Akasofu, S., Dispersion relation of magnetohydrodynamic waves in the ionosphere and its application to the shock wave, Report Ionosphere Research, Japan, 10, 24, 1956.
- Appleton, E. V., Two anomalies in the ionosphere, *Nature (London)*, 157, 691, 1946.
- Balsley, B. B., and Woodman, R. F., On the control of F-region drift velocity by the E-region electric field: Experimental evidence, *J. Atmos. Terr. Phys.*, 31, 865, 1969.
- Beynon, W. J. G., Evidence of horizontal motion in region F₂ ionization, *Nature (London)*, 162, 887, 1948.
- Bhargava, B. N., and Saha, A. K., Memoirs of the Kodaikanal Observatory, Vol. II (An Atlas of Equatorial Ionograms), plates 8-9, Published by the Manager of Publications, Govt. of India Press, Delhi, 1967.
- Bibl, K., Phénomènes dynamiques dans les couches ionosphériques, *C. R. Acad., Sci., Paris*, 235, 734, 1952.
- Bibl, K., Die ionosphärenschichten und ihre dynamischen phänomene, *Zeit. für Geophysik*, 19, 136, 1953.
- Bibl, K., Harnischmacher, E., and Rawer, K., Some observations of ionospheric movements, *Physics of the Ionosphere*, Physical Society, London, 113, 1955.
- Bibl, K., and Rawer, K., Travelling disturbances originating in the outer ionosphere, *J. Geophys. Res.*, 64, 2232, 1959.
- Bramley, E. N., and Peart, M., Diffusion and electromagnetic drifts in the equatorial F₂ region, *J. Atmos. Terr. Phys.*, 27, 1201, 1965.
- Doupnik, J. R., and Schmerling, E. R., The reduction of ionograms from the bottomside and topside, *J. Atmos. Terr. Phys.*, 27, 917, 1965.
- Duncan, R. A., The equatorial F-region of the ionosphere, *J. Atmos. Terr. Phys.*, 18, 89, 1960.
- Faynot, J. M., Vila, P., and Walter, J., Upward moving irregularities in the sub-equatorial ionosphere, *J. Atmos. Terr. Phys.*, 33, 1621, 1971.
- Gautier, T. M., Knecht, R. W., and McNish, A. G., Lunar stratifications of the F₂ layer at Huancayo, Peru, Proc. 2nd Meet. Mixed Commission Ionosphere, Brussels, 100, 1951.
- Hanson, W. B., Sterling, D. L., and Woodman, R. F., Source and identification of heavy ions in the equatorial F-layer, *J. Geophys. Res.* 77, 5530, 1972.
- Martyn, D. F., Atmospheric tides in the ionosphere, *Proc. Roy. Soc.*, A189, 241, 1947.
- Moffett, R. J., and Hanson, W. B., Effect of ionisation transport on the equatorial F-region, *Nature (London)*, 206, 705, 1965.
- Munro, G. H., Short period changes in F-region of the ionosphere, *Nature (London)*, 162, 886, 1948.
- Munro, G. H., and Heisler, L. H., Cusp type anomalies in variable frequency ionospheric records, *Aust. J. Phys.*, 9, 343, 1956a.
- Munro, G. H., and Heisler, L. H., Divergence of radio rays in the ionosphere, *Aust. J. Phys.* 9, 359, 1956b.
- Narcisi, R. S., Processes associated with metal ion layers in the F-region of the ionosphere, *Space, Res.*, 8, 360, 1968.

- Rastogi, R. G., The diurnal development of the anomalous equatorial belt in the F₂ region of the ionosphere, *J. Geophys. Res.*, **64**, 727, 1959.
- Rastogi, R. G., New type of ionospheric disturbance, *Nature (London)*, **225**, 258, 1970.
- Rastogi, R. G., Solar cycle variation of f_oF₂ and h_pF₂ at low latitudes, *Nature (London)*, **229**, 240, 1971a.
- Rastogi, R. G., Upward moving ionospheric irregularities over Kodaikanal, *Proc. Ind. Acad. Sci.*, **73**, 284, 1971b.
- Rastogi, R. G., Upward moving ionospheric irregularities over Huancayo, *J. Atmos. Terr. Phys.*, **34**, 1537, 1972.
- Rastogi, R. G., Upward moving ionospheric irregularity (kink) in the equatorial ionosphere, *Ann. de Geophys* (1973 in Press).
- Rivault, R., Diffusion des echos au voisinage des frequences critiques de F₂, *Proc. Phys. Soc. (London)*, **68**, 126, 1950.
- Seaton, S. L., and Berkner, L. V., Non-seasonal behaviour of F-region, *J. Geophys. Res.*, **44**, 313, 1939.
- Shapley, A. H., World Data Center A, Atlas of ionograms, Report UAG-10, III-25, Published by U. S. Dept. of Commerce ESSA, Boulder, U.S.A., 1970.
- Untiedt, J., A model of the equatorial electrojet involving meridional currents, *J. Geophys. Res.*, **72**, 5799, 1967.
- Woodman, R. F., and Hagfors, T., Methods for the measurement of vertical ionospheric motions near the magnetic equator by incoherent scattering, *J. Geophys. Res.*, **74**, 1205, 1969.
- Woodman, R. F., Vertical drift velocities and east-west electric fields at the magnetic equator, *J. Geophys. Res.*, **75**, 6249, 1970.

Vertical Drift Calculations from upward Moving Ionospheric Irregularities (Kinks) over the Magnetic Equator

K. N. IYER & R. G. RASTOGI

Physical Research Laboratory, Ahmedabad 380009

Received 6 September 1974

The occurrence pattern of ionospheric irregularities observed as sharp discontinuities (kinks), and vertical velocity in the equatorial F region, derived from their upward movement, have been compared for Kodaikanal, Natal and Huancayo. Longitudinal differences in the time of peak occurrence of these kinks and the distribution of vertical velocity are pointed out. The observed vertical velocities are in the range 10-40 m/sec, thereby excluding the possibility of Alfvén waves or magneto-acoustic waves being responsible for the movement of these kinks. It is concluded that the observed vertical drifts represent the $E \times B$ drift in the equatorial F region and that the source of these kinks is metallic ions produced by equatorward neutral winds or gravity waves.

1. Introduction

THE ELECTROMAGNETIC drift theory to explain the Appleton anomaly was first suggested by Martyn¹ and subsequently developed by Rastogi², Duncan³, Bramley and Peart⁴, Hanson and Moffett⁵ and Baxter and Kendall⁶. The latter authors inserted an assumed vertical velocity that was independent of height, and showed that electron concentration profiles in good agreement with those observed can be derived with vertical velocities ~ 10 m/sec. If vertical velocities at the equator can be obtained as a function of time and height, very detailed electron density profiles may be derived for a wide range of latitudes centred on magnetic dip equator. Hence, in the F-region over the magnetic equator such vertical drift measurements will be of great interest. This basically provides the motivation for the present study.

Rastogi noticed a new type of ionospheric irregularity on the ionograms at Thumba (dip lat. 0.6°S)⁷, which he referred to as a 'kink'. Subsequently the occurrence of such an irregularity was confirmed and the method used to calculate vertical drift at Kodaikanal (dip lat. 1.7°N) in the same longitude as that of Thumba⁸, and in the African zone by Faynot *et al.*⁹ at Ouagadougou (dip lat. 4.5°N) and Fort Archambault (dip lat. 1.5°S), at Huancayo (dip lat. 1°N), Chimote (dip lat. 3°N), Natal (dip lat. 0°), Jicamarca (dip lat. 1°N), Ilo (dip lat. 7°S) and Djibouti (dip lat. 3°N) by Rastogi^{10,11}. We studied in detail the diurnal variation of the occurrence pattern and vertical velocity distribution of these kinks at Kodaikanal for the years 1958, 1961 and 1964, covering high, medium and low solar activity conditions¹². In this paper, we compare the occurrence

pattern and vertical velocity of the kinks at difference longitudes.

The stations studied, their coordinates and the period covered are listed in Table 1. The method of deriving the vertical velocity is same as that described by Iyer and Rastogi¹².

On many occasions the velocity remains constant with height, but there are cases when the velocity either increases or decreases with height. The disturbance generally appears at a height of about 120 km and moves up the virtual height-frequency trace in about 2-3 hrs. The occurrence pattern as a function of height is shown in Fig. 1 (b). It is seen that the disturbance is almost equally probable at all heights between 150 and 280 km at Huancayo but at Kodaikanal and Natal it mostly occurs between 180 and 260 km. There seems to be no systematic longitudinal dependence in the height range in which kinks occur. However, at any height, more kinks appear at Kodaikanal than in the western longitudes.

2. Diurnal Variation of the Occurrence of Kinks

Iyer and Rastogi¹² showed that at Kodaikanal, the diurnal variation of the occurrence of kinks shows two peaks around 0900 and 1500 hrs LT. In Fig. 1 (a), the diurnal variation of the occurrence

Table 1—Stations and the Period for which Their Ionograms are Examined

Station	Dip lat.	Geogr. long.	Period of study
Kodaikanal	1.7°N	77°E	1958
Huancayo	0.6°S	75°W	1961
Natal	4.2°N	35°W	1958

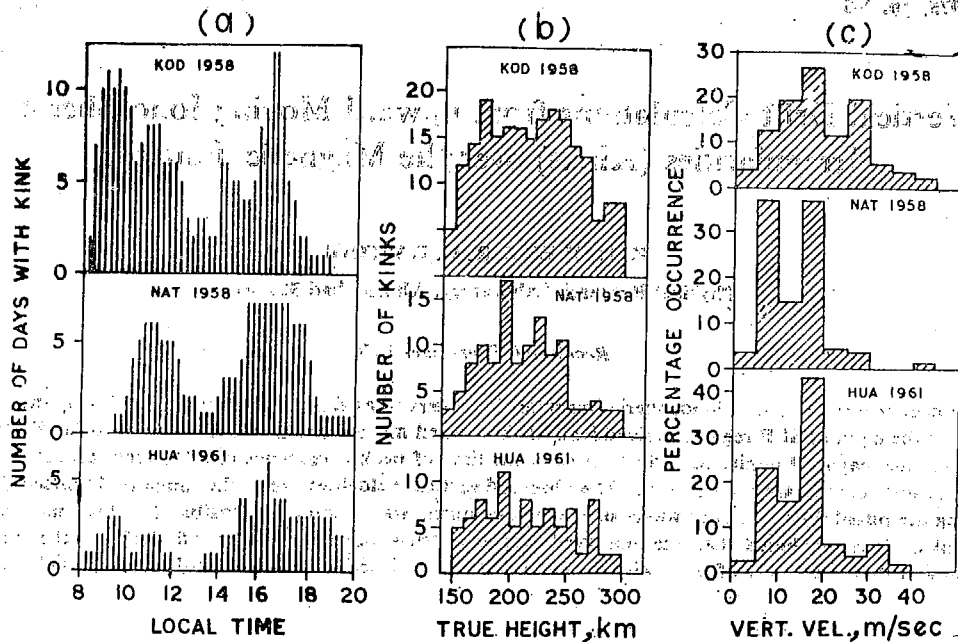


Fig. 1—(a) Occurrence pattern of kink with time of the day for Kodaikanal (KOD), Natal (NAT) and Huancayo (HUA). [Two peaks, one in the morning and the other in the evening with a dip around noon are evident.]; (b) histograms showing the number of kinks observed in different height ranges for Kodaikanal, Natal and Huancayo [The year for which observation is made is also indicated after the station.]; (c) distribution of vertical velocity for Kodaikanal, Natal and Huancayo

pattern for Huancayo and Natal have been compared with that for Kodaikanal. It may be noted that for Natal, the afternoon peak is broader and therefore the afternoon events are definitely more than the forenoon ones. The morning peak occurs at a later hour at Natal than at Kodaikanal in the high sunspot year 1958. At Huancayo also, the evening peak is stronger and broader than the morning one, there being nil events between 1200 and 1330 hrs. It cannot be ascertained now, whether the difference in the behaviour at Natal and Huancayo is due to solar activity change or longitude dependence. However, the difference between Kodaikanal and Natal patterns must be longitude dependent.

3. Distribution of Vertical Velocity in the F-Region

Histograms of the magnitude of vertical velocity are shown in Fig. 1 (c). Vertical velocity ranges from 10 to 40 m/sec. The distribution is sharper for Natal and Huancayo than for Kodaikanal. Velocities more than 20 m/sec seem to be rare at Natal and Huancayo. The median velocities are 18 m/sec, 14 m/sec and 16 m/sec for Kodaikanal, Natal and Huancayo respectively.

4. Diurnal Variation of the Vertical Velocity

The velocities are grouped together for intervals of each hour centred on each half hour, and the mean velocity and standard deviation for each of

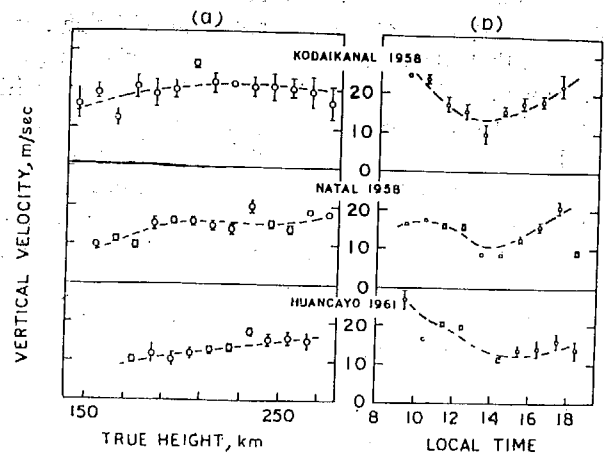


Fig. 2—(a) Variation of the vertical velocity of kinks plotted against true heights of their occurrence; (b) diurnal variation of the vertical velocity of kinks for Kodaikanal, Natal and Huancayo [Velocities are higher towards morning and evening hours with minimum values around noon.]

these hours are plotted against the corresponding hour, in Fig. 2 (b). It seems that at Kodaikanal the velocities tend to be higher in the morning and evening hours with minimum values around midday. At Natal also there is a similar tendency but the morning peak seems to be smaller than the evening one. At Huancayo there is not a clear indication of the rise of the velocity in the evening hours. It also seems that, on the average, velocities are smaller at Natal and Huancayo than those for Kodaikanal in

the morning and evening peak hours. The average velocity for groups of heights 10 km each are computed and plotted against the middle height of the group in Fig. 2 (a). The nature of variation is similar for all the three stations, there being a slight tendency for increase of velocity with height in the range of 140-260 km.

5. Discussion

The movement of the kinks is thought of as representing the vertical drift velocities in the appropriate regions. Condensed ionized formations that move from the upper F-region downward or from lower F-region upward have been studied by Vasilyev¹³ and the latitudinal dependence of the velocity determined from observations on the Schooner Zarya. He finds a strong geomagnetic dependence, the velocity being minimum in a narrow zone of 3° width centred on the magnetic dip equator and attaining maximum values at 4° lat. The height range in which he observes such disturbances, is 250-300 km. The disturbance is seen only in daytime and lasts for 1-4 hr. Various explanations for the mechanism of the observed velocities are attempted by him. Boyenkova and Kushnerevsky¹⁴ assumed that vertical displacements represent magnetohydrodynamic waves. But the velocity of Alfvén waves in the ionospheric plasma at a height of ~ 300 km will be 4.7×10^5 cm/sec, assuming a temperature = 1600 K and density = 5.8×10^{-14} g/cm³. This velocity is two orders of magnitude higher than that observed. The velocity of an accelerated magneto-acoustic wave will be always greater than the Alfvén velocity V_A . Therefore, that cannot explain the observed velocities. The decelerated magneto-acoustic waves are possible only in a hot plasma. In a cold plasma, $\beta = 8\pi p/H^2 \ll 1$ must hold. For the ionospheric plasma in the height region of relevance here, $\beta \leq 1$. Hence, the ionosphere in this region is neither a hot nor a cold plasma. If at all we think of decelerated magneto-acoustic waves as the cause of the observed motion, the velocity of such waves can be written as :

$$V_- = \frac{1}{2} \left\{ V_A^2 + C^2 \pm \left(V_A^4 + C^4 - 2V_A^2 C^2 \cos 2\alpha \right)^{\frac{1}{2}} \right\}^{\frac{1}{2}}$$

where V_A is the Alfvén velocity, C the velocity of sound in the medium, α the angle between the direction of magnetic field and the direction of wave propagation¹⁵. Putting appropriate parameters for a height = 300 km, we get $V_- \approx 840$ m/sec. This is at least two orders of magnitude higher than the observed velocities. Moreover, decelerated magneto-acoustic waves will decay and get attenuated very rapidly whereas the observed disturbances last 2-3 hr.

The vertical drifts of F-region electrons measured by the backscatter technique were reported by Woodman¹⁶. The velocities that they measured (10-40 m/sec) and their general nature are in the same order as our calculation of vertical velocities. This supports the view that the vertical movement of kinks should be due to the electromagnetic drift over the equator. Faynot *et al.*⁹ have computed the electric fields using the observed velocity of these upward moving kinks, assuming the vertical velocity $V_B = c(E \times B)/B^2$. They get values of $E \sim 1$ mV/m which is in good agreement with those measured by vapour cloud releases from rockets. From the above, it is concluded that the observed vertical velocities of the kinks are manifestation of the $E \times B$ drift.

The causes for the production of the irregularities can be numerous. Sharadze and Kvavadze¹⁶ have reported vertically moving disturbances in the ionosphere from observations at Tbilisi and classified them into A1, A2, A3+ and A3- according to the intensity of the changes they produce. They found that a small decrease of about 0.25 to 1.5 MHz of $f_o F_2$ and a lowering of the virtual height in the vicinity of the critical F_2 layer frequency are observed prior to the appearance of vertically moving disturbances. Such changes produced will have progressively decreasing magnitude for A1, A2 and A3 type disturbances respectively. A3+ and A3- are designations for upward and downward moving disturbances respectively. They concluded that A3 (+ and -) type disturbances produce only so small an effect that their occurrence could not be predicted while A1 and A2 types produce their effects even 15-30 min. before their occurrence below the $f_o F_2$ peak. The disturbances described in our paper can be compared to A3+ disturbance of Sharadze and Kvavadze¹⁶, but in the magnitude of their velocity there is only an order of magnitude agreement.

Since the kinks are seen continuously for about 2-3 hr, they may be produced by extra-ionization having long lifetime with loss rates. Metallic ions have low loss coefficients and therefore they can be a possible source of this extra-ionization. Hanson *et al.*¹⁷ have proved the existence of metallic ions over the magnetic equator from RPA data. They have calculated the layer shape, distribution and velocity of these ions. They find that Fe⁺ of mass number 56 could fit best their experimental observation. The vertical velocities they calculate for such ions are in the same range as we obtained. Once these ions cross the collisional domain below 160 km, they would be lifted up by the $E \times B$ drift. The possible sources for these metallic ions could be equatorward neutral winds or gravity waves. Metallic atoms could be

directly supplied by meteoritic dust or aerosols and could be subsequently ionized by solar radiation as suggested by Hanson *et al.*¹⁷. Metallic ions have been recently observed at Thumba¹⁸ by rocket measurements, around 92 km altitude. The fact that many times the kinks develop from strong Es layers also suggests that they must be due to metallic ions of long recombination time.

6. Conclusions

(i) The upward velocities calculated from the movement of kinks show significant longitudinal differences; (ii) the occurrence pattern of these irregularities is also longitude dependent; (iii) the possibilities such as Alfvén waves or magnetoacoustic waves are excluded for the observed velocities; (iv) the mechanism for the uplift of ionization could be $E \times B$ drift; and (v) the possible source of the extra-ionization could be equatorward neutral winds or gravity waves.

Acknowledgements

The authors are grateful to World Data Centre A, Boulder, USA and Indian Institute of Astrophysics, Kodaikanal, India for the data. We are grateful to Dr M. K. V. Bappu for hospitality at the Kodaikanal Ionospheric Laboratory, and to Dr. A. H. Sha-

pley for inviting R. G. Rastogi to the NOAA Laboratories at Boulder, USA.

References

1. MARTYN, D. F., *Proc. R. Soc.*, **A189** (1947), 241.
2. RASTOGI, R. G., *J. geophys. Res.*, **64** (1959), 727.
3. DUNCAN, R. A., *J. atmos. terr. Phys.*, **18** (1960), 89.
4. BRAMLEY, E. N. & PEART, M., *J. atmos. terr. Phys.*, **27** (1965), 1201.
5. HANSON, W. B. & MOFFETT, R. J., *J. geophys. Res.*, **71** (1966), 5559.
6. BAXTER, R. G. & KENDALL, P. C., *Proc. R. Soc.*, **A304** (1968), 1971.
7. RASTOGI, R. G., *Nature, Lond.*, **225** (1970), 258.
8. RASTOGI, R. G., *Proc. Indian Acad. Sci.*, **73** (1971), 284.
9. FEYNOT, J. M., VILA, P. & WALTER, J., *J. atmos. terr. Phys.*, **33** (1971), 1621.
10. RASTOGI, R. G., *J. atmos. terr. Phys.*, **34** (1972), 1537.
11. RASTOGI, R. G., *Annls. Geophys.*, **29** (1973), 421.
12. NARAYANA IYER, K. & RASTOGI, R. G., *J. geophys. Res.*, **79** (1974), 209.
13. VASILYEV, K. N., *Geomagn. Aeronomie*, **7** (1967), 378.
14. BOYENKOVA, N. H. & KUSHNEREVSKY, Yu. V., *Ionosfernyye Issledovaniya*, **9** (1961), 63.
15. WOODMAN, R. G., *J. geophys. Res.*, **75** (1970), 6249.
16. SHARADZE, A. S. & KVAVADZE, D. K., *Geomagn. Aeronomie*, **7** (1967), 71.
17. HANSON, W. B., STERLING, D. L. & WOODMAN, R. F., *J. geophys. Res.*, **77** (1972), 5530.
18. AIKIN, A. C. & GOLDBERG, R. A., *J. geophys. Res.*, **78** (1973), 734.